UNIVERSITÀ DELLA CALABRIA

UNIVERSITÀ DELLA CALABRIA

Dipartimento di Fisica

Dottorato di Ricerca in

Scienze e Tecnologie Fisiche, Chimiche e dei Materiali

XXXII CICLO

Natural derivative polymeric films containing Transition Metal Complexes in between Biomedical and Food Packaging Applications

Settore Scientifico Disciplinare CHIM/03

Coordinatore: Prof.ssa Gabriella Cipparrone Firma Firma oscurata in base alle linee guida del Garante della privacy

Supervisore: Prof.ssa Alessandra Crispini Firma Firma oscurata in base alle linee guida del Garante della privacy

Prof.ssa Iolinda Aiello Firma Firma oscurata in base alle linee guida del Garante della privacy

Dottorando: Dott.ssa Eugenia Giorno

Firma Firma oscurata in base alle linee guida del Garante della privacy

Dedicated to the memory of Prof. Daniela Pucci

At the end of this journey, I want to dedicate a special thought to Prof.ssa Daniela Pucci, under her guidance I moved my first step into the research, with great enthusiasm and dedication. I would be deeply proud to show her goal which, although small, I have reached..

Index

Abstract

I biopolimeri sono principalmente studiati per la progettazione di nuovi materiali utili per l'imballaggio alimentare e/o applicazioni biomediche. Il confezionamento è una componente essenziale nell'industria alimentare, necessaria per preservare la qualità e la sicurezza degli alimenti. La classica funzione del packaging alimentare, che inizialmente si basava sulla protezione, la comunicazione, la convenienza e il contenimento dei prodotti, è notevolmente migliorata con lo sviluppo di un nuovo concetto di imballaggio alimentare che consiste in sistemi di packaging attivi ed ecosostenibili. Attualmente, i principali materiali utilizzati per le applicazioni di confezionamento alimentare sono polimeri plastici prodotti da combustibili fossili, grazie al loro basso costo ed alla loro versatilità d'uso, entrambi fattori che hanno contribuito al loro rapido sviluppo nell'industria dell'imballaggio alimentare. Tuttavia, questi materiali non sono rinnovabili e non sono biodegradabili; il loro riciclaggio non è sempre possibile o economicamente vantaggioso, con conseguenti problemi indotti sull'ambiente. Lo sviluppo di materiali da fonti rinnovabili, in particolare con proprietà biodegradabili, contribuirebbe positivamente a un uso più sostenibile ed ecologico della plastica. Per questo motivo, l'uso di biopolimeri nelle applicazioni di confezionamento alimentare rappresenta una tendenza in rapida crescita. I biopolimeri possono essere ottenuti direttamente dai processi di polisaccaridi naturali o sintetizzati dalle reazioni di polimerizzazione chimica classica a partire dai corrispondenti monomeri rinnovabili. In questa prospettiva, la ricerca si sta concentrando sulla progettazione di materiali innovativi a base di polimeri naturali con prestazioni competitive ed economicamente convenienti rispetto ai materiali convenzionali derivati dal petrolio. I biopolimeri sono utilizzati principalmente nell'industria alimentare come materiali per imballaggio primario e secondario, film flessibili e rivestimenti commestibili. Grazie alle loro eccellenti caratteristiche biocompatibili e non tossiche, i biopolimeri trovano anche ampie applicazioni in campo medico come sistemi di rilascio di farmaci, dispositivi impiantabili, prodotti per la guarigione delle ferite e scaffold per l'ingegneria dei tessuti.

Uno dei biopolimeri più abbondanti in natura è la cellulosa, essa è la componente strutturale della parete cellulare primaria delle piante verdi. I derivati della cellulosa

sono ben noti in quanto possono essere ottenuti attraverso diverse reazioni come ossidazione, esterificazione ed eterificazione della cellulosa. I derivati della cellulosa come la carbossimetilcellulosa (CMC), la metilcellulosa (MC) e l'etilcellulosa (EC), hanno trovato molte applicazioni nell'industria alimentare e biomedica.

Lo scopo generale di questa tesi di dottorato è la progettazione di processi eco-compatibili ed economicamente sostenibili per la preparazione di film polimerici antimicrobici. Nell'ambito di questo progetto di ricerca, l'interesse è stato focalizzato verso l'EC per i suoi numerosi vantaggi rispetto agli altri. L'EC è, infatti, solubile in vari solventi e può essere facilmente processata come film resistenti con una buona stabilità termica e lavorabilità.

L'obiettivo principale di questo lavoro di ricerca è la preparazione di nuovi film polimerici di EC e successiva caratterizzazione. Inoltre l'attività ricercata svolta consiste nel conferire proprietà antimicrobiche ai film polimerici di EC incorporando specifici complessi di metalli di transizione. Come additivi antimicrobici sono stati utilizzati, date le loro note proprietà antimicrobiche, vari complessi di Ag(I) neutri e ionici. In particolare, i complessi acilpirazolonato di Ag(I) neutri sono stati scelti per la loro azione antibatterica esibita contro numerose famiglie batteriche. Inoltre, questi complessi che presentano una varietà di gruppi funzionali e di conseguenza caratteristiche strutturali diverse hanno permesso di studiare le diverse modalità di interazione con la matrice polimerica. Tutti i film EC sono stati preparati con il metodo "solvent casting", le soluzioni di "casting" sono state ottenute miscelando in diversi rapporti in peso degli additivi Ag(I) rispetto all'EC in soluzione o allo stato solido. In entrambi i casi, dopo l'evaporazione del solvente, i film trasparenti sono stati isolati semplicemente rimuovendoli dal supporto di deposito con acqua calda.

Le caratterizzazioni chimico-fisiche dei nuovi film di EC-Ag(I) sono state eseguite attraverso la spettroscopia infrarossa a trasformata di Fourier (FT-IR), l'analisi termogravimetrica (TGA), la calorimetria a scansione differenziale (DSC), diffrazione dei raggi X su polveri (PXRD) e misura dell'angolo di contatto con l'acqua (WCA).

Da un punto di vista applicativo, lo scopo di questa tesi di dottorato è stato quello di preparare nuovi materiali antimicrobici da utilizzare come imballaggi alimentari e nel campo biomedico. A tale scopo, era di fondamentale importanza testare l'attività antibatterica ed eseguire i test di rilascio d'argento dei film ottenuti. Tutti i film

preparati EC-Ag(I) sono stati testati per la valutazione della loro attività antimicrobica contro *l'Escherichia coli*, come modello di ceppi Gram-negativi, in accordo con la normativa standard ISO 22196: 2011. Inoltre, per tutti i film sono eseguiti i test di rilascio della migrazione specifica di ioni Ag(I), secondo la legislazione dell'UE; molti film hanno mostrato valori di rilascio inferiori al limite della legislazione dell'UE. Grazie alle proprietà antimicrobiche dei film ottenuti e del loro limitato rilascio di Ag(I), i film ottenuti rappresentano nuovi materiali molto promettenti per i campi di applicazione sopra riportati.

Il lavoro di ricerca svolto ha dimostrato come il diverso tipo d'interazione che s'instaura tra i complessi metallici Ag(I) e la matrice polimerica svolge un ruolo chiave nelle proprietà complessive mostrate dai film preparati. Tale conoscenza è fondamentale per lo sviluppo di materiali e dispositivi con prestazioni migliorate rispetto a quelli derivanti dall'utilizzo delle singole componenti utilizzate per la preparazione dei film polimerici.

Questo lavoro di ricerca è stato svolto nei laboratori MAT-InLAB del Dipartimento di Chimica e Tecnologie Chimiche dell'Università della Calabria in collaborazione con l'azienda TiFQLab "Centro di Sperimentazione, Ricerca e Analisi Applicata alle Tecnologie Alimentari e dell'Acqua Potabile".

Abstract

Biopolymers are mainly studied for the design of novel materials eventually useful for food packaging and/or biomedical applications. Packaging is an essential component of the alimentary industry, necessary to preserve the quality and safety of food. The classic functionality of food packaging, which has been initially based on product protection, communication, convenience, and containment, has nowadays been enhanced significantly with the development of a new concept of active and eco-sustainable packaging systems. Currently, the principal used materials for food packaging applications are plastic polymers produced from fossil fuels, due to their low-cost and their versatility of use, both factors contributing to their rapid development. However, these materials are non-renewable and not biodegradable; their recycling is not always possible or economically advantageous, resulting in induced environmental issues. The development of materials from renewable sources especially with biodegradable properties would positively contribute to a more sustainable and eco-friendly use of plastics. For this reason, the use of bio-polymers in food packaging applications represents a rapidly growing trend. Bio-polymers can be directly obtained from natural polysaccharide processes or synthesised by classical chemical polymerization reactions starting from renewable monomers. In this perspective, research is focusing on the development of the design of innovative materials based on natural polymers with performances that are competitive and economically convenient compared to conventional materials derived from petroleum.

Bio-polymers are mainly utilized in food industry as primary and secondary packaging materials, flexible films and edible coatings. Owe to their excellent biocompatible and nontoxic features, bio-polymers find also wide applications in the medical field as drug delivery systems, implantable devices, wound healing products, and tissue engineering scaffolds.

One of the most abundant bio-polymer in nature is the polysaccharide Cellulose, the main important structural component of the primary cell wall of green plants. Cellulose derivatives are also well known as they can be obtained through different reactions such as oxidation, esterification and etherification of Cellulose. Cellulose derivatives such as Carboxymethylcellulose (CMC), Methylcellulose (MC) and

Ethylcellulose (EC), have found many applications in food and biomedical industries.

The general purpose of this PhD thesis was the design of eco-friendly and economically sustainable processes to access antimicrobial polymeric films. Within this research project, interest has been focused towards EC for its numerous advantages over the others. EC is indeed highly soluble in various solvents and can be easily processed under tough and tensile films presenting good thermal stability and processability.

The main goal of this research work was to prepare and comprehensively characterize new active polymeric films based on EC. The sought activity consists on imparting antimicrobial properties to the EC polymeric films by incorporating specific transition metal complexes. Various neutral and ionic Ag(I) complexes have been used as active additives into the polymeric matrix, being aware that several silver complexes are indeed well known antimicrobial agents. In particular, neutral Ag(I) acylpyrazolonato complexes were chosen for their antibacterial action exhibited against numerous bacterial families. Furthermore, these complexes presenting a variety of functional groups and consequently different structural characteristics allowed different interaction modes with the polymer matrix. All metal-containing EC films have been prepared by the *"casting method"*: casting solutions have been obtained by mixing in different weight ratio of Ag(I) additives to EC either in solution or in the solid state. In both cases, after the solvent evaporation, transparent films have been isolated by simply removing them from casting support in warm water.

The physical-chemical characterizations of the new Ag-films were performed by Fourier Transform Infrared Spectroscopy (FT-IR), thermogravimetric analysis (TGA), differential scanning calorimetry (DSC), powder X ray diffraction (PXRD) and water contact angle (WCA).

From an application point of view, the aim of this PhD thesis was to prepare new antimicrobial materials to be used in food packaging and in the biomedical field. For this purpose, it was of fundamental importance to test the antibacterial activity and to carry out the silver release tests of the obtained films. All Ag-films have been tested for the evaluation of their antimicrobial activity against *Escherichia coli*, as a model of Gram-negative strains, in agreement to the ISO standard 22196:2011. Moreover,

all films have been tested for the release tests of the specific migration of Ag(I) ions, according to EU Legislation; many films showed release values lower than the EU Legislation limit. Due to the films confirmed antimicrobial properties, and to their limited Ag(I) release, the obtained films represent highly promising new materials for the above reported application fields.

The research work performed has demonstrated the importance of the different structural features of the polymeric films obtained and in particular that the interaction between the active Ag metal-complexes and the polymeric matrix plays a key role in the overall activity displayed by the prepared films. Such knowledge is crucial for the development of materials and devices with improved performance.

This research work was carried out in the laboratories MAT-InLAB of the Department of Chemistry and Chemical Technologies at the University of Calabria in collaboration with the TiFQLab "Centro di Sperimentazione, Ricerca e Analisi Applicate alle Tecnologie Alimentari e dell'Acqua Potabile", company.

Chapter 1

1.1 Food packaging

Food packaging plays a key role in the food industry and more generally in the distribution of goods on a global level. Citing Robertson in his book "Food Packaging: Principles and Practice" "Packaging material provides several functions including protection, containment, convenience, and communication of the product." (**Table 1**). [1] Food packaging represents a field in continuous evolution that received a great attention from both producers and consumers. Producers were highly stimulated in the research of materials and methodologies able to satisfy the needs of this constantly growing sector, on the other hand, the consumers are becoming always more demanding, i.e. easy handling and disposal, portion control, product visibility. [1]

The principal roles of packaging materials are the protection and the preservation of food from environmental contamination and other factors, such as odor, light, microorganisms, dust, temperature changes and humidity, in order to ensure the quality and safety of the contained food [2] [3] [4] [5] [6] In addition, convenience and information play a crucial role. Providing convenience means something referring to utility of use or functionality (range of size, easy handling and disposal, easy opening and dispensing, portion control, reclosability, product visibility). The information reported on the packaging materials regard both legal requirements and marketing objectives such as ingredients (possible allergens), net content, nutrient content, country of origin and so on. These functions, convenience and information, are of highly interest for consumers (**Table 1**).

[1] Advanced, S., and Materials, P. **2018** *Bio-based Materials for Food Packaging*.
[2] Carocho, M., Morales, P., and Ferreira, *Trends Food Sci. Technol.*, 45, 2, 284–295, **2015**
[3] Narayanan, M., Loganathan, S., Valapa, R.B., Thomas, S., and Varghese, T.O. *Int. J. Biol. Macromol.*, 99, 37–45, **2017**
[4] R.Santos, R., Andrade, M., Melo, N.R. de, and S.Silva, A., *Trends Food Sci. Technol.*, 61, 132–140, **2017**
[5] Han, J.W., Ruiz-Garcia, L., Qian, J.P., and Yang, X.T., *Compr. Rev. Food Sci. Food Saf.* 17,4 , 860–877, **2018**
[6] Robertson, G.L. *Food Packaging: Principles and practice*, Boca Rotan: CRC Press: Taylor & Francis Group. **2012**

Table 1

Function	Features
Containment and Protection	*Contains the product* *Mechanical protection* *Barrier to moisture, gases, light, flavors and aromas* *Prevents contamination* *Increases shelf life* *Prevents adulteration and theft*
Convenience	*Product preparation and serving* *Product storage* *Portioning*
Information	*Identification and description of the product* *List of ingredients* *Product features & benefits (storage, preparation, usage and nutritional data)* *Opening instructions* *Promotional messages (sales) and branding* *Safety warnings* *Contact information* *End of life management*

Today we can differentiate three levels of packaging. [6]

Primary packaging: it provides the initial protection barrier, being in direct contact with the packed product and it is also defined as sales packaging units;

Secondary packaging: generally, it is the packaging that has the purpose of enclose and group the products wrapped in the primary packaging, for example the cardboard containing the individual portions of product consumption;

Tertiary packaging: defined as transport packaging, it is the material used for transporting the goods contained in the primary packaging and grouped in the secondary packaging. It is often the outermost layer and also represents the most voluminous and heavy part.

1.2 State of art of functional food packaging

A new concept of food packaging has been introduced in the last decades. The concept of functional packaging includes active or intelligent packaging, providing to the package an active role in the extension of shelf-life (**Fig. 1.1**). [7]

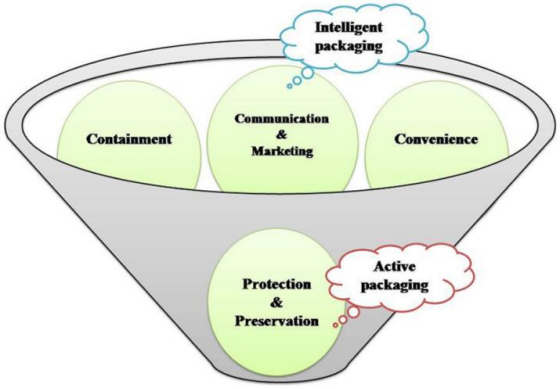

Fig. 1.1 Concept and mode of action, of active and intelligent packaging. [8]

The new packaging concept lead to a multifunctional food-packaging system. In the twenty-first century, many systems for food packaging applications have been designed and launched on the market, like intelligent or smart packaging (IOSP), active packaging (AP), and sustainable or green packaging (SOGP). IOSP are able to monitor the condition of food or its environment by using sensors or indicators. Today, type of intelligent packaging systems commercially available are radio frequency identification, time/temperature indicators, freshness indicators, bio sensors and gas sensors. Intelligent packaging systems can be printed or incorporated into packaging materials to acquire information about food's quality or transfer it to consumers.

The SOGP includes sustainable or green packaging, which are designed as environmental friendly, thought the use of recycled materials and renewable resources, the use of energy-efficient processes for their production and reuse or recycling of food packaging that is biodegradable and/or compostable in order to reduce the problem of municipal solid waste. [9]

[7] Sharma, C., Dhiman, R., Rokana, N., and Panwar, H. *Front. Microbiol.*, 8 , **2017**
[8] Dobrucka, R., LogForum. 9, 2, 103–110, **2013**
[9] Peelman, N., Ragaert, P., De Meulenaer, B., Adons, D., Peeters, R., Cardon, L., Van Impe, F., and Devlieghere, F. *Trends Food Sci. Technol.*, **32,** 2, 128–141, **2013**

Regulation 450/2009 of the European Commission establishes that "active and intelligent materials and articles must be suitable and effective for the intended purpose of use, must not release into food any components that may endanger human health or cause an unacceptable change in the composition or organoleptic characteristics of food, must not mislead the consumer by labelling, presentation or advertising material". [10]

As can be observed from the graph shown in **Fig. 1.2** the number of publications on food packaging innovations has increased steadily.

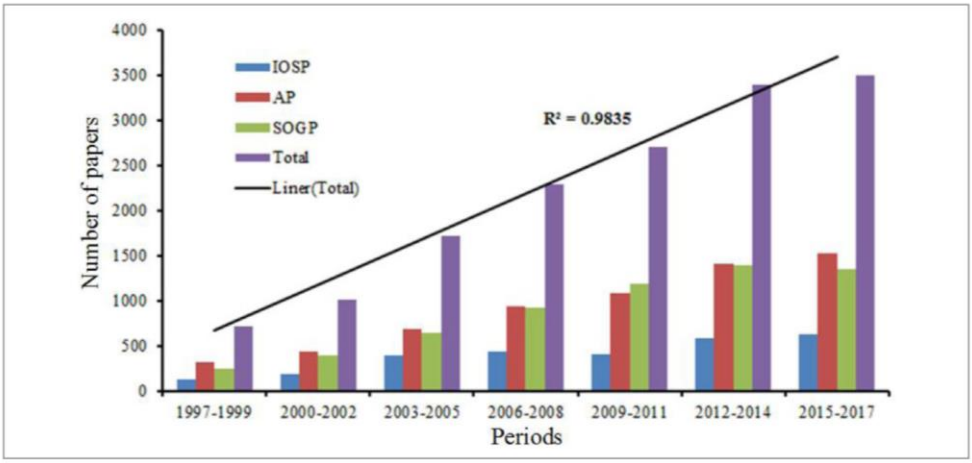

Fig. 1.2 The yearly trend of the total number of publications on IOSP, AP, and SOGP over the past 20 years [11]

One type of functional packaging is the Active Packaging (AP),that is the packaging incorporating active constituents and additives, like antifungal, antimicrobial, antioxidants, other nutrients. [12][13][14] The nature of the active substances that can be added in food packaging materials is very diverse (organic acids, enzymes, bacteriocins, essential oils, fungicides, natural extracts, ions, ethanol etc. and metal based compounds). [15][16][17][18]

---

[10] Guidelines on submission of a dossier for safety evaluation by the EFSA of active or intelligent substances present in active and intelligent materials and articles intended to come into contact with food. *EFSA J.*, **7**, 8, **2018**

[11] Han, J.W., Ruiz-Garcia, L., Qian, J.P., and Yang, X.T. *Compr. Rev. Food Sci. Food Saf.*, 17 , 4 860–877, **2018**

[12] Imran, M., Revol-Junelles, A.M., Martyn, A., Tehrany, E.A., Jacquot, M., Linder, M., and Desobry, S. *Crit. Rev. Food Sci. Nutr.*, **50** (9), 799–821, **2010**

[13] Han, J.H. *Food Technol.*, 54, 3, **2000**

[14] Clarinval, A.-M. and Halleux, J. *Classification of biodegradable polymers, in Biodegradable Polymers for Industrial Applications*, (Woodhead Publishing Limited, Cambridge, England), **2005**

[15] Bikiaris, D.N., and Triantafyllidis, K.S. *Mater. Lett.*, 93, 1–4, **2013**

[16] Lotlikar, S.R., Gallaway, E., Grant, T., Popis, S., Whited, M., Guragain, M., Rogers, R., Hamilton, S., Gerasimchuk, N.G., and Patrauchan, M.A.11, 6, **2019**

[17] COMA, V. *Meat Sci.*, **78** (1–2), 90–103, **2008**

In order to understand, the phenomenon governing the active packaging technology, it is necessary to consider that the packaging system consists of three different components, that are packaging materials, food products and the environment. Independently to its shape and characteristic, the packaging system can be generalized and schematized as shows in **Fig. 1.3:**

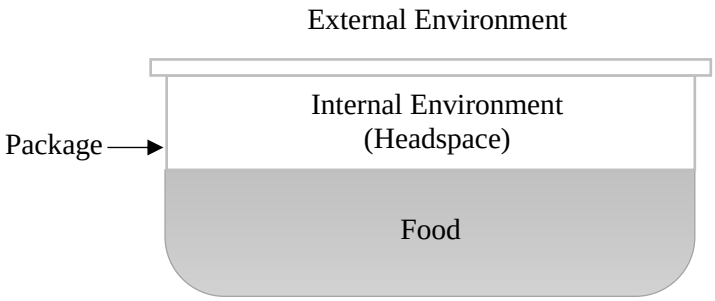

Fig. 1.3 General schematization of a Packaging system

The mass transport phenomena occurring in the food/package/environment system are permeation, migration, and sorption. **Scheme 1.1** schematically describes these interactions. Permeation is the process in which substances are exchanged between the external and internal packaging environments through the package walls. Migration consists in the release of low molecular weight substances from the package into the food. Sorption is the retention of food components within the package structure. The occurrence of the three processes is highly dependent on the affinity between the food and the material that contains it.

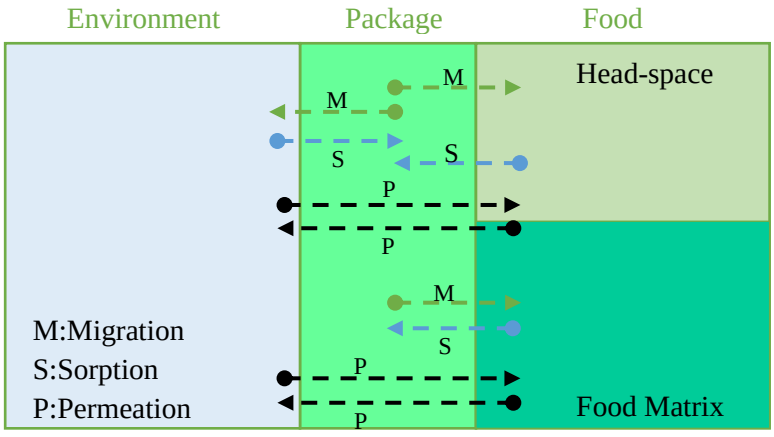

Scheme 1.1 Mass transport phenomena in the food/package/environment system

[18]Appendini, P., and Hotchkiss, J.H. Food Science & Emerging Technologies, 3, 113-126, **2002**

Depending on the mechanism of action, active packaging can be classified in 3 groups: [19]

- Absorbing/scavenging systems: removing undesired compounds present in the food or in the package headspace such as O_2, CO_2, ethylene, excessive water, and other specific compounds. The absorbing systems are mainly moisture absorber pads used to absorb the drip from packed meat and fish. [20][21] The scavenger systems such as O_2 scavengers are those that scavenge or capture residual O_2 from inside the packaging or from the foodstuff itself. The presence of O_2 may result in microbial growth on the food, making it not edible. Ethylene scavengers systems may be used in sachets or incorporated into a polymer film. Ethylene, a natural plant growth hormone, is the key to the ripening process of fruits and vegetables, being released during respiration and then driving the ripening processes itself. [22][23]
- Releasing systems: releasing systems are generally packaging materials or independent devices that contain releasing substances such as preservatives, antioxidants, flavorings, antimicrobial agents, and enzymes. These substances are purposefully added to be released. [24][25]
- Systems with substances grafted or immobilized on the surface of the packaging: generally packaging materials containing additives or enzymes which are grafted on the surface in contact with food and have a technological effect on the food. [26][27][28] This packaging is thus similar to the releasing system with the difference that the active substance is not intentional released, but it stays grafted or immobilized on the surface of the packaging.

[19] Commission of the European Communities Commission Regulation (EU) No 450/2009. *Off. J. Eur. Union*, (L 135), 3–11, **2009**
[20] Brody, A. L., Strupinsky, E. P., and Kline, L.R. *Active packaging for food applications.*, CRC Press. **2001**
[21] Han, J.H. *Innovations in food packaging*, Elsevier Science,Texas, USA, **2014**
[22] Ozdemir, M., and Floros, J.D., *Crit. Rev. Food Sci. Nutr.*, 44 (3), 185–19, **2004**
[23] Ahvenainen, R. *Active and intelligent packaging: an introduction Novel food packaging techniques*, Woodhead Publishing, **2003**
[24] Burt, S. *Int. J. Food Microbiol.*, 94 (3), 223–253, **2004**
[25] Corrales, M., Fernández, A., and Han, J.H. *Food Packaging*, San Diego: Academic Press. **2014**
[26] Appendini, Packaging_Technology_and_Science.pdf, **1997**.
[27] Muriel-Galet, V., Talbert, J.N., Hernandez-Munoz, P., Gavara, R., and Goddard, J.M., *J. Agric. Food Chem.*, 61, 27, 6720–6727, **2013**
[28] Sailaja, R.R.N., and Chanda, M., *J. Appl. Polym. Sci.*, 80, 6, 863–872, **2001**

1.2.1 AP systems: Antimicrobial food packaging

If the active agent of the packaging is an antimicrobial additive, the so-called antimicrobial packaging is obtained. Antimicrobial packaging is defined as a packaging material with biological properties able to reduce, inhibit, or retard the growth of spoilage or pathogenic microorganisms on food surfaces. Unlike the direct addition of the active agents into food, antimicrobial packaging can provide continuous migration of the active agent from the packaging material to the food or to the headspace of the package to maintain an adequate concentration of the antimicrobial agent for extending the shelf life period of the product. [29][30][31] Antimicrobial agents are the most studied active components because the growth of pathogenic and/or spoilage microorganisms are by far the major cause of food spoilage. [32][33][34] The process of Spoilage (degradation) of food can essentially be described as the inevitable alteration of color, consistency and nutritional value to which all food products are subjected. [35][36][37][38][39][40][41][42]

Among the most widespread examples of bacteria responsible for the deterioration of food we find *Salmonella spp.*, *Staphylococcus aureus*, *Listeria monocytogenes*, *Bacillus cereus*, *Escherichia coli*, *Pseudomonas*, *Klebsiella*, *Lactobacillus spp.*; *Rhizopus*, *Aspergillu*; and *Torulopsis*, *Candida*.[32][33] The development of these pathogens involves the onset of serious human pathologies linked to food contamination.[43] The addition of a biocide substance included in the food packaging system is able to reduce the risk of contamination by pathogens and extend the shelf life of foods. Antimicrobial packaging can be reached by different strategies including:

---

[29] Soares, N.F.F., Moreira, F.K.V., Fialho, T.L., and Melo, N.R. *Polym. Adv. Technol.*, 23, 5, 901–908, **2012**

[30] Espitia, P.J.P., Batista, R.A., Otoni, C.G., and Soares, N.F.F. *Antimicrobial Food Packaging Incorporated with Triclosan: Potential Uses and Restrictions*, Elsevier Inc. **2016**

[31]Soares, N.F.F., Pires, A.C.S., Camilloto, G.P., Santiago-Silva, P., Espitia, P.J.P., Silva, W.A. Recent patents on active packaging for food application. issued **2009**

[32]Ahmed, I., Lin, H., Zou, L., Brody, A.L., Li, Z., Qazi, I.M., Pavase, T.R., and Lv, L. *Food Control*, 82, 163–178, **2017**

[33]Otoni, C.G., Espitia, P.J.P., Avena-Bustillos, R.J., and McHugh, T.H. *Food Res. Int.*, 83, 60–73, **2016**

[34]Vilela, C., Kurek, M., Hayouka, Z., Röcker, B., Yildirim, S., Antunes, M.D.C., Nilsen-Nygaard, J., Pettersen, M.K., and Freire, C.S.R. *Trends Food Sci. Technol.*, **80** (April), 212–222, **2018**

[35]Wierda, R.L., Fletcher, G., Xu, L., and Dufour, J.P. *J. Agric. Food Chem.*, **54** (22), 8480–8490, **2006**

[36] Mayr, D., Margesin, R., Klingsbichel, E., Hartungen, E., Jenewein, D., Schinner, F., and Märk, T.D. *Appl. Environ. Microbiol.*, 69, 8, 4697–4705, **2003**

[37] Ioannidis, A.G., Walgraeve, C., Vanderroost, M., Van Langenhove, H., Devlieghere, F., and De Meulenaer, B., *Food Anal. Methods*, 11, 3, 848–861, **2018**

[38] Huang, T., Qian, Y., Wei, J., and Zhou, C. *Polymers (Basel).*, 11**,** 3, **2019**

[39]Lv, R., Huang, X., Aheto, J.H., Mu, L., and Tian, X. *J. Food Saf.*, 38 (6), 1–9, **2018**

[40]Mendes, R., Gonçalves, A., Pestana, J., and Pestana, C. *Eur. Food Res. Technol.*, 221, 3–4, 320–328, **2005**

[41]Jørgensen, L.V., Huss, H.H., and Dalgaard, P. *J. Agric. Food Chem.*, 49, 5, 2376–2381, **2001**

[42] Li, X., Zhu, J., Li, C., Ye, H., Wang, Z., Wu, X., and Xu, B., *Molecules*, 23, 12, 1–20, **2018**

[43] Sung, S.Y., Sin, L.T., Tee, T.T., Bee, S.T., Rahmat, A.R., Rahman, W.A.W.A., Tan, A.C., and Vikhraman, M. *Trends Food Sci. Technol.*, 33, 2, 110–123, **2013**

- Addition of sachets or pads containing volatile antimicrobial agents into packages.
- Incorporation of volatile and non-volatile antimicrobial agents directly into polymers.
- Coating or adsorbing antimicrobials onto polymer surfaces.
- Immobilization of antimicrobials to polymers by ion or covalent linkages. [44]

The antimicrobial food packaging materials have different modes of action, summarized in **Scheme 1.2**

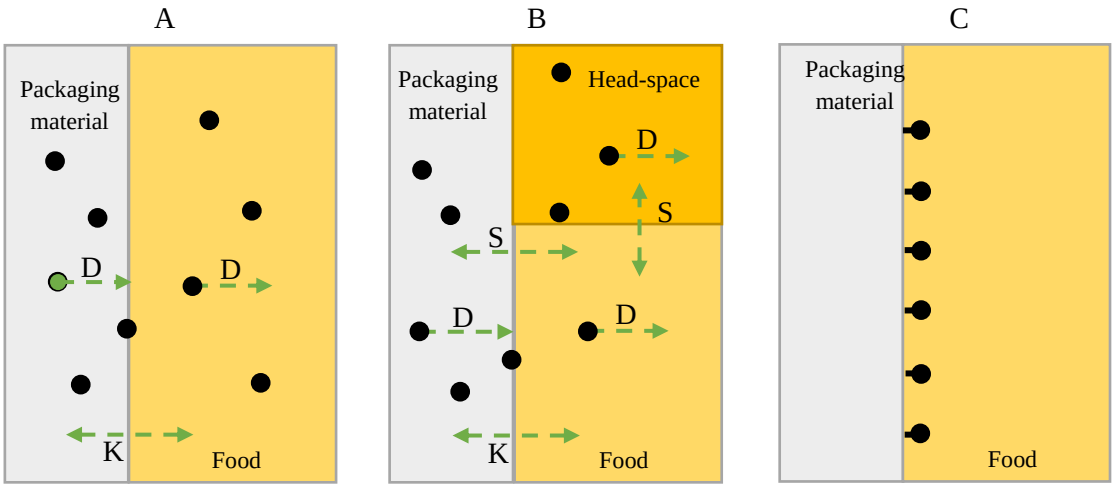

Scheme 1.2 Modes of action of antimicrobial food-packaging materials and mass transport phenomena taking place. (**A**) Packaging material that releases the antimicrobial agent directly onto the food surface in contact, (**B**) packaging material that releases the antimicrobial agent to the headspace and onto the food surface in direct contact, and (**C**) packaging material with the antimicrobial agent immobilized in the polymeric surface. Adapted from [45]

In the system (**A**) the antimicrobial agent is released onto the food surface by direct contact; in (**B**) the release of antimicrobial agent occurs into the package headspace; in (**C**) the antimicrobial agent is immobilized in the polymeric surface and performs its action on the food surface by direct contact.

[44]Lü, F., Ye, X., and Liu, D. *Transactions Chinese Soc. Agric. Mach.*, 40, 6, 138–142, **2009**
[45] Han, J.H., *Antimicrobial food packaging*, Novel food packaging techniques, **2003**

Concerning (**A**) and (**B**) mechanisms, the release of the antimicrobial agent depends on a combination of phenomena. The antimicrobial agent is distributed in all phases, and the concentration ratio at the interfaces is given by the partition coefficient of the antimicrobial agent between the packaging material and the food, more specifically $K = Cp/C_F$, where Cp is the concentration in packaging materials while Cf is the concentration into the food (**Scheme 1.2 A**). D is defined as the mass diffusion coefficient, indicating the rate of release of the antimicrobial agent; S is the coefficient related to the volatile antimicrobial agent, which indicates the solubility of the antimicrobial agent in the headspace and in the package. In particular, $S = Cp/C_{HS}$ and $= Cf/C_{HS}$, where C_{HS} is the concentration antimicrobial agent in headspace (**Scheme 1.2 B**).

1.3 Materials for food packaging

Over the centuries, different packaging materials of various physical-chemical natures have been used: glass, metals (aluminum, tinplate, and tin-free steel), paper and paperboards, and plastics. Many efforts have been made in developing different type of packaging materials to improve their effectiveness with respect to the contained food. The choice of the material used for packaging depends not only on its intrinsic properties (**Table 2**) but also on the product that it will contain. The right selection of the materials for packaging and technologies can ensure the quality and freshness of the product from the packaging to its consumption phase. **Table 2** summarizes the intrinsic properties of the commonly used materials for packaging. [46]

[46] Coles, R., McDowell, D., and Kirwan, M., *Food packaging technology.*, CRC Press Oxford, Egland, **2003**

Table 2

Function	***Features***
Glass	- *Inert with respect to foods* - *Transparent to light and may be colored* - *Impermeable to gases and vapors* - *Rigid* - *Recyclable and reusable* - *Brittle and breakable* - *Widely in use for both single and multi-trip packaging*
Aluminum and Tinplate	- *Rigid material with a high density for steel and a low density to aluminum* - *Good tensile strength* - *An excellent barrier to light, liquids and food* - *Needs closure, seams and crimps to form packs* - *Used in many packaging applications: food and beverage cans, aerosols, tubes, trays* - *Can react with products causing dissolution of the metal*
Paper and paperboard	- *Low density materials* - *Poor barriers to light without coatings or laminations* - *Poor barriers to liquids, gases and vapors unless they are coated or laminated* - *Good stiffness* - *Could be grease resistant upon addition treatment* - *Absorbent to liquids and moisture vapor* - *May be creased, folded and glued* - *Tear easily* - *Not brittle but not so high in tensile strength* - *Excellent substrates for inexpensive printing*
Plastics	- *Wide range of barrier properties* - *Permeable to gases and vapors to varying degrees* - *Low density materials with a wide range of physical and optical properties* - *Usually have low stiffness* - *Tensile and tear strengths are variable* - *May be transparent* - *Functional over a wide range of temperatures depending on the type of plastic* - *Flexible and, in certain cases, can be creased*

Each packaging material has different advantages and disadvantages in its use, such as briefly summarized below:

Glass. Glass is almost impermeable to gas and air and it represents an ideal solution for packaging. Furthermore, foodstuffs can be packed and sterilized by pasteurization directly inside the container. Another extremely important aspect of glass packaging is its unlimited recyclability. In fact, measurable physical differences between virgin glass and recycled glass may not be detected. [1] The disadvantage of choosing glass is its weight and its fragility compared to other materials, making difficult to transport.

Aluminum. Aluminum finds applications in all sectors of the global economy. Although the metal itself is ductile and soft, it can be adapted for use forming alloys by adding low amounts of copper, zinc, silicon, manganese and nickel. In the food sector, aluminum is used in the form of sheets to wrap food or in the form of cans and containers sealed in a vacuum or in a controlled atmosphere.
The chemical, mechanical and physical properties of aluminum such as barrier effect and food contact ability enable a wide range of applications in many different products for food packaging. This material is light but strong and it can be formed and converted into different shapes. Aluminum exhibits good corrosion and temperature resistance and shows a high thermal and electrical conductivity. [47] But in order to produce aluminum, manufacturers need bauxite, which is a mineral that must be mined from the earth. Mining for bauxite is harmful to the environment and can lead to water contamination, erosion, and habitat destruction.

Paper/cardboard. Paper and cardboard are versatile materials used for food packaging. They are made of natural fibers of cellulose or in alternative recycled from recovered materials. Cardboards are very effective and versatile packaging materials and provide protection against contamination and breakage. Paper and cardboard are easy to print on, they are model into secondary packages, and pile on shelves. After use, the cardboard is 100% recyclable and it is often used as raw material for the manufacture of packaging papers and cardboards.

Plastics. Plastic represents an ideal solution for packaging, due to lightness and durability. Plastic is able to provide a layer of protection that is not permeable to air

[47] M. Lamberti, F. Escher, *Food Reviews International*, 23,4, 407-433, **2007**

and other contaminants. Moreover, the extreme versatility of the material in terms of transparency, color, high flexibility (shape, density and thickness) and ability to be printed means that plastic is the packaging material par excellence. The advantages of plastic compared to traditional paper, glass or tin packaging are many: plastic materials can be used for the manufacture of very flexible (pouches, bags, envelopes), semi-rigid (trays, tubs) or stiff materials (bottles, tanks, caps, etc.) in any imaginable size or shape. The most widely used plastics in packaging applications are polyethylene (PE), polypropylene (PP), polystyrene (PS), polyvinyl chloride (PVC), polyurethane (PU), poly(ethylene terephthalate) (PET), poly (butylene terephthalate) (PBT). [48][49]

All these materials are normally used alone but can be also combined with other materials obtaining hybrid materials. Among the latter, the most common is Tetrapak composed of 74% of paper, which forms the central core of the material. Externally, the Tetrapak is coated with a thin polyethylene layer and internally by two layers of polyethylene with a thin aluminum foil interposed. The paper gives the casing rigidity while the plastic ensures a reduced permeability and the ability to seal the material by heat. This composite material has been used since the 1960s for the packaging of long-life sterile milk, fruit juices and other agri-food products.

As stated above, the choice of the packaging material strongly depends on the aliment to be packed. It is additionally true that plastic represents the packaging of more than half of the distributed materials. Consequently, the amount of plastic produced at industrial and domestic level is the main source of environmental pollution.

1.3.1 Plastic food packaging as a source of pollution: Environmental problems

The use of plastic mainly deals with two problems. The first one is that the polymers mainly used to obtain plastics derive from non-renewable resources that are the fossil hydrocarbons. If the growth in plastic production continues at the current rate, in 2050 the plastic industry may account for 20% of the world's total oil consumption. The second problem is the plastic consumption and disposal of waste. The

[48] Campbell, I. M. Promoting polymer properties. In: *Introduction to synthetic polymers*, Oxford, Great Britain: Oxford University Press, 25−73, **1994**

[49] H. Ritchie, M.R., *Plastic Pollution-Our World* in data, **2018**

industrialized countries have a production rate of plastic waste that is decidedly higher than in underdeveloped countries; some countries, like Germany, Holland and the United States have a daily pro capita consumption of plastic between 0.4-0.5 kg.(**Fig. 4)** [50] [51]

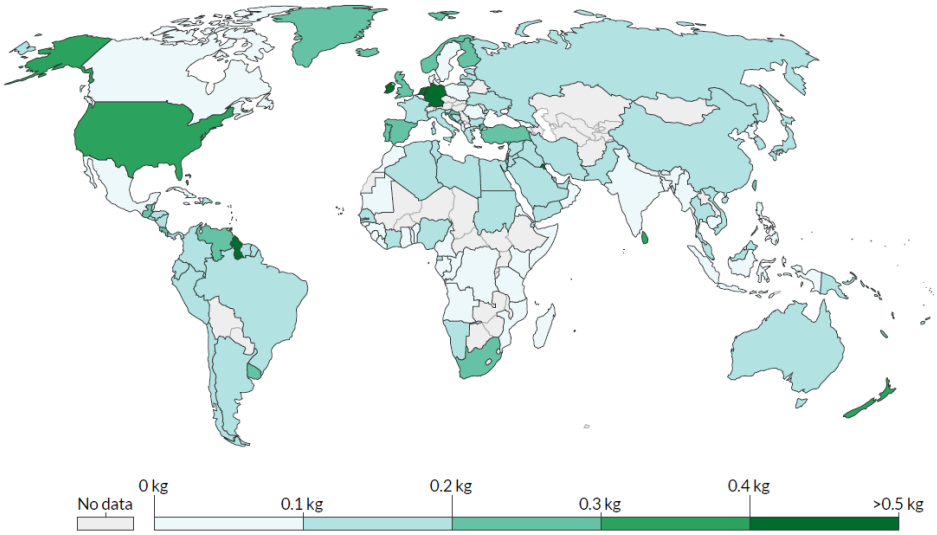

Fig. 1.4 Daily pro capite consumption of plastic 2010 [51]

Nevertheless, these countries are not the major contributors to global pollution. In fact, countries like China, India and South East Asia have an extremely high percentage of inadequately disposed waste, due to poor waste management. The wastes are often sent to be disposed in landfills not adequately controlled neither well-isolated (**Fig. 1.5**). [50]

[50] J. R. Jambeck, R. Geyer, C. Wilcox, T. R. Siegler, M. Perryman, A. Andrady, R. Narayan, K. Lavender Law , *sciencemag.org*, Vol 347 ISSUE 6223, 768, 771, **2015**

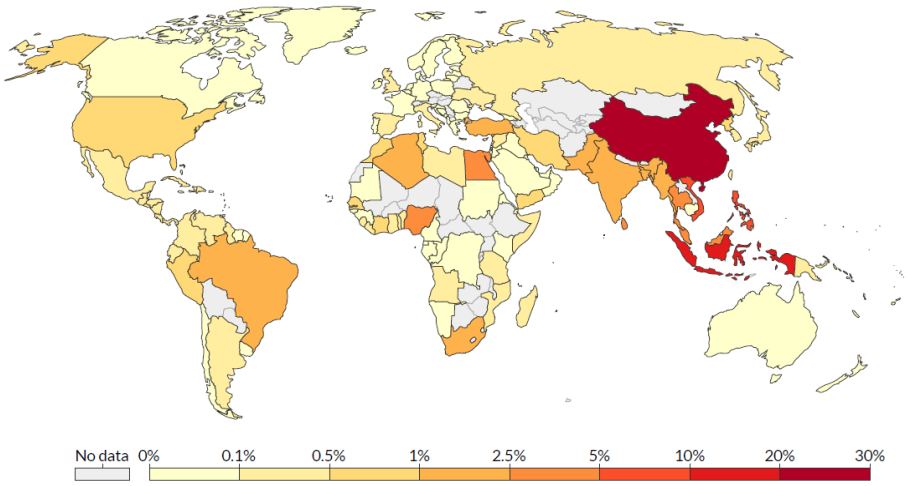

Fig. 1.5 Percentage of incorrect disposal of plastic waste 2010 [51]

Consequently, wastes can enter the waterways and end up in the oceans. Plastic tends to be accumulated by the currents and winds in immense areas of collection on the surface of the oceans. A recent study has estimated that there are over 250,000 tons of floating waste in the oceans. [52] These wastes have a tremendous impact on the marine ecosystem. In particular, plastic debris was found in many species of sea turtle and of bird species by accidental ingestion. [53]

1.3.2 Plastic food packaging as a source of pollution: Human health problems

Since plastic is produced by fossil hydrocarbons, hazardous chemicals present in plastics fatally come in contact with food. These chemicals, such as polymer monomers, additives, solvent residues, plasticizers, and so on, can migrate into food and from there into human organism, giving rise to negative effects on food quality and human health. [54] In order to protect consumers from this problem, several European regulations define the compliance criteria for packaging materials.

The European regulation includes the framework (EC) No 1935/2004 of the European Parliament on materials and articles intended to come into contact with

[51] H. Ritchie, M.R., Plastic Pollution-Our World in data. https://ourworldindata.org/plastic-pollution, **2018**
[52] Eriksen, M., Lebreton, L.C.M., Carson, H.S., Thiel, M., Moore, C.J., Borerro, J.C., Galgani, F., Ryan, P.G., and Reisser, J. Plastic Pollution in the World's Oceans: More than 5 Trillion Plastic Pieces Weighing over 250,000 Tons Afloat at Sea. *PLoS One*, 9, 12, 1–15, **2014**
[53] Bergmann, M., Gutow, L., and Klages, M. *Marine Anthropogenic Litter*, Springer, **2015**
[54] Callegarin, F., Gallo, J.A.Q., Debeaufort, F., and Voilley, A. *JAOCS, J. Am. Oil Chem. Soc.*, 74, 10, 1183–1192, **1997**

foodstuffs. [55] In addition, there is also the regulation (EU) n. 10/2011 on plastic materials, that indicates the rules for measuring overall and specific migration of many hazardous analytes that can migrated in the food. [56] In recent years, many researchers have focused their attention on the identification of the different components that can migrate into food. [57][58][59][60][61][62][63] These are not only the major constituent of the packaging but also the by-product formed during the materials production. [64][65][66] All these compounds represent, above a certain level, a danger for human health. [67][68][69][70][71][72][73]

On the basis of all the above statements, the development of new plastics materials, biodegradable polymer-based, can provide a greener viable alternative for food packaging. The use of bio-polymers represents a valid alternative able to mitigate the problem of pollution from plastic waste and migration additives, providing a solution to the replacement of plastic materials deriving from oil. [74]

1.3.3 Bio-Polymers: cellulose and derivatives as a green alternative

There are a number of plastics called bioplastics, such as bio-Polyethylene terephthalate, bio-Polyethylene or bio-Polypropylene, chemically identical to their fossil fuel-based analogous, but synthesized from biomass, mostly from bioethanol. Even if, the use and development of bioplastics reduce the CO_2 emission resulting

[55] European Union (EU) (2004) *REGULATION (EC) No 1935/2004 OF THE EUROPEAN PARLIAMENT AND OF THE COUNCIL of 27 October **2004** on materials and articles intended to come into contact with food and repealing Directives 80/590/EEC and 89/109/EEC*

[56] European Food Safety Authority. Scientific Opinion on the safety evalutation of the substance, silver zeolite A, silver content 2-5%, for use in the foos contact materials. EFSA J., 9, 12. No Title. **2011**

[57] Vera, P., Aznar, M., Mercea, P., and Nerín, C. **2011**. *J. Mater. Chem.*, 21, 2, 420–431, **2011**

[58] Aznar, M., Vera, P., Canellas, E., Nerín, C., Mercea, P., and Störmer, A., *J. Mater. Chem.*, 21, 12, 4358–4370, **2011**

[59] Metak, A.M., Nabhani, F., and Connolly, S.N. (). *LWT - Food Sci. Technol.*, 64, 2, 781–787, **2015**

[60] Cherta, L., Portolés, T., Pitarch, E., Beltran, J., López, F.J., Calatayud, C., Company, B., and Hernández, F. (). *Food Chem.*, 188, 301–308, **2015**

[61] Onghena, M., Van Hoeck, E., Van Loco, J., Ibáñez, M., Cherta, L., Portolés, T., Pitarch, E., Hernandéz, F., Lemière, F., and Covaci, A. *J. Mass Spectrom.*, 50, 11, 1234–1244, **2015**

[62] Colón, M., and Nerín, C. () . *Food Control*, 57, 419–425, **2015**

[63] Kiyataka, P.H.M., Dantas, S.T., and Pallone, J.A.L. *Food Anal. Methods*, 8 (9), 2331–2338, **2015**

[64] Nerin, C., Alfaro, P., Aznar, M., and Domeño, C. *Anal. Chim. Acta*, 775, 14–24, **2013**

[65] Aznar, M., Rodriguez-Lafuente, A., Alfaro, P., and Nerin, C. *Anal. Bioanal. Chem.*, 404 (6–7), 1945–1957, **2012**

[66] Félix, J.S., Isella, F., Bosetti, O., and Nerín, C. *Anal. Bioanal. Chem.*, 403, 10, 2869–2882, **2012**

[67] Lago, M.A., De Rodriguez-Bernaldo Quiros, A., Sendón, R., Bustos, J., Santillana, M.I., and Paseiro, P. *Anal. Bioanal. Chem.*, 406, 17, 4251–4259, **2014**

[68] Johns, S.M., Jickells, S.M., Read, W.A., and Castle, L. *Packag. Technol. Sci.*, 13, 3, 99–104, **2000**

[69] Jung, T., and Simat, T.J. *Food Addit. Contam. - Part A Chem. Anal. Control. Expo. Risk Assess.*, 31, 4, 743–766, **2014**

[70] Jung, T., Simat, T.J., and Altkofer, W. *Food Addit. Contam. - Part A Chem. Anal. Control. Expo. Risk Assess.*, 27, 7, 1040–1049, **2010**

[71] Lago, M.A., Rodríguez-Bernaldo de Quirós, A., Sendón, R., Bustos, J., Nieto, M.T., and Paseiro, P. (). *Food Addit. Contam. - Part A Chem. Anal. Control. Expo. Risk Assess.*, 32 , 5, 779–798, **2015**

[72] Van Hoeck, E., De Schaetzen, T., Pacquet, C., Bolle, F., Boxus, L., and Van Loco, J. *Anal. Chim. Acta*, 663, 1, 55–59, **2010**

[73] J.L. Aparicio, M.E., *Packag. Technol. Sci.*, 28, 181–203, **2015**

[74] Huang, Y., Mei, L., Chen, X., and Wang, Q., *Nanomaterials*, 8, 10, 1–29, **2018**

from the production of traditional plastics, unfortunately, these kinds of polymers do not solve the environmental problems because they are non-biodegradable. Bioplastics are used in an increasing number of markets, as packaging, catering products, consumer electronics, automotive, agriculture/horticulture, toys, textiles and so on. Packaging represents the largest field of application for bioplastics with almost 1.2 million tons in 2018 (**Fig. 1.6)**.

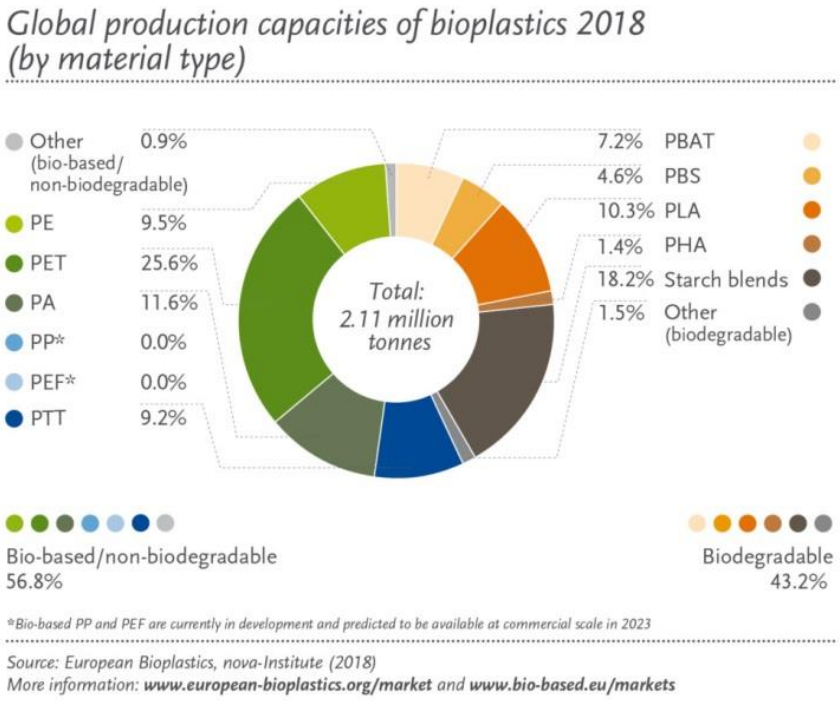

Fig. 1.6 Global production capacities of bioplastics 2018

Bioplastics can be composed by bio-polymers such as starches, cellulose, chitosan or polymers derived from renewable monomers, such as polylactic acid (PLA). [75]
Bio-polymers are considered to be the ideal source of biodegradable and eco-friendly materials with excellent mechanical and barrier properties. [76]
The term “Biodegradable polymers" is attributed to materials that are capable of decomposing into simple compounds like carbon dioxide, methane, inorganic

[75]Feng, X., Xu, Z., and Masliyah, J. 23 (1), 451–456, **2009**
[76] J.L. Aparicio, M.E. *Packag. Technol. Sci.*, 28, 181–203, **2015**

compounds or biomass due to a biochemical enzymatic action of microorganisms and thanks to the biodegradable nature there is no accumulation of waste. [77]

One of the biopolymer used for the production of bioplastics is cellulose, which is the most abundant natural polysaccharide present on Earth. More than 10^{12} tons of cellulose are synthesized every year by photosynthesis from a multitude of living organisms. The cell wall of green plants, algae and oomycetes is mainly composed of cellulose. [78] Cellulose is a homopolymer of D-glucose in which the individual units, monomers, are mutually connected by β-(1-4) glycosidic bond (**Fig. 1.7**).

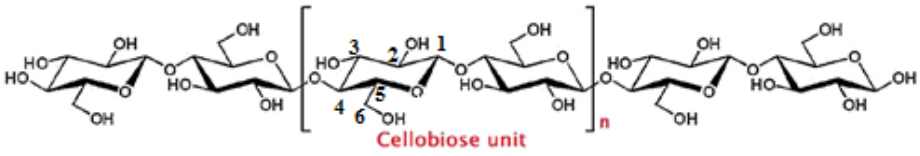

Fig. 1.7 Structure of Cellulose [79][80]

Cellulose-based materials have been used by the packaging industry such as flexible or rigid wrapping materials and containers, for primary and secondary packages. Cellulose cannot be melted and is insoluble in polar solvents or common organic solvents limiting its applications. Cellulose insolubility has been widely studied, leading to two main hypotheses, one of them states that the insolubility of cellulose is due to the relatively high length of the cellulose molecular chain and its close packing through numerous hydrogen bonds, [81] the second hypothesis attributes the insolubility of cellulose to its high crystalline degree. [82][83]

Cellulose can be transformed into a myriad of derivatives, some of these commercially available are shown in **Fig. 1.8**; these products have been reported as environmentally friendly and useful in wide range of applications. [84][85][86][87][88]

[77] Siracusa, V. *Packaging Material in the Food Industry*, Elsevier Inc., **2016**
[78] Sundarraj, A.A., and Ranganathan, T.V., *Drug Invent. Today*, 10 (1), 89–94, **2018**
[79] Ferrer, A., Pal, L., and Hubbe, M. *Ind. Crops Prod.*, 95 ,574–582, **2017**
[80] Jeevahan, J., and Govindaraj, M. a Brief Review on Edible Food, **2017**
[81] Wang, S., Lu, A., and Zhang, L. *Prog. Polym. Sci.*, 53, 169–206, **2016**
[82] Lindman, B., Karlström, G., and Stigsson, L. *J. Mol. Liq.*, 156, 1, 76–81, **2010**
[83] Cazón, P., Velazquez, G., Ramírez, J.A., and Vázquez, M., *Food Hydrocoll.*, 68, 136–148, **2017**
[84] Abdul Khalil, H.P.S., Tye, Y.Y., Saurabh, C.K., Leh, C.P., Lai, T.K., Chong, E.W.N., Nurul Fazita, M.R., Hafiidz, J.M., Banerjee, A., and Syakir, M.I. *Express Polym. Lett.*, 11, 4, 244–265, **2017**
[85] Criado, P., Fraschini, C., Salmieri, S., Becher, D., Safrany, A., and Lacroix, M. *Radiat. Phys. Chem.*, 118, 61–69, **2014**
[86] Ohkawa, K., Hachisu, M., Devarayan, K., and Araki, J., *Fibers Polym.*, 14 (12), 1970–1974, **2013**
[87] Edgar, K.J., Buchanan, C.M., Debenham, J.S., Rundquist, P.A., Seiler, B.D., Shelton, M.C., and Tindall, D. *Prog. Polym. Sci.*, 26 (9), 1605–1688, **2001**
[88] Arvanitoyannis, I., and Biliaderis, C.G., *Carbohydr. Polym.*, 38, 1, 47–58, **1999**

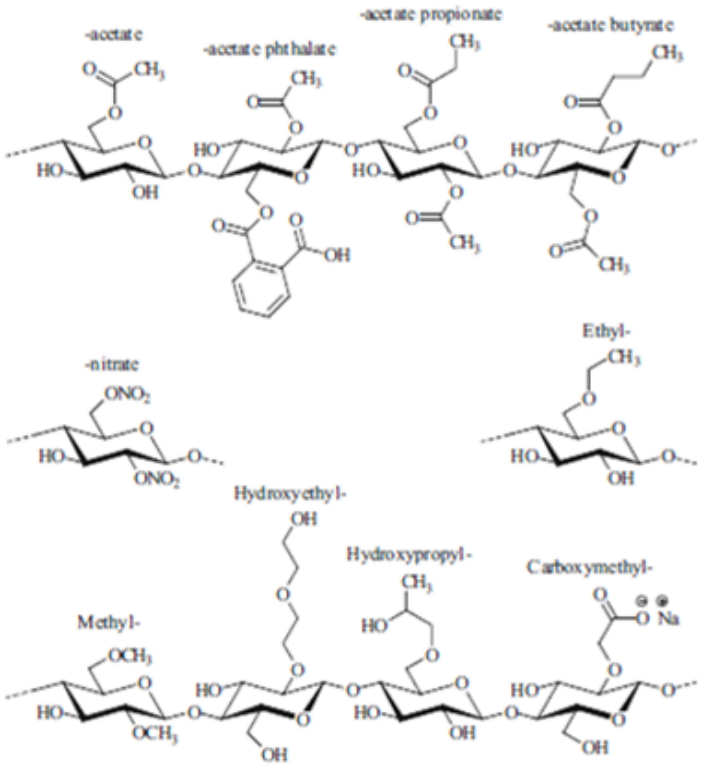

Fig. 1.8 Schematic representation of some commercially available cellulose derivatives. Adapted from [89]

The functionalization of cellulose occurs on the three hydroxyl groups present on the glucosidic unit: the primary hydroxyl group at C-6 (**Fig. 1.8**) and the secondary hydroxyl groups at C-2 and C-3 (**Fig. 1.8**). The functionalization can take place mainly through the typical known alcohols' reactions, such as esterification and etherification. Most of the products manufactured on a commercial scale are partially modified cellulosic compounds still containing free hydroxyl groups. In order to functionalize cellulose, chemical treatments are necessary. These treatments allow to increase the accessibility to the hydroxyl groups and to reduce the intermolecular forces in the backbone, leading to a weakening of the supramolecular structure. [90][91][92]

[89] ISSN 2364-1878 ISSN 2364-1886 (electronic) Springer Series on Polymer and Composite Materials ISBN 978-3-319-73167-4 ISBN 978-3-319-73168-1 (eBook), **2018**
[90] Malm CJ, Tanghe LO, Laird BC, Smith GD, *J Am Chem Soc* , 75, 80–84, **1953**
[91] Jain RK, Agnish SL, Lal K, Bhatnagar HL , *Makromol Chem* 186, 2501–2512, **1985**
[92] Kwatra HS, Caruthers JM, Tao BY, *Ind Eng Chem Res* 31:2647–2651, **1992**

For example, in order to prepare cellulose acetate, a milling process has been performed to activate the cellulose before the reaction with acetic anhydride and super-acid catalyst (SO_4^{2-}/ZrO_2) (**Fig. 1.9**). [93]

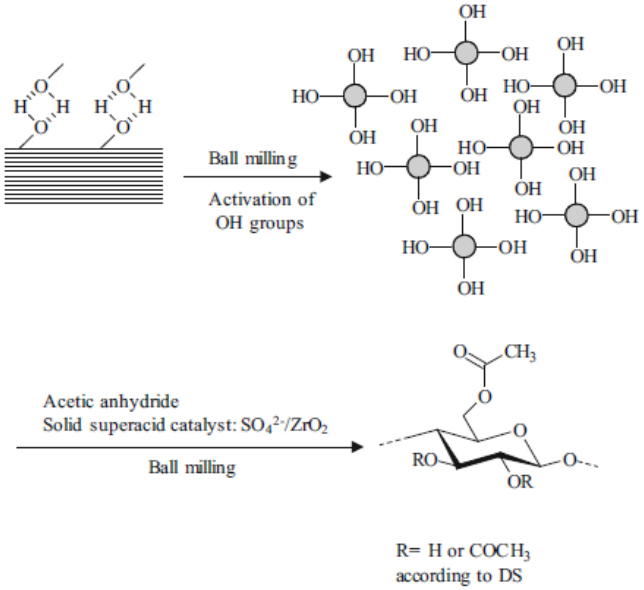

Fig. 1.9 Cellulose activation by ball milling and subsequent solvent-free acetylation. Adapted from [89]

The preparation of cellulose esters can be carried out by following various synthetic strategies, which use organic acids and anhydrides under different reaction conditions. The resulting cellulose esters are soluble in water and not toxic. [94]

For example, cellulose acetate (CA), cellulose acetate phthalate (CAP), cellulose acetate butyrate (CAB), cellulose acetate trimellitate (CAT), hydroxypropyl methylcellulose phthalate (HPMCP) and Ethylcellulose (EC) are common cellulose esters used in commercial products or in pharmaceutical applications. Regarding commercial products, the cellulose esters derivatives are used as coating materials for metal and wood, gravure and flexographic printing inks, inkjet printing inks, graphic arts, automotive clear coats, and general industrial coatings. Cellulose esters are also used for textile application, plastic films such as optical film for LCD technology and anti-fog goggles and filters. [84][95]

[93] Shakeel Ahmed, Bio-based Materials for Food Packaging, *Springer Nature*, **2018**
[94] Heuser F, *The Chemistry of Cellulose* (John Wiley and Sons, New York), 1, **1954**
[95] Shokri, J., and Adibki, K., *Cellul. - Medical, Pharm. Electron. Appl.*47-66, **2013**

Cellulose ethers are prepared through classical nucleophilic reaction under alkaline conditions with one of the following reagents (**Fig. 1.10**):

- Alkyl or aryl halides (Williamson ether synthesis, (a));
- Epoxides (Ring-opening reaction, (b));
- Activated double bonds (Michael addition-type reactions, (c))

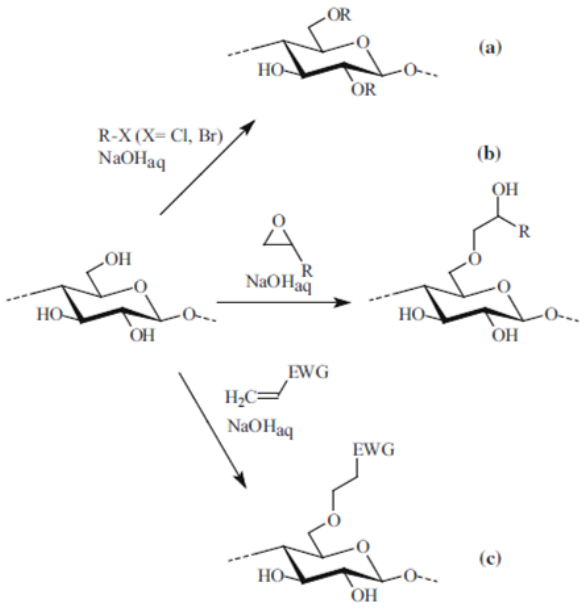

Fig. 1.10 Synthetic pathways for commercial cellulose ethers [89]

Among cellulose derivatives, EC has garnered considerable attention; it is obtained by partial substitution of the hydroxyl groups with ethoxyl functional groups (**Fig. 1.11**).

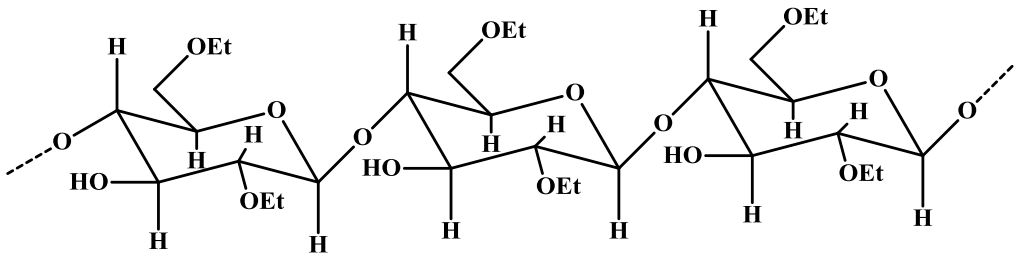

Fig. 1.11 Structure of ethylcellulose

The derivatization is carried out in a basic environment with ethyl chloride as an alkylating agent, the degree of ethoxylation is carefully controlled to have a degree of substitution in the range 44-51%. Four types of EC are commercially available and defined as a function of the degree of ethylene: EC-G (44.5-45.5%), EC-K (45.5-46.8%), EC-N (47.5-49.0%) and EC-T (49.0 or more). [96] EC is insoluble in water, but soluble in various organic solvents, stable in a wide pH range although it tends to swell at extremely acid pH. EC it is also non-toxic, compressible and inert. [97]
Additionally, EC easily forms films when casted by organic solvents, allowing its use as additive and excipient in drug formulations, cosmetics, and food technology. [98]

The property of hydrophobicity coupled with a low oxygen permeability has made EC films appealing as packaging material. [99] In fact, it should be remembered that EC belongs to the category of the Generally recognized as safe (GRAS) by the US Food and Drug Administration (FDA) in the Inactive Ingredients database as well as in the Canadian List of Acceptable Non-medicinal Ingredients. EC can be used in oral capsules, suspensions, tablets, topical emulsions, and vaginal and ocular preparations. As EC is not considered to be a health hazard, the World Health Organization (WHO) has not specified its acceptable daily intake. [100] It is clear that EC films can be considered as materials with high-added value for both food packaging and biomedical applications.

1.4 Bio-Polymers as green materials for devices in biomedical application

Biomedical devices based on the use of polymer plastic include surgical instruments, catheters, coronary stents, pacemakers, catheters, coronary stents, pacemakers, artificial orthopedic prosthesis, surgical gloves, and dermal devices for suture (**Fig. 1.12**). The polymeric plastic devices are mainly developed due to their proprieties

[96] A. S. Narang, S.I.F.B. *Handbook of Pharmaceutical Wet Granulation*., **2019**
[97] Crowley, M.M., Schroeder, B., Fredersdorf, A., Obara, S., Talarico, M., Kucera, S., and McGinity, J.W., *Int. J. Pharm.*, 269, 2, 509–522, **2004**
[98] Davidovich-Pinhas, M., Barbut, S., & Marangoni, A. G., *Cellulose*, 21, 3243-3255, **2014**
[99] Petersen, K., Vae, ggemose Nielsen, P., Bertelsen, G., Lawther, M., Olsen, M.B., Nilsson, N.H., and Mortensen, G., *Trends Food Sci. Technol.*, 10, 2, 52–68, **1999**
[100] Guerra, N.P., Araujo, A.B., Barrera, A.M., Agrasar, A.T., Macías, C.L., Carballo, J., and Pastrana, L. *J. Food Prot.*, 68, 5, 1012–1019, **2005**

such as low cost of production, lightweight, strength, durable, corrosion-resistant, high thermal and electrical insulation. [101]

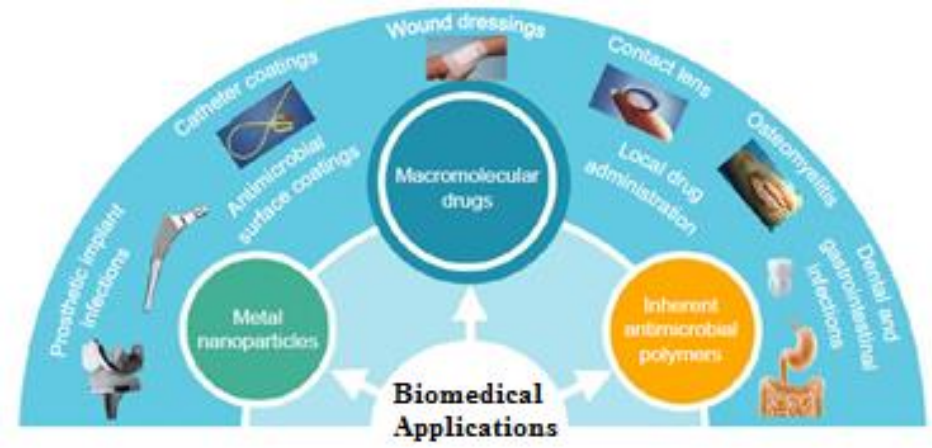

Fig. 1.12 Schematics biomedical applications. Adapted [102]

Nowadays, unfortunately, the use of plastic polymers is associated with a large number of environmental and health issues. Plastic biomedical devices are prepared by chemical substances that have side effects on the atmosphere as well as on the human being. Moreover, synthetic materials often give rise to rejection and incompatibility with the human organism. [103] Organic thin films and coatings, particularly the polymer based ones, are very attractive as biomaterial coatings because they offer great versatility in the chemical groups that can be incorporated on the surface (to control tissue – biomaterial interactions). [104]"Biomaterial" is a term used to categorize materials and devices that directly "interact" with human tissues and organs. The interactions may involve, for example, blood coagulation in the case of blood contacting devices, immune response and foreign body reactions around devices implanted in the body, structural and functional connection between the implant and the host tissue, for examples in the case of dental and orthopedic implants, or antifungals, antibacterial and antimicrobials activities in ointments and patches. [105]

The main areas where these materials can found application are:

[101] Andrady Anthony L., Neal Mike A. 364 *Phil. Trans. R. Soc. B*, 1977-1984 , **2009**
[102] Yang K, Han Q, Chen B, et al.. *Int J Nanomedicine.* 13:2217–2263, **2018**
[103] K. Wasilewska K. Winnicka, *Materials, 12*, 20, 3386, **2019**
[104] Williams , D.F. *The Williams Dictionary of Biomaterials* , Liverpool University Press , Liverpool, **1999**
[105] Vadgama , P. Surface biocompatibility . *Annual Report on the Progress of Chemistry, Section C* , 101 ,14 – 52, **2005**

- biocompatible implants (e.g., protein - repellent coatings, antithrombogenic coatings that
can prevent blood coagulation around implants, and antibacterial coatings);
- tissue engineering;
- drug delivery and gene therapy.

The biological system-biomaterials interaction occurs through the surfaces. In order to reach a full integration between the biomaterial and the host tissue, it is, therefore of high importance to know the surface properties or how to modify these. The overall integration formally makes the material "biocompatible". Very attractive in this direction is the biopolymer chemistry. A rational molecular design can help to build up the right compounds for each specific target, which means implant, tissue engineering and so on. [104] The principal materials for preparation of polymeric thin films are polysaccharides, or their derivatives, with hyaluronic acid (HA); hydrophilic self-assembled monolayers (SAMs); and especially poly(ethylene glycol) (PEG).

Current medical implants systems have been coated in a layer of non-specific proteins immediately after implantation. This causes the activation of an irrevocable host defense mechanism, known as the foreign body reaction. In order to impart a pseudo-biological character to synthetic materials and improve the adhesion of these implants with the surrounding biological tissues, regardless of the material, have been developed surface coatings that impart resistance to nonspecific protein adsorption. [106]

Regarding the application of polymer thin films for drug delivery, the release is used for the longer period delivery, ranging from hours to days. [107] This strategy is utilized in chronic wound treatment that lower the quality of patient's life significantly. In order to limit the problems just described, in recent years, all the advantages of using bio-polymers in the biomedical sector for the ideation of biomedical device based on bio-polymers have been reported. [108][109][110]

[106] S. R. Meyers, M. W. Grinstaff , *Chem Rev*. 14, 112, **2012**
[107] Bahrami, A., Mokarram, R. R., Khiabani, M. S., Ghanbarzadeh, B., & Salehi, R. *Journal of Biological Macromolecules*, **2018**
[108] Yadav, P., Yadav, H., Shah, V.G., Shah, G., Dhaka, G. *Journal of Clinical and Diagnostic Research: Journal of Clinical and Diagnostic Research* , 9, 21, **2015**
[109] Babu, R.P., O'connor, K., Seeram, R., *Progress in Biomaterials*, 2, 1, 8, **2013**
[110]Davidovich-Pinhas, M., Barbut, S., Marangoni, A.G., *Elsevier*, 363-380, **2018**

One of the bio-polymer of considerable interest dedicated to biomedical applications is EC and this is demonstrated by its use in the pharmaceutical industry for over 50 years. For example it has been used to mask the taste of the active ingredients in oral formulations, [111] for the preparation of formulations for the controlled release of active ingredients[112] and for its hydrophobicity has been used to protect tablets and other preparations from environmental humidity. [113] Interestingly, EC has been applied successfully as matrix for preparation of transdermal patches for local delivery of principle active. [114]

Moreover, the plasticity of EC films can be modified through the use of plasticizing agents. In this regard ibuprofen has been successfully used with performances similar to those of conventional plasticizers, for the preparation of molecular dispersion with pharmaceutical applications. [115][116] Furthermore, EC films can be used in the production of composite materials with other materials for the production of membranes with specific permeation characteristics; for example the enrichment with nanoporous graphene allows to efficiently separate mix of low weight alkanes difficult to be separated using traditional methods. [117] In addition, EC was used in combination with pectin for the production of composite films used in the release of active principles locally. [118] It is clear that EC films can be considered as high-added value for both food packaging and biomedical applications.

1.5 Metal-based active polymer materials for food packaging and bio-medical applications

The interest in metal-based active polymer materials for food packaging and biomedical applications arises from the growing concern for the antibiotic resistance developed by many strains bacteria. The development of advanced new antimicrobial materials consists in the use of metals such as: Ag, Au, Pt, Pd, Ir, Cu, Sn, Sb, Pb, Bi, Zn, in order to build up bioactive materials. [119] Metal-based additives are found as: particles, ions absorbed/exchanged in different carriers, salts, hybrid structures and

[111] Sharma, V., and Chopra, H., *J. Pharm. Pharm. Sci.*, 2, 14–18, **2010**
[112] Villa Nova, M., Gonçalves, M.D.C.P., Nogueira, A.C., Herculano, L.D.S., Medina, A.N., Bazotte, R.B., and Bruschi, M.L. *Drug Dev. Ind. Pharm.*, 40, 10, 1308–1317, **2014**
[113] Joshi, S., and Petereit, H.U. , *Int. J. Pharm.*, 457 , 2, 395–406, **2013**
[114] K. Wasilewska and K. Winnicka *Materials*, 12, 3386, **2019**
[115] Kangarlou, S., and Haririan, I., 3, 135–141, **2007**
[116] De Brabander, C., Van Den Mooter, G., Vervaet, C., and Remon, J.P. , *J. Pharm. Sci*., 91, 7, 1678–1685, **2002**
[117] Yuan, B., Sun, H., Wang, T., Xu, Y., Li, P., Kong, Y., and Niu, Q.J., *Sci. Rep.*, 1–11, **2016**
[118] Momin, M., Pundarikakshudu, K., and Nagori, S., *Indian J. Pharm. Sci*., 70, 3, 338–343, **2008**
[119] M. Pollini, A. Sannino, L. Ambrosio *Biomacromolecules*, 16, 7, 1873-1885, 17, **2015**

compounds. The effectiveness of antimicrobial elemental metals is thought to be due to the formation of corresponding metal ions. [120]

In most of the applications of antimicrobial metal-based polymers, the metals can be either incorporated on the surface of a polymer or embedded into the polymeric matrix. [119]

The resulting antimicrobial composite materials find wide applications in both the food packaging and biomedical fields. [119] [121]

1.5.1 Metal complexes as potential antimicrobial agents

Metals have an important role in biological processes, many of them perform essential biological functions and their uses in medicine are varied (**Scheme 3**). [122][123][124][125]

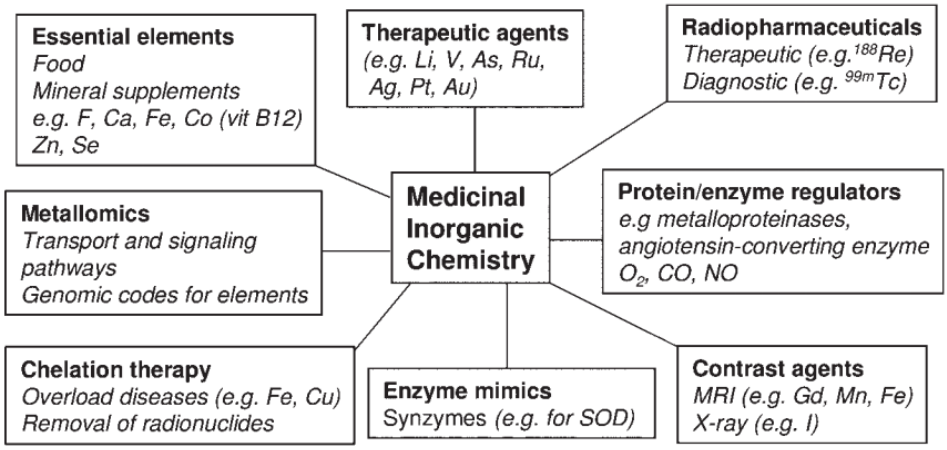

Scheme. 1.3 Some key areas of medicinal inorganic chemistry. [126]

The design and synthesis of a various metal complexes with different metals and ligands, has allowed the preparation of inorganic complexes with various properties, such as antibiotics, antibacterials, antivirals, antiparasitics, anti-HIV [127], anti-

[120] Humberto Palza, *Int. J. Mol. Sci.*, 16, 2099-2116, **2015**
[121] A. Llorens, E.Lloret, P. A.Picouet, R.Trbojevich, A. Fernandez, *Trends Food Sci Technol*, 24, 19-29, **2012**
[122] Keppler, B.K, Curr. *Top. Med. Chem.*, 4, 1575–1583, **2004**
[123] Hambley, T.H., *Dalton Trans.*, 4929–4937, **2007**
[124] Jakupec, M.A., Galanski, M., Arion, V. B., Hartinger, C.G., and Keppler, B.K., *Dalton Trans*., 183–194, **2008**
[125] Hall, M.D., Amjadi, S., Zhang, M., Beale, P.J., and Hambley, T.W., *J. Inorg. Biochem.*, 98, 10, 1614–1624, **2004**
[126] *Bioinorganic Medicinal Chemistry* Edited by Enzo Alessio, WILEY-VCH Verlag GmbH & Co. KGaA
[127] Nubia Boechat, Warner B. Kover, Monica M. Bastos, Nelilma C. Romeiro..*Med Chem Res*. 15: 492–510. **2007**

diabetes, radio-pharmaceuticals agents and anticancer compounds. [128][129][130][131][132][133][134][135][136][137][138][139][140][141]

The antimicrobial capabilities of metals have been known for thousands of years. In the 1920s, the use of metals as antimicrobic agent has stopped due to the discovery of antibiotics by Nobel laureate Sir Alexander Fleming. At the beginning of the twenty-first century, antimicrobial metals is undergoing a renaissance and new studies and research have begun of new antimicrobial agents able to compensate the resistance developed by living organisms, leading to the design of metals compounds alternative to antibiotics. Inorganic complexes, particularly transition metals complexes, have played an important role in the development of new antimicrobial agents. [142] For example, Nickel(II) and Copper(II) complexes and thiourea ligands, whose general structure is shown in the image below **(Fig. 1.13)**, have been synthesized and studied in vitro for their anti-bacterial activity against Gram-positive bacteria (two different standard strains of *Staphylococcus aureus*, *Staphylococcus epidermidis*, *Enterococcus faecalis*, *Streptococcus pyogenes*, *Bacillus cereus*) and Gram-negative bacteria (*Escherichia coli*, *Pseudomonas aeruginosa*, *Enterobacter cloacae*, *Proteus vulgaris*, *Enterobacter aerogenes*). [143] Ligands coordinate to the metal centres in a bidentate mode, yielding complexes with general formula $[ML_2]$.

[128] T. Rosu, A. Gulea, A.Nicolae, R. Georgescu., 12: 782-796, **2007**
[129] Rosu, T.; Pasculescu, S.; Lazar, V.; Chifiriuc, C.; Cernat, R., *Molecul*es.11, 904-914, **2006**
[130] Agarwal, R. K.; Singh, L.; Sharma, D. K., *Bioinorg. Chem. Appl*., 1–10, **2006**
[131] West, D. X. Liberta, E. A.; Padhye, S. B. Chikate, R. C. Sonawane, P. B. Kumbhar, A. S. Yerande, R. G. *Coord. Chem. Rev*. 123:49-71, **1993**
[132] Nora H. Al-Sha'alan. *Molecules*. 12, 1080-1091, **2007**
[133] Ferrari, M. B. Capacchi, S. Pelosi, G. Reffo, G. Tarasconi, P. Alberlini, R. Pinelli, S. Lunghi, P. *Inorg. Chim. Act*. 286: 134-14, **1999**
[134] Elo, H.; Sunila, I.; Lumme, P. *Inorg. Chim. Acta.* 136: 61-63, **1987**
[135] Elo, H.; Lumme, *Inorg. Chim. Acta.* 136;149-153, **1987**
[136] Zhou, J.; Wang, L.; Wang, J.; Tang, N. *Trans. Metal Chem.* 26: 57-63, **2001**
[137] Regina M. S. Pereira, Norma E. D. Andrades, Niraldo Paulino and et al. *Molecules*. 12: 1352-1366, **2007**
[138] T. Suksrichavalit, S. Prachayasittikul, T. Piacham, C.Isarankura-Na-Ayudhya, C. Nantasenamat and V.Prachayasittikul. *Molecules*. 13: 3040-3056, **2008**
[139] Branco, R. J. F.; Fernandes, P. A.; Ramos, M. J.. *J. Mol. Struct*. (THEOCHEM). 729: 141-146, **2005**
[140] Li, Q. X. Luo, Q. H. Li, Y. Z. Shen, M. C. *Dalton Trans.* 2329-2335, **2004**
[141] Spasojevic, I. Chen, Y. Noel, T. J. Yu, Y. Cole, M. P. Zhang, L. Zhao, Y. St Clair, D. K. Batinic-Haberle, I. *Biol. Med*. 42: 1193-1200, **2007**
[142] Md. Saddam Hossain, C. M. Zakaria, Md. Kudrat-E-Zahan,; *American Journal of Heterocyclic Chemistry* , 4,1: 1-21, **2018**
[143] H. Arslan, N.Duran, G. Borekci, C. Koray Ozer and C. Akbay**,** *Molecules.* 14: 519-527, **2009**

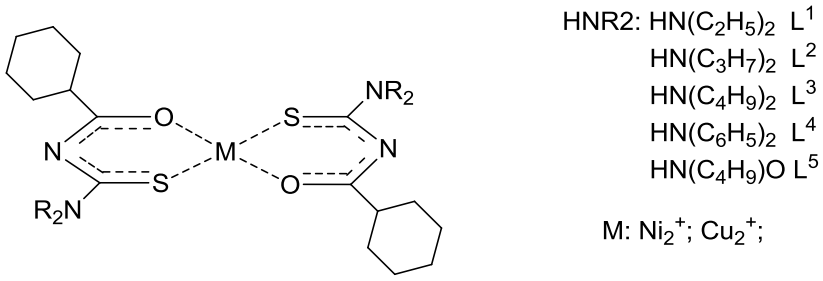

Fig. 1.13 General structure of thiourea derivatives of Nickel(II) and Copper(II) with antimicrobial activity.

The same metals have been coordinated with the N-(R-carbamothioyl)-4-nitrobenzamide (R = diphenyl and ethyl/butyl). **Fig. 1.14**. Comparing the ligands alone with the complexes, for their in vitro antibacterial activities against *S. aureus*, *S. epidermidis*, *E. faecalis*, *E. coli*, *E. cloacae* and *P. valgaris*, the complexes showed greater antibacterial efficacy than the thiourea ligands. [144]

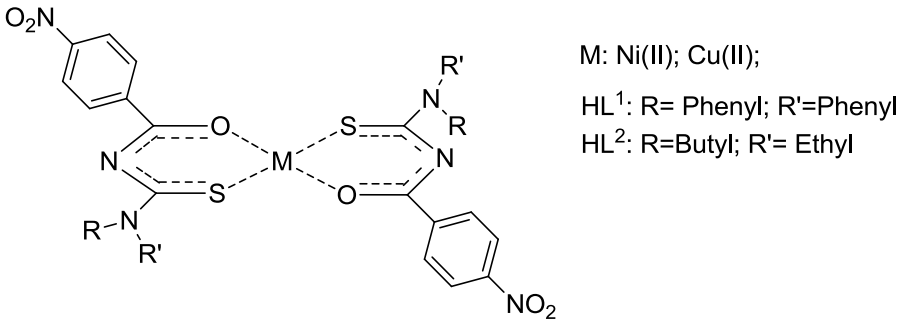

Fig. 1.14 General structure of Nickel and Copper complexes of N-(alkyl(aryl)carbamothioyl)-4-nitrobenzamide.

It is clear, from the above examples, that the formation of complexes between transition metal ions and some ligands has been a winning strategy for the realization of materials with antimicrobial properties. It has been demonstrated that metals and ligands considered separately did not show antimicrobial properties or in any case lower than in the final complexes. As a demonstration of what just now stated, a series of examples including different transition metal ions as well as ligands belonging to different molecular classes are reviewed below.

[144] Sohail Saeed, Naghmana Rashid, Muhammad Ali and Rizwan Hussain, *European Journal of Chemistry.* 1, 3, 200-205, **2010**

Zn(II) and Cu(II) complexes containing cyclohexane-1,3-dione-based ligands have been synthesized (**Fig. 1.15**), and tested against *Escherichia coli*, *Enterococcus faecalis*, *Staphylococcus aureus*, and *Salmonella typhimurium*. The results obtained demonstrate that some of these complexes showed medium-level antibacterial activity against the tested bacteria when compared to ampicillin, a broad-spectrum antibiotic used for this type of infections. [145]

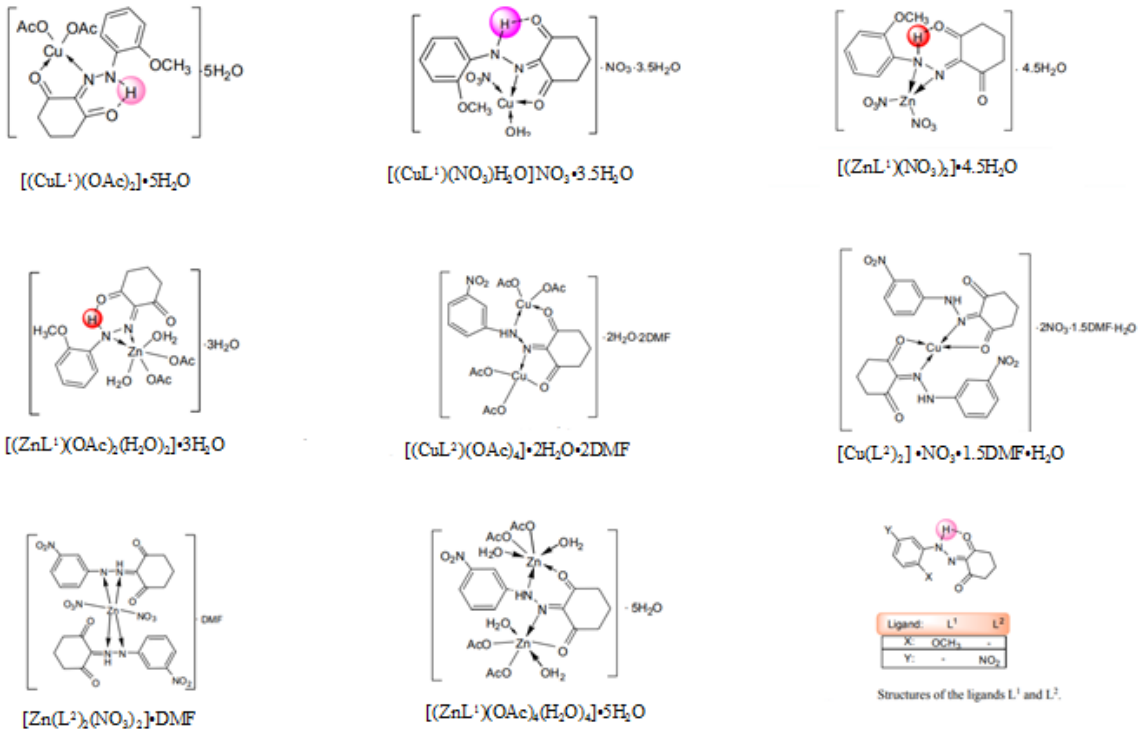

Fig. 1.15. Structure complexes of Zn(II) and Cu(II) with cyclohexane-1,3-dione ligands

Other Cu(II), Co(II), Ni(II), Zn(II) and (3E)-3-[(2-{(E)-[1-(2,4 dihydroxyphenyl)ethylidene]amino}ethyl)imino]-1-phenylbutan-1-one ($DEPH_2$) derived from ethylenediamine, 2',4'-dihydroxyacetophenone and 1-phenylbutane-1,3-dione complexes have been realized and tested allowing to classify them according to their performance in the order Cu(II) > Ni(II) > Co(II) >Zn(II). The results obtained show that the antimicrobial activity of the Cu(II) complexes is higher than the other complexes against Gram-positive bacteria, *Staphylococcus aureus*,

[145]N. Turan, H. Körkoca, R. Adigüzel, N. Çolak and K. Buldurun *Molecules*, 20, 9309-932, **2015**

Streptococcus faecalis, *Bacillus cereus* and three Gram-negative bacteria, *Pseudomonas aeruginosa*, *Escherichia coli*, and *Shigella flexineri*. [146]

Gold is a particularly relevant metal in this context. The first scientific discovery that Au-complexes had antibacterial activity dates back to 1890 when it was observed that Au cyanide, $K[Au(CN)_2]$, was inhibitory to 'tubercle bacilli' in vitro. [147] Subsequently, a large number of Au(I) and Au(III) complexes have been evaluated as possible antimicrobial agents against a broad spectrum of bacteria, fungi and parasites. Indeed, about 50 years later, the introduction of gold complexes has occurred for the treatment of rheumatoid arthritis taking into account that some bacteria, in particular *Pseudomonas putida*, was responsible for this pathology. [148] A series of Au(I) anti-arthritic drugs **(Fig. 1.16)** were shown inhibition against *Pseudomonas putida*, bacterial species related to respiratory tract infections.[149]

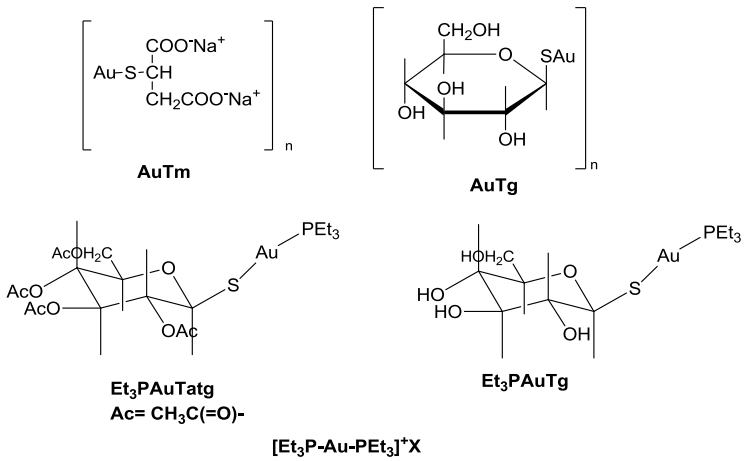

Fig. 1.16 Anti-arthritic drugs structures: AuTm, aurothiomalate; AuTg, aurothioglucose; Et_3PAuTatg, auranofin; Et_3PAuTg, triethylphosphineAu(I)thioglucose.

Au(I) complexes having phosphine and N-heterocyclic carbine ligands showed relevant antibacterial and antifungal activities. In particular, linear phosphine Au(I) complexes having a sulfur atom in the coordination sphere (**Fig. 1.17)** exhibited a good spectrum of activity against several strains of Gram-positive and Gram-negative bacteria, such as *Staphylococcus aureus (Staph. aureus)*, *Staphylococcus*

[146] Ikechukwu P. Ejidike and Peter A. Ajibade, *Molecules*. 20, 9788-9802, **2015**
[147] Koch, *Reber bacteriologische Forschung. Deutsche Medicinische Wochenschrift* 16, 756-7, **1890**
[148] Lande, K. *Die Gunstige Beeinflussung schleichender Dauerinfekte durch Solganol. Munchener Medizinische Wochenschrift* , 74, 1132-4, **1927**
[149] M. D. Rhodes, P. J. Sadler, M. D. Scawen and S. Silver, *J. Inorg. Biochem*., 46, 129, **1992**

epidermidis (Staph. epidermidis), *Escherichia coli (Esch. coli)* and *Pseudomonas aeruginosa (Ps. aeruginosa)*, and fungi *Candida albicans (Ca. albicans)* and *Aspergillus niger*. [150][151][152]

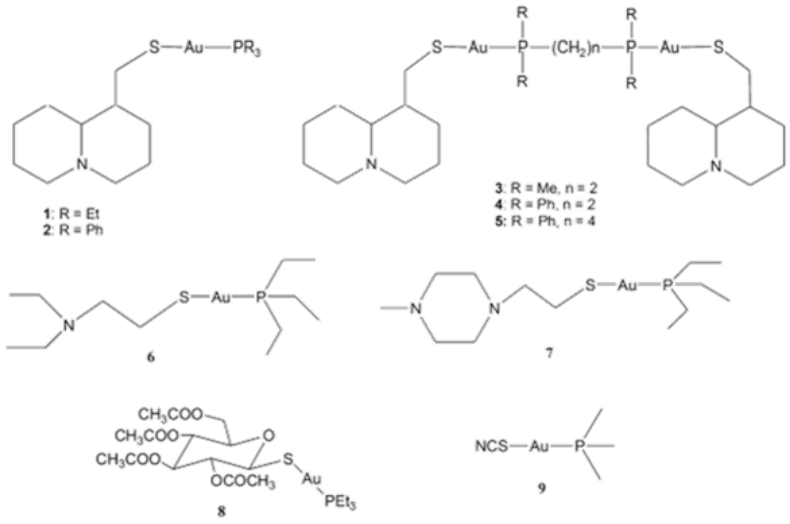

Fig. 1.17 Antibacterial and antifungal phosphine Au(I) complexes containing a coordinated atom.

More specifically, the complex [Au(SCN)(PMe_3)] (complex **9** in **Fig. 17)**, inhibits *Staphylococcus aureus*, *Enterococcus faecalis,* and *P. mirabilis* at low concentrations, and it shows a lower antimicrobial activity for *P. aeruginosa* and *C. albican*, providing in any case, a valid alternative to vancomycin. The vancomycin is the drug normally used for organisms presenting some limits, such as the method of administration, that is by intravenous, and presents resistance problems.[153] The phosphine Au(I) complexes with sulfur containing ligands such as 2-mercaptopropionic acid (2-H_2mpa), 6-mercaptonicotinic acid (6-H_2mna), 2-mercaptonicotinic acid (2-H_2mna), penicillamine (H_2pen), 2-mercaptobenzoic acid (2-H_2mba), 3-mercaptobenzoic acid (3-H_2mba) and 4-mercaptobenzoic acid (4-H_2mba) **(Fig. 1.18)** showed antimicrobial activity against Gram-positive bacteria (*B. subtilis* and/or *S. aureus*). [154]

[150] F. Novelli, M. Recine, F. Sparatore and C. Juliano, *Farmaco*, 54, 232–236, **1999**
[151] A. M. Elsome, J. M. T. Hamilton-Miller, W. Brumfitt and W. C. Noble, J. *Antimicrob. Chemothet*.,37, 911–918, **1996**
[152] S. P. Fricker, *Transition Met. Chem*., 21, 377–383, **1996**
[153] Amanda M. Elsome, Jeremey M. T. Hamilton-Miller, William Brumfitt, William C. Noble *Journal of Antimicrobial Chemotherapy*, Volume 37, Issue 5, Pages 911–918, **1996**
[154] K. Nomiya, S. Yamamoto, R. Noguchi, H. Yokoyama, N. C. Kasuga, K. Ohyama and C. Kato, *J. Inorg. Biochem*., 95, 208–220, **2003**

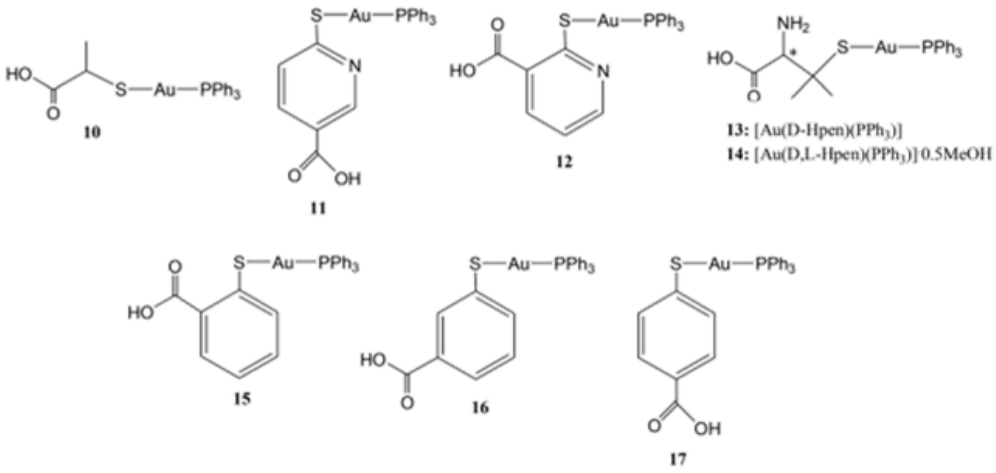

Fig. 1.18 Phosphine Au(I) complexes with sulfur-containing ligands

The substitution of sulfur-containing ligands in the above mentioned phosphine Au(I) complexes with heterocyclic nitrogen containing ligands lead to complexes (**Fig. 1.19**) showing selective and high activity against two Grampositive bacteria *Bacillus subtilis* and *Staph. aureus* and modest activity against yeasts *Ca. albicans* and *Sacch. Cerevisiae*. [155]

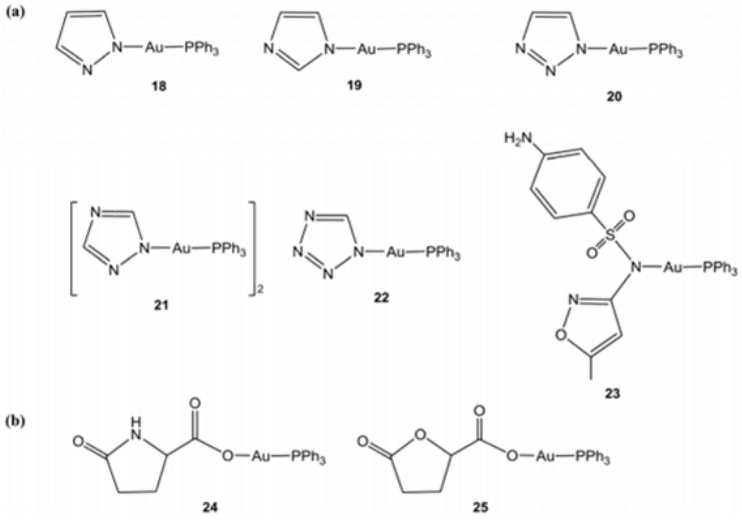

Fig. 1.19 Phosphine Au(I) complexes with nitrogen (a) and oxygen (b) donor ligands showing a different spectrum of antibacterial and antifungal activity.

[155] K. Nomiya, R. Noguchi and M. Oda, *Inorg. Chim. Acta*, 298, 24–32, **2000**

Other complexes highly selective against bacteria and fungi are gold complexes containing N-heterocyclic carbenes (NHC). [156] Their antibacterial activity strongly depends on the nature of the substituents on the nitrogen atoms of the NHC ligand. In fact, complexes (a) and (c) in **Fig. 1.20** were found to inhibit the growth of Gram-positive Bacteria *Staph. aureus* and *Ent. faecalis*, while having no effects toward Gram-negative bacteria *Esch. coli* and *Ps. aeruginosa* and fungi *Ca. albicans* and *Ca. tropicalis*. [157] Instead, the presence of a penta-methylbenzyl group as a substituent on the nitrogen atoms, complex (b) in **Fig. 1.20**, resulted only in good antifungal activity. Complex (d) in **Fig. 1.20** was found active against Gram-positive *Bacillus subtilis*, but did not inhibit the growth of Gram-negative *Esch. coli*. [158]

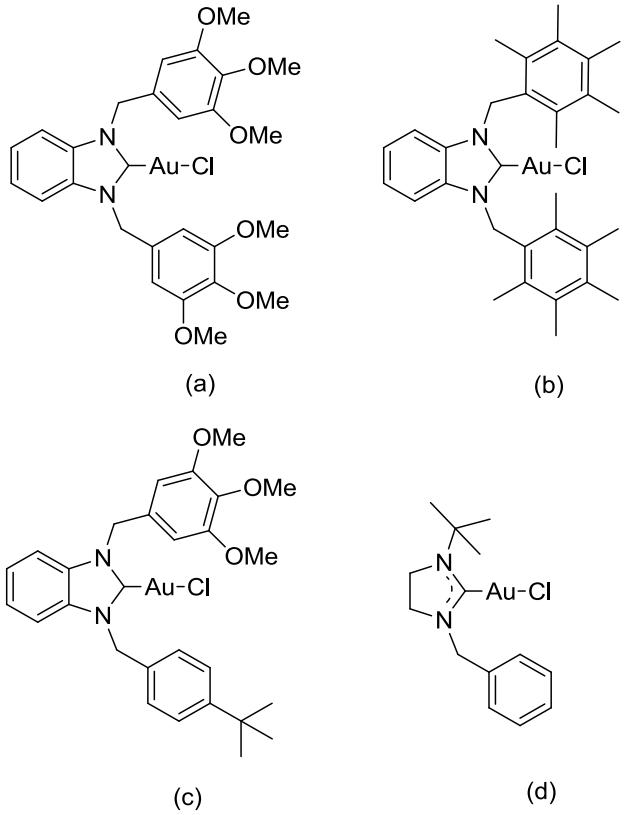

Fig. 1.20 Antibacterial and antifungal Au(I) complexes having coordinated N-heterocyclic carbene ligands.

These are just few examples that aim to demonstrate how the research for new antimicrobial transition metal complexes is a subject in constant growth in the

[156] K. M. Hindi, M. J. Panzner, C. A. Tessier, C. L. Cannon and W. J. Youngs, *Chem. Rev*., 109, 3859–3884, **2009**
[157] İ. Özdemir, N. Temelli, S. Günal and S. Demir, *Molecules*, 15, 2203–2210, **2010**
[158] S. Ray, R. Mohan, J. K. Singh, M. K. Samantaray, M. M. Shaikh, D. Panda and P. Ghosh, *J. Am. Chem. Soc*., 129, 15042–15053, **2007**

current scientific panorama. Among transition metal complexes, Ag(I) based derivatives have been widely studied and many of these have displayed significant antimicrobial activity.

Since the main target of this PhD work is the realization of polymeric films incorporating different silver complexes we will dedicate the subsequent paragraphs to the state of art of silver, in different forms, as antimicrobial agent.

1.6 Silver as an antimicrobial agent: Historical background

Romans, Greeks and Egyptian were well aware of the benefits related to the use of silver, since they used this metal to prevent food spoilage, facilitate the heal of open wounds and even to treat mental illness when the knowledge regarding bacteria and infection was practically not existent. A historical source states that silver spoon may be used for milk to prolong its shelf life and it was known that cooking or storing water or wine in silver pots would keep it safe. [159] In the late 900, a well-known Muslim philosopher and doctor, Avicenna reported the use of silver as a blood purifier, for bad breath and for heart palpitations. In the 17th and 18th century, silver was used in the form of silver nitrate in the treatment of venereal diseases, fistulae, and abscesses. Subsequently, in the 19th century, researches showed that silver not only prevented wounds from being infected, but it also allowed healing. [160] A combination of multiple factors in the study of antibacterial agents has promoted silver as an antimicrobial agent and silver rapidly raised to the forefront in the development of antimicrobial systems. Antibacterial agents play an important role not only for general hygiene but also as disinfectant in places such as hospitals. Our society is increasingly more aware of the ubiquitous presence of microbes in all aspects of daily life. The development of microbes resistant to antibiotics is constantly growing and the research and development of new antibiotics is not able to follow this increase. The medicine should find new antimicrobial systems to fight the increasing number of nosocomial infections and guarantee the proper functioning of the public health system. [161] Nowadays, silver and its derivatives are mainly used as antimicrobial components for the preparation of cosmetics, medical ointment and

[159] Grier N. Silver and its compounds. In: Block SS, ed. *Disinfection, Sterilization and Preservation. Philadelphia*. Lea & Febiger, 375–398, **1968**
[160] Hill WR, Pillsbury DM., *Argyria–The Pharmacology of Silver. Baltimore*. Williams & Wilkins, **1939**
[161] Hetrick, E.M., and Schoenfisch, M.H., *Chem. Soc. Rev.*, 35 (9), 780–789, **2006**

patches, materials for food and industrial packaging, water treatment and so on. More generally, silver can confer the antibacterial property to materials used for different purpose. [162][163][164]

1.6.1 Mechanism of silver antimicrobial action

The specific antibacterial activity of silver seems to be related to the release of Ag(I) ions.

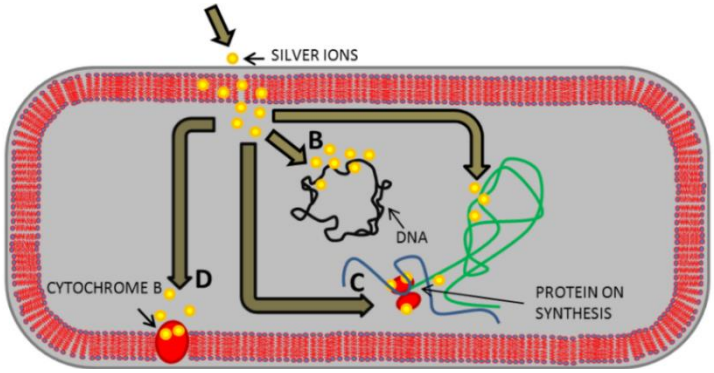

Fig. 1.21 Mechanism of antimicrobial action of Ag(I) ions [165]

The exact mechanism of action that Ag(I) ions perform is not known, but a mechanism was supposed which involves the following steps:

(A) Ag(I) ions penetrate the bacterial cell wall and bind to the phospholipid layer of the cytoplasmic membrane;

(B) Ag(I) ions bind the bacterial DNA with subsequent disrupting of DNA replication;

(C) Ag(I) ions impair the ability of ribosomes to transcribe messenger RNA;

(D) Ag(I) ions bind to the sulfhydryl group of the cytochrome b. [165]

The antimicrobial activity of silver depends on the presence of silver cations which strongly bind to the electron donor groups of biological molecules containing

[162] Vaidyanathan, R., Kalishwaralal, K., Gopalram, S., and Gurunathan, S. *Biotechnol. Adv.*, 27, 6, 924–937, **2009**
[163] Chen, X., and Schluesener, H.J., *Toxicol. Lett.*, 176, 1, 1–12, **2008**
[164] W. Sim, R. T. Barnard, M.A.T Blaskovich, Z.M. Ziora, *Antibiotics, 7*, 4, 93, **2018**
[165] D. Chudobova, L. Nejdl, J. Gumulec, O. Krystofova, M.A.M. Rodrigo, J. Kynicky, B. Ruttkay–Nedecky, P. Kopel, P. Babula, V. Adam, R. Kizek, *Int. J. Mol. Sci*., 14, 7, 13592-13614, **2013**

sulphur, oxygen or nitrogen, since silver presents an extreme chemical affinity for sulfur groups, like thiols (-SH) contained in biomolecules. [166][167] Silver ions react with the thiol group of enzymes and inactivate them, resulting in the ending of DNA replication. [168] This interaction occurs with the inactivation of enzymes in the outer membrane, permeability and trans membranous energy metabolism are disrupted leading to the cellular breakdown **Fig. 1.22** [169][170][171][172] Furthermore, depletion of protective enzymes produces an increase in reactive oxygen species (ROS), which further contribute to damage the vital functions of the cell in aerobic conditions. [172][173]

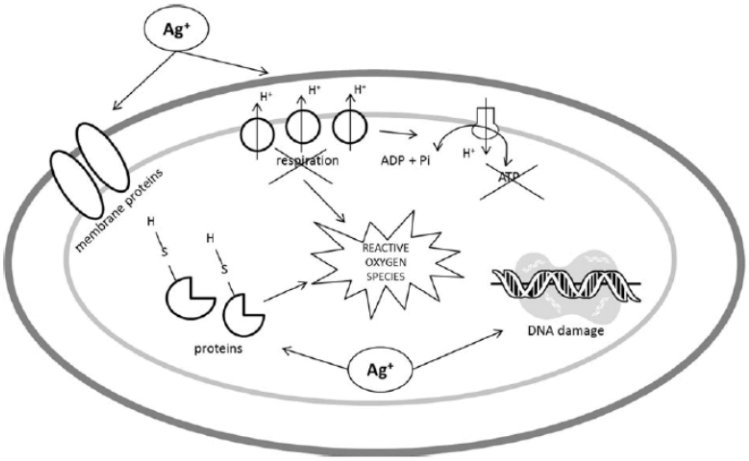

Fig. 1.22 Antimicrobial effects of Ag+ in the interaction with membrane proteins by blocking respiration and electron transfer; inside the cell, Ag+ ions interact with DNA, proteins and induce ROS production. [173]

Moreover, the ions can bind to DNA components, stabilizing DNA closed conformation, which is evidenced by a condensed region in the center of the cell, preventing replication. It is not yet clear if the replication inhibition happens because silver ions are bound to the phosphate residues [167][169169] or if they intercalate between N-H bonds in purines and pyrimidines. [170]

Bacterial defense mechanisms against the damage caused by the presence of silver ions at low concentrations may be able to re-establish homeostasis and thus survive.

[166] Liau, S.Y., Read, D.C., Pugh, W.J., Furr, J.R., and Russell, A.D. *Lett. Appl. Microbiol.*, 25 (4), 279–283, **1997**
[167] Choi, O., Clevenger, T.E., Deng, B., Surampalli, R.Y., Ross, L., and Hu, Z., *Water Res.*, **43** (7), 1879–1886, **2009**
[168] Matsumura, Y., Yoshikata, K., Kunisaki, S. ichi, and Tsuchido, T. *Appl. Environ. Microbiol.*, 69 (7), 4278–4281, **2003**
[169] Feng, Q.L., Wu, J., Chen, G.Q., Cui, F.Z., Kim, T.N., and Kim, J.O. *J. Biomed. Mater. Res.*, 52 (4), 662–668, **2000**
[170] Guggenbichler, J.P., Böswald, M., Lugauer, S., and Krall, T. *Infection*, 27, **1999**
[171] Lok, C.N., Ho, C.M., Chen, R., He, Q.Y., Yu, W.Y., Sun, H., Tam, P.K.H., Chiu, J.F., and Che, C.M. , *J. Proteome Res.*, 5 (4), 916–924, **2006**
[172] Mijnendonckx, K., Leys, N., Mahillon, J., Silver, S., and Van Houdt, R., *BioMetals*, 26 (4), 609–621, **2013**
[173] Park, H.J., Kim, J.Y., Kim, J., Lee, J.H., Hahn, J.S., Gu, M.B., and Yoon, J., *Water Res.*, 43 (4), 1027–1032, **2009**

Above a certain concentration instead, the bacterial damage would be irreversible, leading to cell death.

According to a series of studies reported in the literature, the antibacterial activity appears to be dependent on the bacterial species under examination. The studies suggest that Gram negative bacteria are more sensitive to the presence of silver than Gram positive ones. [169]

1.6.2 Silver ions and Silver nanoparticles as potential material for food packaging and biomedical applications

From past to today, silver has been used in many fields of applications. Compared to other natural antimicrobial agents with recognized antimicrobial properties, silver has the advantage of the excellent thermal and chemical stability and its relatively low cost make it the ideal candidate for its incorporation in a wide variety of materials. In addition, silver has a broad inhibition spectrum versus unlimited strains of bacteria, fungi, algae and possibly some viruses. [174] Since silver is easily incorporated into many materials, the application to the packaging technology has been extended in a short time especially in Japan. [175] In **Table 3** some examples of packaging materials with the relative active form of silver compounds are reported.

[174] Rhim, J.W., Wang, L.F., and Hong, S.I., *Food Hydrocoll.*, 33, 2, 327–335, **2013**

Table 3 [175]

Trade name	**Active compound**	**Producer**	**Country**
Piatech	Silver Oxide	Daikoku Kasei Co.	Japan
Silvi Film		Nimiko Co.	Japan
Okamoto Super Wrap		Okamoto Industries, Inc.	Japan
Apacider	Silver Zeolite	Sangi Co.	Japan
Zeomic		Shinanen New Ceramics Co.	Japan
Backekiller		Kanebo Co.	Japan
Cleanaid		Gyunghyang Ind. Co.	Korea
Aglon	Silver	Aglon Technologies LLc	USA
Ageless SE		Mitsubishi Gas Chem.	Japan
MicroFree	Silver, copper oxide, zinc silicate	DuPont	USA
Novaron	Silver Zirconium phosphate	Miliken Co.	USA
Surfacine	Silver halide	Surfacine Development Co.	USA
Ionpure	Silver/glass	Ishizuka Glass Co.	Japan

Nowadays, silver can be applied to the food packaging industry as antimicrobial agents and can be classified into two categories depending on the presence of silver ions (Ag^{+}) or silver nanoparticles (Ag^{0}). One of the most used system is Silver-zeolite (AgZ) which is mostly preferred for films due to its capability to slow release silver (I) ions towards the food surface. [176] Zeolites are microporous, zinc sodium ammonium aluminosilicate minerals commonly used as commercial adsorbents. In silver zeolites, naturally occurring sodium ions are partially replaced by silver ions using simple ion-exchange methods. [177] Following contact with moisture, silver ions are yet again substituted by sodium ions present in the release environment and sustainably leach from the surface **Fig. 1.23**.

[175] de Abreu, D.A.P., Cruz, J.M., and Losada, P.P.*Food Rev. Int.*, 28, 2, 146–187, **2012**
[176] Kaba, N., and Duyar, H.A., Antimikrobiyal Paketleme. 25 (2), 181–185, **2008**
[177] Rai, M., Yadav, A., and Gade, A, *Biotechnol. Adv.*, 27, 1, 76–83, **2009**

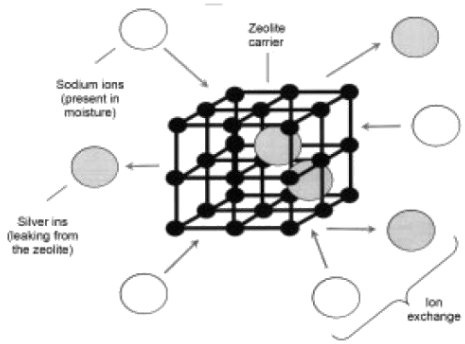

Fig. 1.23 Schematic representation of the ion-exchange induced release mechanism in silver exchanged clays and porous minerals.

The release of silver ions depends on the amount of saline moisture, which is a crucial risk factor for the development of microbes on surfaces. If the migration rate is very low zeolites became very appealing with respects to others natural and synthetic substances. In the food field, zeolites can be applied in many foods processing equipment: cutlery, cutting boards, countertops, containers, or any other food contact surface. Silver zirconium phosphates (AgZrP) has been realized following the same mechanism used for silver-sodium exchange. [178]

Silver nanoparticles (AgNPs) may be incorporated to biodegradable and non-biodegradable polymers for the production of food packages with antimicrobial properties, leading to greater safety and longer shelf life. [179] However, it is difficult to quantify the migration of nanoparticles within food matrices, due to the lack of standardized analytical guidelines for the AgNPs migration studies. [180] In addition, there is still no specific legislation that regulates the use of silver nanoparticles for applications in the food field.

Silver nanoparticles (AgNPs) are also widely used in textiles, water-filtration and health care due to their outstanding antimicrobial properties. [181][182][183][184][185] Silver nanoparticles performance depend on many factors, such as size and shape,

[178] Busolo, M.A., Fernandez, P., Ocio, M.J., and Lagaron, J.M. *Food Addit. Contam. - Part A Chem. Anal. Control. Expo. Risk Assess.*, 27, 11, 1617–1626, **2010**
[179] E.Orlando Simbine, L. da Cunha Rofrigues, J. Lapa-Guimaraes, E. Setsuko Kamimura, C. Humberto Corassin, C. Augusto Fernandes de Oliveira, *Food Sci. Technol*, 39, 4, 793-802, **2019**
[180] L. de Oliveira Morais, E. Valverde Macedo, J. Mauro Granjeiro,I. Fernandes Delgado, *Critical Reviews in Food Technology and nutrition*, 1-20, **2019**
[181] Boisselier, E., and Astruc, D., *Chem. Soc. Rev.*, 38, 6, 1759–1782, **2009**
[182] Edwards-Jones, V. *Appl. Microbiol.*, 49, 2, 147–152, **2009**
[183] Larimer, C., Ostrowski, N., Speakman, J., and Nettleship, I. *Mater. Charact.*, 61, 4, 408–412, **2010**
[184] Martínez-Abad, A., Lagaron, J.M., and Ocio, M.J., *J. Agric. Food Chem.*, 60, 21, 5350–5359, **2012**
[185] Osório, I., Igreja, R., Franco, R., and Cortez, J., *Mater. Lett.*, 75, 200–203, **2012**

concentration, morphology, composition and crystallinity. [186] AgNPs are particles of Ag(0) with size ranging from 1 to 100 nm, with specific physiochemical characteristics different from those of bulk materials of the same composition, mainly due to the high surface-area-to volume ratio. [187] In fact, nanoparticles with higher specific area are significantly efficient in releasing silver ions, influencing their performance as antibacterial agent.

Furthermore, the enhanced antibacterial effect of AgNPs as compared to Ag(I) ions could be due to the higher chemical stability of the nanoparticles, which would enable them to penetrate more efficiently inside the cells. [188] The AgNPs broad-spectrum of antibacterial activities made them very popular in several medical applications, in milk bottles and toys for children, clothing, sheets and pillows, cosmetics, refrigerators, vacuum cleaners, washing machines, plenty of personal care applications and many others. This extensive use leads to an increased release of AgNPs in the environment, which consequently might have harmful ecological effects. [189][190]

The concern of a number of researchers is linked to the mobility of silver nanoparticles in the human body. Silver nanoparticles could be able to distribute in almost all human organs, as well as to penetrate cell membranes. [191]

The exceptional success of silver, both in the form of ions and nanoparticles, concern also the biomedical application, as can be seen from the image below **Fig. 1.24**.

[186]Azlin-Hasim, S., Cruz-Romero, M.C., Ghoshal, T., Morris, M.A., Cummins, E., and Kerry, J.P. *Innov. Food Sci. Emerg. Technol.*, 27, 136–143, **2015**
[187] Rai, M.K., Deshmukh, S.D., Ingle, A.P., and Gade, A.K. *J. Appl. Microbiol.*, 112, 5, 841–852, **2012**
[188] Li, W.R., Xie, X.B., Shi, Q.S., Zeng, H.Y., Ou-Yang, Y.S., and Chen, Y. Ben, *Appl. Microbiol. Biotechnol.*, 85, 4, 1115–1122, **2010**
[189] Fabrega, J., Luoma, S.N., Tyler, C.R., Galloway, T.S., and Lead, J.R. *Environ. Int.*, 37, 2, 517–531, **2011**
[190] Pokhrel, L.R., and Dubey, B. *Environ. Sci. Technol.*, 46, 14, 7755–7762, **2012**
[191] Chaloupka, K., Malam, Y., and Seifalian, A.M. *Trends Biotechnol.*, 28, 11, 580–588, **2010**

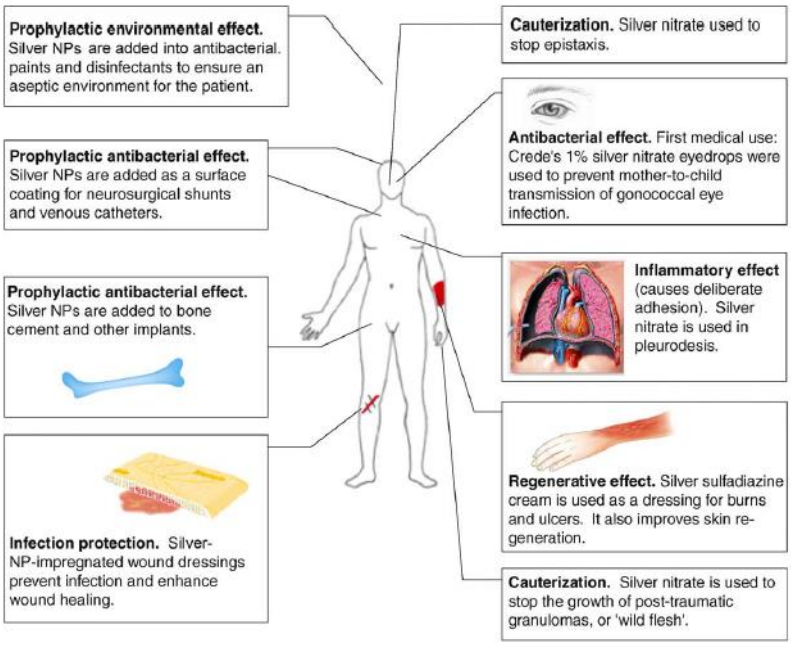

Fig. 1.24 Some common uses of cationic Silver (right) and silver nanoparticles (left) in medicine [192]

Dressings such as Silvercell®, Urgotul®, Silverex®, etc., are the result of the incorporation of silver sulfadiazine into hydrogels, while the dispersion in alginates is the basis of systems such as catheters, for example, Bardex Ic®. [193][194]

1.6.3 Antimicrobial Ag(I) complexes

A large number of Ag(I) based compounds have been developed and tested against numerous bacterial species. In 1968s the first Ag(I) complex combining Ag(I) ions sulfadiazine was produced, a cream with a broader bactericidal spectrum that even today continues to be prescribed for the management of burns. [195] In 1975s the crystallography structure of silver sulfadiazine (SSD) complex was determined, proving that each silver ion, is in a distorted tetrahedral configuration coordinated to three nitrogen atoms and one oxygen atom of the sulphadiazine molecules (**Fig. 1.25**). [196]

[192] Chaloupka, K., Malam, Y., and Seifalian, A.M. *Trends Biotechnol.*, 28, 11, 580–588, **2010**
[193] Ip, M., Lui, S.L., Poon, V.K.M., Lung, I., and Burd, A. *J. Med. Microbiol.*, 55, 1, 59–63, **2006**
[194] Lo, S.F., Hayter, M., Chang, C.J., Hu, W.Y., and Lee, L.L. *J. Clin. Nurs.*, 17, 15, 1973–1985, **2008**
[195] C.L. Fox, S.M. Modak. *Antimicrob. Agents Chemother*., 5, 582, **1974**
[196] D.S. Cook, M.F. Turner. *J. Chem. Soc., Perkin Trans*., 2, 1021, **1975**

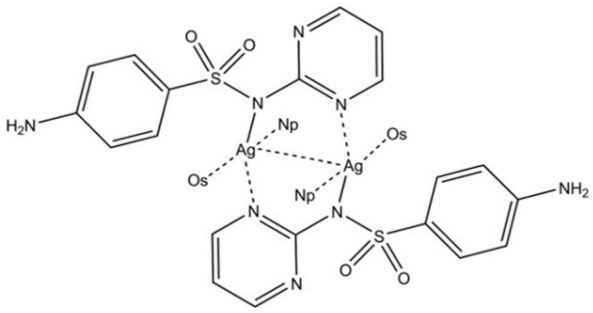

Fig. 1.25 Ag(I) [(4-aminophenyl)sulfonyl](pyrimidin-2-yI)azanide or SSD. OS: Oxygen from sulfonyl group. Np: Nitrogen from pyrimidine ring

Recently Ag(I) complexes have been extensively studied. The antimicrobial activity of the Ag(I) complexes is strongly correlated to the non-metal atom which silver is linked too. For examples, it is reported below that with Ag(I)-S, Ag(I)-N and Ag(I)-P.

The oligomeric complexes with the linkage Ag(I)-S have displayed effective antimicrobial activities against selected bacteria, yeast and mold, but their spectra of action are found very narrow. Complexes containing imidazoles ligands, so with the Ag(I)-N linkage showed wide spectra with remarkable antimicrobial activities against bacteria, yeast and mold, but particularly versus mold. This activity is performed also by the monomeric species cationic Ag(I)-N. **(Fig. 1.26)**

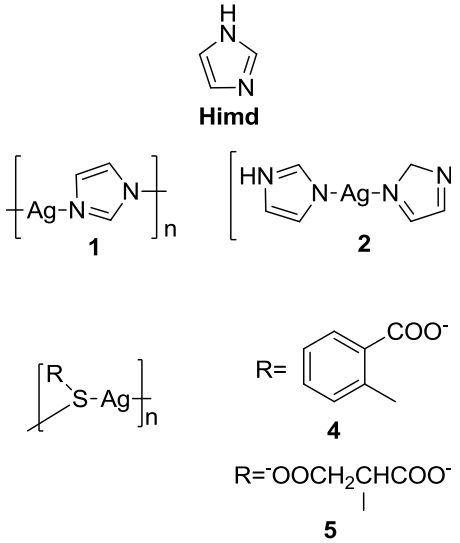

Fig. 1.26 Structures of complexes with the linkage Ag(I)-S and Ag(I)-N.

Other interesting examples are that with complexes containing the linkage Ag(I)-C and Ag(I)-P. Ag(I) complexes with N-Heterocyclic Carbenes (NHC) were synthesized from corresponding ligands and silver acetate or silver oxide to yield the desired product. [197][198] Thus, Ag(I)-carbene complexes were synthesized, with antimicrobial properties (**Fig. 1.27**). After complexes preparation, the antimicrobial properties were tested against a series of bacterial species, both Gram-positive and Gram-negative, *E. coli*, *S. aureus*, and *P. aeruginosa*. [199][200]

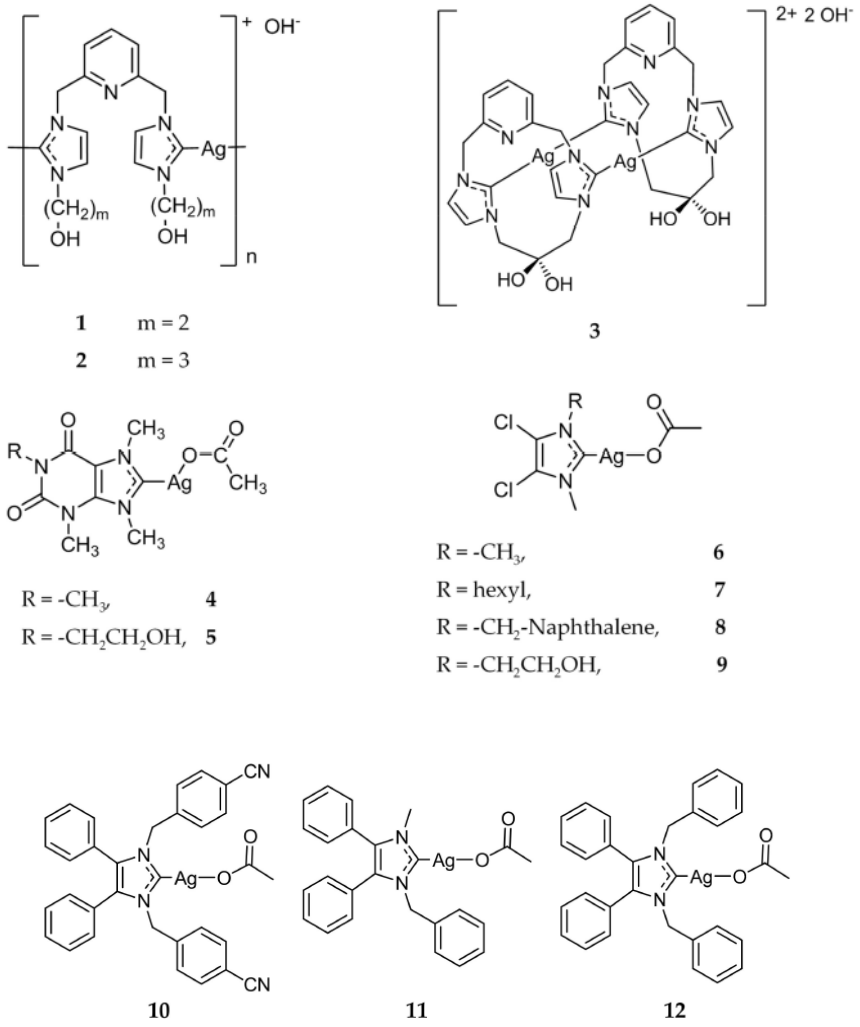

Fig. 1.27 Structure of Ag(I)-NHC complexes

[197] S. Patil, A. Deally, B. Gleeson, H. Muller-Bunz, F. Paradisi, M. Tacke, *Metallomics*, 3, 74-88, **2011**
[198] A. Melaiye, R.S. Simons, A. Milsted, F. Pingitore, C. Wesdemiotis, C.A. Tessier, W.J. Youngs, *Journal of Medicinal Chemistry*, 47 , 973-977, **2004**
[199] Youngs,W.J.; Knapp, A.R.;Wagers, P.O.; Tessier, C.A., *Dalton Trans.*, 41, 327–336, **2012**
[200] Melaiye, A.; Simons, R.S.; Milsted, A.; Pingitore, F.; Wesdemiotis, C.; Tessier, C.A.; Youngs, W.J. *J. Med. Chem.* **2004**, 47,
973–977

The results obtained show that complexes **1** and **2** have better bacteriostatic activity than $AgNO_3$. This surprising result soon lead to the synthesis of other complexes of the same family as complexes **3** and **4**. Complex **4** was tested against of Gram-positive and Gram-negative bacteria, showing good activity. (**Fig. 1.27**) Complex **4** also showed antimicrobial activity against *Burkholderia cepacia* (*B. cepacia*), a bacterium that mainly affects the respiratory tract. Moreover, complexes **5** and **6** show a good antibacterial activity against *B. cepacia*, while complexes **6**–**9** (**Fig. 1.27**) demonstrated good results against *B. pseudomallei* and *B. mallei*. [201] Complexes **10**, **11** and **12** (**Fig. 1.27**) showed a better antibacterial activity than the previous ones, probably attributed to the lipophilicity of these complexes, which allowed an increased penetration through the lipid cellular membrane and so an easier access to the targets. These complexes showed a good antimicrobial activity against both Gram-positive and Gram-negative bacteria, while their NHC precursors showed significantly lower activity, again indicating the utility of Ag(I) ions in antimicrobial.[202][203][204] The Ag(I)-NHC complexes show structural differences in the side chains linked to the nitrogen atoms, giving rise to a series of variations in properties related to lipophilicity, solubility and stability of the relative complexes. [205] Such complexes normally exert their antimicrobial action through interaction with cellular membranes, enzymes and DNA/RNA. [205]

Ag(I)-phosphine complexes and O-ferrocenyldithiophosphonates, $[Ag_2\{FcP(OMe)S_2\}_2(PPh_3)_2]$ are reported in **Fig. 1.28 (**a) e **1.28** (b). Both complexes (a) and (b), which were inserted into electrospun nanofibers in order to evaluate their antibacterial properties, moderate levels of antimicrobial activity have been obtained against *Micrococcus luteus* and *E. coli*. [206]

[201] Cannon, C.L.; Hogue, L.A.; Vajravelu, R.K.; Capps, G.H.; Ibricevic, A.; Hindi, K.M.; Kascatan-Nebioglu, A.; Walter, M.J.; Brody, S.L.; Youngs,W.J. *Antimicrob. Agents Chemother*, 53, 3285–3293, **2009**
[202] Patil, S.; Deally, A.; Gleeson, B.; Muller-Bunz, H.; Paradisi, F.; Tacke, *Metallomics*, 3, 74–88, **2011**
[203] Tacke, M. J. O*rganomet. Chem.*, 782, 17–21, **2015**
[204] Nicholas A. Johnson, Marie R. Southerland and Wiley J. Youngs, *Molecules*, 22, 1263, **2017**
[205] S. Medici, M. Peana, G. Crisponi, V. M. Nurchi, J. I. Lachowicz, M. Remelli, M. Zoroddua, *Coordination Chemistry Reviews*
[206] M. Karakus, Y. Ikiz, H.I. Kaya, O. Simsek, *Chem. Cent. J.*, 8, 1–8. **2014**

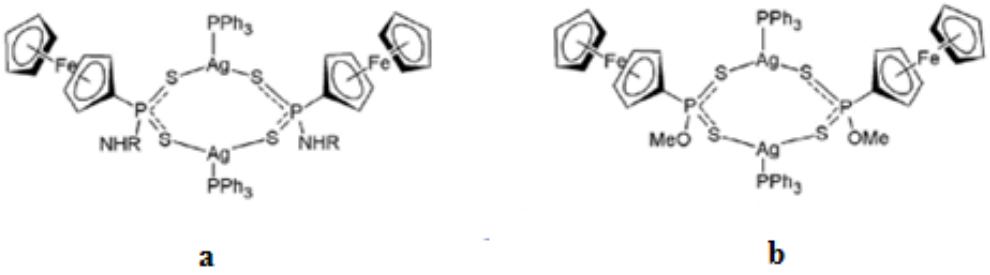

Fig. 1.28 Structures of complexes.

Moreover two complexes, $[Ag(mPTA)_4](Tpms)_4(BF_4)$ (**Fig. 1.29** (a)) and $[Ag(Tpms)(mPTA)](BF_4)$ (**Fig. 1.29** (b)) where mPTA is N-methyl-1,3,5-triaza-7-phosphaadamantane and Tpms is the scorpionate tris(1-pyrazolyl)methanesulfonate anion, were synthesized and tested for their activity against different bacterial strains. The results obtained for $Ag(mPTA)_4]^{5+}$ show an activity comparable to that of $AgNO_3$, while $[Ag(Tpms)(mPTA)]^+$ is a little less efficient.

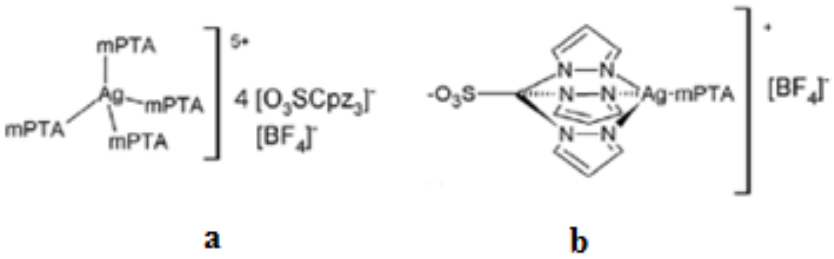

Fig. 1.29 Structures of mPTA complexes.

For both species, the proposed antimicrobial mechanism of action is the interaction with DNA, through a strong electrostatic attraction and then the complexes displayed a good binding ability toward the BSA protein. [207]

Ag(I)-N heterocycles are the last examples here reported. Ag(I) complexes such as Ag(I)-pyridinedicarboxylate compounds with pyridine derivatives such as pyridine-2,3-dicarboxylic (quinolinic), pyridine-2,4-dicarboxylic (lutidinic) and pyridine-2,5-dicarboxylic (isocinchomeronic) acids (**Fig. 1.30** (a–c)), were tested as antimicrobial agents against *E. coli*, *L. monocytogenes*, *S. typhi* and *S. aureus*.

[207] P. Smolen´ ski, C. Pettinari, F. Marchetti, M.F.C. Guedes da Silva, G. Lupidi, G.V. Badillo Patzmay, D. Petrelli, L.A. Vitali, A.J.L. Pombeiro, *Inorg. Chem.* 54, 434–440, **2015**

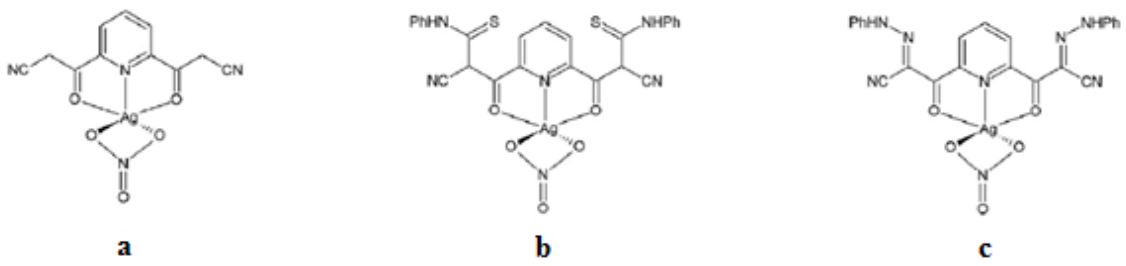

Fig 30. Ag(I)-pyridinedicarboxylate compounds with pyridine derivatives

Quinoline derivatives were employed in a study where the relative Ag(I) complexes (**Fig. 1.31** (a-b)) were screened against 15 different multidrug-resistant strains of bacteria isolated from diabetic foot ulcers and compared to the antimicrobial activities of the reference drug, silver sulfadiazine. $[Ag(8\text{-nitroquinoline})_2]NO_3 \cdot H_2O$ was the most active compound in this series, slightly more effective than silver sulfadiazine against all the bacterial strains tested. The complex $[Ag(5\text{-nitroquinoline})_2]NO_3$, showed better results than $AgNO_3$ against the standard nonresistant bacterial strains of *S. aureus*, *P.aeruginosa*, *Proteus mirabilis*, and *Streptococcus pyogenes*. [208]

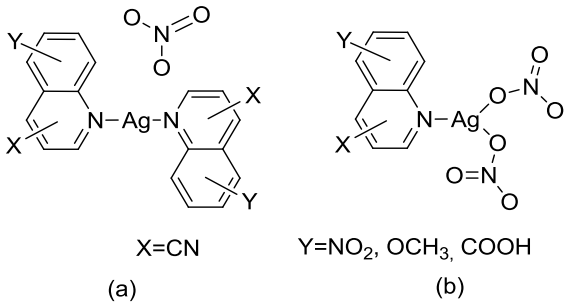

Fig. 1.31 Quinoline derivatives complexes.

Finally, Ag(I) complexes containing pyridine and benzimidazole phosphate derivatives as ligands (**Fig. 1.32** (a-b)). These complexes demonstrated good antimicrobial activity against *C. albicans* strains. In particular, complex $[Ag(2\text{-bimOpe})_2]NO_3$ (2-bimOpe = 1H-benzimidazol-2-ylmethyldiethylphosphate) was highly effective against *P. aeruginosa*. [209]

[208]U. Kalinowska-Lis, E.M. Szewczyk, L. Che¸cin´ska, J.M.Wojciechowski,W.M.Wolf, J. Ochocki, *ChemMedChem.*,9, 169–176, **2014**
[209]L. Ortego, M. Meireles, C. Kasper, A. Laguna, M.D. Villacampa, M.C. Gimeno, *J. Inorg. Biochem.* 156, 133–144, **2016**

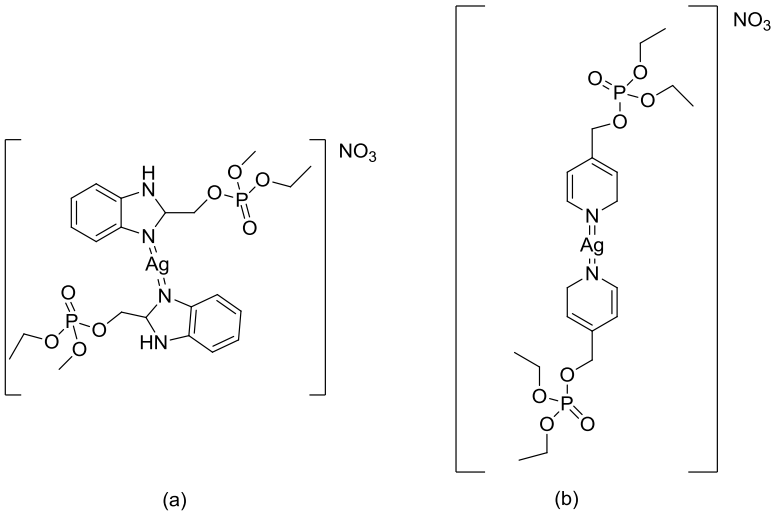

Fig. 1.32 Examples of silver complexes with N-heterocycles.

It was widely demonstrated that the antimicrobial activity is closely related to the type of donor atom that binds the metal center (silver) so the structure-activity relationship is highlighted. In fact, many works reported in the literature show that the antibacterial activity of Ag(I) complexes depend more on the Ag–ligand bond than from solubility, chirality, or the degree of polymerization of these complexes. [210][211][212][213][214][215][216] [217]

1.7 Silver effects on human health: toxicity and legislation

In order to discuss silver toxicity, it is necessary differentiate among silver metallic, silver ions or silver nanoparticles. Silver ions in small concentrations are not cause of concern to humans but a silver accumulation for ingests can form deposits of different silver species which may induce skin alteration consisting of blue-greyish skin coloration, due to the argyria pathology. This pathology ca be solved with the removal of the sick subject from the source of silver ions. [218] Nowadays general safety principles are reported in the Regulation EC No 1935/2004 on materials and

[210] K. Nomiya, S. Takahashi, R. Noguchi, S. Nemoto, T. Takayama, M. Oda. Inorg. Chem., 39, 3301, **2000**
[211] I. Tsyba, B.B. Mui, R. Bau, R. Noguchi, K. Nomiya. Inorg. Chem., 42, 8028, **2003**
[212] M.A.M. Abu-Youssef, S.M. Soliman, V. Langer, Y.M. Gohar, A.A. Hasanen, M.A. Makhyoun, A.H. Zaky, L.R. Öhrström. Inorg. Chem., 49, 9788 , **2010**
[213] S. Patil, J. Claffey, A. Deally, M. Hogan, B. Gleeson, L.M. Menéndez-Méndez, H. Müller-Bunz, F. Paradisi, M. Tacke. *Eur. J. Inorg. Chem.*, 7, 1020, **2010**
[214] R. Rowan, T. Tallon, A.M. Sheahan, R. Curran, M. McCann, K. Kavanagh, M. Devereux, V. McKee. *Polyhedron*, 25, 1771, **2006**
[215] B. Coyle, M. McCann, K. Kavanagh, M. Devereux, V. McKee, N. Kayal, D. Egan, C. Deegan, G.J. Finn. *J. Inorg. Biochem*., 98, 1361, **2004**
[216] M.A.M. Abu-Youssef, R. Dey, Y. Gohar, A.A. Massoud, L. Öhrström, V. Langer. *Inorg. Chem*., 46, 5893, **2007**
[217] K. Nomiya, A. Yoshizawa, K. Tsukagoshi, N.C. Kasuga, S. Hirakawa, J. Watanabe. *J. Inorg. Biochem*., 98, 46, **2004**
[218] Russell, A.D., and Hugo, W.B. *Prog. Med. Chem.*, 31 (C), 351–370, **1994**

articles intended to come into contact with food. Article 3 of EC No 1935/2004 claims that any material or object intended to come into contact directly or indirectly with food shall be manufactured in compliance with good manufacturing practices so that, under normal or foreseeable conditions of use, they do not transfer their constituents to food in quantities which could: (a) endanger human health or (b) bring about an unacceptable change in the composition of the food or (c) bring about a deterioration in the organoleptic characteristics thereof. This Regulation applies to all materials and articles intended to be in contact with foodstuff, including active and intelligent materials, for which are established specific requirements for their marketing. Active materials and articles are defined as "materials and articles that are intended to extend the shelf-life or to maintain or improve the condition of packaged food; they are designed to deliberately incorporate components that would release or absorb substances into or from the packaged food or the environment surrounding the food".

The framework Regulation establishes general principles for each packaging material but it does not describe how they must be accomplished depending on its nature. It is the Regulation (EC) No. 450/2009 which lays down the specific provisions for active and intelligent materials and articles in addition to the general requirements established in Regulation (EC) No. 1935/2004 for their safe use. According to the active packaging Regulation, only substances that are included in the 'Community or positive list' of authorized substances may be used in components of active materials and articles. For new active substances, an application for their authorization shall be submitted. The Community list should include the identity, conditions of use, restrictions and/or specifications of use of the substance or of a combination of substances and, where necessary, of the component or of the material or of the article in which they are added to or incorporated into.

For the active substances, which are intended to be released into food or are immobilized on the packaging surface in contact with food should only be used under the conditions set out in Food Law Regulation. New food additives or an extension of use are subject to an authorization procedure laid down in Regulation (EC) No. 1331/2008 that establishes a common authorization procedure for food additives, food enzymes and food flavorings. Then, European food safety authority (EFSA) performs a risk assessment of the substance and publishes a Scientific

Opinion about its use. Finally, it is the European Commission who approves the use and the applicable restrictions for these substances.

Regarding the passive parts in which the active substances are incorporated, they should be covered by the specific Community or national provisions applicable to those materials and articles. For example, if an active substance is incorporated in a polymeric matrix, the polymer has to comply with the Regulation (EU) No. 10/2011 on plastic materials and articles intended to come into contact with food. In this way, Articles 11 and 12 of plastic Regulation specify the applicable restrictions regarding specific migration limits (SML) and overall migration limits (OML), respectively. The SML is the maximum permitted amount of a given substance released from a material or article into food or food simulants, and those limits are established in the Union list of the Regulation. Plastic materials and articles shall not transfer their constituents into food simulants in quantities exceeding 10 mg of total constituents released per dm^2 of food contact surface (mg/dm^2). At European level, EFSA has authorized the use of silver zeolites, silver zirconium phosphate with specific migration limits. [56] EFSA provisionally accepts the use of silver in food-contact materials with a maximum of 5% silver in the form of silver zeolites or silver zirconium phosphate. The more recent council directive on materials and plastics intended to come in contact with foodstuffs establishes both the standard analysis protocols for determining specific migration that maximum limit of Ag^+ to foodstuffs is restricted to max 0.05 mg/kg food for the whole group in the EFSA provisional list of additives used in plastics 11th update: 28/10/2011.

Chapter 2

Ag(I) complexes as active ingredients for Ethylcellulose thin films

Based on what has been reported so far, the goal of this doctoral thesis is to prepare and to investigate novel Ag(I) active packaging materials, based on the natural derived polymer ethylcellulose, EC, and selected antimicrobial Ag(I) complexes. In order to prepare the new EC-Ag(I) films, the choice of the Ag(I) complexes has been correlated to the type of forces involved in the physical interactions responsible for the homogeneous inclusion of the metal based active molecules into the EC substrate. Knowing the EC structure, reversible noncovalent interactions such as van der Waals, electrostatic or hydrogen bonding can be expected to form between the Ag(I) complexes and the EC substrate. Neutral and ionic silver complexes have been selected as additives, and within the neutral derivatives, the choice of the ligands surrounding the metal centre have been realized in the attempt to modulate the overall polarity and the significance of the hydrogen bonds functional groups.

As neutral silver complexes, Ag(I) acylpyrazolonato complexes (**Fig. 2.1**) have been chosen based on their recognized antimicrobial activity and, from a structural point of view, based on two main structural features. The presence on the 4-acyl-5-pyrazolones of the trifluoromethyl (-CF_3) group, due to the ability of the so called "organic fluorine" groups increase the specific non-covalent intermolecular interactions or nano-segregation of incompatible segments of molecules. [219] Moreover, it is well known that the insertion of a fluorine atom or a -CF_3 group, at least in organic molecules significantly affects their biological properties and increases their metabolic stability. [220]

The second structural difference is that on the imidazole ring. Some complexes are characterized by the presence of different functional groups, instead some others show, in the same position, an H-atom on the nitrogen in position 1. The presence/absence of this N-H bond confers a hydrophilic/hydrophobic character to the overall complex. [221]

[219] O. Jeanni, M. Fourmiguè, *Chem. Eur. J.,12*, 2994 – 3005, **2006**
[220] P. Yadav, K. Lal, L. Kumar, A. Kumar, A.K. Paul, R. Kumar, *Eur. J. Med. Chem,155*, 263-274, **2018**
[221] F. Marchetti, J. Palmucci, C. Pettinari, R. Pettinari, F. Condello, S. Ferraro, M. Marangoni, A. Crispini, S. Scuri, I. Grappasonni, M. Cocchioni, M. Nabissi, M. R. Chierotti, R. Gobetto, *Chem. Eur. J., 21*, 836 – 850, **2015**

The presence of the N-H hydrogen bond donor on the imidazole ligands can favor the formation of hydrogen bonds with the suitable acceptor groups present on the polymeric EC matrix, both on the surface and in the inner structure, giving rise to different aggregation mode in the formation of the derived films.

The selected neutral silver complexes exhibit a different functionalization on the imidazole ring. More specifically, as can be seen from the **Fig. 2.1**, complexes **1** and **2** differ in the functionalization in position 1 of the imidazole ring, respectively with an aromatic ring and an alkyl group. The complexes **3-5** show different functional groups in the position 2 of the imidazole ring.

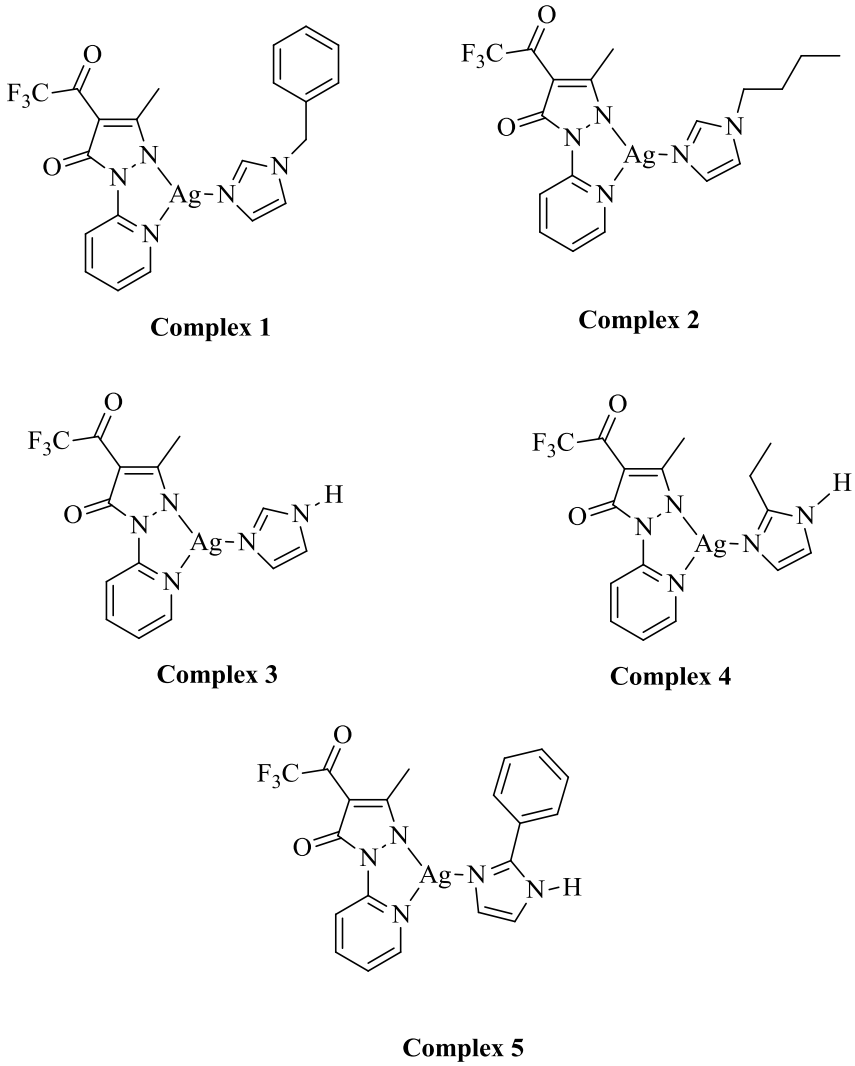

Fig. 2.1 Ag(I) acylpyrazolonato complexes

Moving from neutral and positively charged silver complexes to ionic Ag(I) derivatives, a structurally different system has been selected. The neutral 2,2'-

bipyridine ligand characterized by the presence of two hydroxyl groups (-OH), has the ability to bis-chelate silver ion, forming stable ionic complexes with different counter ions [222][223][224][225][226][227], so the acetate derivative reported in **Fig.2.2** has been tested in the insertion into the polymeric EC matrix. Ethylcellulose is only partially substituted in terms of OH groups, but, similarly to cellulose, the polymer chains are arranged in a parallel manner and are organized in sheets stabilized by interchain OH--O hydrogen bonds, whereas the stacking of sheets is stabilized by both van der Waals dispersion forces and weak CH–O hydrogen bonds. This structural organization imply that polymer has a strong affinity to itself and materials containing hydroxyl groups. [228]

The ionic complex showed in **Fig. 2.2** displays the metal centre surrounded by hydroxyl groups (complex **6**), which, as expected have a fundamental role in the interaction with the EC substrate.

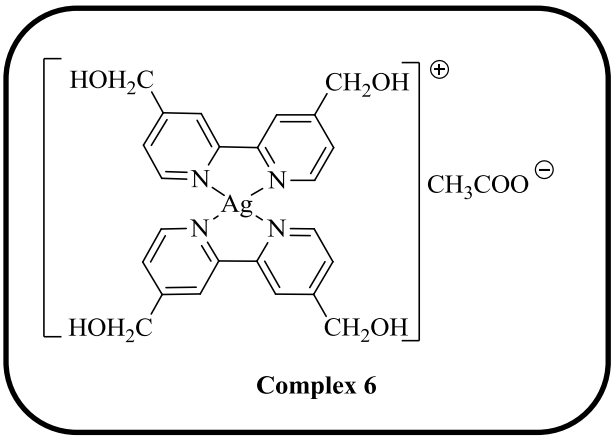

Fig. 2.2 Ag(I) ionic complex

This ionic complex **6** has never been tested for its potential antibacterial activity until now. Therefore, its use as active additive in the preparation of EC films with potential various applications is for the first time verified in this research project.

[222] D. Pucci, G. Barberio, A. Bellusci, A. Crispini, M. La Deda, M. Ghedini and E. I. Szerb, *Eur. J. Inorg. Chem.*, 2457– 2463, **2005**
[223] D. Pucci, G. Barberio, A. Bellusci, A. Crispini, M. Ghedini and E. I. Szerb, *Mol. Cryst. Liq. Cryst.*, 441, 251–260, **2005**
[224] D. Pucci, G. Barberio, A. Bellusci, A. Crispini, B. Donnio, L. Giorgini, M. Ghedini and E. I. Szerb, *Chem.–Eur. J.*, 12, 6738–6747, **2006**
[225] A. Bellusci, M. Ghedini, L. Giorgini, F. Gozzo, E. I. Szerb, A. Crispini and D. Pucci, *Dalton Trans.*, 7381–7389, **2009**
[226] D. Pucci, A. Crispini, M. Ghedini, E. I. Szerb and M. La Deda, *Dalton Trans.*, 4614–4622, **2011**
[227] E. I. Szerb, D. Pucci, A. Crispini and M. La Deda, *Mol. Cryst. Liq. Cryst.*, 573, 34–45, **2013**
[228] D. Pucci, B. Sanz Mendiguchía, C. M. Tone, E. I. Szerb, F. Ciuchi, M. Gao, M. Ghedini, A. Crispini, *J. Mater. Chem. C*, 2, 8780, **2014**

In order to achieve EC films with potential biomedical and food packaging applications, it has been necessary to organize the work in various steps sequentially accomplished as follows:

- Synthesis and characterization of the Ag(I) active additives complexes;
- Evaluation of different methods for incorporation of the Ag(I) complexes into EC polymer;
- Choice of the solvent used for the preparation of the new Ag(I) films in order to make the preparation environmentally sustainable;
- Investigation of the structural role of the ligands surrounding the metal centre in the interaction with the Ethylcellulose matrix;
- Tests for specific migration of Silver ions, according to EU Legislation on the migration of chemicals from plastic, for the evaluation of the compliance of these materials to be applicable in the food packaging sector;
- Tests of the antibacterial activity of all films

2.1 Ag(I) Acylpyrazolone complexes: structural features and applications

In the Chapter 1, metal coordination complexes with antimicrobial activity was described. In this scenario, recently Ag(I) coordination complexes have attracted a great deal of attention for their important antibacterial action exhibited against numerous bacterial families. [221] This new class of complexes is characterized by the presence of 4-acyl-5-pyrazolonate (Q) ligands, with different electronic and steric features, as main coordinated ligands and phosphine or various imidazoles L as ancillary ligands. 4-acyl-5-pyrazolones are an interesting class of asymmetric β-dichetonic ligands containing a pyrazolic unit functionalized with an O,O chelating group of the diketonic type. They were first synthesized in the late nineteenth century, but it was only in 1959 that Jensen reported an advantageous method of preparation, specifically for 1-phenyl-3-methyl-4-acylpyrazol-5-oni. [229]

[229] Jensen, B.S., Meier, H., Lundquist, K., and Refn, S. *Acta Chem. Scand*., 13, 1668–1670, **1959**

Acylpyrazolones are generally indicated with HQ where H is the enolizable proton (**Fig. 2.1.1a)** and Q indicates the substituents R^1, R^2, R^3. The general structure is reported below (**Fig. 2.1.1b)**.

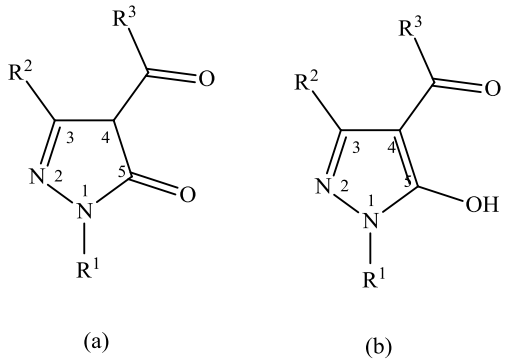

2.1.1 Generally structure of acylpyrazolones HQ: (a) chetonic form and (b) enolic form

Neutral acylpyrazolones are present in different tautomeric forms both in solid state and in solution, as reported in **Fig. 2.1.2**

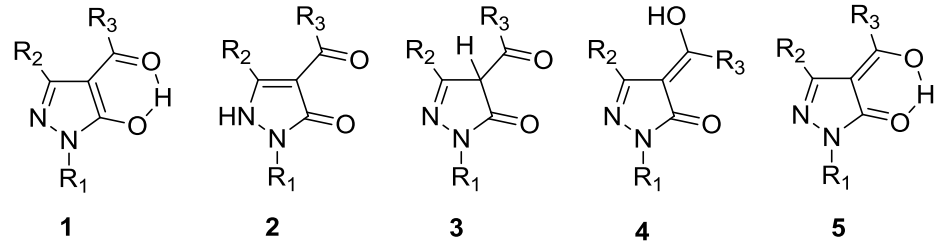

Fig. 2.1.2 Tautomer forms that of acylpyrazolones.

The enolic form **1** is preferred in polar solvents, while the presence of a phenolic ring in R^2 stabilizes the diketonic structure **2**. Acylpyrazolones in their neutral form can coordinate a metal centre in different coordination modes, as indicated in **Fig. 2.1.3.**

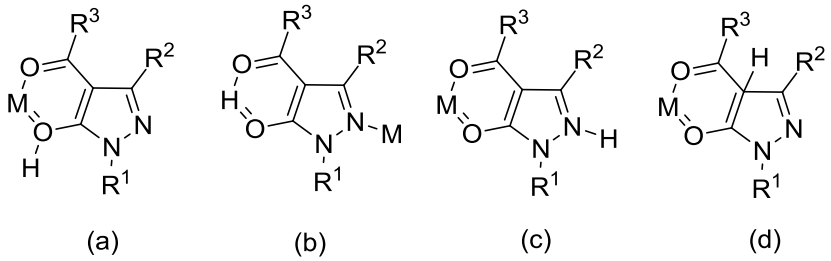

Fig. 2.1.3 Different metal coordination ways of Acylpyrazolones.

The enolic tautomer can coordinate to the metal centre both in a bidentate (see **Fig. 2.1.3a, c, d**) and in a monodentate mode through the nitrogen of the pyrazole ring (**Fig. 2.1.3b**). When acylpyrazole ligands are deprotonated by treatment with a base, in their anionic form the usually observed coordination way occurs through both oxygen atoms, therefore behaving as bidentate chelating ligands. (**see Fig. 2.1.3 a, c, d**) There so versatile ligands have been used as binders in analytic chemistry for the determination and isolation of many metals thanks to such important properties like high extraction capacity, the color of the extracted complexes and the different solubility of the complexes in numerous solvents. [230]

Ag(I) is a very versatile metal centre for designing acylpyrazolonato complexes. Indeed, a large number of novel acylpirazolonato coordination polymers based on Ag(I) as metal centre, have been synthesized. [231]

Ag(I) is a very versatile metal centre for designing acylpyrazolonato complexes. A large number of novel Ag(I) acylpirazolonato coordination polymers, have been synthesized. As can be seen from the following examples, the reaction of different acylpyrazolones with Ag(I) salts and their reactivity with N- and P-donor ligands, leads to Ag(I) complexes with different structural and physicochemical properties. In **Fig.2.1.4** are reported the HQ and HQ^{py} proligands. More specifically the HQ one lead different R groups, the linear fluorinated propyl group (HQ^{fb}), the cyclohexyl moiety (HQ^{cy}), the 2-methyl-2-butenoyl (HQ^{be}) and the phenyl moiety (HQ^{ph}). The1-(2-pyridyl)-3-methyl-4-trifluoroacetyl-5-pyrazolone (HQ^{py}), clearly differs from the others due to the presence of the pyridine ring in the HQ structure.

[230] Pettinari, C., Marchetti, F., Cingolani, A., Leonesi, D., Mundorff, E., and Rossi, M., *J. Organomet. Chem.*, 557, 187–205, **1998**

[231] Marchetti, F., Palmucci, J., Pettinari, C., Pettinari, R., Scuri, S., Grappasonni, I., Cocchioni, M., Amati, M., Lelj, F., and Crispini, A., *Inorg. Chem.*, 55, 11, 5453–5466, **2016**

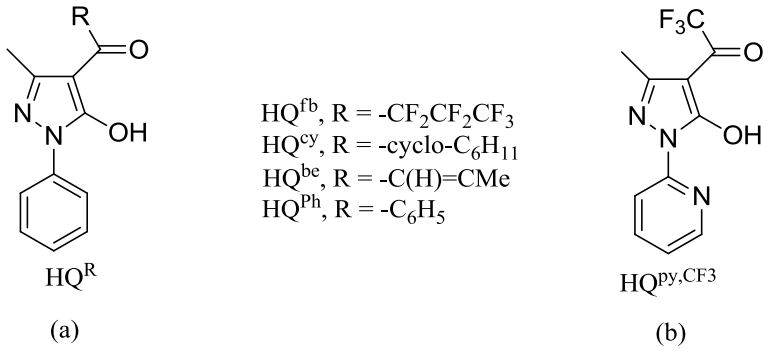

Fig.2.1.4 Structures of HQ Proligands

From the general scheme of reaction (**Scheme 2.1.1**) it is possible to note that the mono-, di-, and even polynuclear Ag(I) complexes were obtained by reaction between $AgNO_3$ and HQ^R in methanol using NaOMe as deprotonating agent.

The coordination modes between HQ^R and HQ^{py} with respect to Ag(I) significantly changes; in the first case the Ag(I) is O_2 chelated on one side and N-linked on the other side, in the latter is instead reported an N_2 chelation on one side and a single oxygen linkage on the other one. (**Scheme 2.1.1**)

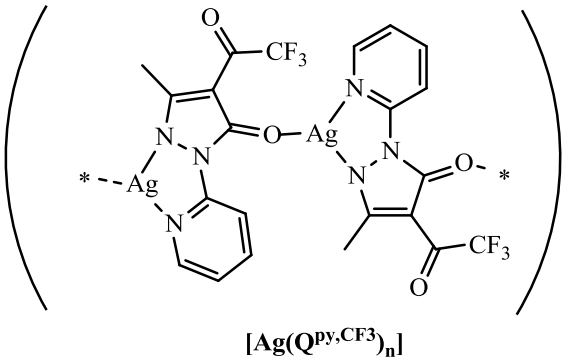

Scheme 2.1.1 Synthetic procedure of the $[Ag(Q^R)_n]$ and $[Ag(Q^{py,CF3})_n]$

Several imidazole derivatives as well as a pyridine and phosphine as ancillary ligands (L) have been used in order to obtain the final complexes (**Fig.2.1.5**).

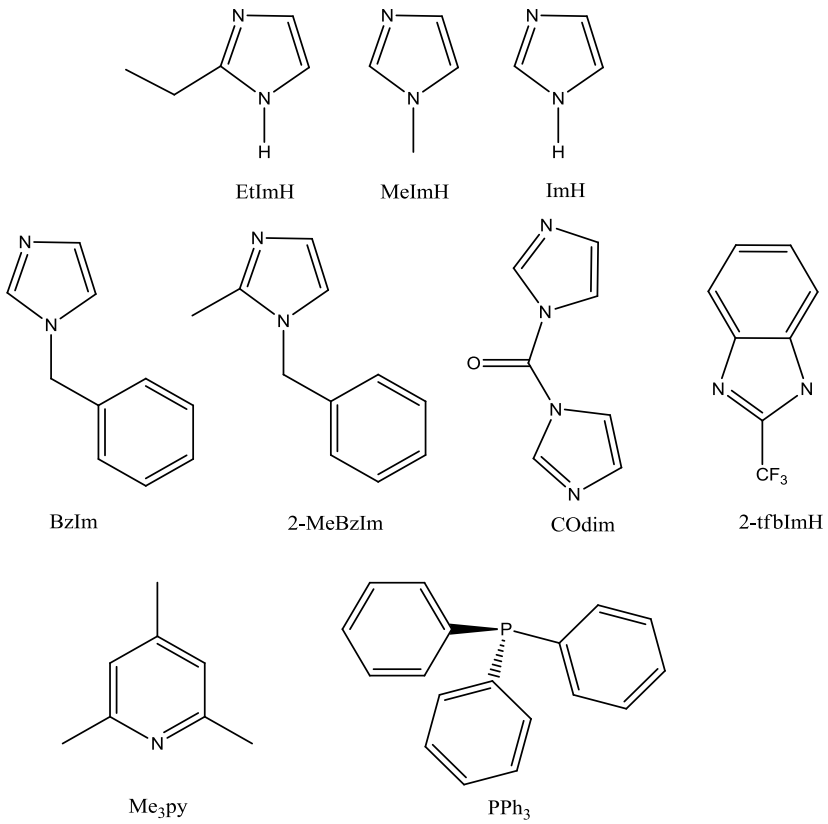

Fig.2.1.5 Structures of Imidazoles, Phosphine and Pyridine

In the **Scheme 2.1.2** is reported the reaction between the polymer backbone and the ancillary ligands. The interaction with these ligands causes the HQ-Ag sub-units formation from the polymer chain, this lead to the desired mononuclear complexes. The different complexes obtained not only depend from the ligand but strongly depends from the reaction environment. [232][233][234][235]

[232] Cingolani, A., Effendy, Marchetti, F., Pettinari, C., Pettinari, R., Skelton, B.W., and White, A.H., *Inorg. Chem.*, 41, 5, 1151–1161, **2002**
[233] Cingolani, A., Effendy, Marchetti, F., Pettinari, C., Pettinari, R., Skelton, B.W., and White, A.H. *Inorg. Chem.*, 43, 14, 4387–4399, **2004**
[234] Lorenzotti, A., Marchetti, F., Pettinari, C., Pettinari, R., Skelton, B.W., and White, A.H. *Inorg.Chim. Acta*, 358 , 11, 3190–3200, **2005**
[235] Cingolani, A., Effendy, Martini, D., Pellei, M., Pettinari, C., Skelton, B.W., and White, A.H. *Inorganica Chim. Acta*, 328, 1, 87–95, **2002**

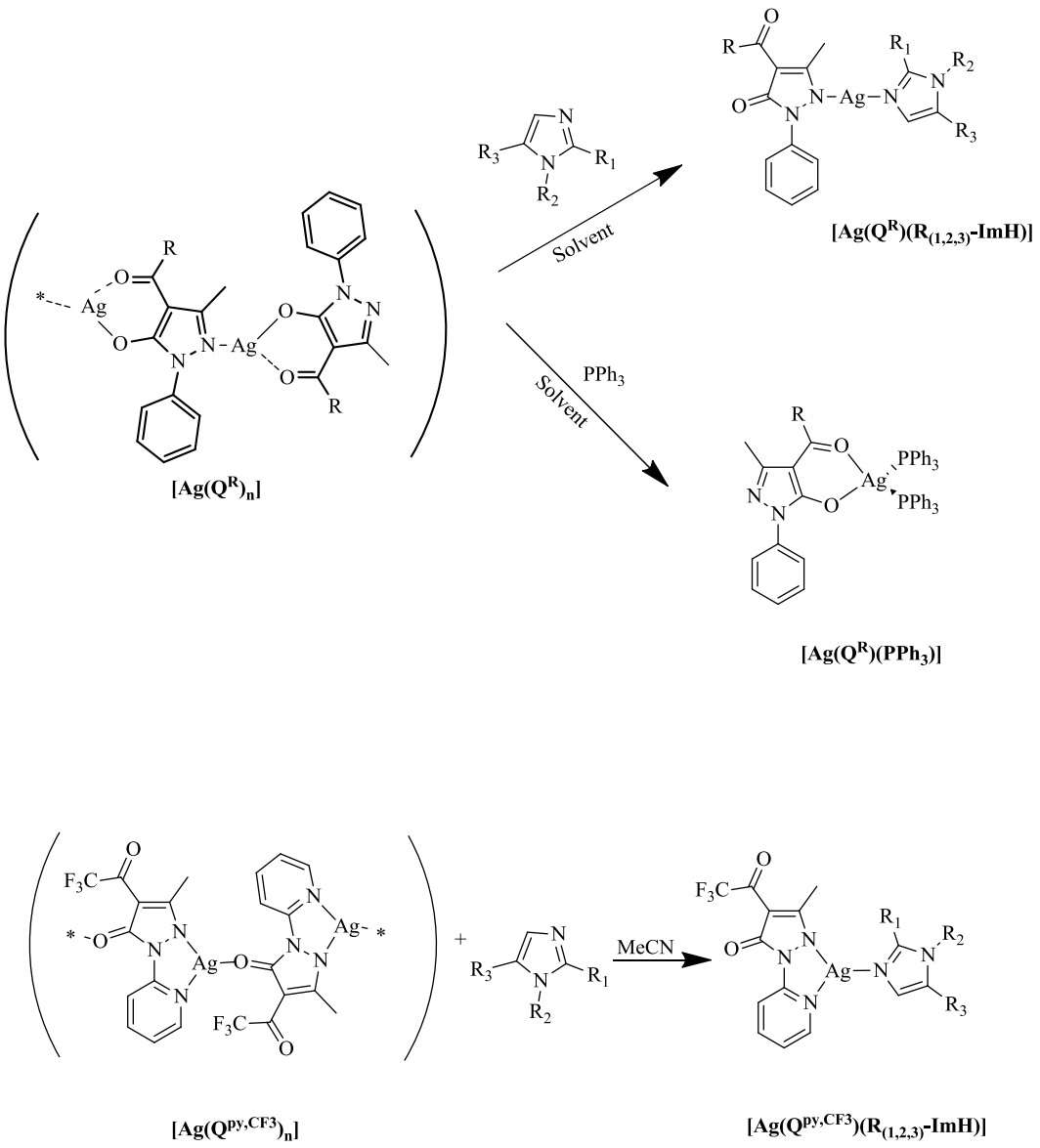

Scheme 2.1.2 General synthetic procedure leading to complexes formation

Several complexes can be obtained and they are reported in **Fig.2.1.6**. These show important variation both from a structural and properties point of view, *i.e.* geometries, solubility, solvation and antibacterial activity.

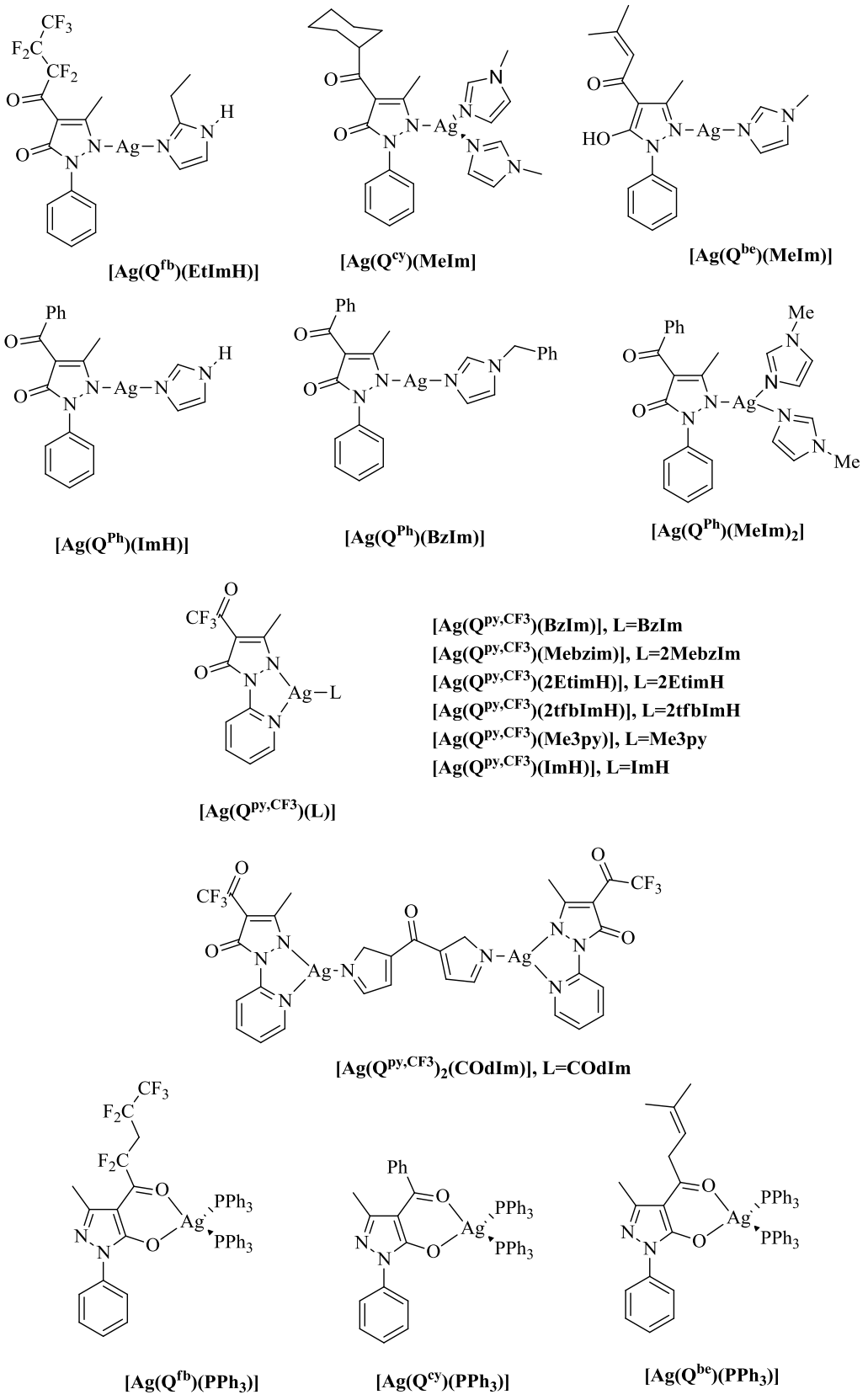

Fig.2.1.6 Structures of the final complexes.

2.1.1 Antibacterial activity

The antibacterial activity of the polynuclear complexes and the mononuclear complexes has been investigated against bacterial species such as Escherichia coli and Staphylococcus aureus, both in terms of MIC (minimal inhibition concentration) and grows trends. The results obtained, compared with those of free ligand and $AgNO_3$ salt, show a high and almost stable antibacterial activity and their values are. (**Fig. 2.1.1.1**)

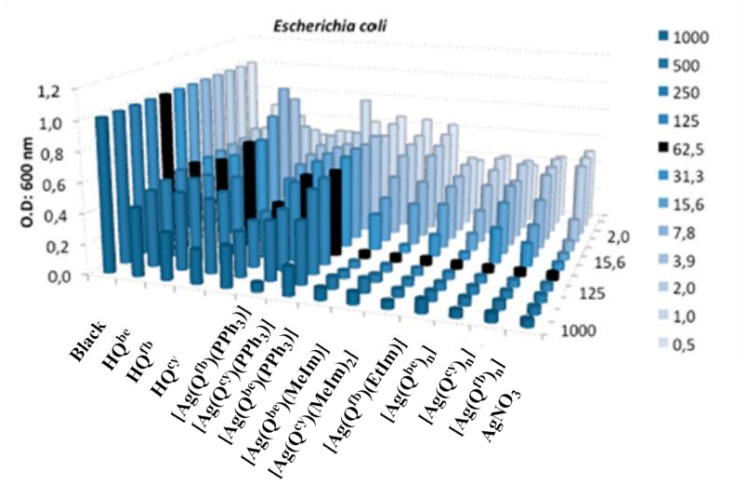

(a)

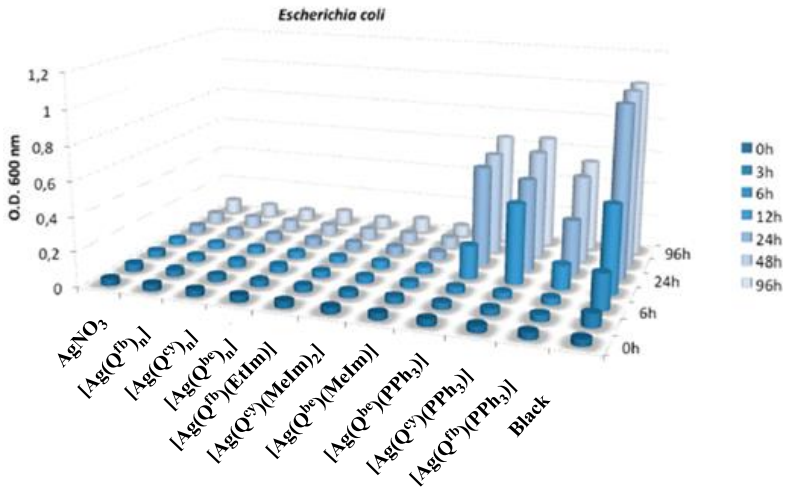

(b)

Fig. 2.1.1.1 a) MIC values of HQ^R proligands, polymers and complexes $[Ag(Q^R)(R_{(1,2,3)}\text{-ImH})]$ and $[Ag(Q^R)(PPh_3)]$ against Escherichia coli, where $AgNO_3$ is

the positive control and blank is the negative control **b)** Growth trends of E. coli in 62.5 ppm solutions of complexes [Ag(Q^R)($R_{(1,2,3)}$-ImH)] and [Ag(Q^R)(PPh_3)].

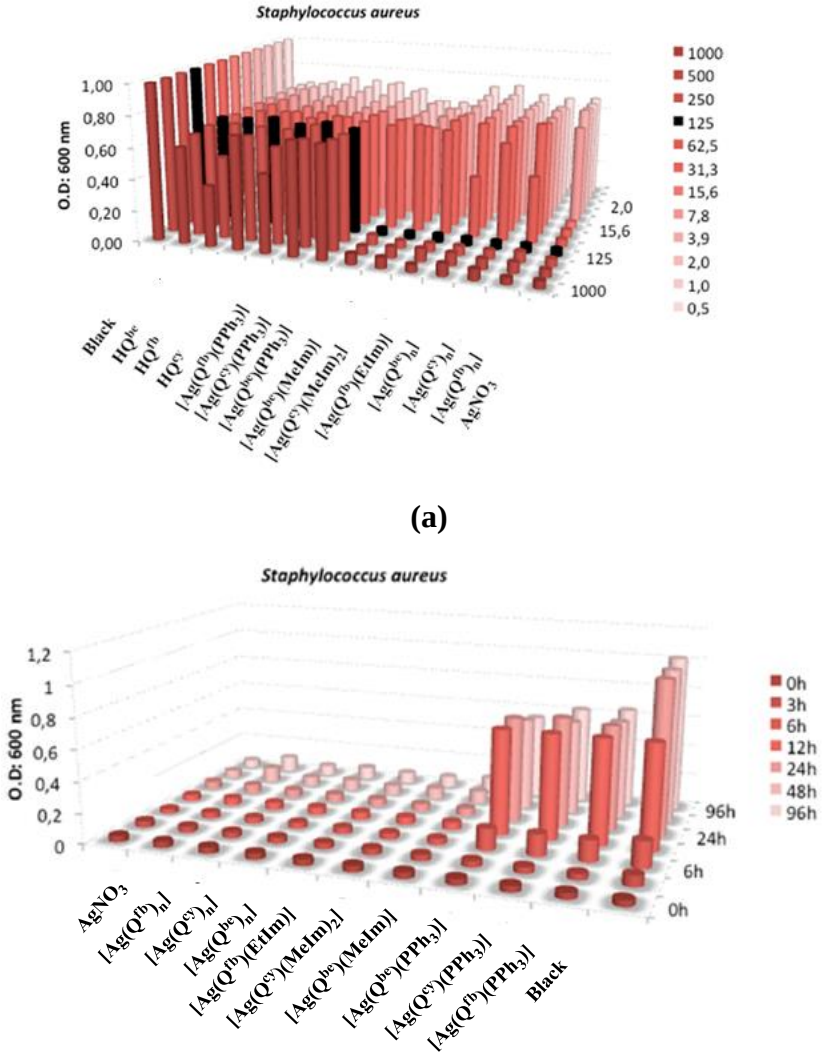

(a)

(b)

Fig. 2.1.1.2 a) MIC values of HQ^R proligands, polymers and complexes [Ag(Q^R)($R_{(1,2,3)}$-ImH)] and [Ag(Q^R)(PPh_3)] against Staphylococcus aureus, where $AgNO_3$ is the positive control and blank is the negative control.**b)** Growth trends of S. aureus in 125 ppm solutions of complexes [Ag(Q^R)($R_{(1,2,3)}$-ImH)] and [Ag(Q^R)(PPh_3)].

From the graphs in **Fig. 2.1.1.1** and **Fig. 2.1.1.2** it can be observed that the antibacterial activity of polymer $[Ag(Q^R)]_n$, of the mononuclear complexes $[Ag(Q^R)$-(imidazole)], and of the $[Ag(Q^R)(imidazole)_2]$ are very high against both *Escherichia Coli* and *Staphylococcus aureus* cultures, comparable to that of the $AgNO_3$. In contrast, the coordination of the PPh_3 to the metal centre leads to complexes with a lower activity. This is probably due to a major steric hindrance causing a reduced Ag^+ availability. [236][237][238][239]

After the deep study in solution, which allowed the disclosing of the chemical-physical properties as well as the antibacterial activity, the above reported polymers and complexes were used for the preparation of polyethylene composites. These materials are of high interest for composite plastics with low intrinsic value such as filters, bottles, and containers.

Polyethylene (PE) is one of the most common plastics, and is extensively used in packaging and containers for safe drinking water including bottles and taps. The addition of additives during the embedding process has been realized by using a different composition w/w of Ag(I) additive/polyethylene ratio. [221] The composites are prepared through a reaction in solid phase between the matrix and the Ag(I) additive, and, subsequently, the reaction mixture is heated up to 150 °C, above the melting point of the polyethylene, afterward when stirred for half an hour, the liquid is deposited thus obtaining a composite disk. This process is called "dry thermoplastic process" and relies on the thermoplastic behavior displayed by some substances.

Two main processes can achieve formation of films packaging; the one of the methods used for the preparation of films for food packaging. Formation of films packaging can be achieved by two main processes; the one, "wet process" involves polymer dispersion or solubilization in a solution-casting followed by evaporation of the solvent. The second, "dry process" is based on use on thermoplastic behavior that some polymers display at low moisture levels in compression molding and extrusion. [240] [241][242]

[236] Nomiya, K.; Tsuda, K.; Sudoh, T.; Oda, M. J. *Inorg. Biochem*., 68, 39−44, **1997**
[237] Nomiya, K.; Tsuda, K.; Kasuga, N. C. *J. Chem. Soc., Dalton Trans.*, 1653−1659, **1998**
[238] Nomiya, K.; Noguchi, R.; Oda, M. *Inorg. Chim. Acta*, 298, 24−32, **2002**
[239] Nomiya, K.; Tsuda, K.; Tanabe, Y.; Nagano, H. *J. Inorg. Biochem*., 69, 9−14, **1998**
[240] Cuq, B., Gontard, N., and Guilbert, S., 38,16 , 4071–4078, **1997**
[241] Pommet, M., Redl, A., Guilbert, S., and Morel, M.H., *J. Cereal Sci.*, 42, 1, 81–91, **2005**
[242] Liu, L., Kerry, J.F., and Kerry, J.P., *Int. J. Food Sci. Technol*., 41, 3, 295–302, **2006**

The process can involve any or all of the following operations: heating, cooling, feeding, conveying, compressing, shear-in, reacting, mixing, melting, homogenizing, "amorphization" (converting polymer crystalline domains to amorphous domains), cooking, and shaping. [243]

The composite plastic materials contenting Ag(I) Acylpyrazolonato additives has been tested against three bacterial strains, *E. coli, P. aeruginosa and S. aureus* and results showed high and persistent values of bactericidal and bacteriostatic activity, comparable to PE embedded with $AgNO_3$. Except for composites containing as complexes of Silver those presenting the phosphines as ancillary ligands, the resulting composites exhibit a reduced antibacterial action. This low activity is likely related to the degree of saturation of the Silver center and to the presence of different ancillary ligands in the diverse typologies of complexes. [231] These bacterial classes are being chosen because they represent well-known pathogens of medical relevance. Moreover, these bacteria are very resistant to classic antibiotics, which are difficult to treat and eradicate worldwide. S. aureus is associated with skin infections, responsible for many hospital- and community-acquired infections and occasionally causes food poisoning. [244] *P. aeruginosa* is a pathogen able of causing several infections in humans, including cystic fibrosis, urinary tract infections, and surgical wounds. [245] *E. Coli* is usually associated with food poisoning, causing infections of the gastrointestinal tract such as diarrhea and hemolytic uremic syndrome. [246]

The contact and release tests, according to EU Legislation on the migration of chemicals from plastic materials, in several conditions for specific migration of Ag^+ from plastics, are shown a very limited but time persistent release of Silver ions from composites, thus suggesting that they are potential antibacterial materials for future food packaging applications. Finally, it has been shown that the quantity of ions released, is not only lower than the limit set by the legislation, but it is so low as not to be toxic both for the environment and for humans. This was confirmed

[243] Hernandez-Izquierdo, V.M., and Krochta, J.M., *J. Food Sci.*, 73 (2), 30–39, **2008**
[244] Maguire, G.P., Arthur, A.D., Boustead, P.J., Dwyer, B., and Currie, B.J., *Med. J. Aust.*, 164, 12, 721–723, **1996**
[245] Leitão, J.H., Sousa, S.A., Cunha, M. V., Salgado, M.J., Melo-Cristino, J., Barreto, M.C., and Sá-Correia, I. *Eur. J. Clin. Microbiol. Infect. Dis.*, 27, 11, 1101–1111, **2008**
[246] Besser, R.E., Lett, S.M., Weber, J.T., Barrett, T.J., Doyle, M.P., and Griffin, P.M., *J. Am. Med. Assoc.*, 269, 17, :2217-2220, **1992**

respectively by evaluate cytotoxic effect in CD34+ cells by MTT assay and by D.magna test of ecotoxicity. [247]

The excellent characteristics of polyethylene composites and Ag(I) complexes push research towards the study of their possible incorporation into different matrices, in order to prepare new materials that can be used in the food package field. From this idea comes the central heart of this doctoral thesis.

2.2 Synthesis and characterization of the neutral Ag(I) acylpyrazolonato complexes selected as active additives.

The chosen ligand $HQ^{py,CF3}$ [(1-(2-pyridyl)-3-methyl-4-trifluoroacetyl-5-pyrazolone] has been provided by the School of Science and Technology, Chemistry Section, University of Camerino (UNICAM), while all Ag(I) complexes reported have been synthesized by adapting synthetic strategies according to the literature. [248] All complexes have been characterized both in solution and in the solid state. In particular, being necessary for the comprehension of the interactions between the Ag(I) complexes and the EC matrix a full solid state characterization, all complexes have been structurally and thermally analyze though powder and single crystal X-Ray Diffraction analysis, thermogravimetric and differential scanning calorimetry analysis (TGA and DSC).

2.2.1 Synthesis and characterization of the polymer $[Ag(Q^{py,CF3})]_n$

The synthetic methodology of the Ag(I) acylpyrazolonato complexes involves, as first step, the synthesis of the precursor polymer $[Ag(Q^{py,CF3})]_n$ This has been synthetized following the procedure reported in literature. [221]

[247] ISO 6341: Water quality "Determination of the Inhibition of the Mobility of Daphnia magna Straus (Cladocera, Crustacea)" Acute toxicity test. **2012**

[248] F. Marchetti, J. Palmucci, C. Pettinari, R. Pettinari, F. Condello, S. Ferraro, M. Marangoni, A. Crispini, S. Scuri, I. Grappasonni, M. Cocchioni, M. Nabissi, M. R. Chierotti, R. Gobetto, *Chem. Eur. J.*, 21, 836-850, **2015**

2.2.2 Synthesis and characterization of the selected [Ag(Q ^{py,CF3})(L)] complexes, 1-5

The synthesis of complexes **1-5** and their structures are shown in **Scheme 2.2.2** Complexes **1** and **2** are characterized by a different functionalization in position 1 of the imidazole ring: the first one show a benzyl-ring instead the second an alkyl chain. These types of functionalities confer to them a hydrophobic character. Complexes **3** and **4** show the N-H bond in position 1 and respectively a CH_3CH_2- and H-linkage in position 2. The N-H functionality confers an overall hydrophilic character to these complexes with respect to the others. Complex **5**, is a particularly interesting, since, it is characterized both by the presence of a hydrophobic substituent on the imidazole ring, similarly to complexes **1** and **2** but also by the presence, on the same imidazole ring, of the N-H substituent. This particular molecular structure could influence the interactions between the complex and the EC matrix after its incorporation.

Three of the five complexes (**1**, **3** and **4**) have been obtained following the synthetic procedure reported in literature. [221] Complexes **2** and **5** have been synthesized for the first time within this project, following the methodology reported in literature and reported in the following **Scheme 2.2.2** .

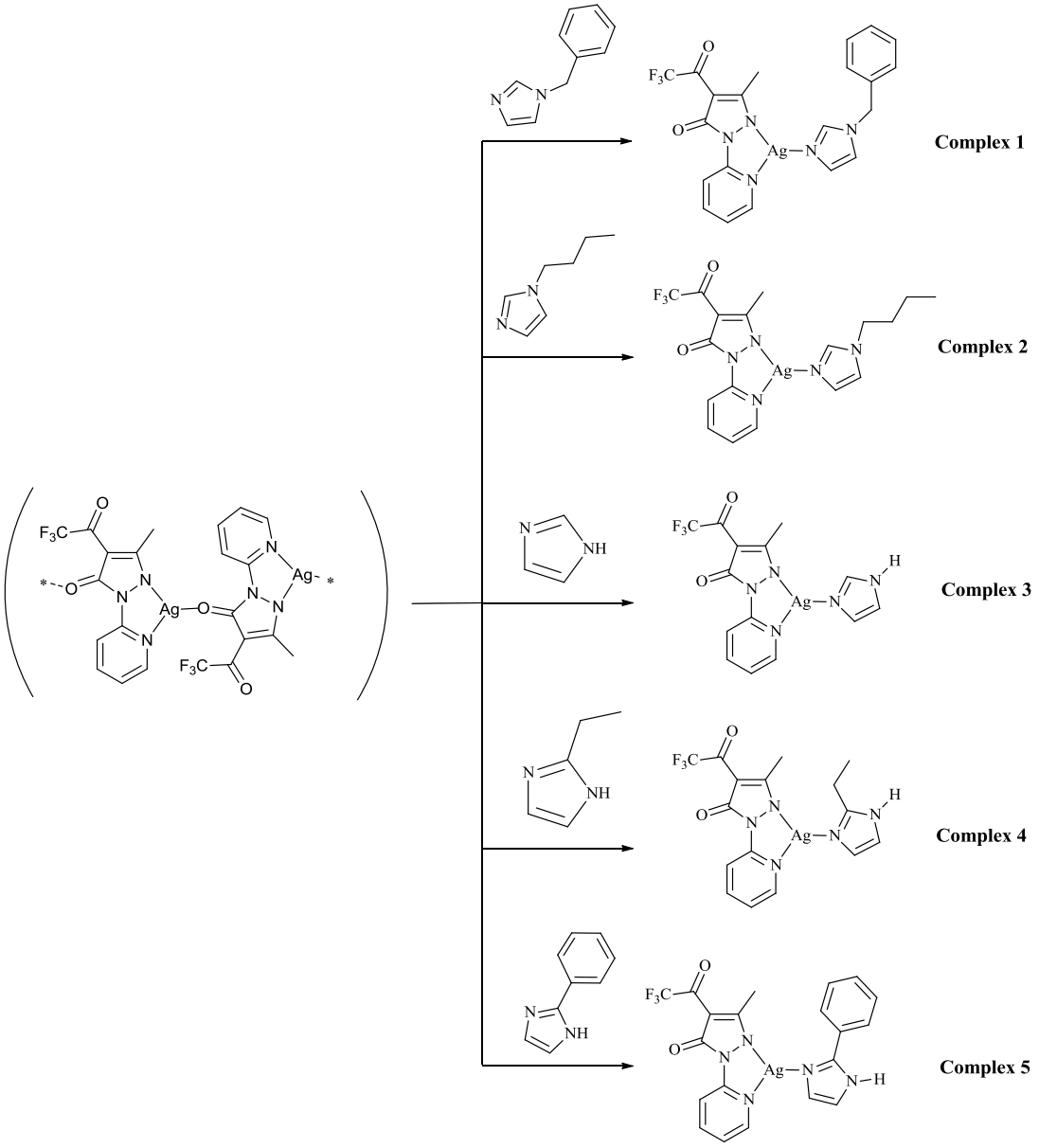

Scheme 2.2.2 Synthetic pathways of the complexes 1-5**.**

The elemental analysis data performed of all the complexes confirmed the proposed structures presented in **Scheme 2.2.2**, for the complexes which were obtained in good yield.

All the characterizations are in agreement with the date reported in literature. [221]

The discussion reported above is about general concerns and comparisons among the five complexes, the complete and specific characterizations (Elemental analyses, IR and NMR) for each complex are reported in the Chapter 4.

Structural and thermal characterizations will be discussed in the following paragraph.

2.2.3 Structural and thermal characterization of the selected [Ag($Q^{py,CF3}$)(L)] complexes, 1-5

Within the silver derivative series under study, deep structural information have been achieved by the single crystal X Ray analysis of complex **1** and **2**, as representative of the first group of Ag(I) complexes, and complexes **3** and **4** as examples of the second type of derivatives. While the structural determination of complexes **3** and **4** has been already reported [221], the ones of complexes **1** and **2** are reported herein for the first time.

Suitable single crystals of both complexes **1** and **2** have been obtained from an ethanol solution. Selected bond lengths and angles are reported in **Table 2.2.3**.

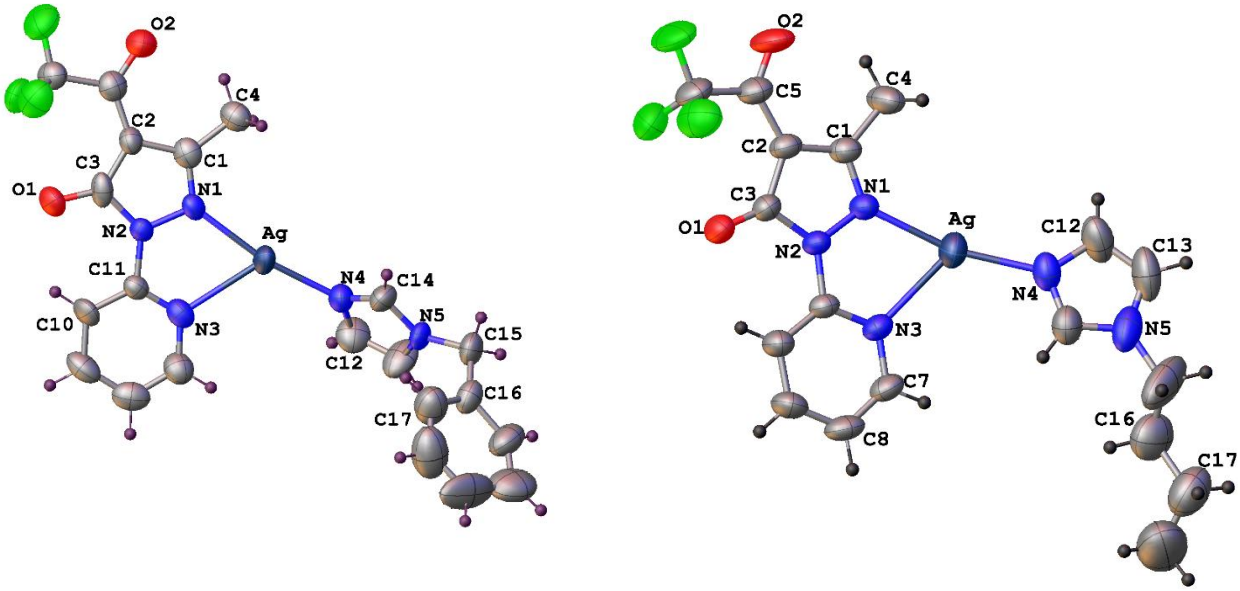

a) **b)**

Fig. 2.2.3.1 Perspective view of the asymmetric unit content of complexes **1** (a) and **2** (b) with atomic numbering schem

Table 2.2.3. Bond lengths [Å] and angles [°] for complexes **1** and **2**.

	1	**2**
Ag-N(1)	2.165(11)	2.194(3)
Ag-N(3)	2.433(12)	2.417(3)
Ag-N(4)	2.118(12)	2.125(3)
Ag-Ag#1		3.2725(7)
N(1)-Ag-N(4)	169.0(5)	165.31(12)
N(3)-Ag-N(4)	120.4(5)	120.75(12)
N(1)-Ag-N(3)	69.6(4)	71.02(10)
N(4)-Ag-Ag#1		109.38(10)
N(1)-Ag-Ag#1		83.63(8)
N(3)-Ag-Ag#1		61.41(7)

Symmetry transformations used to generate equivalent atoms: #1 -x+1,-y+1,-z+2

Both crystal structures **(Fig. 2.2.3.1)** show the mono-anionic N_2-chelating mode of the $Q^{py,CF3}$ ligand, where the nitrogen atom of the imidazole ring complete the Ag(I) coordination sphere. The tri-coordination of the metal centre gives rise to a highly distorted trigonal-planar geometry, where the N(1)-Ag-N(4) angle points towards linearity, particularly in the case of complex **1**. In both complexes **1** and **2**, a grater distortion from the trigonal geometry is observed when compared with complexes **3** and **4**, as reported in literature (Figure **2.2.3.2**). [221] Indeed, in the last complexes, while the value of the "bite" angle within the metallacycle of about 71° is comparable with the values observed in 1 and 2, the other two angles are found very different, with values in the range of 151-155 ° and 134-139 ° for the N(1)-Ag-N(4) and N(3)-Ag-N(4) angles, respectively.

Moreover, the Ag-N bonds in the N_2-chelating ring are now characterized by a greater asymmetry with respect to both complexes **3** and **4**, with distances at the

pyridine ring of 2.433(12) and 2.417(3) Å compared to the values of 2.376(3) and 2.358(3) Å for complex **3** and 2.392(3) Å for complex **4**.

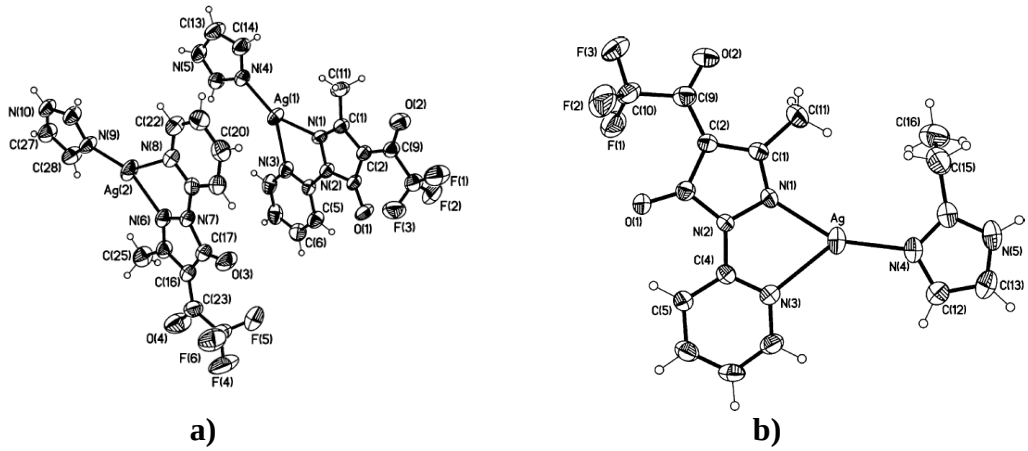

a) **b)**

Fig. 2.2.3.2 Perspective view of the asymmetric unit content of [Ag($Q^{py,CF3}$)(imH)] (**3**) a) and [Ag($Q^{py,CF3}$)(2EtimH)] b) **(4)** with atomic numbering scheme (ellipsoids at the 40% level). [231]

The main structural features arising from the analysis of both the crystal structure and the crystal packing of complexes **1** and **2**, regard the nature and type of intermolecular interactions, also able to determine the inner conformation of the single molecules.

The crystal packing of complex **1** is characterized by the formation of dimers within which centrosymmetric molecules interact via π- π stacking interactions between the pyridine and the pyrazole rings and weak C-H---O hydrogen bonds, as pictured in **Fig. 2.2.3.3**. The imidazole ring is not coplanar with the mean plane passing through the Ag(I) metallacycle (dihedral angle between the mean planes of 53.1(1)°), being basically orthogonal to the mean plane passing through the above molecule within the dimer. The orientation of the imidazole ring favors, therefore, the C-H---O hydrogen bond interactions.

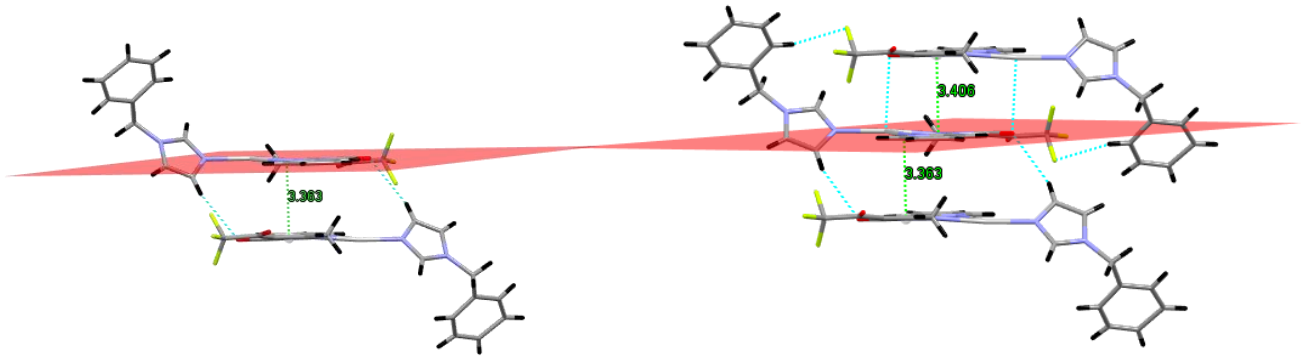

a) **b)**

Fig. 2.2.3.3 Crystal packing views showing the association of molecules of **1** in dimers a) and the interaction of dimers in the formation of columns via π- π stacking interactions and C-H---F contacts b). Values of interplanar distances are reported in the figure.

As shown in **Fig. 2.2.3.3** (**b**) the repetition of dimers gives rise to columns, within which C-H---F contacts and further significant π- π stacking interactions are present. Even if the crystal packing of complex **2** is characterized again by the presence of dimers of molecules, repeating them self in the formation of columns, the way in which molecules pack is noticeably different than that observed in complex **1**. The main intermolecular interaction holding molecules into dimers, is the argentophilic one, with an Ag---Ag distance of 3.273(1) Å. Some relevant differences in the intramolecular arrangement of the coordinated ligands with respect to the Ag(I) metallocycle arise observing how molecules pack into dimers. As shown in **Fig. 2.2.3.4** (a), although the imidazole ring is slightly tilted with respect to the mean plane passing through the silver metallacycle (dihedral angle between the mean planes of 13.7(1)°), its mean plane is far from the metallocycle of about 0.7 Å.

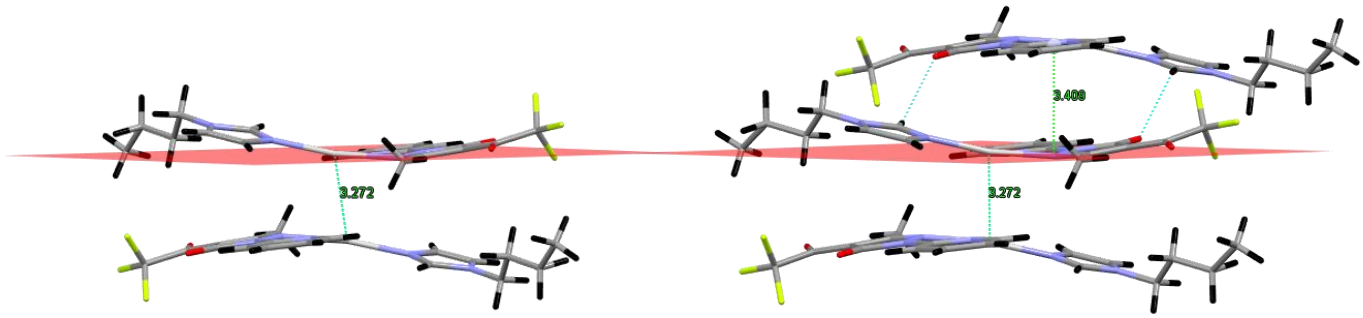

a) **b)**

Fig. 2.2.3.4 Crystal packing views showing the association of molecules of **2** in dimers (a) and the interaction of dimers in the formation of columns via π- π stacking interactions and C-H---O contacts (b). Values of Ag---Ag and interplanar distances are reported in the figure.

Dimers of complex **2** forms columns where each dimer interact via p-p stacking interactions between symmetrically related pyridine ring of the acylpyrazolonate ligands, and weak C-H---O hydrogen bonds (**Fig. 2.2.3.4 (b)**.

Differently than what seen for complexes **1** and **2**, the structural packing motif at the base of complexes **3** and **4** molecular packings is the N-H group on the imidazole ligands. As reported in literature, the presence of strong N–H···O hydrogen bonds drives to the formation of both chains and columns, both synthons reinforced by the presence of intermolecular interactions involving the fluorine atoms of the CF_3 groups and hydrogen atoms of both the acylpyrazolonate and imidazole ligands (**Fig. 2.2.3.5 b**).

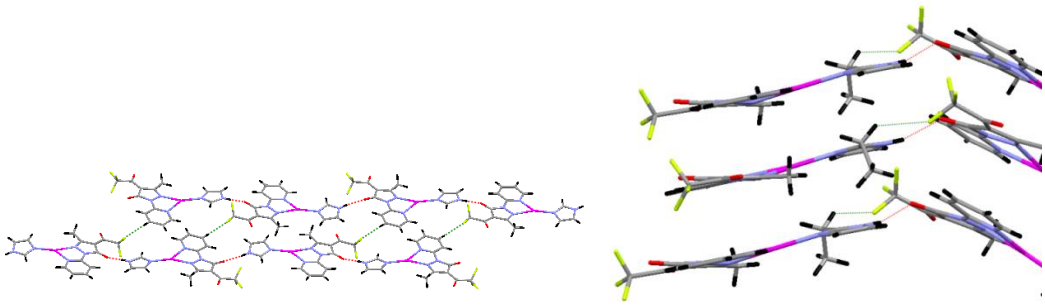

a) **b)**

Fig. 2.2.3.5 Molecular dimers of complex **3 (a)** and **4 (b)** formed by N-H···O and C-H···F hydrogen bonds reproduced from reference data [221]

The following characterizations (TGA and DSC) that have been realized are of utmost importance because not only gives as the possibility to disclose the all complexes thermal properties and behaviour, but will allow to easily understand the chemical-physical properties of the films which will have a more complex bulk.

The thermal behaviour and phase sequence of all silver complexes have been investigated by thermogravimetric analysis (TGA) and differential scanning calorimetry (DSC).

The TGA analysis and its derivate (DTG) (**Fig.2.2.3.6** and **Fig**. **2.2.3.7**) show the loss of weight corresponding to a sub-sequential complex fragmentation.

A heating range from 30 to 600 °C with a speed of 5 °C/min has been applied to all the complexes. All the thermograms show many decomposition stages, with a step particularly relevant at which can be associated the loss of the Q coordinated ligand portion. The Ag(I) complexes can be grouped in **1**, **2**, **5** and **3**, **4**, as a function of their similar thermal behaviour. The first group show a very wide decomposition stage starting at around 150 °C until 550 °C. (**Fig. 2.2.3.6)**

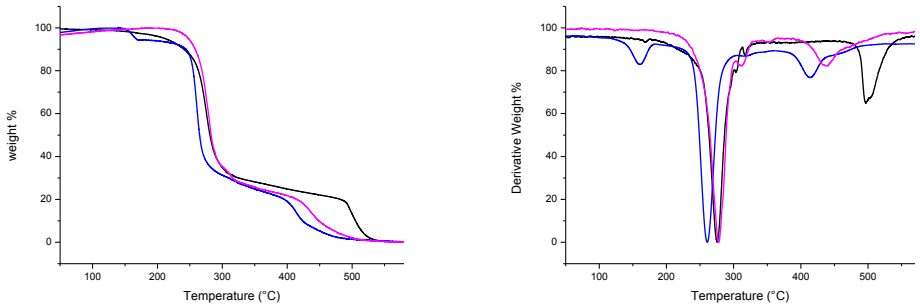

a) **b)**

Fig. 2.2.3.6 TG curves **(a)** and DTG curves **(b)** of complexes **1** (black line), **2** (blue line) and **5** (magenta line).

The thermograms of the **3** and **4** (**Fig. 2.2.3.7)** compounds is so similar that can be overlapped, in particular in the region of 300-370 °C. Up to 600 °C, a small amount of mass residue of the total mass is detectable, less than 10% for all complexes.

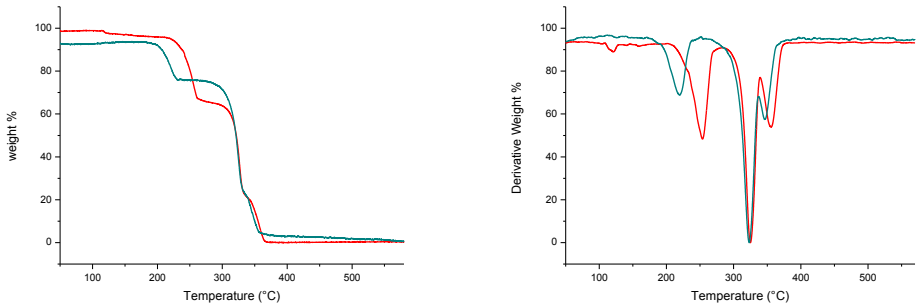

a) **b)**

Fig. 2.2.3.7 TG curves (a) and DTG curves (b) of complexes **3** (green line) and **4** (red line).

The results obtained from the TG and DTG curves show thermal decomposition behavior and the thermal stabilities are clearly observed for the complexes.

The DSC analysis performed on all derivatives, clearly prove the thermal similarities between structurally analogous Ag(I) complexes. Indeed, as reported in **Fig. 2.2.3.8**, complexes **1** and **2** show an endothermic peak in the range 158-160 °C corresponding to their melting point, while **3**, **4** and **5** derivatives melt at higher temperature values, that is 236-239 °C. **Fig. 2.2.3.9**

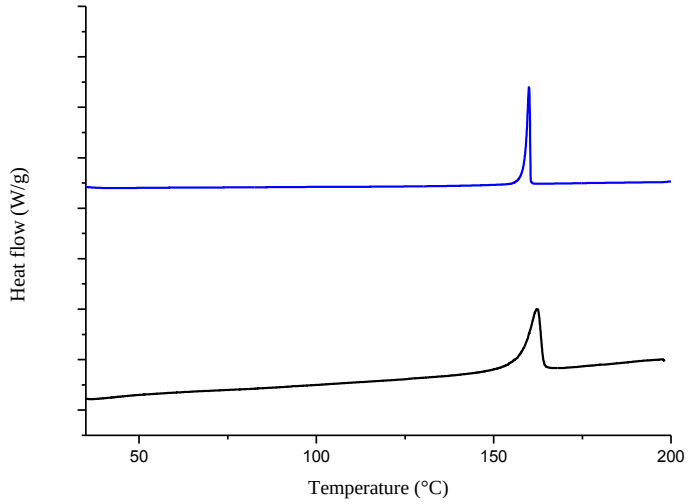

Fig. 2.2.3.8 DSC traces of complexes **1** (black line) and **2** (blue line).

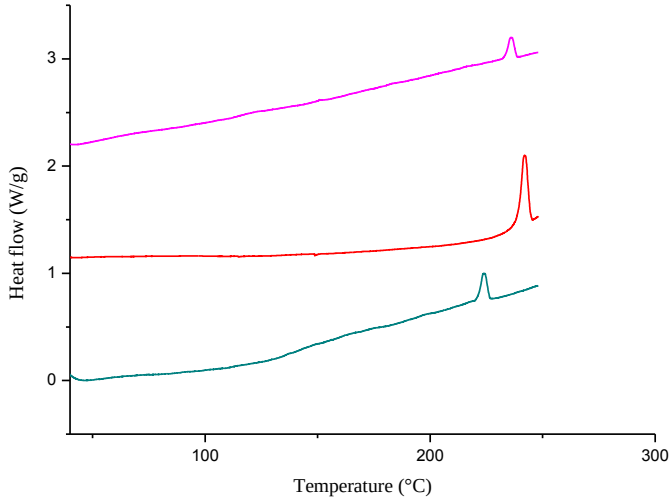

Fig. 2.2.3.9 DSC traces of complexes **3** (green line), **4** (red line) and **5** (magenta line).

From the analysis of the DSC of the two groups of complexes it can be observed that the melting point values relating to the first group **1**-**2** are very close to each other as well as the second group **3**, **4** and **5** shows a very small melting point range. Although this is a field of difficult prediction since it is the result of the contribution of various factors such as the arrangement of the molecules within the crystalline structure, the symmetry of the molecule, the intermolecular interactions and the conformational energy of the molecules it can be deduced that the packing in the solid crystalline state of the two groups of complexes could be related to their similar response to the energy necessary for their transition to the liquid state.

2.3 Synthesis and characterization of the ionic Ag(I) derivative selected as active additive

The complex **6** [(bpy-OH)$_2$Ag][CH_3COO] has been synthesized and characterized for the first time in the Mat-In Lab laboratories. [2218] The presence of the hydroxyl substituents on the bipyridine ligand induce water solubility and induce the interaction via hydrogen bonds. This last aspect is particularly relevant for the

purpose of this PhD project, since it is expected to form supramolecular structures with the EC polymer.

In order to prepare the complex **6**, it is necessary to synthesize the bipyridine ligand that constitutes it.

2.3.1 Synthesis and characterization of ligands 4,4'- bis(hydroxymethyl)-2,2'-bipyridine (bpy-OH) and the complex 6 [(bpy-OH)$_2$Ag][CH$_3$COO]

Synthesis of the [(bpy-OH)$_2$Ag][CH$_3$COO] and ligand 4,4'- bis(hydroxymethyl)-2,2'-bipyridine (bpy-OH) were prepared according to the method reported in literature with small modifications. [249][221]

2.3.2 Synthesis and characterization of [(Bpy-OH)$_2$Ag][CH$_3$COO], 6

The [(Bpy-OH)$_2$Ag][CH$_3$COO] complex has been isolated from reaction of Ag(I) acetate with the equimolar quantity of ligand bpy-OH in EtOH, under nitrogen atmosphere, in a vessel protected from light, for 4 hours (**Scheme 2.3.2.1**). The complex was obtained as a yellowish solid in a relative high yield as 80 %, after recrystallization from EtOH/Hexane. The complex was dried for several days under high pressure vacuum and subsequently was fully characterized and its proposed structures was confirmed by IR, ^{1}H NMR and elemental analysis.

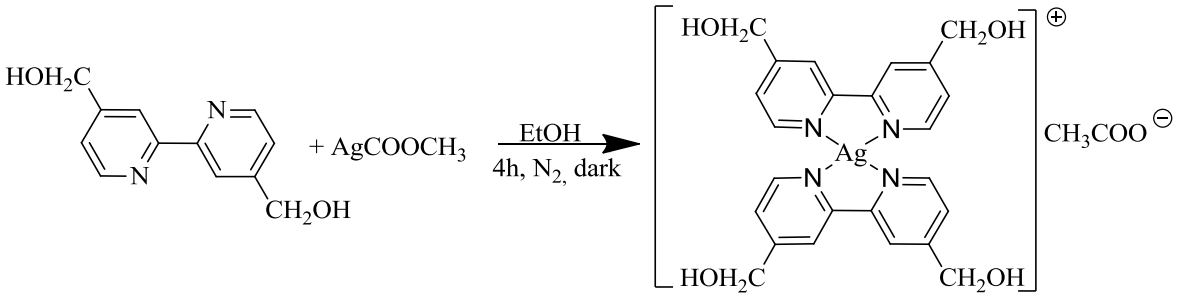

Scheme 2.3.2.1 Syntheses of Complex **6**.

The IR spectra of the complex shows a large band at 3369 cm^{-1}, regardless of several attempts to dry the powders, and therefore reasonably attributable to the 2,2'-bipyridine and –CH$_2$OH substituents. Furthermore, is observed a corresponding

[249] G.Will, G. Boschloo, S. Nagaraja Rao and D. Fitzmaurice, J. Phys. Chem. B, 103, 8067-8079, **1999**

asymmetric and symmetric stretching vibration frequencies for the carboxylate counterions at around 1560 cm^{-1} (ν_{as} (COO-)) and at 1390 cm^{-1} (ν_{asy}(COO-)), respectively. [250] The ^{1}H NMR spectra of the complex **6**, recorded in CD_3OD solutions shows the signals corresponding to the protons of the carboxylate counterions and the protons of the coordinated ligand, the integration being indicative of the 2:1 ratio between the ligand and the counterion. In particular, it is possible to observe in the aromatic region the signals corresponding to the 12 protons of the Bpy-OH ligands, while in the aliphatic region the singlet corresponding to the methylene group of the Bpy-OH at 4.91 ppm and a singlet corresponding to the alkyl protons of the carboxylate counterion at 1.89 ppm. The elemental analysis data performed on complex **6** confirmed the proposed structure presented in scheme **2.3.2.1**.

2.3.3 Structural and thermal and characterization of ionic Ag(I) derivative selected as active additive, 6

The crystal structure of complex **6**, (**Fig. 2.3.3.1)** proving the ionic nature of the derivative and the tetra-coordination geometry around the metal centre of the cation, with two chelated bypiridine ligands, has been already reported. [228]

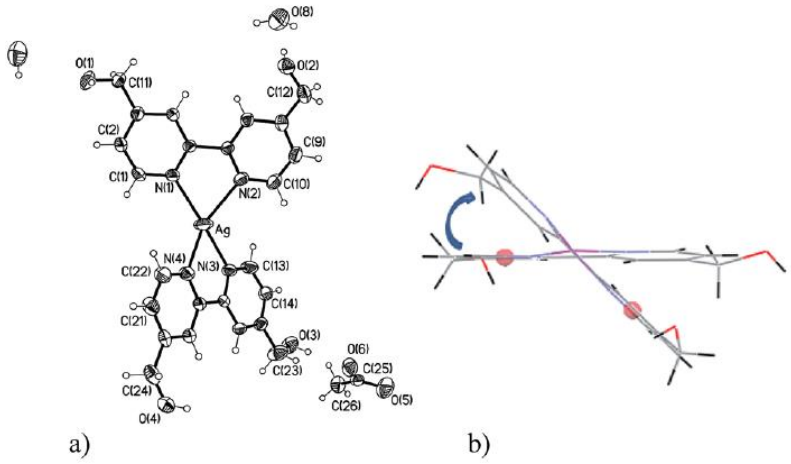

Fig 2.3.3.1 Perspective view of ionic complex **6** with an atomic numbering scheme (ellipsoids at the 50% level) (a) and the crystallographic independent complex **6** cation in Λ configuration (b).

[250] N. W. Alcock and V. M. Tracy, *J. C. S. Dalton*, 2243-2246, **1976**

Considering the structure of complex **6**, the relative orientation of the two ligands creates a helicity around the metal ion, and the absolute configuration has been properly resolved. To date, a wide pool of liquid crystals based on Ag(I) coordinated to differently substituted pyridines have been synthesized. The nature of ligands, substituents and/or counterions define the symmetry of the mesophase formed by these Ag(I) complexes. [228]

Chromonic liquid crystals are characterized by their particular features combining the liquid crystalline properties (self-ordering, alignment, sensitivity to conditions) and optical and electro-optical properties. Two principal chromonic mesophases may be defined, the N (nematic) and M (hexagonal) phases. In the N phase the columns are organized in a nematic array with no positional order, while the M phase is formed by columns ordered in a hexagonal lattice (**Fig. 2.3.3.2**). [251].

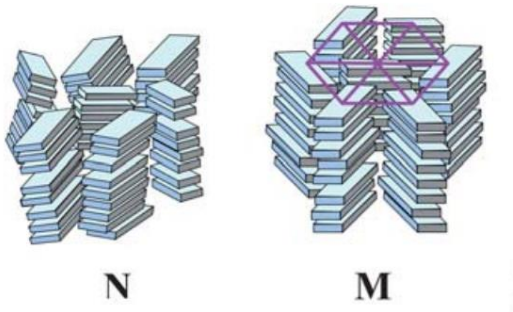

Fig. 2.3.3.2 The schematic chromonic N and M phases

The stability of the N and M phases depends on temperature and phase concentration. The majority of chromonic liquid crystals systems are obtained from molecules with an aromatic planar core featuring solubilizing groups at the periphery of the molecular structure, which self-assemble in columns through electrostatic and π–π interactions. [252] Through the analysis of the intermolecular interactions within the asymmetric unit of complex **6** and its 3D crystal packing the relationships between the structure and chromonic liquid crystal properties of complex **6** may be established. [228] The formation of water aggregates species is due to the presence of water molecules either in the powder and in the crystalline solid state is due to the properly functionalized 2,2'-bipyridine with hydroxyl groups as well as to the acetate counterions. Hydrogen bonds established between the hydroxyl groups at the

[251] J. Lydon, *J. Mater. Chem*., 20, 10071–10099, **2010**
[252] P. J. Collings, A. J. Dickinson and E. C. Smith, *Liq. Cryst*., 37, 701–710, **2010**

periphery of the Ag(I) containing cation induces the formation of cation dimeric repeating units despite the potential electrostatic repulsion. The most peculiar feature in PXRD pattern of **6 (Fig 2.3.3.3 a** and **b)** confirming the presence of a chromonic M phase is a sharp high-angle reflection corresponding to the stacking repeat distance of 3.51 Å. This value is slightly larger than the stacking repeat distance of 3.40 Å, typical for organic chromonic molecules. This increase is due to the stacking within columns of non-planar molecules, which are aggregated through aromatic interactions between facing bipyridine fragments and consistent with the aromatic π–π stacking distance of about 3.6 Å found in the crystalline solid state.

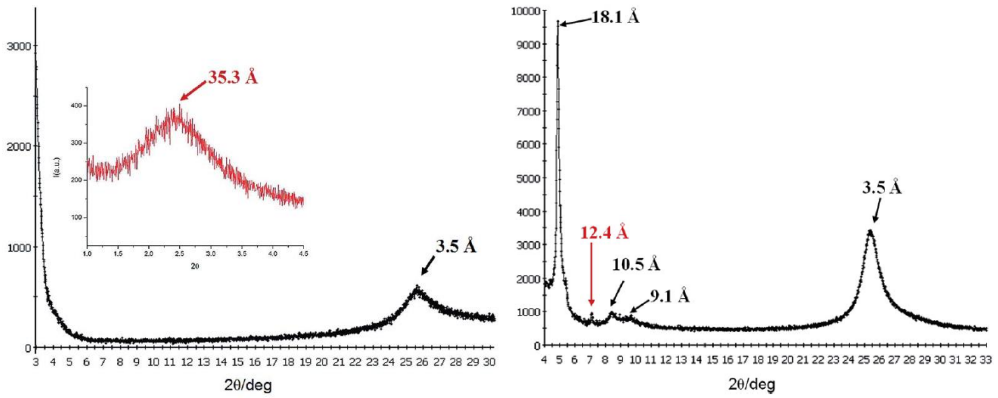

a) **b)**

Fig 2.3.3.3. Complex **6** X-Ray diffraction pattern (low angle region in the inset) in the nematic phase at 20%wt concentration (a) and in the hexagonal phase at 60%wt concentration at room temperature (b).

The phase diagram of complex **6** was determined by POM analysis and the relative mesophases were confirmed by X-Ray diffraction analysis. Water solutions of complex **6** exhibit LC phases in the concentration range from 15% to 60%.

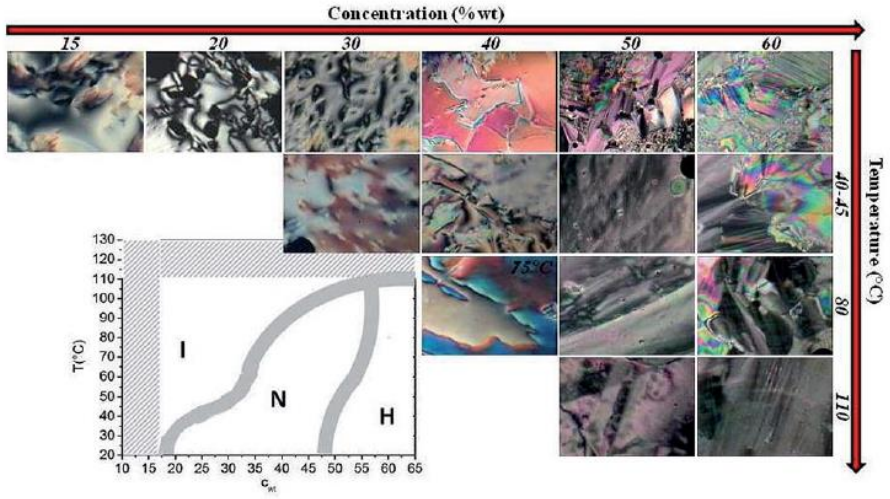

Fig 2.3.3.4 Phase diagram of complex **6** and POM pictures of the texture observed at different temperatures and concentrations, confirming the presence of LC phases.

From 15% to *ca.* 50% of concentration, at room temperature, complex **6** displays nematic (N) regions as evidenced by the typical textures observed. By increasing temperature, this phase directly melts into the isotropic phase. At higher concentrations, complex **6** assembles into a hexagonal phase (M) at room temperature. While at 50% the M phase converts to the N phase by increasing temperature before isotropization (I). At 60%, the nematic phase is suppressed, and the hexagonal phase results stable until isotropization at 120°C.

In order to evaluate how the ionic Ag(I) complex **6** can interact with the polymeric EC matrix, it has been characterized trough PXRD, TGA and DSC. [228] The characterization PXRD, which confirms the already reported data, has been realized is important because gives as the possibility to understand the chemical-physical properties of the films which will obtain through incorporation of this complex. The thermal behaviour and phase sequence of the complex **6** has been investigated TGA and differential scanning calorimetry DSC. The TGA analysis is in agreement with the data reported in literature. [2218] Thermal analysis of the complex is performed by the DSC analysis (**Fig**. **2.3.3.5)**. The complex **6** show an endothermic peak in the range 178-180 °C corresponding to the complex melting point.

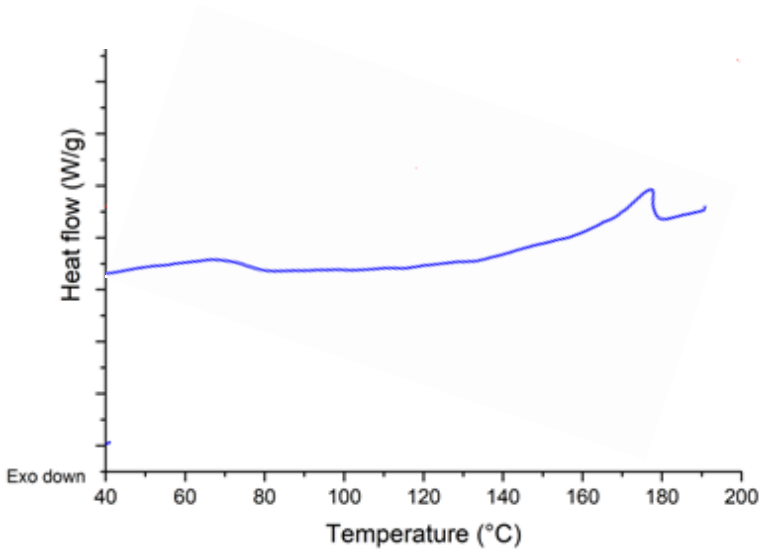

Fig.**2.3.3.5** DSC curves of complex 6**.**

Chapter 3

Preparation and Characterization of Silver(I) Ethylcellulose thin films

As stated in Chapter 1, ethylcellulose (EC) is the polymeric matrix chosen to build up active films within this PhD thesis project. EC has a semirigid nature and interesting physical and chemical properties making it quite attractive for many applications. [253] Compared to the abundant and biodegradable cellulose, EC overcomes the limitation due to the scarce cellulose solubility in almost any solvent. EC is soluble in a wide variety of solvents, making it easier to work, very stable, resistant to alkalis, both diluted and concentrated even if sensitive to acids. EC takes up very little water from moist air or during immersion. Light, visible or ultraviolet, has no discoloring action on EC.

EC is a linear polysaccharide obtained by etherification on the C6 position of cellulose, implying the partial substitution of the cellulose hydroxyl groups with ethoxyl ones along the polymer backbone. This functionalization plays a significant role in the decrease of the interchain hydrogen bonds causing an increase of the amorphous region. Nevertheless, the semicrystalline nature characteristic of EC is preserved by the remaining hydroxyl groups on the polymer backbone. [254]

EC displays thermotropic and lyotropic behavior with the formation of chiral nematic mesophases (cholesteric type). [255][256] This particular mesophase may be represented by the right- and left-handed helicoidal arrangements of twisted nematic planes where the polymer chains organize in layers with approximately parallel positional ordering (**Fig. 3.1**).

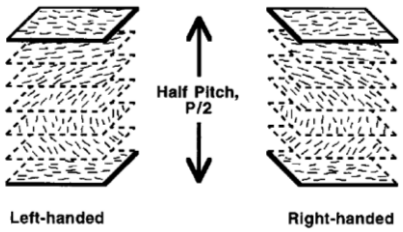

Fig. 3.1 Basic structural type of chiral nematic (cholesteric) mesophases of side-chain LC polymers. P is the helix pitch. [256]

[253] Gurvinder Singh Rekhi Sunil S. Jambhekar, *A Polymer Review*, Pages 61-77, **2008**
[254] C.Jianan, H.Yifang, Y. Jinyue, Y. Shaoqiong, and Y. Hua, *Journal of Applied Polymer Science*, Vol. 45, 2153-2158, **1992**
[255] Guo, J.-X.; Gray, D. G. *Macromolecules*, *22*, 2086-2090, **1989**
[256] S. Shimamoto, D. G. Gray, *Chem. Mater.*, *10*, 1720-1726,**1998**

However, the liquid crystalline behavior is observable in EC only when the content of ethoxyl groups on the cellulose polymer backbone reaches the 45% in weight. In this case, the EC thermotropic mesophase is recorded in a temperature range of 150-205 °C, where the texture of a cholesteric mesophase has been observed through polarized optical microscopy (POM) (**Fig. 3.2**). [256] [257]

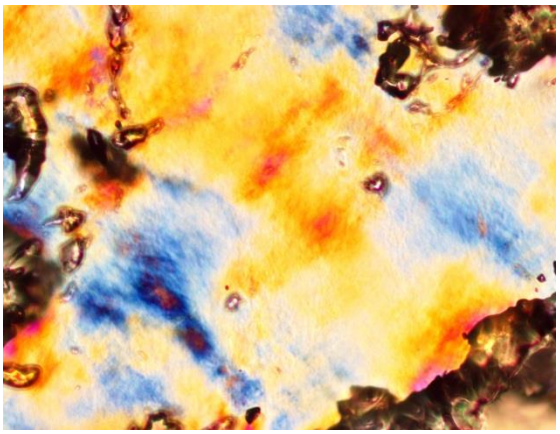

Fig. 3.2 Typical POM photograph of an EC (45% of Ethoxyl content) at 170 °C.

As regarding its lyotropic behavior, EC shows a liquid-crystalline mesophase when dissolved in halogen solvents (dichloromethane and chloroform), glacial acetic acid, and acrylic acid. As for any lyotropic liquid crystal, the mesophase is observable within a specific range of concentration that also depends on the nature of the solvent used. All the previously reported solvents induce a chiral nematic phase, similar in features to the thermotropic previously described mesophase. [258][259]

Noteworthy, EC cholesteric mesophase organisation is maintained from the solution to the solid thin film state upon slow evaporation of the solvent. [260][261][262] This particularity, which is not encounter for other lyotropic liquid crystals, is probably due to the presence of solvent molecules that are entrapped/incorporated into the polymeric film allowing the preservation of the chiral nematic organization. [256]

[257] Z. Zhang, H. Zhang, Q. Zhang, Q. Zhou, H. Zhang, Z. Mo, X. Zhao, X. Wang, *J. Appl. Polym. Sci*., **2006**, *100*, 584-592.
[258] Vogt, U. and Zugenmaier, P. (), Berichte der Bunsengesellschaft für physikalische Chemie, 89: 1217-1224, **1985**
[259] Budgell, D. R. Ph.D. Thesis, McGill University, Montreal, **1989**
[260] Gray, D. G. *Faraday Discuss. Chem. Soc. 79*, 257-264, **1985**
[261] Gilbert, R. D.; Patton, P. A. *Prog. Polym. Sci*., *9*, 115-131, **1983**
[262] Gilbert, R. D., Ed.; Hanser: New York, pp 47-70, **1994**

In the present PhD work, the EC lyotropic liquid crystalline behavior has been found fundamental for understanding the structural effects induced by the addition of Ag(I) complexes on the polymer matrix. Indeed, through Powder X-Ray Diffraction (PXRD), Diffential Scanning Calorimetry (DCS) and Polarizing Optical Microscope (POM), it has been possible to probe the effects induced by the additives into the supramolecular organization of the polymeric matrix. Furthermore, it was possible to understand how the hydrophilic or hydrophobic nature and the neutral or ionic character of the Ag(I) complexes may induce additional EC phases, with an increased amount of order within the supramolecular structure.

3.1 Preparation of the EC-*n*x films

Differently than a previous study reporting on the synthesis of Ag(I) polyethylene (PE) composite materials prepared following the dry method (based on heating, above the melting point of the plastic matrix, the mixture of PE and the biocidal additive),[263] the preparation of the EC-*n*x films has been realized following the casting method. Therefore, the EC-*n*x films have been prepared by slow evaporation of a solution in dichloromethane (CH_2Cl_2) obtained mixing the EC polymeric matrix and the different Ag(I) complexes (**1-6**) in various weight ratios.

The obtained EC-*n*x solutions were left to evaporate at room temperature when deposited on disks of silica glass in order to yield transparent films (**Fig. 3.3**), subsequently desorbed with distilled water from the silica glass disks.

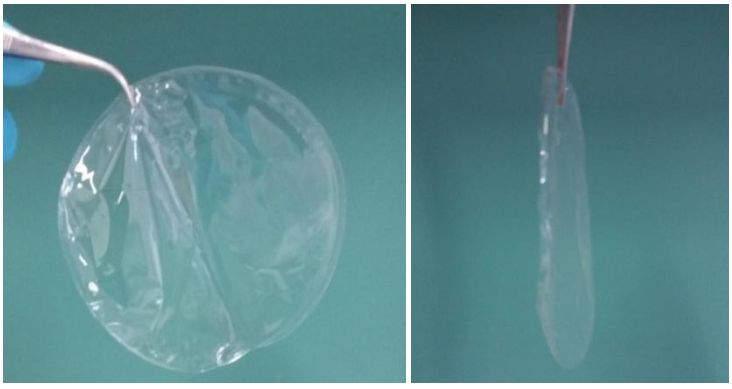

Fig. 3.3 EC-*n*x films image

[263] F. Marchetti, J. Palmucci, C. Pettinari, R. Pettinari, M. Marangoni, S. Ferraro, R. Giovannetti, S. Scuri, I. Grappasonni, M. Cocchioni, F. J. Maldonado Hodar, R. Gunnella, *Appl. Mater. Interfaces, , 8,* 29676-26687, **2016**

The combination ratio between the Ag(I) complexes and the EC polymer has been chosen following a progressive reduction of the Ag(I) complexes content into the matrix (**Table 3.1**), while the starting solutions have been prepared by different mixing procedures.

Table 3.1 Specific ratios used for the preparation of the **EC-*n*x** film, expresses in terms of w/w

	x (w/w)	n[a] (g)	EC (g)
EC-0	-	-	0.5
EC-*n*a	1:40	1.25×10^{-2}	0.5
EC-*n*b	1:2000	2.5×10^{-4}	0.5
EC-*n*c	1:5000	1×10^{-4}	0.5

[a] *n* = complexes **1**-**5,6** and **$AgNO_3$**; x = a-c, weigh ratios n/EC

Following the same preparation procedures and in the same ratio w/w used for the EC-*n*x films, (**Table 3.1**), EC-0 and EC-($AgNO_3$)x films were prepared as comparison. The EC-0 is the pure ethylcellulose polymer matrix, considered as blank, instead EC-($AgNO_3$)x is composed by ethylcellulose and silver nitrate. $AgNO_3$ is well-known for its antibacterial activity and for this reason represents the ideal reference compound. The full physical-chemical characterization of the new EC-*n*x films was performed. For those films prepared at concentration lower than 1:40 weigh ratios, between the Ag(I) complexes and the EC polymer, no significant changes in terms of physical-chemical characteristics with respect to EC-0 were observed, both at room and variable temperature. This is probably due to the high degree of dilution. EC-*n*a films, instead, represent the right balance that allowed to study and understand the nature and the relative effects of the non-covalent interactions between Ag(I) additives and the polymeric EC matrix.

The preparation of the film-forming solution of the new supramolecular aggregates, was achieved realized both in solution and in the solid states.

3.1.1 Solution procedure

The film-forming solution has been prepared dissolving the EC matrix and the Ag(I) additives in CH_2Cl_2 as solvent and leaving under stirring the solution mixture for several hours at room temperature. The choice of the solvent has been made considering that, as already described, the EC polymer transforms into the lyotropic cholesteric phase when dissolved at a specific concentration in CH_2Cl_2, and keeps the same supramolecular organization when filmed. [256] Therefore, in this condition, it has been possible to use the liquid crystalline structural organization and characterization of the EC film before the insertion of the Ag(I) complexes (named in the discussion as EC-0), in order to follow all the modification due to the interactions between the polymeric matrix and the silver additives. Moreover, once the understanding of the type and the strength of the intermolecular interactions has been achieved, an eco-sustainable and green solvent, more environmental friendly and equivalent to chlorinated solvents as dictated by the principles of green chemistry, has been chosen to prepare the new films. [264][265][266][267][268]

The green solvent, chosen for preparation of EC-*n*x films, is 2-methyltetrahydrofuran (2-MeTHF) that can be produced by biomass treatment and its use has been demonstrated in several applications. [269][270][271][272]

As it will be show in the characterization paragraph, the films obtained from 2-MeTHF show the same characteristics than those obtained from dichloromethane.

3.1.2 Solid state preparation by Liquid Assisted Grinding (LAG)

An interesting option for the preparation of EC-*n*x films has been experimented by using the mechanochemical synthesis through the Liquid Assisted Grinding (LAG) routine. [273][274][275]

---

[264] M. Smoleń, A. Marczyk, W. Kośnik, B. Trzaskowski, A. Kajetanowicz, K. Grela, *Eur. J. Org. Chem.*, 640–646, **2019**
[265]M. Nelson, in *Green solvents for chemistry: perspectives and practice*, Oxford University Press, **2003**
[266]G. Jessop, *Green Chem*., *13*, 1391–1398, **2011**;
[267]R. A. Sheldon, *Green Chem.,7*, 267–278, **2005**
[268]K. Grela, Ł. Gułajski, K. Skowerski, in *Metal-Catalyzed Reactions in Water* (Eds.: P. Dixneuf, V. Cadierno), Wiley-VCH, *8*, pp. 291–333, **2013**;
[269] A. Pellis, F. P. Byrne, J. Sherwood, M. Vastano, J. W. Comerford ,T. J. Farmer, *Green Chem.,21*, 1686-1694, **2019**
[270] R. Alcantara, P. D. de Maria, Curr. *Green Chem., 5*, 86–103, **2018**
[271] V. Antonucci, J. Coleman, J. B. Ferry, N. Johnson, M. Mathe, J. P. Scott, J. Xu, *Org. Process Res. Dev.*, *15*, 939–941, **2011**
[272] V. Pace, P. Hoyos, L. Castoldi, P. D. De María, A. R. Alcántara, *Chem. Sus. Chem.*, *5*, 1369–1379, **2012**

The reactions carried out in solution have always been used for the synthesis of new molecules but, in recent years, attention has shifted to alternative techniques such as mechanochemistry. Mechanochemistry is the branch of chemistry that is based on solid-state synthesis also called "mechanosynthesis". The mechanosynthesis includes all the reactions induced by mechanical energy and the studies the chemical-physical properties of substances subjected to the action of mechanical forces. The applications of mechanochemistry date back to prehistoric times, the first documented mechanochemical reaction occurred from the grinding of cinnabar with acetic acid, in a copper vessel, to give elemental mercury (4th century BC), the first documented method for obtaining an elemental metal from a compound. [276]

The IUPAC (International Union of Pure Applied Chemistry) defines mechanochemistry as a chemical reaction induced by the direct absorption of mechanical energy. The grinding of powdery substances and the liquid-assisted grinding (which provides the use of one or more solvents as the initiator of the reaction) generate reactive chemical species that can be subjected to mechanical chemical reactions. [277][278][279][280][281]

Mechanochemistry presents different advantages compared to traditional synthesis procedures, such as simplified process, environmental and working safety. [282] These last advantages are of considerable importance since mechanochemical reactions are conducted in absence of any solvent, or at least catalytic quantities.

Mechanochemistry is used today frequently, in many fields such as metallurgy, crystal engineering, materials engineering, the coal industry, construction, agriculture, pharmaceuticals and waste treatment. [283] Nowadays, it is well known that through mechanochemical synthesis new molecules, with the formation of covalent bonds between the reagents, with completely different properties can be

---

[273] S. L. James, C. J. Adams, C. Bolm, D. Braga, P. Collier, T. Friscic´, F. Grepioni, K. D. M. Harris, G. Hyett, W. Jones, A. Krebs, J. Mack, L. Maini, A. Guy Orpen, I. P. Parkin, W. C. Shearouse, J. W. Steedk, D. C. Waddelli, *Chem. Soc. Rev.*, , *41*, 413–447, **2012**

[274] G. Gorrasi, A. Sorrentino, *Green Chem.*, 17, 2610-2625, **2015**

[276] L. Takacs, *J. Mineral Met. Mater. Soc.*, 52, 1, 12, **2000**

[277] G.R.Desiraju, *J.Mol. Structure*, 374, 191, **1996**; b (c); d) e) F. Cavalieri, F. Padella, *Waste Manage.*, *22*, 913-916, **2002**

[278] H.Hassaballa, J.W. Steed e P.C. Junk, *Chem Comm*., 577, **1998**;

[279] C.A. Hunter e J.K.M. Sanders, J.Am. *Chem.Soc*., 112, 5525, **1990**

[280] E.l. Kim, S Paliwal e C.S. Wilcox, *J.Am. Chem.Soc*,120, 11192, **1998**

[281] Margaret C. *Etter, Acc. Chem. Res*., 23, 120-126, **1990**

[282] X.Guo, D. Xiang, G. Duan, P. Mou, *Waste Management*, Vol. 30, Issue 1, Pages 4-10, **2010**

obtained, as well as supramolecular species, such as co-crystals or salts, consisting of the formation of intermolecular interactions between reagents.

In the present work, the use of mechanochemistry represents an interesting alternative to the classic synthetic pathway for the film solution preparation since there is an almost total solvent removal and substantial particle size reduction. The particles reduction causes a major amount of surface exposure inducing a maximization of the interaction between the Ag(I) complexes and the matrix.

More specifically, the mechanochemistry has been used for the preparation of EC films with weight ratio 1:40 of Ag(I) complexes and EC polymer. As stated above, the choice of this weight ratio is due to the possibility to detect clearly the modification induced by the complexes into the EC matrix. The EC and the Ag(I) complexes have been placed in an agate ball miller, with a small amount of solvent (CH_2Cl_2 or 2-MethylTHF). After the milling process, the obtained powder was solubilized in CH_2Cl_2 or 2-MethylTHF. The dispersion has been deposited on a Petri disk obtaining a transparent film.

Speed and reaction time are surely important parameters to be taken into account. The grinding speed was fixed as high as possible, instead, the reaction time was evaluated following the reaction through PXRD, in order to disclose the best time reaction condition. As shown in **Fig. 3.4**, where the progress of the solid state mixing of complex **4** and the EC powder is reported as example title, no differences between the grinding after two hours and four hours are observed. Therefore, for all preparation, the reaction time was fixed at two hours.

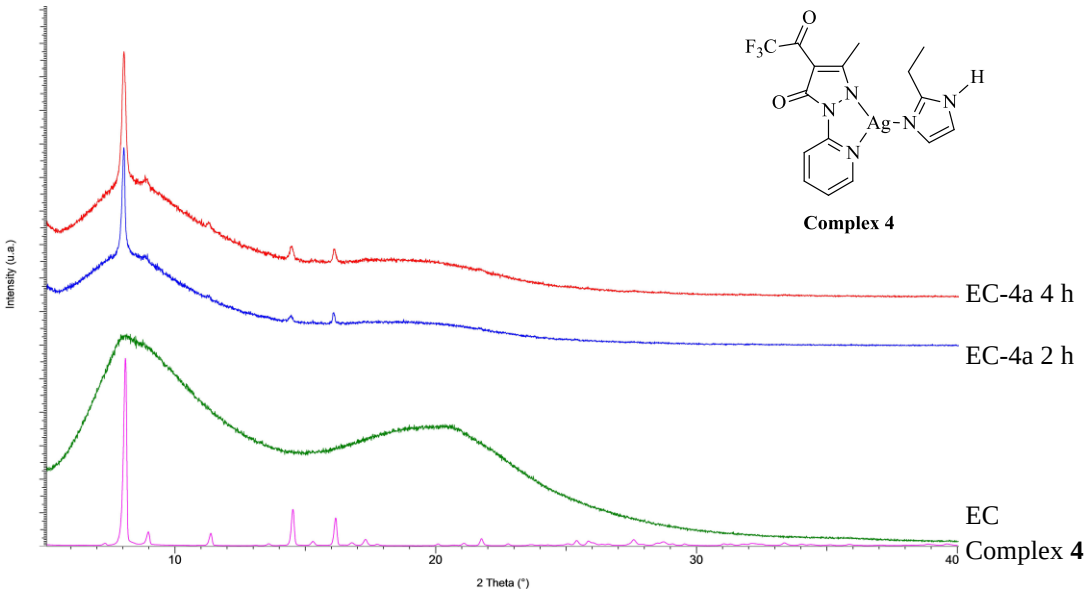

Fig. 3.4 PXRD patterns of EC-4a films obtained through LAG method as a function of time: reaction time 2h (blue line) and reaction time 4h (red line).

3.2 Chemical-physical characterization of the EC-*n*a films

All the new polymeric films have been characterized in by infrared spectroscopy (IR) and Powder X-Ray diffraction (PXRD) in order to obtain structural information and by thermogravimetric (TGA) and differential scanning calorimetry (DSC) analysis to disclose the thermal behavior. Morphological and optical investigation have been performed with polarized light optical microscope (POM), atomic force microscopy (AFM) and Contact angle measurements.

The characterization of ethylcellulose in its film state (EC-0) is mandatory in order to do the subsequent comparisons with all films incorporating the Ag(I) additives. All the characterization results obtained are in good agreement with those reported in literature.

The IR spectrum shows the typical bands such as the -OH stretching vibration at 3480 cm^{-1}, the -CH stretching at 2970 and 2878 cm^{-1}, the -CH_3 and -CH_2 bending 1450 and 1379 cm^{-1} and the -C-O-C- stretching 1060 cm^{-1}. [284] In addition, the EC-0 spectrum shows a band at 1631 cm^{-1} corresponding to the stretching and bending

[284] Desai, K. Alexander, A. Riga, *Int. J. Pharm.., 308,* 115-123, **2006**

modes of the H-O-H of the absorbed water molecules by the EC film, such as reported in literature. [285]

The thermal decomposition of EC-0 was investigated by TGA and DSC in order to study the heat resistance and the physical-chemical changes in comparison with the subsequently prepared EC-*n*x films. The thermogravimetric analysis performed in the present study shows that the EC-0 decomposition reactions occur in two main steps at maximum temperatures (T_{max}) of 347 °C and 461 °C (**Fig. 3.5**). In the first step, there is the greatest weight loss of EC-0 (87 % *ca.*) and the main decomposition compounds are water, carbon dioxide, ethanol, ethylene, unsaturated hydrocarbons, ethers, etc. In the second one a further mass reduction occurs (9 % *ca.*) and other products are formed, similar to those obtained from the thermal decomposition of cellulose but ethoxyl groups in place of hydroxyl groups. [286][287][288] Hence, at 600°C, only 4% *ca.* residual mass remains, indicating an almost complete degradation of EC-0. These stages are even more evident in the corresponding DTG curve (**Fig. 3.5**, green line). The EC-0 thermogram shows also a tiny step at 200°C *ca.*, which corresponds to a weight loss of less than 0.6%. Since this last weight loss represents a negligible weight loss and does not undergo variations across these samples, it will not be considered in this study.

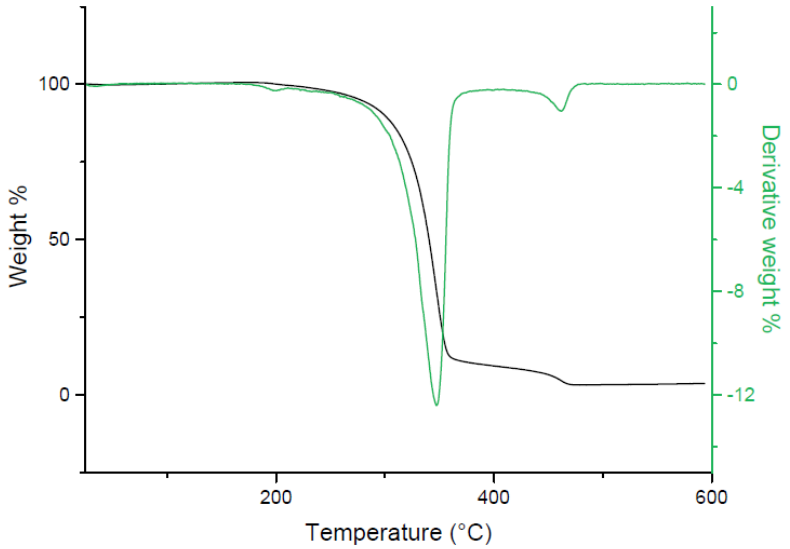

Fig. 3.5 EC-0 TGA curve (black line) and DTG curve (green line).

[285] S. Bai, S. Sridhar, A.A. Khan, *J. Membr. Sci.*, *174*, 67-79, **2000**
[286] S.C. Moldoveanu, Elsevier Science, Amsterdam, pp. 217–273, **1998**
[287] W. P. Brown and C. F. H. Tipper, *Journal of Applied Polymer Science*, Vol. 22,1459-1468, **1978**
[288] S.C. Moldoveanu, Elsevier Science, Amsterdam, pp. 217–273, **1998**

Further information on the thermal behaviour of the EC-0 film was obtained from the DSC analysis. The DSC curve of EC-0, acquired between 30 and 200 °C, (**Fig. 3.6**) shows several thermal events. [289] In particular, during the first heating run (**Fig. 3.6**, black line), a broad endothermic peak, occurring between 40 and 60 °C, emerges. This peak can be attributed to the evaporation of residual dichloromethane, being absent in the second heating curve (**Fig. 3.6**, green line). In addition, the EC-0 glass transition and melting are observed at *ca.* 130 °C and *ca.* 183 °C, respectively. These thermal events are completely reversible, as demonstrated by the presence in the cooling curve of the inverse processes, i.e. vitrification (*ca.* 126 °C) and crystallization (*ca.* 178 °C), and by the reappearance of the same events during the second heating-cooling cycle (**Fig. 3.6**, green line). The presence of both glass transition and melting is a clear evidence of the semicrystalline nature of EC-0, since the glass transition can be attributable to the amorphous areas of the polymer, whereas melting can be ascribed to the crystalline domains of ethylcellulose. [290]

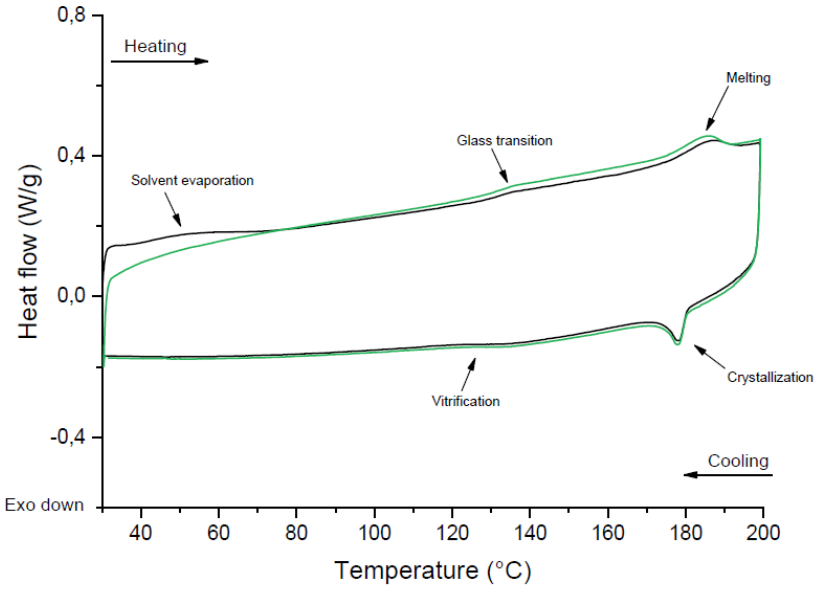

Fig. 3.6 DSC curves of the EC-0 film sample; first heating-cooling cycle: black line; second heating-cooling cycle: green line.

The semicrystalline nature of EC has been widely investigated in literature through PXRD [290][291][292][293] and SAXS (Small-Angle X ray Scattering) analysis. [294] The

[289] M. Davidovich-Pinhas, Shai Barbut, A.G. Marangoni , Annual Review of Food Science and Technology 7:1, 65-91, **2016**
[290] a) L. Bruno, S. Kasapis, P.W.S. Heng, *Carbohydr. Polym*, *88*, *1*, 382-388., **2012**
[291]L. Bruno, S. Kasapis, V. Chaudhary, K. T. Chow, P.W.S. Heng, L. P. Leong, *Carbohydr. Polym.*, *86*, *2*, 644-651; **2011**
[292]S.M. Lomakin, S.Z. Rogovina, A.V. Grachev, E.V. Prut, Ch.V. Alexanyan, *Thermochim. Acta*, *521*,*1*, 66-73, **2011**

PXRD profile of the EC-0 film (**Fig. 3.7)** is characterized by two reflections centred at 2θ of 8.2° (d value of 10.8 Å) and 19.2° (d value of 4.6 Å), respectively.

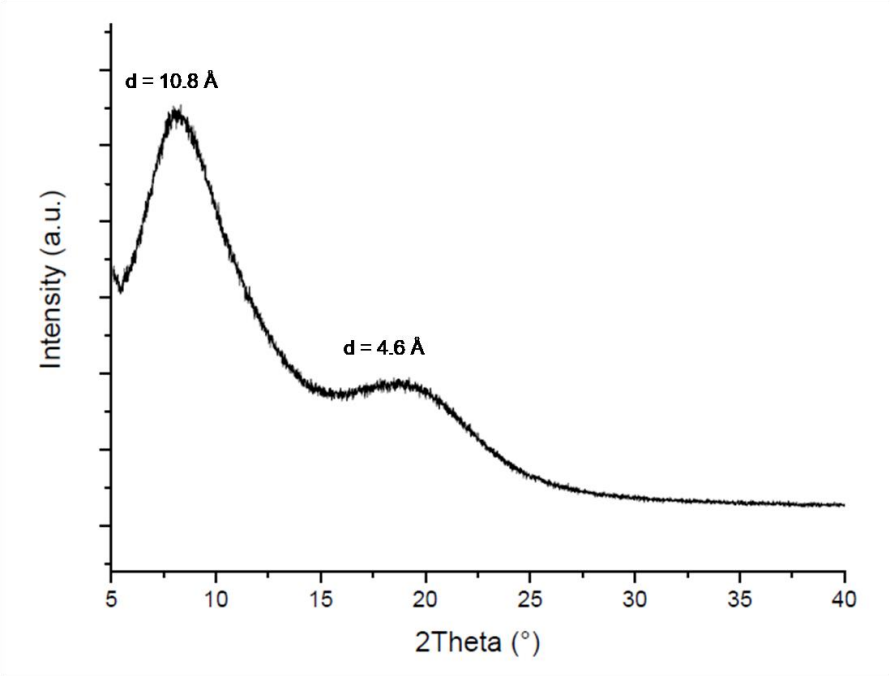

Fig. 3.7 PXRD pattern of EC-0 recorded at room temperature.

The first reflection represents the interlayer distance of the ordered polymer structures, while the high angle one gives information about the interchain distance. [295][296][297][298][299][300][301] These reflections appear as broad bands, rather than sharp peaks, indicating that EC exhibits only short range order. Hence, being the PXRD analysis performed on the EC-0 film, the pattern can be associated to the liquid crystalline nature of the EC polymer retained in the film. Indeed, since the EC-0 film retains the lyotropic liquid crystalline organization obtained in the dichloromethane solution, the PXRD pattern is the characteristic one of a nematic cholesteric liquid crystalline phase. [302]

---

[293] Y. Bingbing, S. Haixiang, W. Tao, X. Yanyan, L. Peng, K. Ying, N. Q. Jason, *Sci. Rep.*, *6*, 28509, **2016**
[294] M. Davidovich-Pinhas, S. Barbut, A.G. Marangoni, *Food Sci. Technol.*, *7,1*, 65-91, **2016**
[295] a) Hui Ling Lai, Kendal Pitt, Duncan Q.M. Craig, *International Journal of pharmaceutics*, Volume 386, 1–2,178-184, **2010**
[296] Jianan, C., Yifang, H. , Jinyue, Y. , Shaoqiong, Y. and Hua, Y., J. Appl. Polym. Sci., 45: 2153-2158, **1992**
[297] Nishio Y., Sato J., Sugimura K. *Advances in Polymer Science*, Vol 271. Springer, **2015**
[298] L. Bruno, S. Kasapis, P.W.S. Heng, *Carbohydr. Polym*, *88*, *1*, 382-388., **2012**
[299] L. Bruno, S. Kasapis, V. Chaudhary, K. T. Chow, P.W.S. Heng, L. P. Leong, *Carbohydr. Polym.*, *86*, *2*, 644-651, **2011**
[300] S.M. Lomakin, S.Z. Rogovina, A.V. Grachev, E.V. Prut, Ch.V. Alexanyan, *Thermochim. Acta*, *521,1*, 66-73, **2011**
[301] Y. Bingbing, S. Haixiang, W. Tao, X. Yanyan, L. Peng, K. Ying, N. Q. Jason, *Sci. Rep.*, *6*, 28509, **2016**
[302] U. Vogt, P. Zugenmaier, Berichte der Bunsengesellschaft für physikalische Chemie, *89*, 1217-1224, **1985**

The lyotropic mesomorphism of EC-0 has been investigated by POM analysis (**Fig. 3.8**), and the observation has been performed in two different procedures. In the first method, the EC-0 film has been dissolved into a solution at 9% of dichloromethane, exhibiting distorted fingerprint textures, similar to those observed for cholesteric liquid crystals, as reported in literature (**Fig. 3.8 a**). [303] In the second method, the lyotropic mesomorphism has been observed under POM by placing small sample pieces of the EC-0 film between two glass plates and allowing then drops of dichloromethane to enter by capillary action, ("drop-experiment") (**Fig. 3.8 b**).

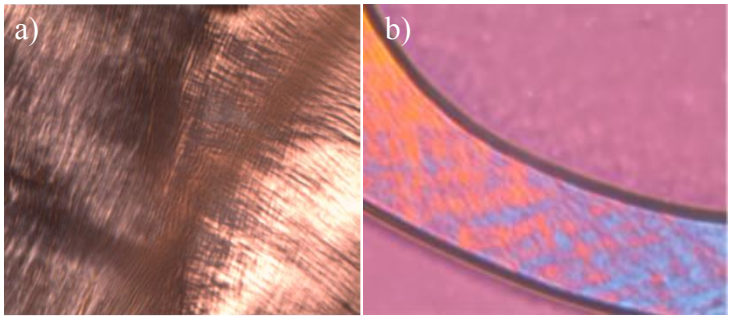

Fig. 3.8 POM textures of EC-0: 9 % (w/w) CH_2Cl_2 solution (a); dried film wet from drops of CH_2Cl_2 (b).

Also in this case EC-0 film shows distorted fingerprint textures, characteristic of a cholesteric nematic liquid crystalline phase. [304]

3.2.1 EC-($AgNO_3$)a film

EC-($AgNO_3$)x films were prepared, following the same preparation routine, incorporating $AgNO_3$ salt into the EC matrix, in the same ratio w/w used EC-*n*x films. EC-($AgNO_3$)x films have been used as a term of comparison both in the for chemical-physical characterization and in the evaluation of antibacterial properties and silver release capability of all the prepared films. $AgNO_3$ salt is a strong electrolyte, and this property compared with the complexes used for the preparation of all films, plausibly influences the rate of antibacterial activity and the release of Ag(I) ions expected to be extremely high. Moreover, the structural, thermal and

[303] M. Kléman *J. Physique*, *46*, 1193-1203, **1985** b) C. C. Yen, S. Edo, H. Oka, M. Tokit, J. Watanabe, *Macromolecules, 41*, 3727-3733, **2008**
[304] Gray, D.G.; Mu, X. *Materials* , *8*, 7873-7888, **2015**

morphologic characterizations performed on the EC-($AgNO_3$)a film has fundamental importance for understanding how a silver salt, in which the Ag(I) is not in a complex cation, interacts with EC substrate.

The FT-IR spectrum of EC-($AgNO_3$)a compared to EC-0 (**Fig. 3.9**) shows similar bands, with some differences observed in the lower wavenumber region. In EC-$AgNO_3$ film spectrum the bands to 2808 cm^{-1} and 2761 cm^{-1} (O-C-H stretching bands) of ethoxyl groups of EC matrix show the shift probably due at the closeness of Ag(I) ions. Furthermore, the EC-($AgNO_3$)a FT-IR spectrum shows a decrease in intensity of the band at 1630 cm^{-1}, relative to the H-O-H bending of absorbed water, which suggests a replacement of the water absorbed molecules with metal ions. [305] This experimental evidence, in agreement with the literature, suggests the formation of a homogeneous film where the silver nitrate salt is surrounded by ethoxyl and hydroxyl groups.

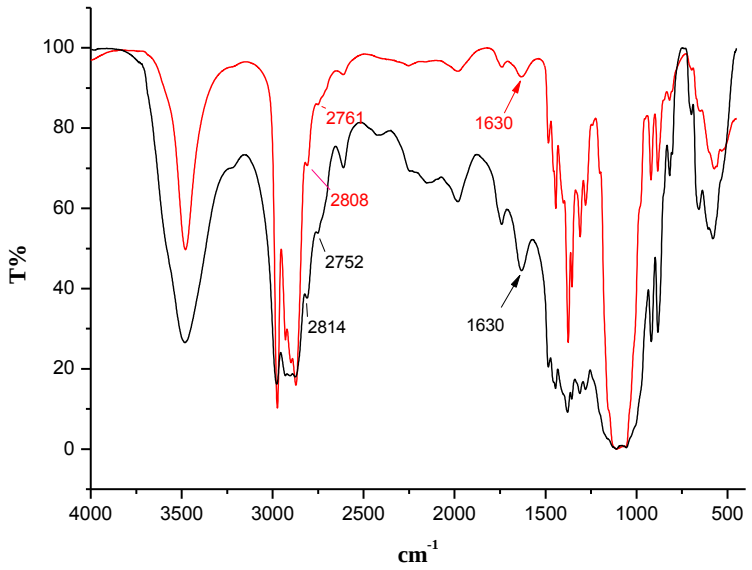

Fig. 3.9 Comparison between the FT-IR spectra of EC-0 (black line) and EC-($AgNO_3$)a film (red line)

The EC-($AgNO_3$)a thermal profile (**Fig. 3.10**) is similar to that of EC-0: the main decomposition peak occurs at the same temperature of the polymer and the second one takes place at a temperature value lower than EC-0 (416 °C). However, the

[305] S. Bai, S. Sridhar, A.A. Khan, *J. Membr. Sci.*, *174*, 67-79, **2000**

pyrolysis is faster with respect to EC-0, this effect is probably due to the oxidizing power exerted at high temperatures by silver nitrate on the ethylcellulose residue. The pyrolysis of EC-$AgNO_3$ film ends at values at lower temperature values respect EC-0, and, it is less complete than EC-0, since the residual mass accounts for 5.03 %.

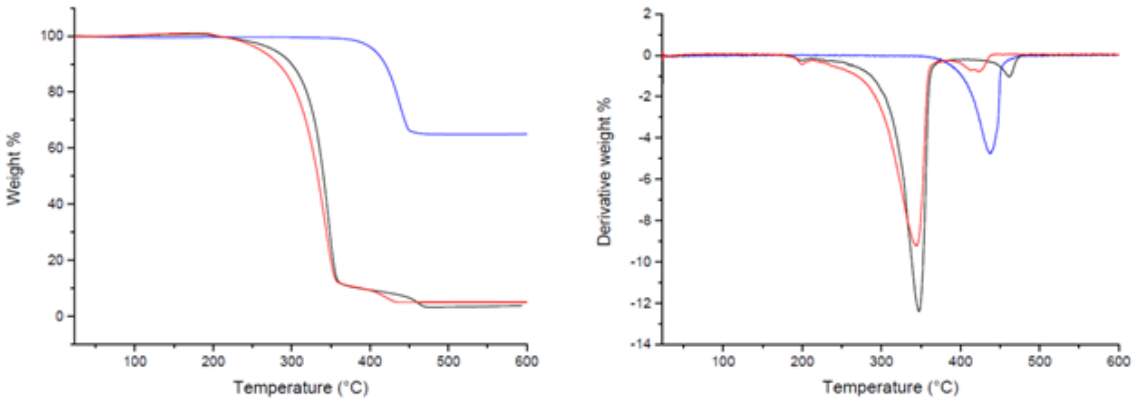

Fig. 3.10 TG curves (a) and DTG curves (b) of EC-0 (black line), $AgNO_3$ (blue line) and composite EC-($AgNO_3$)a (red line).

The DSC profile of the EC-($AgNO_3$)a is perfectly superimposable to that of EC-0, featuring the same temperature transitions and showing no trace of the silver salt upon melting (**Fig. 3.11**).

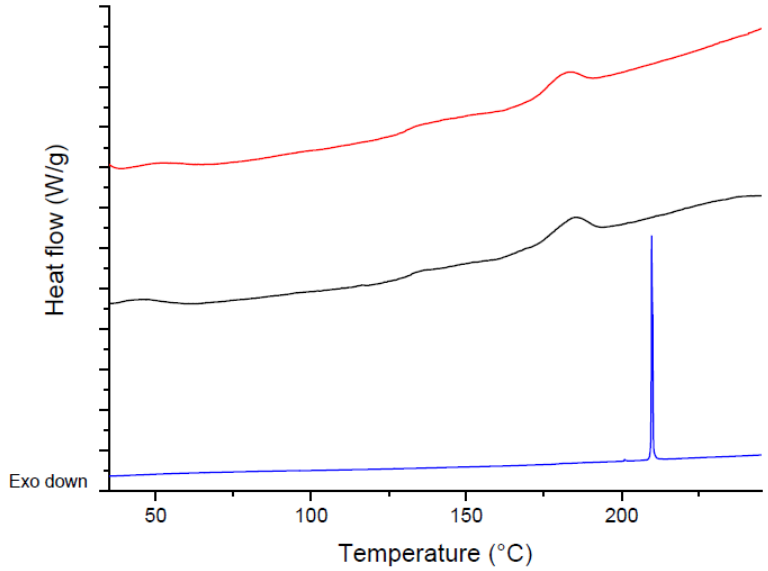

Fig. 3.11 DSC curves of EC-0 (black line), $AgNO_3$ (blue line) and composite EC-$AgNO_3$a (red line).

The EC-($AgNO_3$)a PXRD diffractogram, reported in **Fig. 3.12** is perfectly superimposable to that of EC-0. The typical $AgNO_3$ powder diffraction peaks are not detected and the PXRD profile of the EC-($AgNO_3$)a film is that of a typical amorphous film. There is no trace of the salt because it is assumed that it no longer exists in the matrix in the form of a crystalline solid but, as previously described for the IR characterization, the silver nitrate salt dissolves into the EC matrix, in a kind of "solvate" mode, by the ethoxy and hydroxy groups of the EC matrix. The highly homogeneity of the film leaves to guess that the silver salt is deeply dispersed within the matrix.

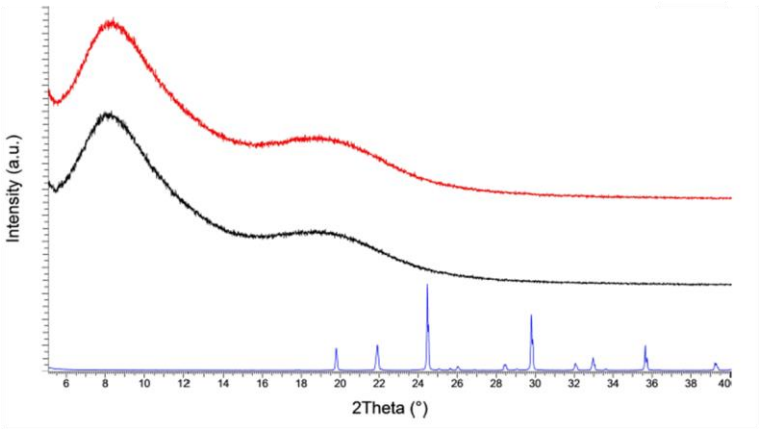

Fig. 3.12 PXRD patterns of EC-0 (black line), $AgNO_3$ (blue line) and composite EC-$AgNO_3$a (red line).

The POM analysis was performed to disclose the mesophase and to evaluate the homogeneity of the sample. The surface of the EC-($AgNO_3$)a film (**Fig. 3.13**) shows weakly birefringence and quite homogeneous texture as that already observed for EC-0.

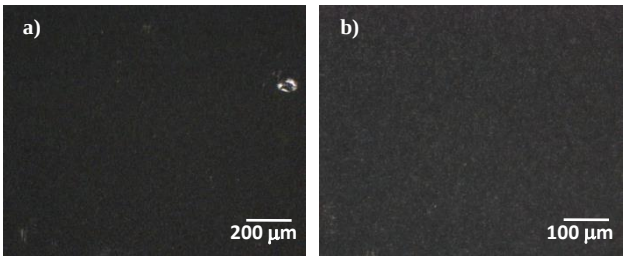

Fig. 3.13 POM images on two different scales of EC-($AgNO_3$)a sample recorded at room temperature.

In order to verify if the addition of the $AgNO_3$ salt into the polymeric matrix leaves unchanged the lyotropic liquid crystalline behavior of the neat EC-0 film, film samples were prepared both dissolving EC-($AgNO_3$)a at 9% (w/w) in dichloromethane and placing a dried film of EC-($AgNO_3$)a between two glass plates wet by drops of CH_2Cl_2. As shown in **Fig. 3.14** in both cases, the POM textures show the same birefringent textures observed in the case of EC-0 sample, pointing out that the inner structure of the polymer in its liquid crystalline organization has been preserved (**Fig. 3.8**).

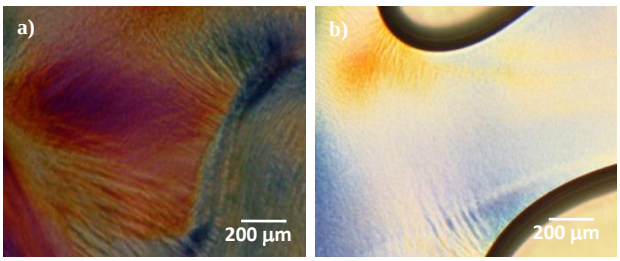

Fig. 3.14 POM textures of EC-($AgNO_3$)a: 9% (w/w) CH_2Cl_2 solution a); dried film wet from drops of CH_2Cl_2 b).

All the characterizations of the EC-($AgNO_3$)a film allow to conclude that the silver nitrate salt dissolves into the EC matrix, where ethoxyl and hydroxyl groups within the EC polymeric backbone surround the Ag(I) ions. Thus, the polymeric organization has been maintained.

3.2.2 EC-*n*a films with Ag(I) neutral complexes as additives

As introduced at the beginning of this chapter, the films prepared at 1:40 weigh ratios represent the right balance to obtain significant information on the interaction between Ag(I) additives and the polymeric EC matrix. In **Fig. 3.15** a schematic representation of combination of the EC powder the Ag(I) complexes and the picture of the final films is reported.

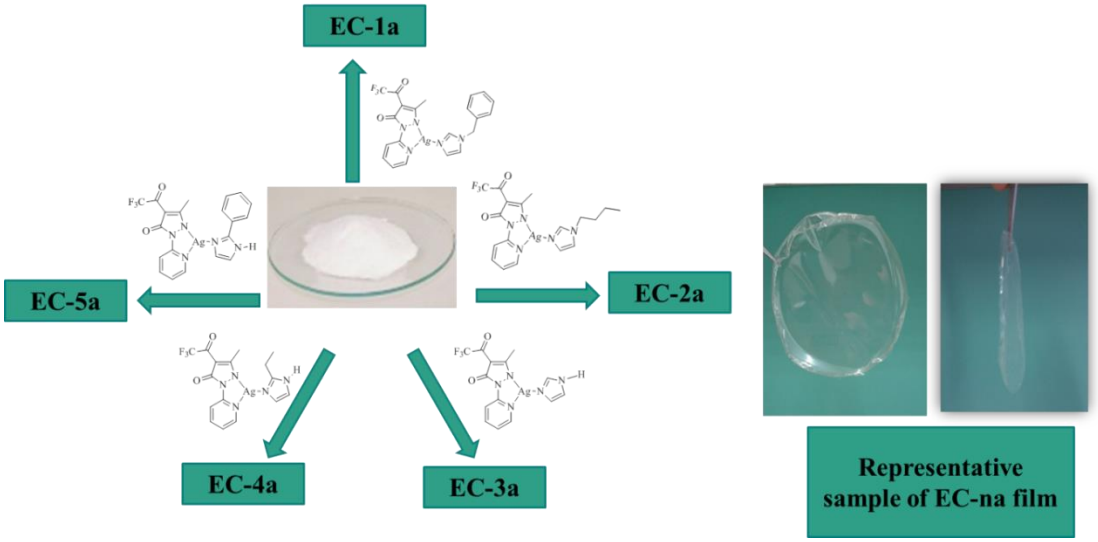

Fig. 3.15 Schematic representation of combination of the EC powder the Ag(I) complexes and the picture of the final films.

The physical-chemical characterizations of the new EC-*n*a films are discussed below. The discussion has been done grouping the films as a function of the different structural features of the Ag(I) complexes, which is the functionalization on the imidazole ring.

.

3.2.2.1 EC-1a and EC-2a films

The grouping of films EC-1a and EC-2a was made according to the functionalization on the imidazole ring; these films were prepared by using complexes **1** and **2**, both lacking of the N-H synthon, potentially able to establish hydrogen bonds with and within the polymeric matrix.

As first characterization, the FT-IR spectra have been recorded. The IR spectra of EC-0, complexes **1** and **2** and the correspondent films EC-1a and EC-2a are reported in **Fig. 3.16**. The FT-IR spectra of EC-1a and EC-2a films do not show any significant difference in the wavenumber range between 4000-2500 cm-1 between them and with respect to that of EC-0 spectrum. Some differences are instead observed with respect to the FT-IR spectra of the starting complexes **1** and **2**, at least in the lower wavenumber region.

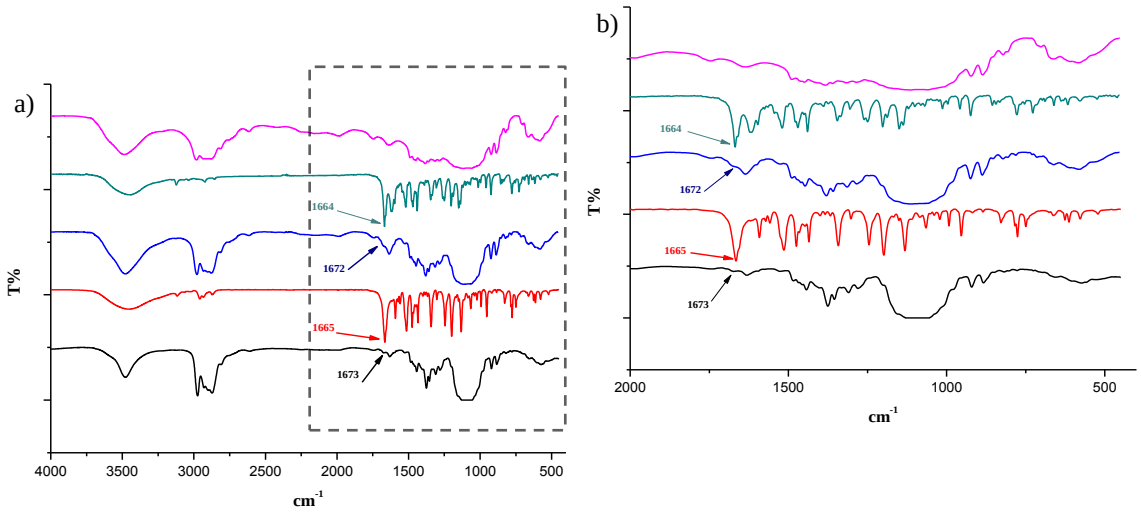

Fig. 3.16 a) FT-IR spectra of EC-0 (magenta line), complex **1** (green line), complex **2** (red line), EC-1a (blue line) and EC-2a (black line) b) inset of 2000-500 cm^{-1} of EC-0 (magenta line), complex **1** (green line), complex **2** (red line), EC-1a (blue line) and EC-2a (black line)

In particular, in the case of EC-1a film the band at around 1664 cm^{-1} (**Fig. 3.16**), attributable to the C=O stretching vibration of the Ag(I) complex **1** carbonyl group, is found slightly shifted at 1672 cm^{-1}, while the C=O stretching vibrations of the Ag(I) complex **2** carbonyl group is shifted from 1665 cm^{-1} to 1673 cm^{-1}. This band moves to higher wavenumber suggesting the existence of weak van der Waals interactions between the complexes and the EC matrix, similarly to what has already been observed in polyethylene composites containing Ag(I) acylpyrazolonato additives. [306]

The thermal behaviour of EC-1a and EC-2a films differs from that of EC-0 as the decomposition occurs in a single step rather than two steps, as proved by the TG analysis (**Fig. 3.17**). Nevertheless, it is worth to note that in the case of EC-1a, a shoulder at 363 °C accompanies the single peak with the maximum at 342 °C. In the case of EC-2a, this peak at 333 °C is rather broad and not very sharp as the first one detected in the EC-0 spectra. Thus, it can be concluded that the pyrolysis of both films is faster than that of EC-0. In addition, the decomposition peak of the films presents only slight differences, in terms of onset temperature and T_{max}, with respect to the first pyrolysis step of EC-0. Interestingly, it should be noted that at the end of

[306] F. Marchetti, J. Palmucci, C. Pettinari, R. Pettinari, M. Marangoni, S. Ferraro, R. Giovannetti, S. Scuri, I. Grappasonni, M. Cocchioni, F. J. Maldonado Hodar, R. Gunnella, *Appl. Mater. Interfaces*, *8*, 29676-26687, **2016**

pyrolysis, the mass of the EC-1a and EC-2a, are respectively 0.40 % and 0.34% of the total mass, indicating that the thermal decomposition of the films is more complete than that of EC-0 (**Fig. 3.17 a** and **b)**. Thus, the EC-1a and EC-2a are slightly less stable, at high temperatures, than EC-0.

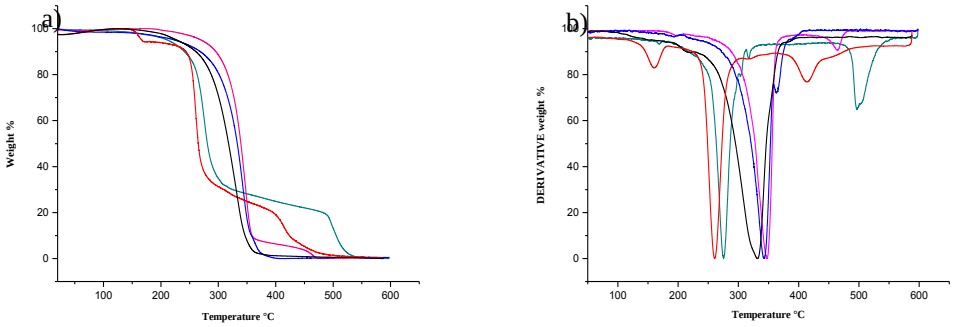

Fig. 3.17 TG curves (a) and DTG curves (b) of EC-0 (magenta line), Ag(I) complex **1** (green line), Ag(I) complex **2** (red line), EC-1a (blue line) and EC-2a (black line).

The thermal characterization of the new films has been completed with the DSC analysis.

The comparison between EC-0, complexes **1** and **2** and their films is shown in **Fig. 3.18**. The EC-1a DSC profile, together with the presence of the endothermic peak deriving from dichloromethane residues evaporation, as observed for EC-0, exhibits a single thermal event at 158 °C *ca* attributable to a glass transition. The presence of a single transition in the DSC curve of EC-1a film indicates compatibility and miscibility among the film components. [307][308] Indeed, the complete disappearance of the typical transitions observed for EC-0, as well as the melting peak of the Ag(I) complex **1**, states the formation of a new phase, in which complex **1** is perfectly embedded into the polymer backbone.

The DSC trace of EC-2a shows two transitions, the glass transition and melting, at 131°C and 183°C, respectively, similarly to those observed for EC-0, even if the melting peak of complex **2** is not present. Nevertheless, the clear evidence of the formation, even in this case, of a new homogeneous phase with inner interactions

[307] C. de Brabander, C. van den Mooter, G., Vervaet, C., Remon, J.P. *Journal of Pharmaceutical Sciences* , Vol. 91 , Issue 7 , 1678 – 1685, **2002**
[308] X. Wang, H. Novoa de Armas, N. Blaton, A. Michoel, G. Van den Mooter, *International Journal of Pharmaceutics*, Vol. 345, 1–2, Pages 95-100, **2007**

between complex **2** and the EC matrix, is proved by PXRD analysis and will be discussed hereafter.

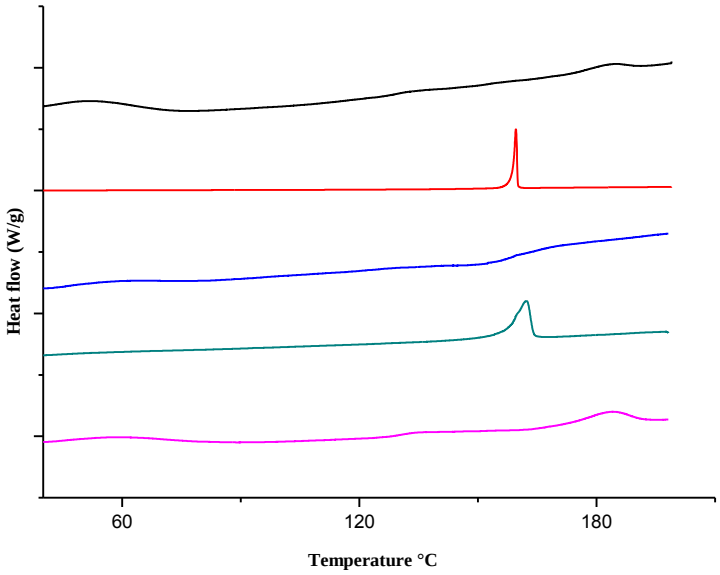

Fig. 3.18 DSC curves of EC-0 (magenta line), complex **1** (green line), complex **2** (red line), EC-1a (blue line) and EC-2a (black line).

Indeed, a deep and fundamental characterization has been then performed through PXRD analysis.

The PXRD patterns of both films show a similar shape to that of EC-0, presenting the same two broad reflections centred at 2θ 8.2° and 19.2° (*d* values of 10. 8 and 4.6 Å), thus retaining the nematic cholesteric LC phase of the EC-0 film (**Fig. 3.19 a** and **b**).

a)

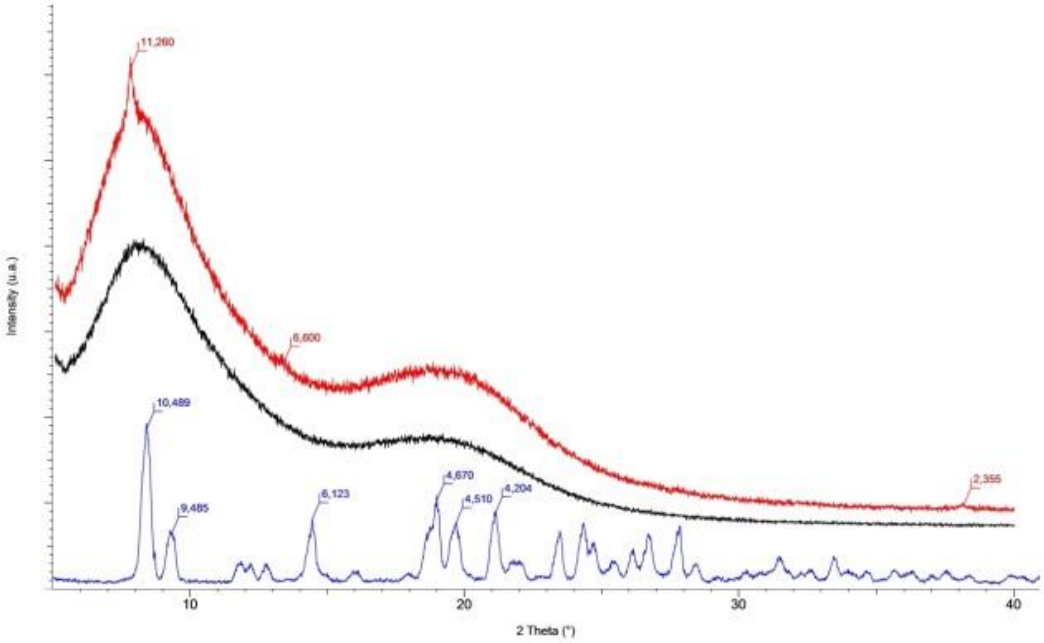

b)

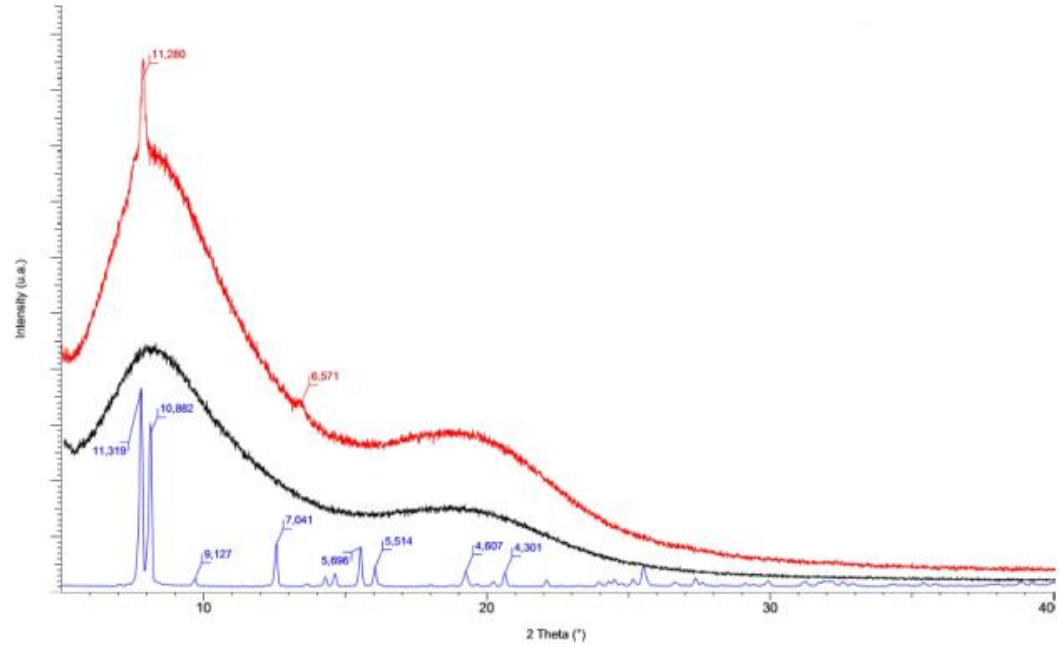

Fig. 3.19 PXRD patterns, recorded at room temperature, of EC-0 (black line), complex **1** (blue line) and EC-1a (red line) (a) and of EC-0 (black line), complex **2** (blue line) and EC-2a (red line)

Moreover, three new reflections appear in the PXRD patter of EC-1a, that cannot be attributable to the characteristic PXRD pattern of complex **1**. These new diffraction peaks correspond to *d* values of 11.26, 6.60 and 2.35 Å, which indexation (performed

through LCDixRay program) [309] highlights to the formation of a two-dimensional lattice of a hexagonal columnar phase (**Table 3.2**). Hence, the addition of complex **1** into the EC matrix induces the generation of a new local sub-organization of the polymer matrix in its liquid crystalline phase, with the coexistence of local hexagonal (H) and chiral nematic orders (N*). This coexistence apparently incompatible was observed in literature for other polymeric systems such as the poly-γ-benzil-L-glutamate and DNA. [310][311]

In the EC-2a PXRD pattern, two new reflections appear, corresponding to *d* values of 11.28 and 6.57 Å (**Fig. 3.19 b)**. Also in this case, these new diffraction peaks correspond to the formation of a two-dimensional lattice of a hexagonal columnar phase (**Table 3.2**). The addition of complex **2** into the EC matrix leads, such as for complex **1**, new local sub-organization of the polymer backbone. It can be assumed that the interaction of both complexes **1** and **2** with the polymeric matrix is the same, probably due to the similar hydrophobic nature of the complexes and the absence, in both cases, of suitable hydrogen bonding synthons.

Table 3.2 Indexation of EC-1a and EC-2a PXRD pattern

EC-1a	d_{obs}(Å)	d_{calc}(Å)[a]	h	k	Cell parameter
	11.26	11.26 [b]	1	0	a_h = 13.00 Å
	6.60	6.50	1	1	RMSD = 0.127[c]
	2.35	2.46	4	1	
EC-2a	d_{obs}(Å)	d_{calc}(Å)[a]	h	k	Cell parameter
	11.28	11.26 [b]	1	0	a_h = 12.91 Å
	6.57	6.50	1	1	RMSD = 0.095[c]

[a] Calculated data obtained using LCDixRay program [309]; [b] Data chosen for calculations; [c] Root-mean-square-difference for the calculation.

Polarized optical microscopy (POM) investigation was used to evaluate the optical homogeneity of the different films. At room temperature, EC-1a and EC-2a films

[309] N. Godbert, A. Crispini, M. Ghedini, M. Carini, F. Chiaravalloti, A. Ferrise, *J. Appl. Cryst.*, 47, 668-679, **2014**
[310] M. Kléman *J. Physique*, *46*, 1193-1203, **1985**
[311] C. C. Yen, S. Edo, H. Oka, M. Tokit, J. Watanabe, *Macromolecules*, *41*, 3727-3733, **2008**

show a quite uniform texture homogeneous with a slight birefringence similarly observed for EC-0 (**Fig. 3.20**).

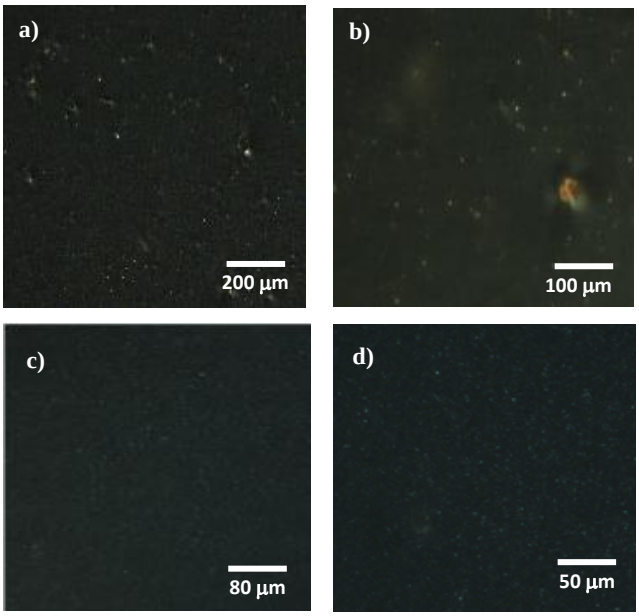

Fig. 3.20 POM images on two different scales of EC-1a (a and b) and EC-2a (c and d) films acquired at room temperature.

Further POM investigation was performed in order to understand the changes of eventual liquid crystalline behavior of the films with respect to the EC polymeric matrix. The lyotropic mesomorphism has been investigated by POM analysis (**Fig. 3.21**), and the observation has been performed in two different procedures such as previously described for EC-0 film.

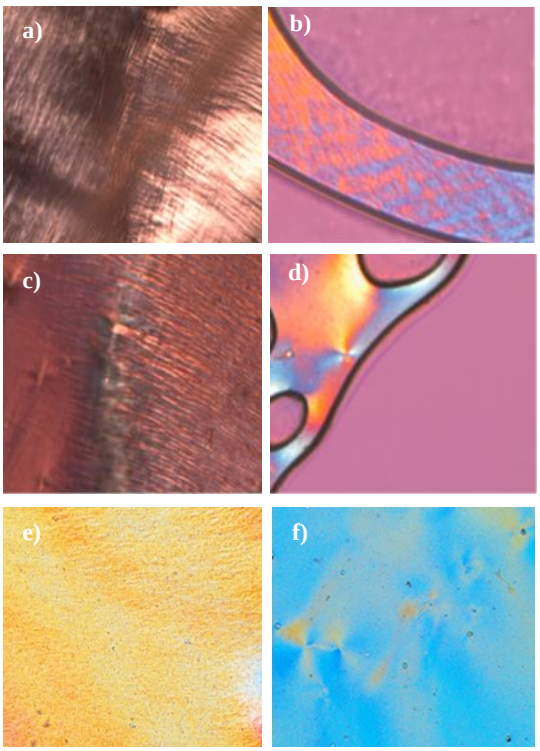

Fig. 3.21 POM textures of EC-0, (a) EC-1a (c) EC-2a (e) at 9% (w/w) CH_2Cl_2 solution; EC-0 (b), EC-1a (d) and EC-2a (f) dried film wet from drops of CH_2Cl_2.

In the conditions at 9 %(w/w) of CH_2Cl_2 solution, both EC-1a EC-2a films exhibit distorted fingerprint textures, similar to those observed for EC-0 film (**Fig. 3. 21 a**, **c, e)**. When film samples are paced between two glass plates, in both cases an undefined birefringent appears as soon as the solvent drop reaches the samples. The textures become more defined after 3 hours and in particular, the banded structure of a nematic chiral organization emerges in both EC-1a and EC-2a cases (**Fig. 3.21 c** and **e**). Furthermore, in some regions of the film samples, a focal conic fan textures, typical of a hexagonal columnar phase appears (**Fig. 3.21 d** and **f**).

This last observation confirms the PXRD analysis findings: the addition of complexes **1** and **2** into the EC polymer triggers a structural change of its supramolecular organization in the LC phase, with the coexistence of two different liquid crystalline phases.

A possible model representing the coexistence of the cholesteric and the hexagonal phases reached by the addition of complexes **1** and **2** into the polymeric matrix is reported in **Fig. 3.22**:

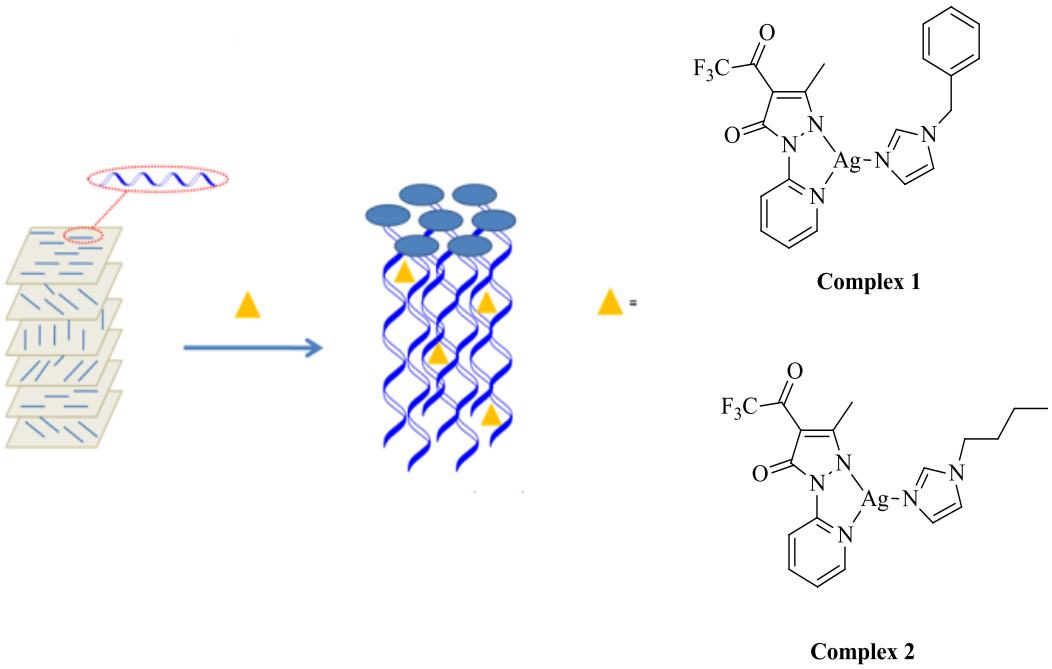

Fig. 3.22 Schematic representation of the polymer transition from the cholesteric to the hexagonal structure obtained by the addition of complexes **1** and **2**.

The schematic representation of the local supramolecular structure of the hexagonal liquid crystalline phase shows how the Ag(I) complexes,**1** or **2**, are presumably placed among the EC chains, keeping the overall cholesteric arrangement typical of the polymer backbone.

3.2.2.2 EC-3a, EC-4a and EC-5a films

The second grouping of films EC-3a, EC-4a and EC-5a was made according with the similar functionalization on the imidazole ring. In fact, complexes **3**, **4** and **5** are characterized by the presence of the hydrogen bond on the N-atom of the imidazole group. This N-H group plays a very significant role in the complex-matrix interaction and confers a hydrophilic character to these complexes. More specifically, complexes **3-5** show different functional groups in the position 2 of the imidazole ring, with an H atom in **3**, an ethyl group in **4** and an aromatic ring in **5.**

The IR spectra of EC-0, complexes **3**, **4** and **5** and their relative films EC-3a, EC-4a and EC-5a are reported in **Fig. 3.23 a** and **c**. As for the other films, also these show a very similar spectra to EC-0 one.

Interestingly, the band at around 1665 cm^{-1}, associated to the C=O stretching vibrations of Ag(I) complexes **3**, **4** and **5**, slightly shifts to lower wavenumbers (respectively, at 1656, at 1658 and 1601 cm^{-1}) in the corresponding EC-*n*a films. The observed different shifts of the carbonyl band between first group, represented by EC-1a and EC-2a, respect the second group, consists EC-3a, EC-4a and EC-5a films, suggest a different interaction mode of complexes with the EC matrix. In fact, for the latter group of films, the slight shift of carbonyl group can potentially be indicative to the formation of hydrogen bond between C=O of complexes and the hydroxyl groups of EC matrix. [312][313] In addition to what has just been described regarding the C=O stretching vibrations of IR-spectrum of EC-5 film (Fig. 3.23 c), it can be observed a further band shift, of the complex **5**, from 1663 cm^{-1} to 1678 cm^{-1}; this suggests the existence of weak van der Waals interactions between the hydrophobic substituent (benzyl group) on the imidazole ring of complex **5** and EC matrix.

[312] I. V. Rubtsov, K. Kumar, R.M. Hochstrasser, *Chem. Phys. Lett.*, *402***,** 439-443, **2005**
[313] J. Shi, W. Wang, Z. Feng, D. Zhang, Z. Zhou, Q. Li, *Polymer*, 175, 152-160, **2019**

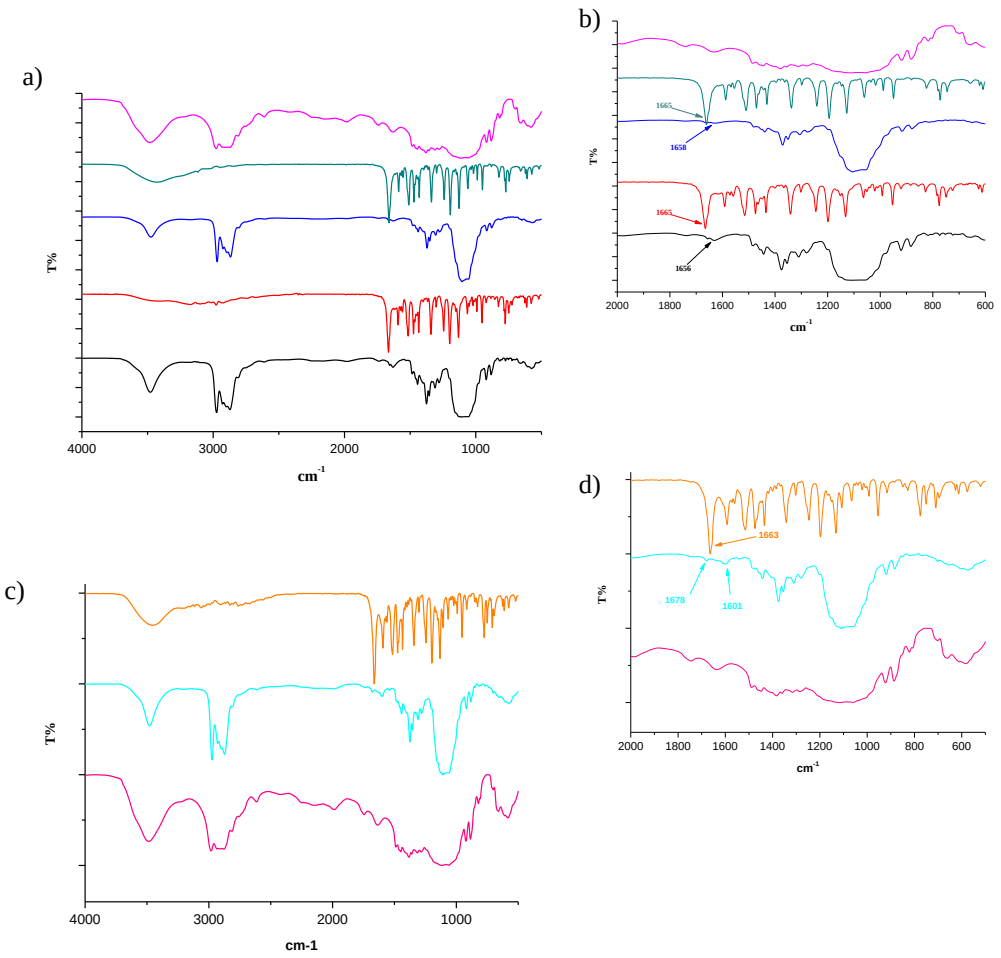

Fig. 3.23 FT-IR spectra of: **a)** EC-0 (magenta line), complex **3** (green line), complex **4** (red line), EC-3a (blue line) and EC-4a (black line) **b)** inset of 2000-500 cm^{-1} of EC-0 (magenta line), complex **3** (green line), complex **4** (red line), EC-3a (blue line) and EC-4a (black line) **c)** complex **5** (orange line) and EC-0 film (magenta line) and EC-5a (cyan line) **d)** inset of 2000-500 cm^{-1} of complex **5** (orange line) and EC-0 film (magenta line) and EC-5a (cyan line).

The thermal behaviour of EC-3a, EC-4a and EC-5a films differs from that of EC-0 as the decomposition occurs in a single thermal event rather than two. (**Fig. 3.24 a** and **c**) The EC-3a decomposition occurs which a sharp peak centred at 332 °C while the EC-4a and EC-5a present a shoulder respectively at 365 °C and 335 °C that accompanies the single peak with the maximum respectively at 349 °C and 307 °C. For all three films, the last pyrolysis process takes place at lower temperature values than EC-0, thus, it can be concluded that their pyrolysis is faster than that of EC-0. In addition, the decomposition peak of the films presents some differences, in terms of

onset temperature and T_{max}, with respect to the first pyrolysis step of EC-0 at 347 °C. Interestingly, it should be noted that at the end of pyrolysis, the mass of EC-3a and EC-5a, is 0.84% and 2.11% respectively of the total mass, indicating that the thermal decomposition of the films is more complete than that of EC-0. Conversely, the mass of the EC-4a film residues account to 5.4%, that is higher than that of EC-0, revealing that the thermal decomposition of EC-4a is less complete than that of EC-0. The thermal decomposition of all films is faster and more complete than that of EC-0, thus, revealing that these films are less thermally stable than EC-0.

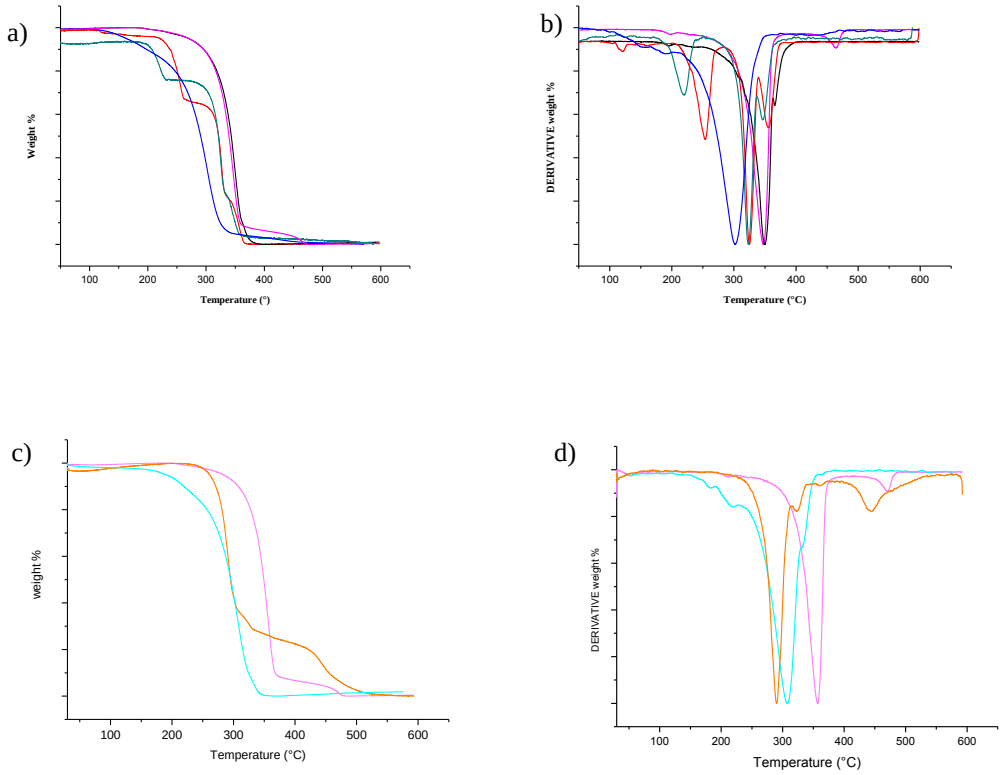

Fig. 3.24 a) TG curves and **b)** DTG curves of: EC-0 (magenta line), Ag(I) complex **3** (green line), Ag(I) complex **4** (red line), EC-3a (blue line) and EC-4a (black line) **c)** TG curves and **d)** DTG curves of EC-0 (magenta line), complex **5** (orange line) and film EC-5a (cyan line).

The thermal characterization of the films EC-3a, EC-4a and EC-5a was completed by the DSC analysis. The DSC curves obtained for EC-*n*a films have been compared with that of the EC-0 film and the respectively complexes (**Fig. 3.25 a** and **b**).

The DSC profile of EC-3a and EC-5a show two transitions, the glass transition and melting at 130 °C and 184 °C respectively, that occur at similar temperatures of EC-0. In the same way, the DSC profile of the EC-4a film shows two transitions, the glass and melting transitions at 128 °C and 179 °C respectively **(Fig. 3.25 a)**. Thus, the DSC curves of all three films, display the same transitions at the similar temperature values that of EC-0, both in term of glass transition and melting point, suggesting a type of interaction that does not significantly changes the structural design of the polymeric matrix occur with the addition of complexes **3**, **4** and **5**.

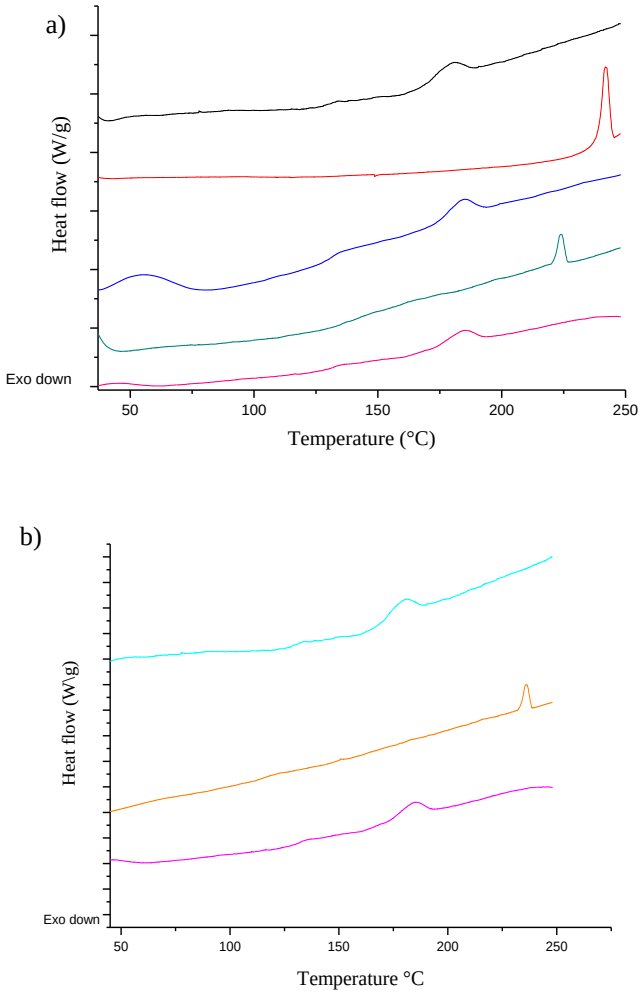

Fig. 3.25 DSC curves of **a)** EC-0 (magenta line), the Ag(I) complex **3** (green line), the Ag(I) complex **4** (red line), EC-3a (blue line) and EC-4a (black line) **b)** EC-0 (magenta line), complex **5** (orange line) and film EC-5a (cyan line).

In order to better understand this different scenario, PXRD analysis was performed and provides explanation that is more detailed. In fact, the PXRD patterns obtained for the EC-3a, EC-4a and EC-5a films, shown in **Fig. 3.26 a-c** appear to be the overlapping of the diffractograms of each individual component. The PXRD patterns of the three films show two broad reflections similar to that of EC-0, and in each film the diffraction peaks of the respective complexes are present without any significant modification in terms of shifts. The PXRD results suggest that not intimate interactions are formed between the complexes **3**, **4** and **5** and the polymer matrix, hypothetically the complexes molecules remain on the EC surface establishing superficially interactions.

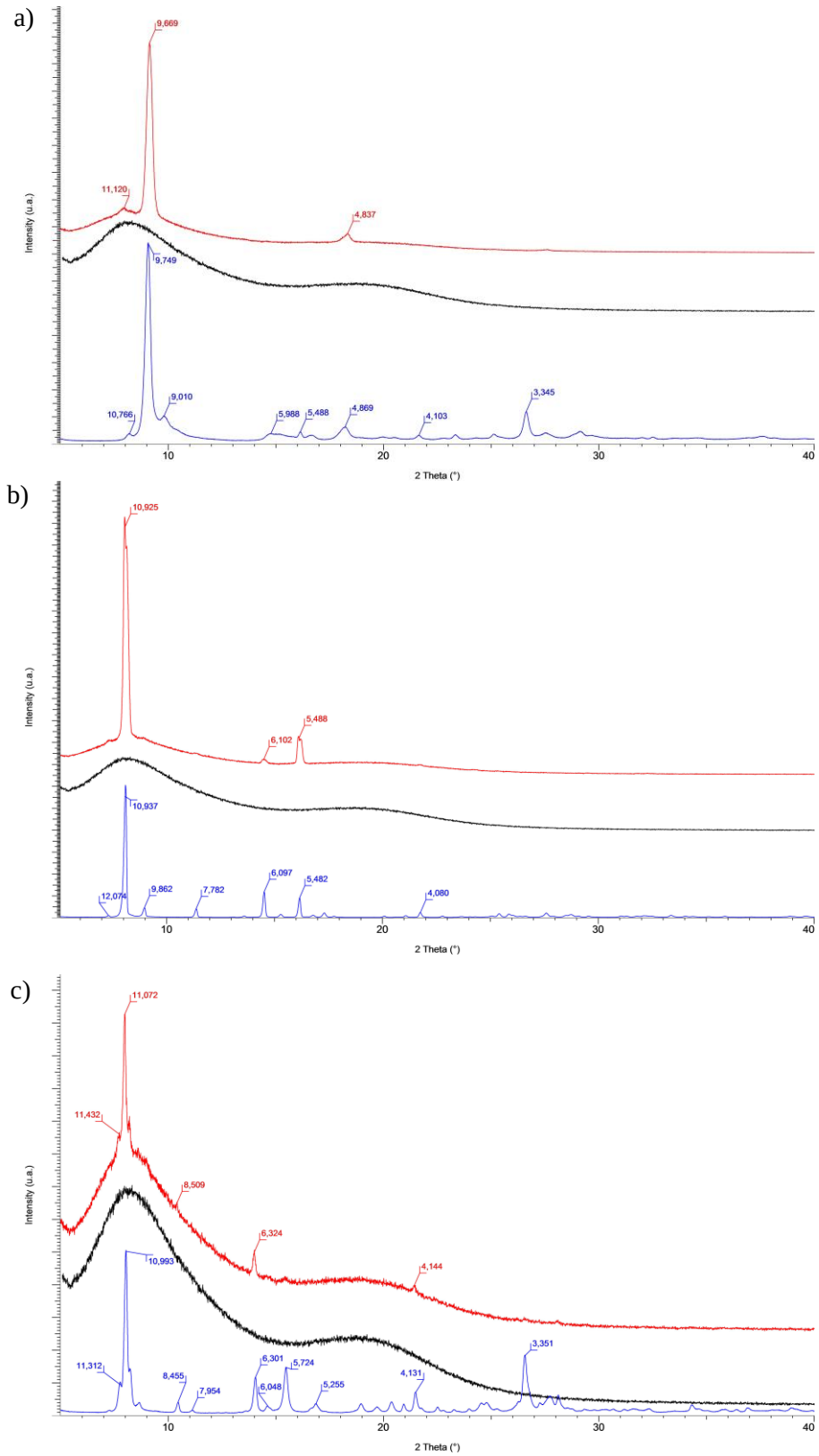

Fig. 3.26 PXRD patterns, recorded at room temperature, of a) EC-0 (black line), complex **3** (blue line) and EC-3a (red line), b) EC-0 (black line), complex 4 (blue line) and EC-4a (red line) c) EC-0 (black line), complex **5** (blue) and EC-5a (red line) (c).

The result, described above, observed through PXRD finds a further confirmation by POM analysis, performed at room temperature, of films EC-3a, EC-4a and EC-5a. The POM micrograph of EC-3a shows the presence of birefringent elongated structures with a length of more than 130 μ (**Fig. 3.27 a** and **b)**. In the EC-4a POM image these birefringent elongated structures (**Fig. 3.27 c** and **d)** possess a length of more than 80 μ. Also in the case of EC-5a the collection of images performed presents a numerous of birefringent structures (**Fig. 3.27 e** and **f**) with length less than 50 μm.

These birefringent structures are probably formed from clusters of self-aggregate complexes molecules, randomly distributed on the EC matrix surface.

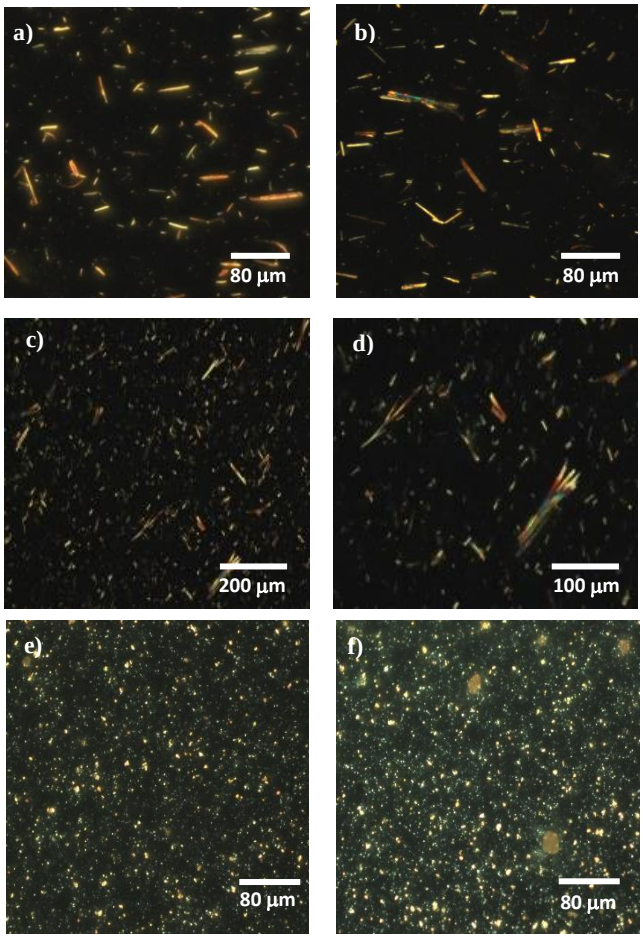

Fig. 3.27 POM images of EC-3a film (**a** and **b**), EC-4a film (**c** and **d**) and EC-5a film (**e** and **f**)

The presence of the N-H synthon on the imidazole ligand is responsible for the formation of strong intermolecular N-H···O hydrogen bonds with the carboxylic

oxygen atom of the coordinated acylpyrazole ligand, as shown by the reported structural determination of complex **3** and **4**. The crystal packing of these complexes is characterized by the formation of dimers held together through intermolecular N-H···O hydrogen bonds and, in the case of complex **4**, by intermolecular interactions involving the fluorine atoms of the -CF_3 groups and one of the methylene hydrogen atoms. (**Fig. 3.28**).

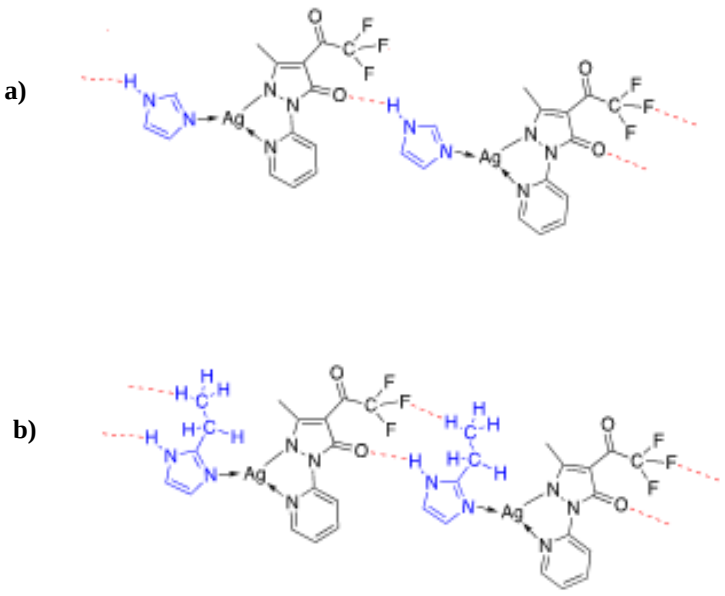

Fig. 3.28 Molecular dimers of: **a)** complex **3** formed by N-H···O and C-H···F hydrogen bonds reproduced from reference data [231] and **b)** complex **4** hypothesized on the basis of the complex analogue **3**, formed by N-H···O hydrogen bonds.

The ability of the complexes to form hydrogen bonds between itself, as described above, suggests that these complexes can interact in the same way with the polymer matrix. In fact, as observed by the chemical-physical characterizations, the complex molecules remain on the EC matrix surface with which these establish hydrogen bond interactions without significantly changing of its structure.

In the case of EC-5a, the physical-chemical characterization displays the formation of microcrystals of complex **5** dispersed on the surface of the polymeric matrix. In the EC-5a the hydrophilic character conferred by the group N-H of the imidazole ring of complex **5** prevails on the presence of the hydrophobic substituent on the same imidazole ring. The interactions established between complex **5** and the

polymeric matrix probably via hydrogen bonds, are similar to those occurring for films EC-3a and EC-4a on the EC matrix surface. The results obtained from the chemical-physical characterizations performed on the EC-3a EC-4a and EC-5a films suggest that the addition of complex **3**, complex **4** or complex **5** to the EC polymer does not cause deep structural changes of the EC-0 supramolecular architecture. Indeed, the complex molecules remain on the EC matrix surface establishing hydrogen bond interactions without significantly changing of its structure.

3.2.3 EC-*n*a film with an example of a Ag(I) ionic complex

The EC-6a film is prepared using a ionic complex as silver additive. Complex **6**, such as previously described in Chapter 2, shows that the Ag(I) ion is in a tetra-coordination geometry bis-chelated by two bipyridine ligands and forming a stable ionic complex with acetate as counter ion. The ionic complex **6** showed in **Fig. 3.35** displays the metal center surrounded by hydroxyl groups which may have a fundamental role in the interaction via hydrogen bond with EC matrix.

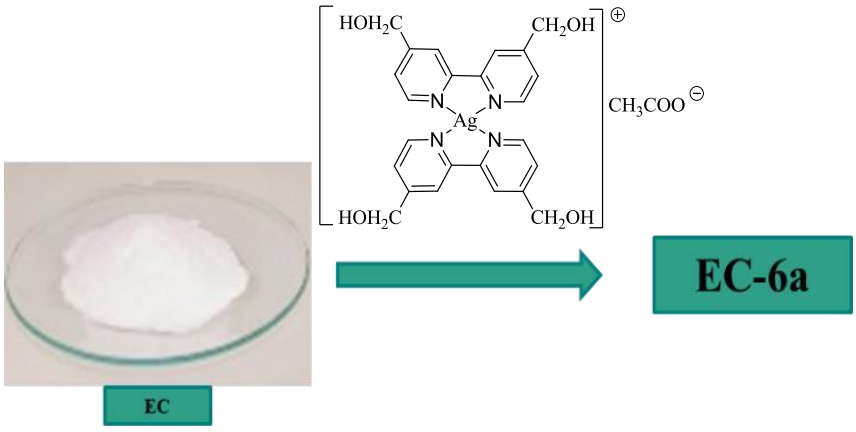

Fig. 3.35 Schematic representation of the EC matrix and the structures of the ionic complex.

Structural, thermal and morphological characterizations were performed in order to disclose the effect caused on the film by the introduction of the ionic complex.
FT-IR spectra of the Ag(I) complex, the EC-6a film and EC-0 are reported in **Fig. 3.36**.

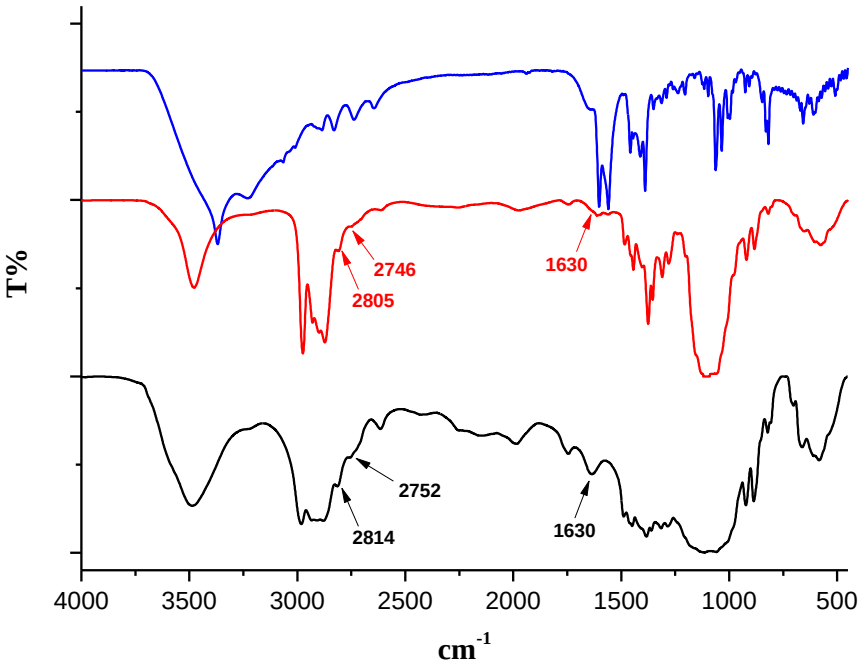

Fig. 3.36 FT-IR spectra of EC-0 film (black line), EC-6a (red line) and complex **6** (blue line)

The comparison of FT-IR spectrum of the EC-6a, complex **6** and EC-0 films shows some differences between them. The FT-IR spectrum of EC-6a displays a slight shift of the bands at 2814 cm^{-1} and 2752 cm^{-1} (O-C-H stretching bands ethoxyl groups of EC), probably it can be assumed that the ethoxyl groups of EC matrix are involved in hydrogen bonding with the hydroxyl groups of the bipyridine ligand. Furthermore, in EC-6a FT-IR spectrum the band at 1630 cm^{-1}, relative to the H-O-H bending of adsorbed water, has significant reduced-intensity respect for the same band in the EC-0 FT-IR spectrum, suggesting a plausible formation of hydrogen bonding between the hydroxyl groups on bipyridine ligand of the complex **6** with EC. Probably the interaction via hydrogen bonds to occur between the hydroxyl functions of bipyridine ligand and hydroxyl group of either polymeric backbone and of molecules of water adsorbed which are better proton acceptors than ethoxyl groups of EC. [314]

In order to study the thermal behavior and eventual chemical-physical changes of the EC-0 structure with the introduction of the ionic complex **6**, TGA and DSC analysis are performed. The decomposition of the EC-6a film occurs in a single step

[314] De Brabander C, Van Den Mooter G, Vervaet C, Remon JP., *J Pharm Sci*., 91, 7, 1678-85, **2002**

completed at a temperature value of 366 °C. The mass residue relative of EC-6a film is only 0.85% of the total mass, much lower than the mass residue of EC-0 which is 4% (**Fig 3.37 a** and **b**). The thermal decomposition of EC-6a is faster and more complete than that of EC-0, thus, revealing that the EC-6a film has a thermal stability lower than EC-0.

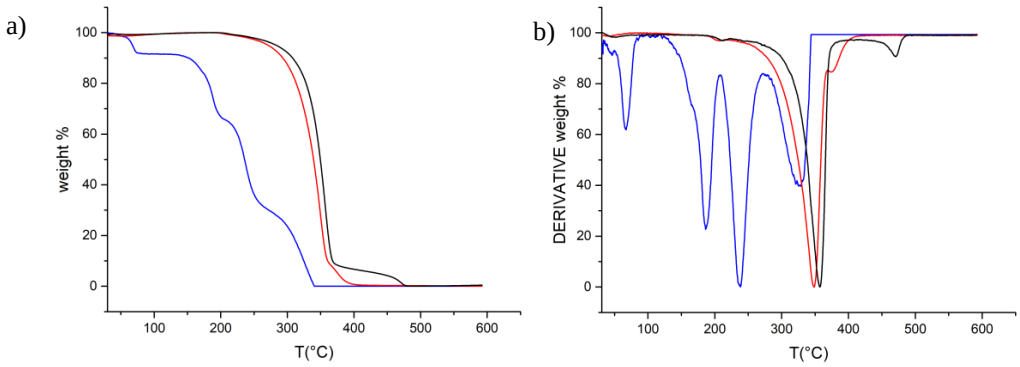

Fig. 3.37 a) TG curves **b)** DTG curves of EC-0 (black line), the Ag(I) complex **6** (blue line) and film EC-6a (red line).

Thermal behavior of the EC-6a film is completed by the DSC analysis. The DSC curve obtained for EC-6a film has been compared with that of the EC-0 film and complex **6** (**Fig. 3.38**). The DSC curve of EC-6a film shows no trace of complex **6** melting peak, while two transitions are observed, the glass transition at 130 °C and the melting at 184 °C that occur at similar temperature values than EC-0 film.

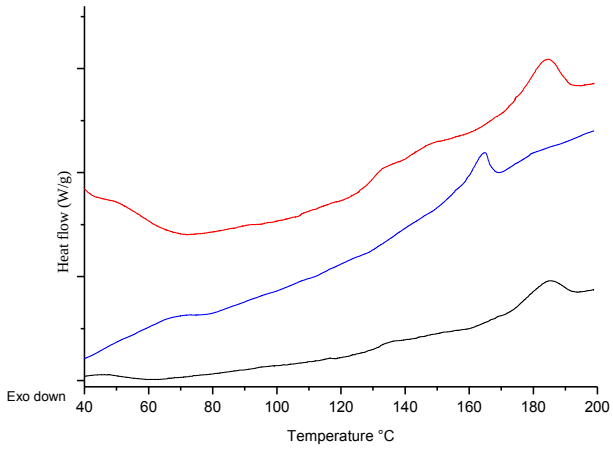

Fig. 3.38 DSC curves of EC-0 (black line), complex **6** (blue line) and film EC-6a (red line).

From the comparison between the diffractograms of film EC-6a and EC-0, reported in **Fig. 3.39**, it is clear that EC-6a XRD pattern shows the distinctive diffraction peaks of complex **6** arising from the typical PXRD profile of EC-0 (**Fig. 3.39**). Thus, the PXRD pattern of EC-6a appears to be the overlap of the diffractograms of each individual component.

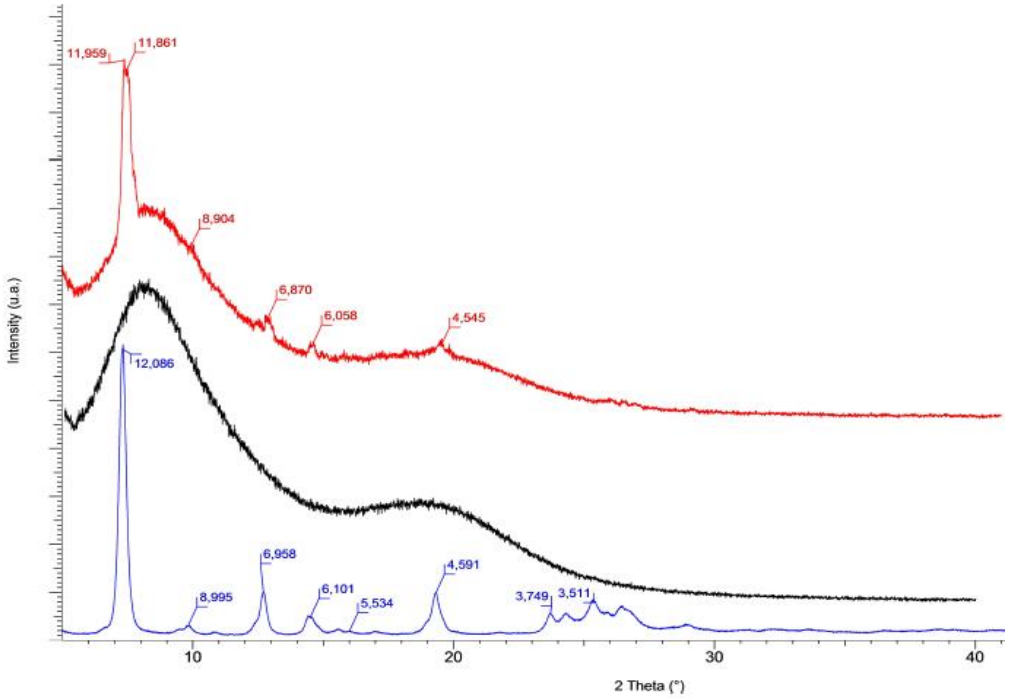

Fig. 3.39 PXRD patterns, recorded at room temperature, of EC-0 (black line), complex **6** (blue line) and EC-6a (red line).

When EC-6a is analyzed under polarized light optical microscopy at room temperature, the micrograph clearly shows birefringent punctual structures with dimensions smaller than 50 µm (**Fig. 3.40**).

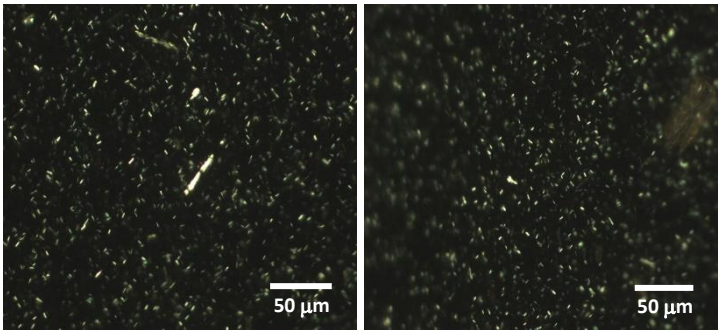

Fig. 3.40 POM images of EC-6a film.

The addition of the ionic complex **6**, such as complexes **3**, **4** and **5**, not induces an intimate interaction between complex **6** and EC matrix, which formally maintains its structural identity. The presence of the $–CH_2OH$ substituents on the bipyridine ligands in the complex cation of **6** is probably responsible for the formation of hydrogen bonds with on its surface, inducing the formation of microcrystals of complex dispersed on the surface of the polymeric matrix.

3.4 EC-*nx* films: Atomic Force Microscopy (AFM) characterization

In order to evaluate the surface topography of all films, Atomic Force Microscopy (AFM) was used. In **Fig. 3.41 a** and **b** the typical morphologies observed for EC-0 film at two different scales are reported. The EC-0 film surface appears homogenous with a granular structure when it is acquired at high resolution.

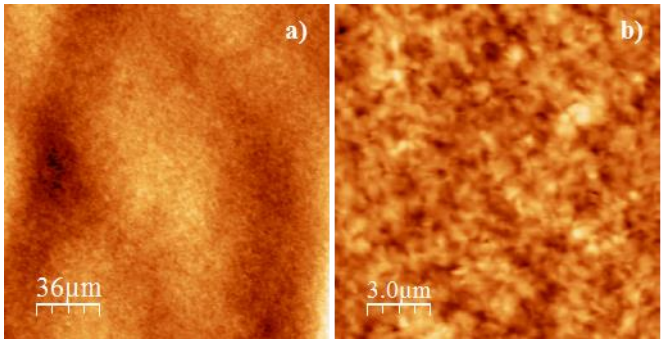

Fig. 3.41 AFM images showing the topography on two different scales of samples EC-0 (a and b).

The AFM analyses of the EC-($AgNO_3$)a film surface results homogenous with a granular structure similar to that of EC-0 film, pointing out the complete blending of the silver salt in the polymeric matrix (**Fig. 3.42**).

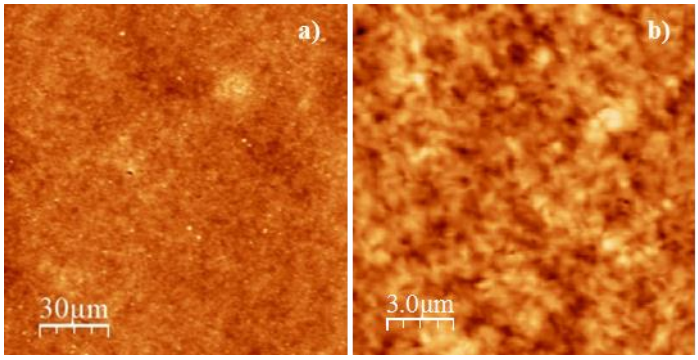

Fig. 3.42 AFM images showing the topography on two different scales of EC-($AgNO_3$)a film (**a** and **b**).

Analyzing in the same way the different films containing the Ag(I) complexes, it can be observed that the EC-1a (**Fig. 3.43 a** and **b**) and EC-2a (**3.43 c** and **d**) surfaces are similar to the observed EC-0 film (**Fig. 3.43 a** and **b**). Also in these cases the

homogeneous surface highlights the deep embedding of the complexes into the polymeric matrix.

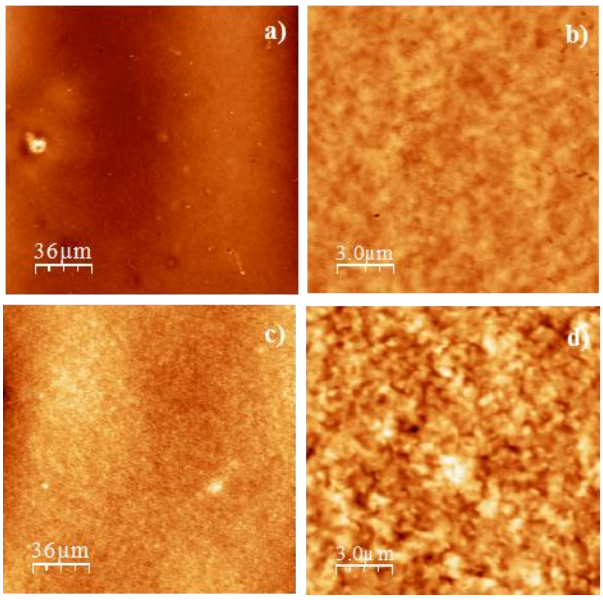

Fig. 3. 43 AFM images showing the topography on two different scales of samples EC-1a (**a** and **b**) and EC-2a (**c** and **d**).

On the contrary, EC-3a, EC-4a, EC-5a and EC-6a films, show a quite different topography with several elongated structures whose dimension changes depending on the different film, (**Fig. 3.44** and **3.45**)

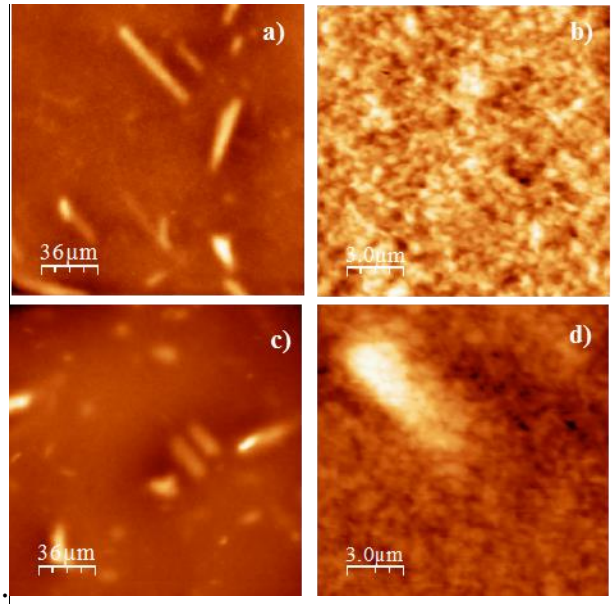

Fig. 3.44 AFM images showing the topography on two different scales of samples EC-3a (**a** and **b**) and EC-4a (**c** and **d**)

The elongated structures in the EC-3a and EC-4a films have a dimension ranging about 50 microns and around 40 microns in length, respectively (**Fig. 3.44**). In **Fig. 3.45 a** and **b** the topography of EC-5a is reported, showing agglomerates of the Ag(I) complex on the film surface. The size of the agglomerates is about 13 microns of length. In the case of EC-6a film (**Fig. 3.45 c** and **d**) the AFM pictures show a presence of several elongated structures whose dimension ranges from few microns to about 15 microns in length.

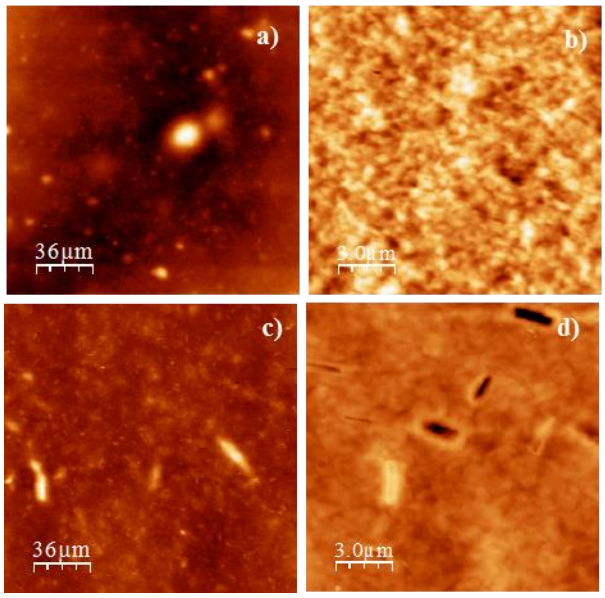

Fig. 3.45 AFM images showing the topography on two different scales of samples EC-5a (**a** and **b**) and EC-6a (**c** and **d**)

Summarizing it is observed that for the films EC-1a and EC-2a, in which the complex is complete blending in the polymer matrix, the surface of these films is similar to EC-0 and EC-($AgNO_3$)a films. For the other films, EC-3a, EC-4a, EC-5a and EC-6a, where the complexes remain on the surface, the AFM images completely different to EC-0 and EC-($AgNO_3$)a, due to the formation of microcrystals of the complexes dispersed on the EC matrix surface.

From the AFM analysis it is possible to measure the surface roughness. In recent years, the surface topography of the antibacterial materials has been studied as propriety of surface that influences the interaction with bacteria. Many works reported in the literature demonstrated the relationship between bacterial adhesion and surface topography and the possible mechanisms which are involved from the

interactions among surface topographic features and bacterial cells. Recent works have highlighted that increasing surface roughness involves a greater of bacteria cell adhesion. [315][316] Thus, in this work, the roughness analysis of the prepared films was carried out in order to evaluate how the roughness of the surface could influence the proprieties of films prepared such as the wettability [317] and antibacterial. [318]

In **Table 3.3** are reported the measurement of roughness of all films prepared.

Table 3.3. Roughness of films measurements.

Sample	nm
EC-0	**22±4**
EC-($AgNO_3$)a	**13±2**
EC-1a	**17±1**
EC-2a	**12±1**
EC-3a	**69±8**
EC-4a	**170±50**
EC-5a	**116±10**
EC-6a	**73±9**

The results of measurements of roughness show that EC-1a and EC-2a film have a similar morphological characteristic of EC-0 and EC-($AgNO_3$)a which confirms the same chemical and physical properties previously described. Indeed, for EC-3a, EC-4a, EC-5a, and EC-6a films the presence of aggregates on the film surface is reflected in a much higher value of the roughness than the EC-0 and EC- ($AgNO_3$)a film.

[315] V. K. Truong, R. Lapovok, Y. S. Estrin, S. Rundell, J. Wang, C. J. Fluke, R. J. Crawford, and E. P. Ivanova, Biomaterials 31, 3674, **2010**
[316] E. Preedy, S. Perni, D. Nipic, K. Bohinc, and P. Prokopovich, Langmuir 30, 9466, **2014**
[317] R. Norman R. Morrow, G. Mason, *Colloids and Surfaces A: Physicochem. Eng.* Aspects, 436, 392– 401, **2013**
[318] Songze Wu, Botao Zhang, Yi Liu, Xinkun Suo, Hua Li, *Biointerphases*, 13, 6, 60801-60809, **2018**

3.5 Characterization of EC-*n*x films as active materials for food packaging

3.5.1 EC-*n*x films: Water Contact Angle Measurements

The hydrophobicity, and therefore, the wettability of the all EC-*n*x films have been investigated by contact angle measurements as a function of the type of Ag(I) complexes additives and their concentration into the EC matrix. The study of this parameter is important since it will affect the properties of the final materials in terms of their potential application as active materials for food packaging (**Table 3.4**). [319]

Table 3.4. Contact angle measurements.

Sample	Θ (°) ± 2				
EC-0	66				
Samples	Θ (°) ± 2	**Samples**	Θ (°) ± 2	**Samples**	Θ (°) ± 2
EC-($AgNO_3$)a	78	**EC-($AgNO_3$)b**	68	**EC-($AgNO_3$)c**	68
EC-1a	76	**EC-1b**	74	**EC-1c**	68
EC-2a	75	**EC-2b**	64	**EC-2c**	60
EC-3a	75	**EC-3b**	71	**EC-3c**	70
EC-4a	67	**EC-4b**	77	**EC-4c**	73
EC-5a	63	**EC-5b**	66	**EC-5c**	66
EC-6a	72	**EC-6b**	74	**EC-6c**	66

The results of contact angle measurements highlighted that a discrete increase in hydrophobicity is observed in the case of EC-($AgNO_3$)a, EC-1a and EC-2a films with respect to EC-0. This is probably due to the fact that the $AgNO_3$ salt and complexes **1** and **2** establish intimate interactions with the EC matrix, forming films with new structures.

It is well known that water contact angle increases with an increase in surface hydrophobicity, this effect for the biopolymers could be due to intermolecular interactions existing under the film surface. This means that the surface obtained from embedding complex **1** or **2** it is more hydrophobic than EC-0, due to the change

[319] L.W. Chan, K.T. Chow, P.W.S. Heng, *Pharm. Res.*,*23, 2*, 408-421, **2006**

of the inner molecular organization of the EC polymer matrix given by the intermolecular interactions under the film surface. [320]

For the other films EC-3a, EC-4a, EC-5a, and EC-6a the presence of randomly distributed crystalline clusters on the surface did not allow a good comparison, with respect to the EC-1a and EC-2a films, in terms of water contact angles. Nevertheless, from **Table 3.4** can be seen that EC-3a and EC-6a show an increase of hydrophobicity respect EC-0. While the EC-4a and EC-5a films have hydrophobicity values comparable or slightly higher than the EC-0 film. The non-linear trend observed for EC-*n*x films (n=**3**-**6**) can be related to their disordered and disparity of the distribution of the protrusions on the surface due to the crystalline clusters.

As regarding the diluted EC-1x, EC-2x and EC-($AgNO_3$)x (x=b,c) films can be observed a decrease of contact angle decreasing with the Ag(I) concentration of relative films. Nevertheless, the **Table 3.4** shows for EC-1c and EC-2c films the lowest value, respectively of 68°± 2 and 60°± 2, at the lowest concentration of 1:5000 w/w in Ag(I) complex. While for other diluted films EC-3x, EC-4x, EC-5x and EC-6x (x=b,c) films is observed that some complexes induce an increase of hydrophobicity with the decrease of the Ag(I) concentration.

The wettability can be correlated directly with surface properties such as the roughness thought a number of complex factors defined by different models. [321][322]

In the histogram (**Fig. 3.46**) are reported the values of contact angle compared with roughness value. It is clear, from **Fig. 3.46**, that the values of water contact angle are higher for the EC-1a, EC-2a and EC-($AgNO_3$)a films are characterized by a smooth and homogeneous surface with roughness values comparable to EC-0. While, the other films such as EC-3a, EC-4a, EC-5a and EC-6a greater roughness values are recorder since as proved by the AFM and POM observation, the complexes molecules are randomly distributed on the surface of the EC polymeric matrix forming crystalline clusters. (**Fig.3.46**).

[320] T. J. Gutiérrez, G. González, *Food Bioprocess Technol*., *9*, *11*, 1812-1824, **2016**
[321] T. Pisuchpen, N. Chaim-ngoen, N. Intasanta, P. Supaphol, V. P. Hoven, *Langmuir*, *27*, 3654–3661, **2011**
[322] M. Sun, A. Liang, G. S. Watson, J. A. Watson, Y. Zheng, J. Ju, L. Jiang, *Plos One*, *7*,*4*,e35056, **2012**

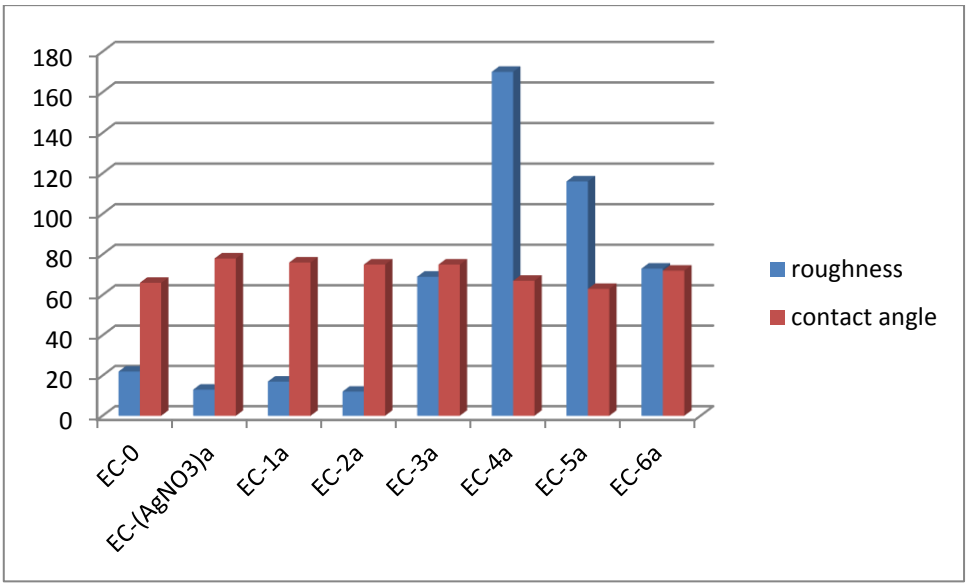

Fig. 3.46 Measurements of contact angle and correlation of the roughness of EC-*n*a films.

3.5.2 Ag(I) release towards food simulants: migration tests

Ag(I) migration from the new EC-*n*x films has been tested by using three food simulants, corresponding to a different food class, depending on the pH. In particular, distilled water (A), ethanol 10% v/v (B) and acetic acid 3% v/v (C) have been chosen and all used under two assay conditions, 70 °C for 2 h and 40 °C for ten days, according to the EU Legislation on the migration of chemicals from plastic materials. [323] Currently, Food and Drug Administration (FDA/CFSAN) allows the application of silver nitrate ($AgNO_3$) in bottled waters and the European Food Safety Authority (EFSA) has declared specific migration limit of equal or lower than 0.05 mg Kg^{-1} of food. [324][325] EC-0 and EC-($AgNO_3$)a-c were tested as negative and positive control, considering the total absence of Ag(I) components in EC-0 and assuming the maximum migration of free Ag(I) ions from EC-($AgNO_3$)a-c films. The controls and EC-*nx* films were used for all tests as squares of dimensions 5×5 cm. The measurements have been performed in order to correlate Ag(I) migration as

[323] EU Food Contact Regulations for Plastics (food packaging and food Regulations 1935/2004, 79/112/EEC and 89/109/EEC) and EU Regulation 10/2011 (The Plastics Regulation), which indicates the rules for measuring overall and specific migration. http://ec.europa.eu/food/food/chemicalsafety/foodcontact/index_eu.htm
[324] A. Martinez-Abad, M.J. Ocio, J. M. Lagaron, *J. Appl. Polym. Sci.,131*, 41001-41012, **2014**
[325] FDA/CFSAN. Food Additives Permitted for Direct Addition to Food for Human Consumption, Silver nitrate-172.167. http://www.accessdata.fda.gov/scripts/cdrh/cfdocs/cfCFR/CFRSearch.cfm?fr=172.167

function of contact liquid type, temperature and relative exposure time, and amount of Ag(I) complexes in the EC polymer. The overall Ag(I) migration values expressed in terms of milligrams per volume of the amount of Ag(I) ions detected at the various different concentration are reported in **Table 3.5** and **Table 3.6**, and plotted as reported in **Fig. 3.47** and **Fig. 3.55**.

Table 3.5. Specific Ag(I) migration from EC-*nx* square films, expressed in mg L^{-1} release in several simulants by heating at 70 °C for 2 hours. Data represent mean of least three independent measurements.

Sample	***Simulant*** [a] ***A***	***Simulant B***	***Simulant C***
EC-0	0	0	0
EC-1a	0,160	3,950	0,408
EC-1b	LOQ[326]	< 0,05	< 0,05
EC-1c	LOQ	< 0,05	< 0,05
EC-2a	0,240	1,012	0,253
EC-2b	< 0,05	LOQ	< 0,05
EC-2c	LOQ	LOQ	LOQ
EC-3a	1,180	< 0,05	2,100
EC-3b	< 0,05	LOQ	0,005
EC-3c	LOQ	LOQ	LOQ
EC-4a	1,100	< 0,05	1,630
EC-4b	LOQ	LOQ	LOQ
EC-4c	LOQ	LOQ	< 0,05
EC-5a	0,870	0,476	1,440
EC-5b	< 0,05	< 0,05	< 0,05
EC-5c	LOQ	LOQ	LOQ
EC-6a	0,480	0,128	0,386
EC-6b	0,006	< 0,05	< 0,05
EC-6c	LOQ	LOQ	LOQ
EC-($AgNO_3$)a	0,330	0,286	0,286
EC-($AgNO_3$)b	< 0,05	LOQ	< 0,05
EC-($AgNO_3$)c	< 0,05	LOQ	< 0,05

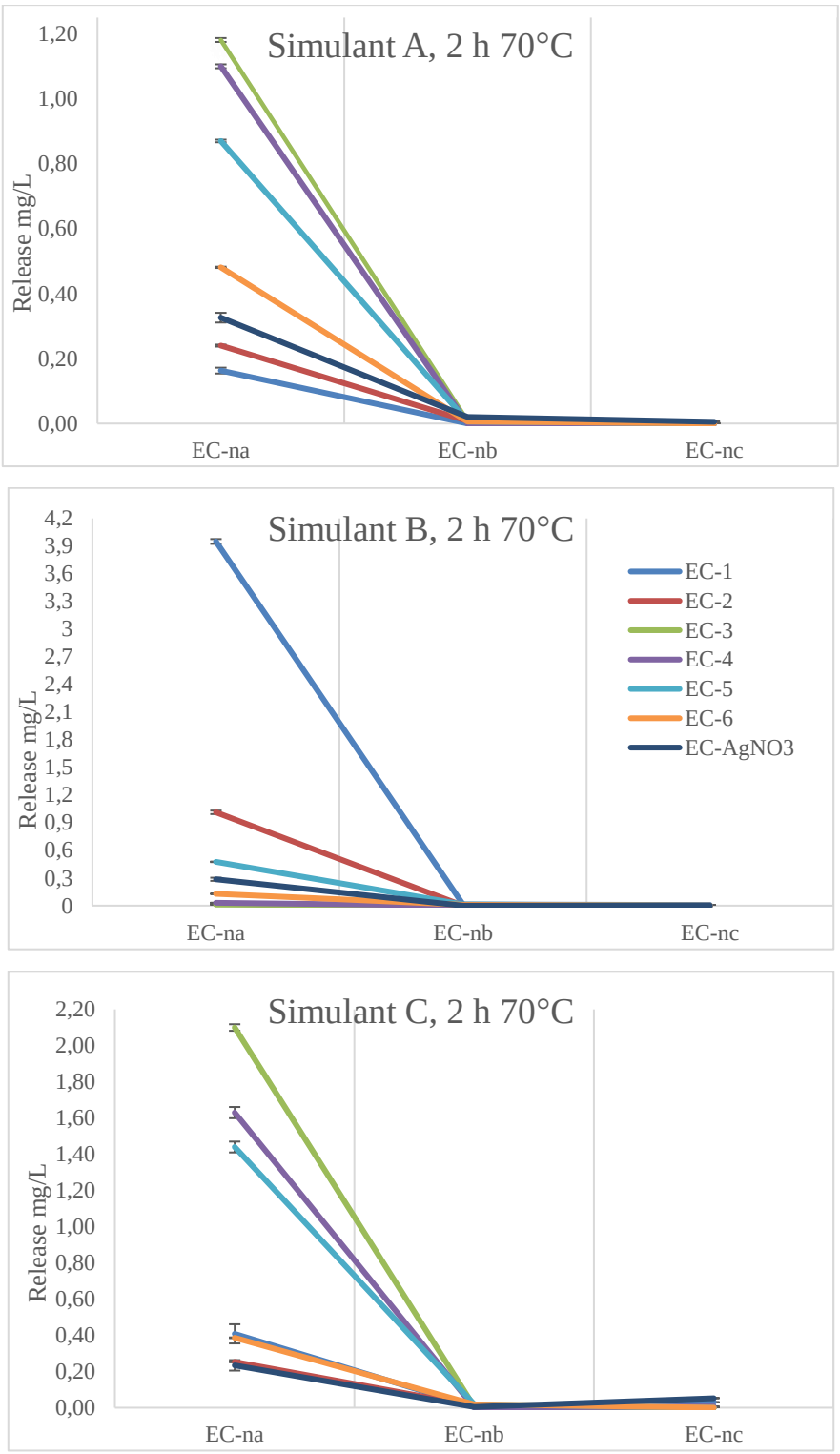

Fig. 3.47 Scatterplot showing the correlation between Ag(I) release amount in mg L^{-1} and the Ag (I) concentration in the EC matrix, at 70 °C and 2 h left, in distilled water (a), ethanol 10% v/v (b) and acetic acid 3% v/v (c).

As reported in **Table 3.5**, as well as in **Fig. 3.47**, in all cases, at concentration lower than 1:40 w/w, the EC-*n*x films show a release of Ag(I) ions below the limit set by the EU legislation of 0.05 mg Kg^{-1} or the instrumental limit of quantification (LOQ) of 0.004 mg L^{-1}. [326] Differences are then observed and discussed only in the case of the EC-*n*a films, where the behaviour is different depending on the simulant and, with the same simulant, as it will be shown, on the temperature and relative exposure time. The high temperature, with relatively low exposure time, favors the maximum release of Ag(I) ions both in distilled water and acetic acid 3% v/v, in the case of EC-3a, EC-4a, EC-5a and EC-6a films.

As it has been already discussed, all these films are characterized by the presence of silver complexes distributed on the surface of the film more than deeply included within the polymeric matrix. Therefore, the superficial interactions between the silver additives and the matrix surface could be responsible for their transfer into distilled water solution as well as their instability in acidic condition.

In the case of simulant A, EC-1a and EC-2a films shows, the minimum value of Ag(I) migration, lower than that of the EC-($AgNO_3$)a film control, probably due to the higher interaction of both complexes with the EC matrix.

As regarding the amount of Ag(I) ions detected from the diluted films (EC-*n*b and EC-*n*c, *n*=1,2,3,4,5), were lower or slightly greater than 0.004 mg L^{-1}, while in the case of both EC-($AgNO_3$)b and EC-($AgNO_3$)c films, values of about 0.02 mg L^{-1} and 0.005 mg L^{-1} respectively are recorded.

In the case of simulant B, ethanol 10% v/v, an opposite trend was observed. The maximum values of Ag(I) migration are recorded in the case of both EC-1a and EC-2a films. This finding can probably be attributed to the swelling effect exerted by ethanol on the EC polymeric matrix. The EC swelling in ethanol is due to its solubility in this solvent and, since the simulant B is made up of 10% of ethanol, it induces an increase of the release Ag^+ ion from the EC-*n*x films. [327]

The swelling effect of EC-1a and EC-2a films allows a fast release of the Ag(I) ions into simulant B because in this films the complexes are deep included in the polymeric matrix presumably within the EC chains. As further confirmation of the role played by ethanol simulant on Ag(I) ions release, a comparison of PXRD

[326] ISO-11885: Waters quality – Determination of selected elements by inductively coupled plasma optical emission spectrometry (ICP-OES);
[327] M. Larsson, J. Hjärtstam, J. Berndtsson, M. Stading, A. Larsson, *Eur. J. Pharm. Biopharm.*, 76, 428-432, **2010**

patterns of the EC-0, EC-1a and EC-2a films before and after soaking in ethanol, 10% v/v at 70 °C for 2 h, has been performed (**Fig. 3.48-3.50**).

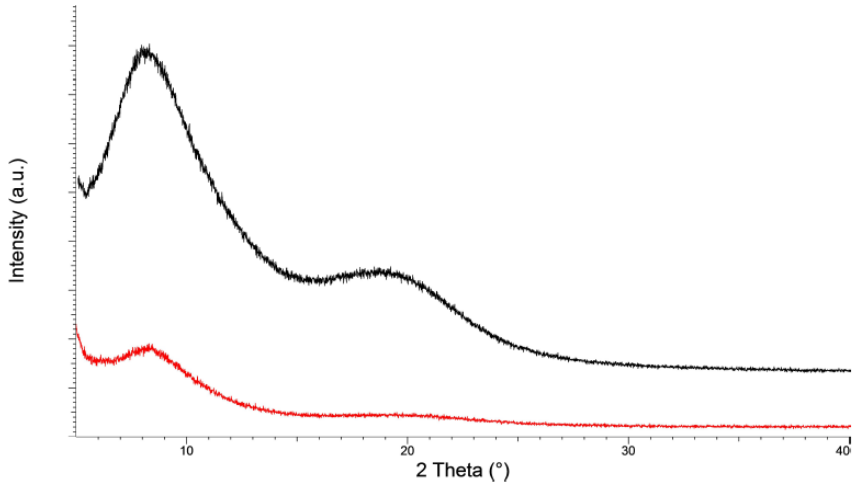

Fig. 3.48 PXRD patterns of EC-0 film before (black line) and after (red line) soaking in food simulant B for 2 h at 70°C.

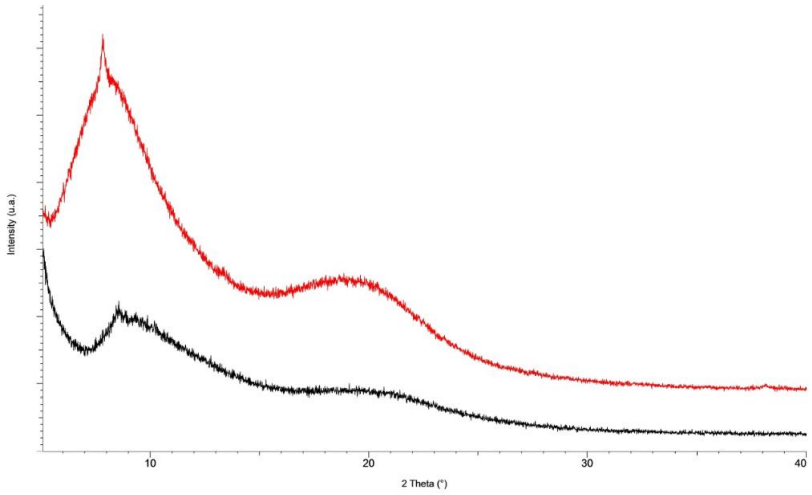

Fig. 3.49 PXRD patterns of EC-1a film before (red line) and after (black line) soaking in food simulant B for 2 h at 70°C.

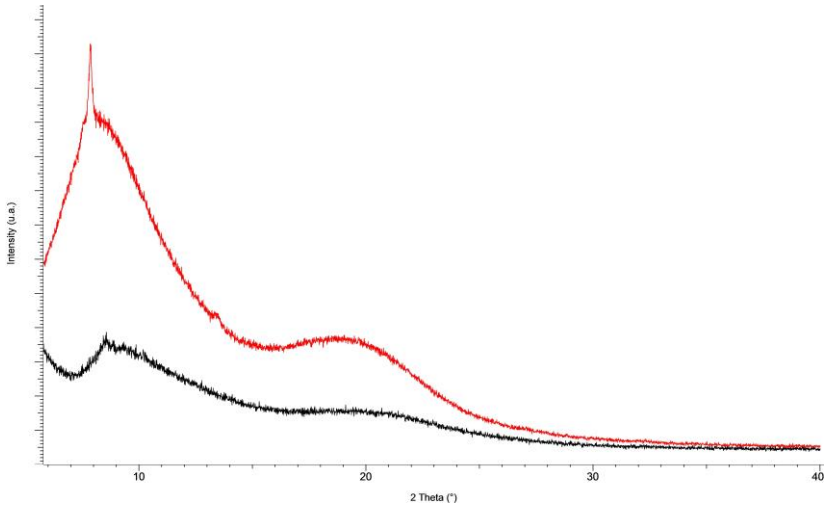

Fig. 3.50 PXRD patterns of EC-2a film before (red line) and after (black line) soaking in food simulant B for 2 h at 70°C.

The diffractograms of the swollen EC-0, EC-1a and EC-2a films show a marked increase of amorphism respect to the same samples before swelling, probably attributable to the partial disentanglement of the polymer chains triggered by the solvent molecules penetration, with an increase of the chains mobility and partial destruction of the polymer crystalline regions.

However, the ethanol effect on the Ag(I) ions release appears to be complex and not predictable, considering that in the case of the EC-3a, EC-4a and EC-5a films significantly lower values of Ag(I) ions were detected in the ethanol migration medium. A significant result regards the very low amount of Ag(I) migration detected in the case of EC-3a and EC-4a films in the ethanol migration medium at 70 °C for 2 hours with respective values recorded of 0.031 and 0.045 mg L^{-1} (**Tab. S5**).

The EC-3a, EC-4a, EC-5a and EC-6a films did not swell after soaking in ethanol solution, delaying the release of Ag(I) ions to the simulant. The PXRD patterns are almost comparable to those of the same samples before soaking, presenting both the polymer and the Ag(I) complex reflection peaks (**Fig. 3.51-3.54**).

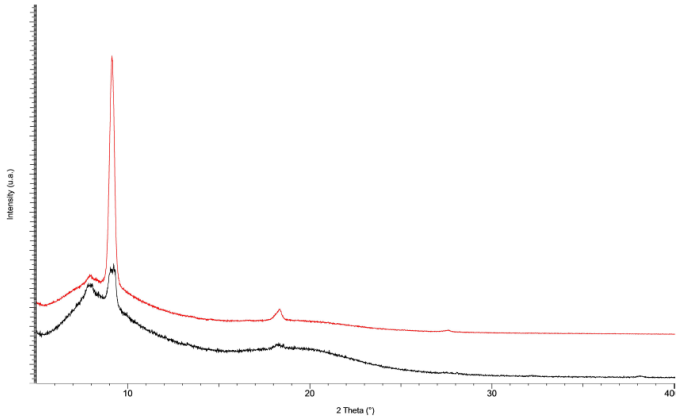

Fig. 3.51 PXRD patterns of EC-3a film before (red line) and after (black line) soaking in food simulant B for 2 h at 70°C.

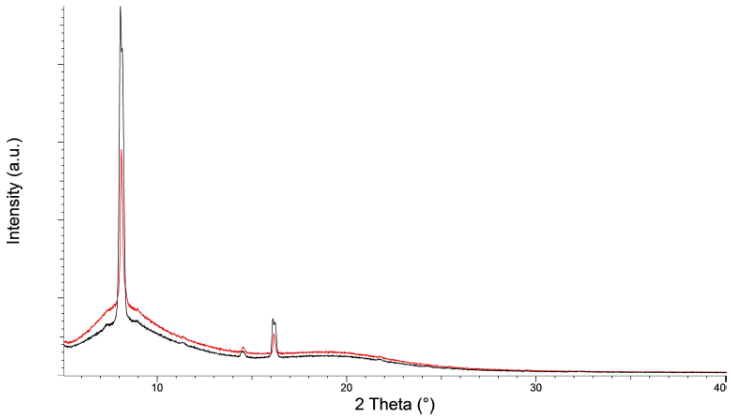

Fig. 3.52 PXRD patterns of EC-4a film before (red line) and after (black line) soaking in food simulant B for 2 h at 70°C.

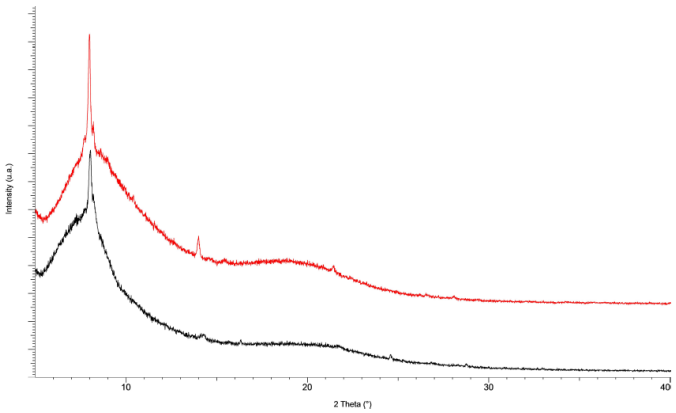

Fig. 3.53 PXRD patterns of EC-5a film before (red line) and after (black line) soaking in food simulant B for 2 h at 70°C.

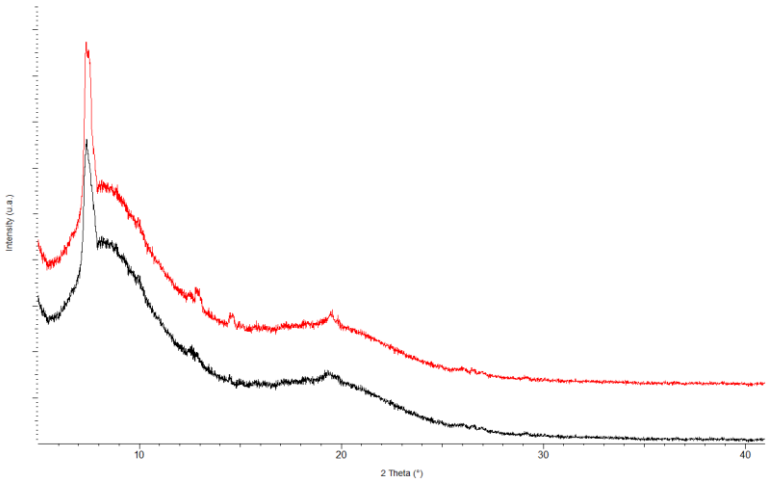

Fig. 3.54 PXRD patterns of EC-6a film before (red line) and after (black line) soaking in food simulant B for 2 h at 70°C.

Thus, it is reasonable to assume that EC-3a, EC-4a, EC-5a and EC-6a films do not under-go swelling, probably due to the presence of the complex crystallites on the film surface, which presumably, forming as well as a surface layer, partially protect it from the solvent molecules penetration.

With simulant C, at 70 °C and 2 h working condition, none of significant differences in terms of ion release were observed between all EC-*n*a films with respect to the EC-($AgNO_3$)a films. At lower concentration, the EC-*n*b and EC-*n*c (*n*=1,2,3,4,5,6), were recorded value Ag(I) ions release below the instrumental limit of quantification (LOQ) or values around 0.05 mg Kg^{-1}, while for EC-($AgNO_3$)b,c, the release is always around 0.05 mg Kg^{-1}.

Changing working condition to longer exposure time, 10 days, and reduced temperature of 40 °C, no relevant differences between all EC-*n*a films are observed in the case of simulant A, distilled water (**Table 3.6**) and (**Fig. 3.55**).

Table 3.6 Specific Ag(I) migration from EC-*nx* square films, expressed in mg L^{-1} release in several simulants by heating at 40 °C for 10 days. Data represent mean of least three independent measurements.

Sample	***Simulant*** [a] ***A***	***Simulant B***	***Simulant C***
EC-0	0	0	0
EC-1a	0,210	< 0,05	1,790
EC-1b	LOQ	LOQ	LOQ
EC-1c	LOQ	LOQ	LOQ
EC-2a	0,52	< 0,05	0,998
EC-2b	< 0,05	0,028	< 0,05
EC-2c	LOQ	LOQ	LOQ
EC-3a	1,01	2,00	1,640
EC-3b	< 0,05	< 0,05	< 0,05
EC-3c	LOQ	LOQ	LOQ
EC-4a	0,540	2,100	1,650
EC-4b	LOQ	LOQ	< 0,05
EC-4c	LOQ	LOQ	< 0,05
EC-5a	0,42	1,12	2,275
EC-5b	< 0,05	< 0,05	< 0,05
EC-5c	LOQ	LOQ	LOQ
EC-6a	0,12	0,12	1,246
EC-6b	< 0,05	< 0,05	< 0,05
EC-6c	LOQ	LOQ	LOQ
EC-($AgNO_3$)a	0,53	< 0,05	0,108
EC-($AgNO_3$)b	< 0,05	LOQ	< 0,05
EC-($AgNO_3$)c	< 0,05	LOQ	< 0,05

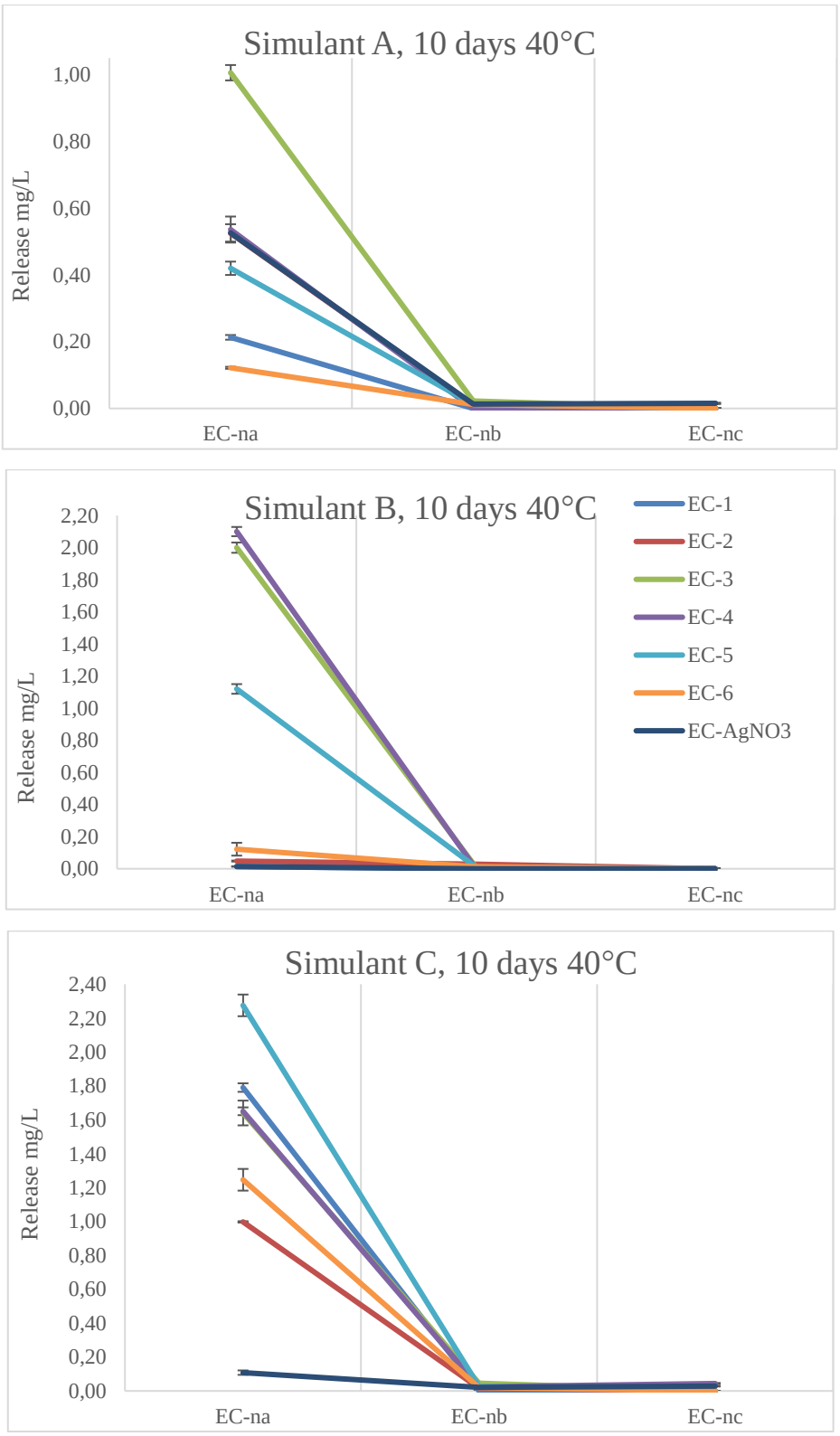

Fig. 3.55 Scatterplot showing the correlation between Ag(I) release amount in mg L^{-1} and the Ag (I) concentration in the EC matrix, at 40 °C and 10 days left, in distilled water (a), ethanol 10% v/v (b) and acetic acid 3% v/v (c).

Indeed, the highest Ag(I) ions migration in distilled water was again recorded in the case of EC-3a, followed by the analogous films EC-4a and EC-5a with respect to control EC-($AgNO_3$)a, but for diluted films, the release of Ag(I) ions is below the limit set by the EU legislation of 0.05 mg Kg^{-1} or the instrumental limit of quantification (LOQ) of 0.004 mg L^{-1}.

In the case of simulant B a different behaviour with respect to previous working condition, was observed. Indeed, even in ethanol 10% v/v, the maximum value of Ag(I) release is recorded in the case of the EC-3a, EC-4a and EC-5a films, while a value even below to the EU legislation of 0.05 mg Kg^{-1} is found in the case of EC-1a and EC-2a films (**Fig. 3.55**). Also for the EC-6a film, the observed release is higher than the values found for EC-1a and EC-2a films, probably due to the week interactions between the complex, dispersed on the of the film, and polymer matrix.

Moreover, all diluted EC-*n*b and EC-*n*c films show Ag(I) ions release even below the EU legislation of 0.05 mg Kg^{-1} or the instrumental limit of quantification (LOQ) of 0.004 mg L^{-1}. It appears, then, that the bursting ethanol effect previously observed, is not working in this condition. Indeed, the PXRD patterns of EC-0 matrix before and after soaking, in simulant B at 40° C for 10 days (**Fig. 3.56**), are almost comparable, demonstrating, in this case, the absence of swelling effect.

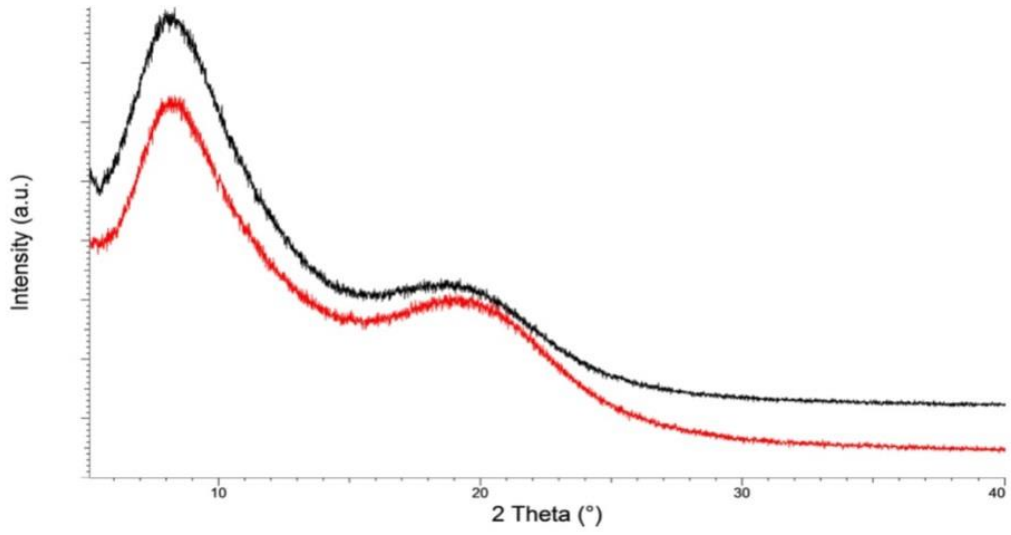

Fig. 3.56 PXRD patterns of EC-0 film before (black line) and after (red line) soaking in food simulant B for 10 days at 40 °C.

With simulant C, none of the significant differences seen for all EC-*n*x films in terms of ion release, are observed (**Fig. 3.55**). At lower concentration, as in the case of EC-1b and EC-*n*c (n=1,2,3,4,5,6), Ag(I) ions release even below the instrumental limit of quantification (LOQ) was recorded, while in all other films, including EC-($AgNO_3$)b,c, values around 0.05 mg Kg^{-1} were observed.

Summarizing, for EC-1a and EC-2a films in almost any simulant conditions the release of Ag(I) ions is less than for EC-3a, EC-4a, EC-5a, and EC-6a films probably due to the different mode of interaction between this type of complexes and EC polymeric matrix, such as previously described. Nerveless, an opposite trend is observed in simulant B, 70 °C for 2 hours, where the swelling effect improves a higher Ag(I) release for EC-1a and EC-2a films respect EC-3a, EC-4a, EC-5a, and EC-6a films. At lower concentration, for all EC-*n*x (x=b,c) films, Ag(I) ions release even below the instrumental limit of quantification (LOQ) or values around 0.05 mg Kg^{-1} was observed and in most cases less than EC-($AgNO_3$)b,c films.

3.6 Characterization of EC-*n*x films as antimicrobial materials for biomedical and food packaging applications

Antimicrobial polymers have emerged as promising candidates against microbial contamination. The fabrication of antibacterial surfaces for biomedical and food packaging applications has been accomplished with various antimicrobial agents comprising inorganic metal ions, organic molecules and metal-based complexes. [328][329][330]

Antimicrobial polymers can act according to different mechanism. One approach is the release of a chemical or antibacterial agent from the device surface which targets the surrounding bacteria (release mechanism). In the other approach, antibacterial agent can be grafted on the device surface that prevent the bacterial attachment to the surface or kill the attached bacteria (contact mechanism). (**Fig. 3.57)** [331][332][333]

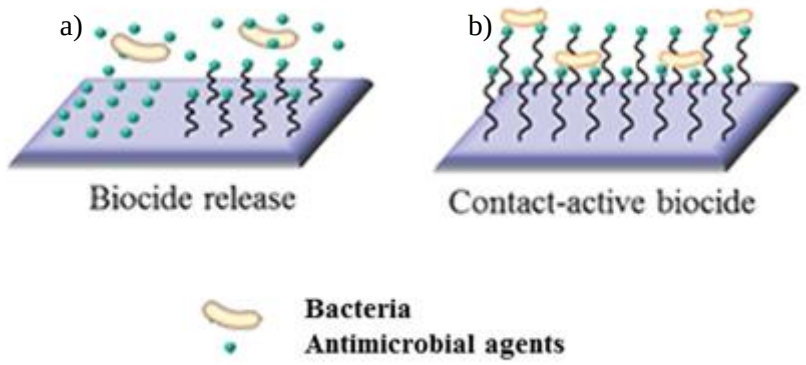

Fig. 3.57 Mechanism of antimicrobial action **a)** by release of the active component **b)** by contact. Adapted from [334]

The production of antibacterial surfaces for biomedical and food packaging applications has been accomplished with various antimicrobial agents including inorganic metal ions, organic molecules and metal-based complexes. [335][336][337][338]

[328] B. O. Jung, C. H. Kim, K. S. Choi, Y. M. Lee and J. J. Kim, J. Appl. Polym. Sci., 72, 1713–1719, **1999**
[329] E. R. Kenawy and H. Xiao, Royal Society of Chemistry, **2013**
[330] E. R. Kenawy, F. I. Abdel Hay, R. El Shanshoury, E. R. Abd and M. H. El Newehy, J. Polym. Sci. Part A: *Polym. Chem*., 40, 2384–2393, **2002**
[331] D. Sun, M. Babar Shahzad, M. Li, G. Wang and D. Xu Sun, Vol 30, **2015**
[332] J. Hasan, R. J. Crawford and E. P. Ivanova: Trends Biotechnol., , 31, 295–304, **2013**
[333] K. Vasilev, J. Cook and H. J. Griesser: 'Exp. Rev. Med. Dev.,6, 553–567, **2009**
[334] K. Bazaka, M. V. Jacob,b W. Chrzanowskic and K. Ostrikovacd, RSC Adv., 5, 48739, **2015**
[335] Bikiaris, D.N., and Triantafyllidis, K.S. *Mater. Lett.*, 93, 1–4, **2013**

The antibacterial activity of all new EC-*n*x films has been studied against *Escherichia coli* (*E. coli*) as model of Gram-negative bacterial strains, usually related to food poisoning, diarrhoea and haemolytic uremic syndrome. *E. coli* is commonly found in the lower intestine of humans and warm-blooded animals. *E. coli* is part of the normal flora of the gastrointestinal tract and are the dominant species in the aerobic faecal flora humans. Although most *E. coli* strains are harmless, some strains can cause serious illnesses (*E. coli* O157:H7). Transmission of *E. coli* is by faecal-oral contact, usually by ingestion of contaminated food and water. [339] Furthermore, the *E. coli* strain is the reference recommended by Clinical and Laboratory Standards Institute (CLSI).

The antibacterial activity by contact of all EC-*n*x films was tested in agreement to the ISO standard. [340] EC-($AgNO_3$)x films and EC-0 film were used in the test as positive and negative controls, respectively. The colony forming units (CFUs) were assessed by enumerating the total colony after incubation for 24 h at 37 °C, and this parameter compared with EC-0 **(Table 3.7**).

[336]Lotlikar, S.R., Gallaway, E., Grant, T., Popis, S., Whited, M., Guragain, M., Rogers, R., Hamilton, S., Gerasimchuk, N.G., and Patrauchan, M.A.11, 6, **2019**
[337]COMA, V. *Meat Sci.*, 78, 1–2, 90–103, **2008**
[338]Appendini, P., and Hotchkiss, *J.H. Food Science & Emerging Technologi*es, 3, 113-126, **2002**
[339] *Iran J Microbiol*., 2, 2, 59–72., **2010**
[340] ISO-22196: Plastics –Measurement of Antibacterial Activity on Plastics Surface, **2011**

***Table 3.7**. Antibacterial activity (C.F.U. values) of the EC-nx films and relative killing percentage (%), according to ISO standard*

	E. coli **(24 h)** **C.F.U.**	***E. coli*** **(24 h)** **%**
EC-0	215	0
EC-1a	0	100
EC-1b	28	87
EC-1c	89	59
EC-2a	0	100
EC-2b	60	72
EC-2c	140	35
EC-3a	0	100
EC-3b	65	70
EC-3c	176	18
EC-4a	0	100
EC-4b	2	99
EC-4c	155	28
EC-5a	0	100
EC-5b	69	68
EC-5c	159	26
EC-6a	0	100
EC-6b	161	25
EC-6c	196	9
EC-($AgNO_3$)a	0	100
EC-($AgNO_3$)b	0	100
EC-($AgNO_3$)c	75	65

The performed tests made on the film samples intended to prove inhibition of bacteria growth on the contact surface. EC-0 and EC-($AgNO_3$)x at various concentrations were tested as negative and positive control, respectively. From the data reported in Table 3.7 it is evident that the introduction of Ag(I) complexes, both neutral and charged, into the EC polymeric matrix induces bactericidal activity. All

the films belonging to the series EC-*n*a, that is the one with weight ratio 1:40, display killing percentages of 100%. **(Fig. 3.58)**

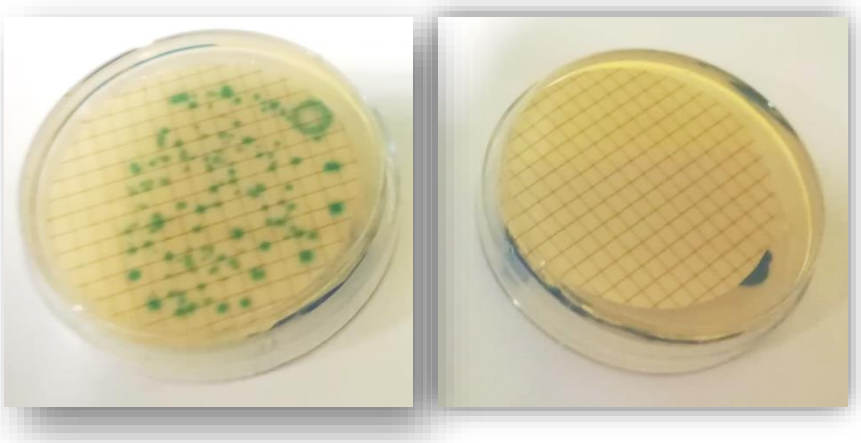

(a) (b)

Fig. 3.58 Solution of *E. coli* (a) and solution after contact with EC-*n*a (b)

For the EC-*n*b films the killing percentage ranges between 25% - 99%. Particular relevant is the 99% of antibacterial activity found for EC-4b, which is also accompanied by a release in water under the LOQ (**Fig. 3.59**).

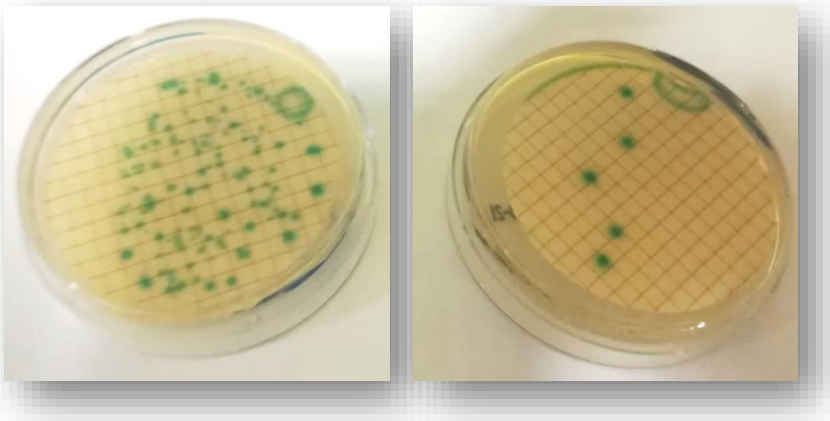

(a) (b)

Fig. 3.59 Solution of *E. coli* (a) and solution after contact with EC-4b (b)

The EC-*n*c films seem to provide the worst results, but it is very important to underline that 1:5000 is a very diluted working operation condition. Nevertheless, the

killing percentage value of 59% observed for EC-1c is an outstanding result, also considering that the silver ion release is less than the LOQ limit **Fig. 3.60**.

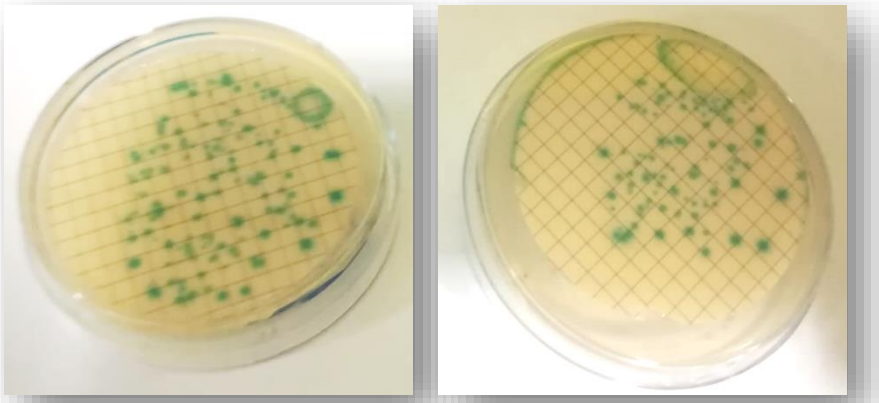

(a) (b)

Fig. 3.60 Solution of *E. coli* (a) and solution after contact with EC-1c (b)

The EC-6b and EC-6c films containing the ionic complex show a very low antibacterial activity, probably due to a higher steric hindrance of the silver cation, which does not allow an easily access to bacterial cell membrane.

Believing that these new silver containing films could be used in biomedical applications, it is clear that we would like to realize systems working with the lower amount of active additives with a higher antibacterial activity and the smaller release of silver ions in water. In this contest, we successfully reached this goal since the most of films prepared with a very small amount of additives show excellent antibacterial activity and minimum values of Ag(I) release, lower than the human toxicity limit.

Chapter 4

EXPERIMENTAL SECTION

Materials and Methods

All commercially reagents and solvents were purchased from Sigma Aldrich and were used without further purification. The Ethylcellulose used has a degree of substitution equal to 48.0-49.5% (w/w) Ethoxyl basis. The ligands $HQ^{py,CF3}$ were prepared by the Chemistry Department of the University of Camerino. [341]

Characterization with Infrared Spectroscopy (FT-IR)

IR spectra were recorded on a FT-IR spectrometer Perkin-Elmer Spectrum One. Fourier Transform Infrared (FT-IR) analysis was carried out on the film samples in the mid-infrared area (4000-400 cm^{-1}) with a Perkin Elmer Spectrum 100 FT-IR spectrometer. KBr pellets were used only to obtain the ligands and Ag(I) complexes spectra.

Characterization ^{1}H Nuclear Magnetic Resonance spectroscopy (^{1}H-NMR)

^{1}H-NMR spectra were recorded on a Bruker WH-300 spectrometer in deuterated solvents with TMS as an internal standard.

Morphological and Optical measurement (AFM)

Atomic Force Microscopy (AFM) was used to evaluate surface topography. AFM, a Multimode 8 (Bruker), was operated in tapping mode, to avoid any sample damage, using probes with an elastic constant of 5 N/m and a nominal tip radius of 10 nm (TAP 150A, Bruker). All measurements were performed in air and at room temperature. The scan line speed was optimized between 1 and 3 Hz over 256×256

[341] F. Marchetti, C. Pettinari, R. Pettinari, *Coord. Chem. Rev*., 249, 2909– 2945, **2005**

pixels. Image treatment and analysis were carried out using the free software WSxM.[342]

Water Contact Angle Measurements

Static contact angles to deionized water were measured with a CAM 200 contact angle meter (KSV Instruments LTD, Helsinki, Finland) at room temperature. A drop (5 µL) of deionized water was put onto the sample surface by a micropipette, and measurements were carried out by setting the tangents on both visible edges of the droplet the contact angle. All experiments were carried out at room temperature (22 ± 1 ºC) and the contact angle was measured in triplicate and a mean value was obtained for each films. [343][344][345] The images were processed by ImageJ free software using the contact angle plugin. [346] The program then fits the profile of the drop and calculates the contact angle using the sphere approximation or the ellipse approximation.

Characterization with Thermogravimetric analysis (TGA)

The thermal stability was measured on a Perkin-Elmer Thermogravimetric Analyser Pirys 6 TGA. Approximately 3 mg of each sample was placed in an alumina crucible and heated from 20°C to 600°C, at a heating rate of 5 °C min^{-1}, under a dry nitrogen atmosphere. The DTG (Differential Scanning Calorimetry) curves were obtained from the first derivative of the thermogravimetric profiles.

Characterization with Differential Scanning Calorimetry (DSC)

DSC analysis was performed using a TA DSC Q2000 instrument with a refrigerated cooling unit (RCS 90). Indium metal standard was used for the temperature

[342] Horcas, R. Fernández, J. M. Gómez-Rodríguez, J. Colchero, J. Gómez-Herrero, *Rev. Sci. Instrum.*, *78*, 013705, **2007**
[343] G. De Filpo, E. Pantuso, K. Armentano, P. Formoso, G Di Profio, T. Poerio, E. Fontananova, C. Meringolo, A.I. Mashin and F.P. Nicoletta, *Membranes, 8, 35*, 1-15, **2018**;
[344] C. Oliviero Rossi, P. Caputo, N. Baldino, F.R. Lupi, D. Miriello, R. Angelico, *Int. J. Adhes. Adhes*.,70, 297-303, **2016**;
[345] C. Oliviero Rossi, P. Caputo, N. Baldino, E. Ildyko Szerbc, B. Teltayev, *Int. J. Adhes. Adhes*,*72*, 117-122, **2017**
[346] a) G. Lamour and A. Hamraoui, *J. Chem. Educ.*, *87*, 1403-1407, **2010** b) W. Rasband, *National Institute of Health*, **2009** http://rsbweb.nih.gov/ij/index.html (accessed Sep 2010) c) M.Brugnara, **2006**, http://rsbweb.nih.gov/ij/plugins/contact-angle.htm (accessed Sep **2010**)

calibrations. The samples were accurately weighted (1.5-2 mg) and crimped in non-hermetic aluminium pans. The samples were heated at a heating rate of 5 °C min^{-1}, under a dry nitrogen atmosphere (flow rate 50 ml min^{-1}), using an empty non-hermetic aluminium pan as reference.

Characterization with Polarizing Optical Microscope (POM)

Melting points and mesophase textures were examined with a Leica DMLP polarizing microscope equipped a Leica DFC290 camera and CalCTec (Italy) heating stage.

Characterization with Powder X-Ray Diffraction (PXRD)

The PXRD patterns were acquired on a Bruker D2-Phaser equipped with a Cu Kα radiation (λ = 1.5418 Å) and a Lynxeye detector, at 30 kV and 10 mA, with step size of 0.01° and step time of 2 s, over an angular range of 5–40° 2θ. The obtained diffractograms were analysed with DIFFRAC.EVA diffraction software. The interplanar distances (d) were calculated according to the Bragg equation.

Characterization X-Ray single crystal analysis (X-Ray)

X-ray data, for the complex 3, were collected at room temperature on a Bruker-Nonius X8 Apex CCD area detector equipped with a graphite monochromator and Mo Ka radiation (l = 0.71073 Å). Data were processed through the SAINT [347] reduction and SADABS [348] absorption software. The structures were solved by standard Patterson methods through the SHELXTL NT [349] structure determination package and refined by full-matrix least squares based on F2. In general, all nonhydrogen atoms were refined anisotropically and hydrogen atoms were included as idealized atoms riding on the respective carbon atoms with C–H bond lengths appropriate to the carbon atom hybridization. Hydrogen atoms of the co-crystallized

[347] SAINT, *Version* 6.45 Copyright©, Bruker Analytical X-Ray Systems Inc., **2003**
[348] Sheldrich, G. M. SADABS. *Version* 2.10, Bruker AXS Inc., Madison, USA, **2003**
[349] SHELXTL-NT, *Version* 5.1 Copyright©, Bruker Analytical X-Ray Systems Inc., 199

water molecules have been included in calculated positions and restrained bond distances and angles have been used.

Preparation of the EC-*n*a films in Liquid Assisted Grinding

Preparation of the EC-*n*a films in Liquid Assisted Grinding was carried out using a mixer mill MM 400 Retsch.

Release tests for specific migration of Ag(I) from the EC-*n*x films

ICP Analyses for specific Ag(I) ions migration were carried out with inductively coupled plasma spectroscopy with Optical Emission Spectrometry (ICP-OES), Varian 710 ES and the instrumental limit of quantification considered of (LOQ) of 0.004 mg L^{-1} was determined with the white method and corresponds to that provided by the ISO-11885: Waters quality – Determination of selected elements by inductively coupled plasma optical emission spectrometry (ICP-OES). [326]
All release tests were performed at the TifqLab Laboratory, Centro di sperimentazione, ricerca e analisi applicate alle tecnologie alimentari e dell'acqua potabile – Department DIMES, University of Calabria.

4. Synthesis procedures

4.1 Synthesis and characterization of polymer $[Ag(Q^{py,CF3})]_n$

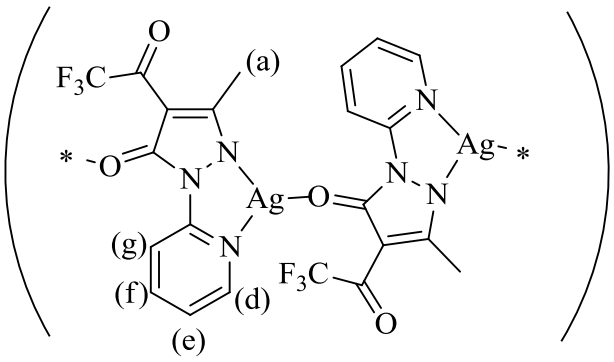

To a solution of the ligand $HQ^{(py,CF3)}$ (0.135 g, 0.5 mmol) in methanol (30 mL) was added NaOMe (0.027 g, 0.5 mmol). Subsequently, was added a solution of silver nitrate (0.085 g, 0.5 mmol) in water (10 mL) and a white precipitate slowly formed. The resulting reaction mixture was further stirred for 1 h, and later the solvent was removed and the precipitate afforded, which was filtered off, washed with Et_2O (10 mL). After filtration, the polymer has been obtained as gray powder and was dried in vacuo to constant weight. Yield 98%. It is soluble in DMSO, acetone and acetonitrile.

Characterization

Molecular weight:	376.97 g mol^{-1}
Molecular formula:	$C_{11}H_7AgF_3N_3O_2$
Melting point:	295-297 °C

Elemental analysis (%):

Theoretical:	C= 35.01 H= 1.86 N= 11.11
Experimental:	C= 34.95 H= 1.65 N= 10.68

IR (KBr) (ν_{max}/cm^{-1}): 1653vs, 1605m ν(C=O), 1508s, 1439s ν(C=C, C=N, C-N), 1355s, 1247m, 1185s, 1123s, 1078m, 949s, 771s.

^{1}H NMR (300MHz, CD_3CN): δ_H 8.79 (1H, d, J= 7.68 Hz, H^d), 8.26 (1H, d, J = 4.36 Hz, H^g), 7.12 (1H, J = 7.41 Hz, H^e), 7.12 (1H, d, J = 7.61 Hz, H^f), 2.40 (3H, s, -CH_3) ppm.

TGA-DTA (mg% vs. °C): heating from 30 to 600°C with a speed of 8°C/min; from 260 to 600°C progressive decomposition, with a final black residual of 40% weight.

4.2 Synthesis of [Ag($Q^{py,CF3}$)(Bzim)], complex 1

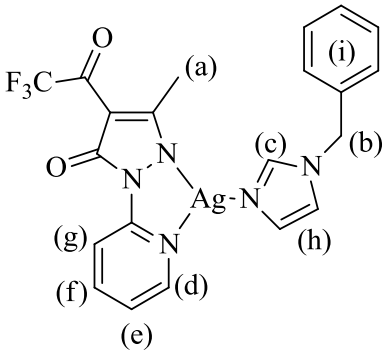

To a suspension of [Ag($Q^{py,CF3}$)] (**1**) (0.250 g, 0.66 mmol) in acetonitrile (30 mL) was added 2-benzylimidazole (0.316 g, 2.0 mmol). A colorless precipitate slowly formed and the mixture of reaction was stirred at room temperature for 1 h. Subsequently, the solvent removed on a rotary evaporator and the precipitate was filtered, and washed with methanol. The powder obtained dried in vacuo to constant weight and shown to be complex **1**. Yield: 75%. It is soluble in acetone, acetonitrile, chlorinated solvents and DMSO.

Characterization

Molecular weight:	535.04 g mol^{-1}
Molecular formula:	$C_{21}H_{17}AgN_5O_2F_3$
Melting point:	136-138 °C
Elemental analysis (%):	

Theoretical: C= 47.03 H= 3.21 N= 13.06

Experimental: C= 46.38 H= 2.80 N= 12.68

IR (KBr) (ν_{max}/cm^{-1}): 3118w ν(Carom-H), 1664s, 1617vs ν(C=O), 1592m, 1466m, 1384s, 1341m, 1245m ν(C=C, C=N, C-N), 1196s, 1145vs, 1009m, 920m, 774vs.

^{1}H NMR ((300MHz, $CDCl_3$): δ_H 8.80 (1H, d, J= 8.73 Hz, H^d), 8.03 (1H, d, J= 6.09 Hz, H^g), 8.10 (1H, s, H^c), 7.95 (1H, t, J= 9.03 Hz, H^e), 7.45-7.30 (6H, m, H^h+H^i), 7.20 (1H, t, J= 6.87 Hz, H^f), 7.09 (1H, s, H^h), 5.15 (2H, s, H^b). 2.34 (3H, s, H^a) ppm.

TGA-DTA (mg% vs. °C): heating from 30 to 600°C with a speed of 8°C/min; from 100 to 600°C progressive decomposition, with a final black residual of 8% weight.

4.3 Synthesis of [Ag($Q^{py,CF3}$)(BuIm)], complex 2

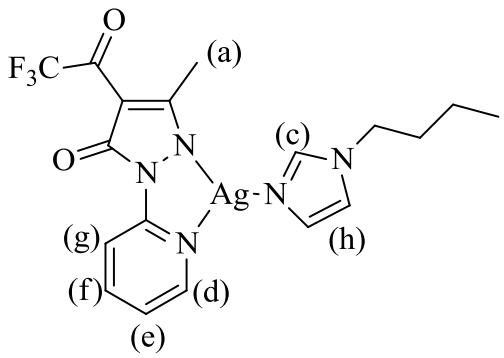

Derivative **2** was obtained similarly to **1**. Yield 91%. It is soluble in acetone, acetonitrile, chlorinated solvents and DMSO.

Characterization

Molecular weight: 501.05 g mol^{-1}

Molecular formula: $C_{18}H_{19}AgF_3N_5O_2$

Melting point: 162-165 °C

Elemental analysis (%):

Theoretical: C= 43.11 H= 3.79 N= 13.97

Experimental: C= 41.25 H= 3.04 N= 11.29

IR (KBr) (ν_{max}/cm^{-1}): 3245w ν(C arom-H), 1665s ν(C=O), 1570m, 1558m, 1514s, 1474s ν(C=C, C=N, C-N), 1342s, 1302m, 1245s, 1198s, 776vs.

^{1}H NMR (DMSO-d6): δ_H 8.6 (1H, d, J(H-H)= 8.46 Hz, H^d) 8.26 (1H, d, J(H-H)= 4.92 Hz, H^g), 7.92-7.85 (2H, m, H^c, H^e), 7.33 (1H, s, H^h), 7.13 (1H, t, J(H-H)= 6.03Hz, H^f), 7.01 (1H, s, H^h), 3.97 (2H, t, J(H-H)= 4.52 Hz, -CH_2 Butil), 2.25 (3H, s, H^a), 1.67-1.62 (2H, m, -CH_2 Butim), 1.17-1.15 (2H, m, -CH_2 Butim), 0.85 (3H, t, J(H-H)= 5.5 Hz) ppm.

TGA-DTA (mg% vs. °C): heating from 30 to 600°C with a speed of 8°C/min; from 100 to 600°C progressive decomposition, with a final black residual of 7% weight.

4.4 Synthesis of [Ag($Q^{py,CF3}$)(imH)], complex 3

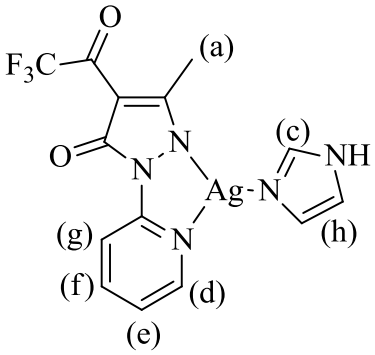

Derivative **3** was obtained similarly to **1**. Yield 85%. It is soluble in acetone, acetonitrile, chlorinated solvents and DMSO.

Characterization

Molecular weight:	444.99 g mol^{-1}
Molecular formula:	$C_{14}H_{11}AgF_3N_5O_2$
Melting point:	145-147°C

Elemental analysis (%):

Theoretical:	C= 37.69 H= 2.49 N= 15.70
Experimental:	C= 37.25 H= 2.74 N= 14.29

IR (KBr) (ν_{max}/cm^{-1}): 3434m ν, 3050w ν(Carom-H), 1664s ν(C=O), 1591m, 1570m, 1514s, 1474s ν(C=C, C=N, C-N), 1341s, 1302m, 1245s, 1198s, 776vs

^{1}H NMR (DMSO-d6): δ_H 12.47 (1H, s, -NH), 8.59 (1H, d, J(H-H)= 8.25 Hz, H^d), 8.28 (1H, d, J(H-H)= 4.96 Hz, H^g), 7.87 (2H, t, J(H-H)= 6.7 Hz, H^e, H^c), 7.15 (3H, t, J(H-H)= 5.58 Hz, H^f, H^h), 2.29 (3H, s, H^a) ppm.

TGA-DTA (mg% vs. °C): heating from 30 to 600°C with a speed of 8°C/min; from 100 to 600°C progressive decomposition, with a final black residual of 5% weight.

4.5 Synthesis of [Ag($Q^{py,CF3}$)(2EtimH)], complex 4

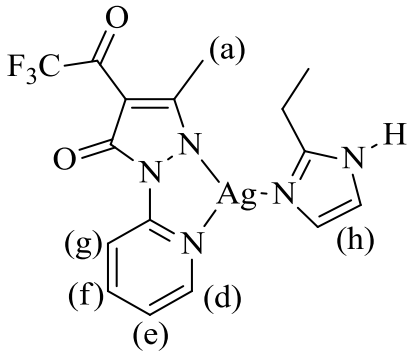

Derivative **4** was obtained similarly to **1**. Yield 89%. It is soluble in methanol and DMSO.

Characterization

Molecular weight:	473.02 g mol^{-1}
Molecular formula:	$C_{16}H_{15}AgN_5O_2F_3$
Melting point:	186-188 °C

Elemental analysis (%):

Theoretical:	C= 40.53 H= 3.19 N=14.77
Experimental:	C= 40.27 H= 2.97 N=14.25

IR (KBr) (ν_{max}/cm^{-1}): 3177w ν(Carom-H), 1665s ν(C=O), 1591m, 1483m, 1464s, 1434s ν(C=C, C=N, C-N), 1375s, 1301m, 1953s, 775s, 723vs.

^{1}H NMR (DMSO-d6): δ_H 12.49 (1H, s, -NH), 8.61 (1H, d, J= 8.49 Hz, H^d), 8.26 (1H, d, J= 4.92 Hz, H^g), 7.86 (1H, t, J= 6.9 Hz, H^e), 7.13 (2H, t, J= 6.03 Hz, H^f), 7.07 (1H, s, H^h), 2.74 (2H, q, 7.59 –CH_2 EtimH), 2.30 (3H, s, H^a), 1.20 (3H, t, J=7.59Hz, –CH_3 EtimH) ppm.

TGA-DTA (mg% vs. °C): heating from 30 to 600°C with a speed of 8°C/min; from 100 to 600°C progressive decomposition, with a final black residual of 27% weight.

4.6 Synthesis of [Ag($Q^{py,CF3}$)(2-PhenIm)], complex 5

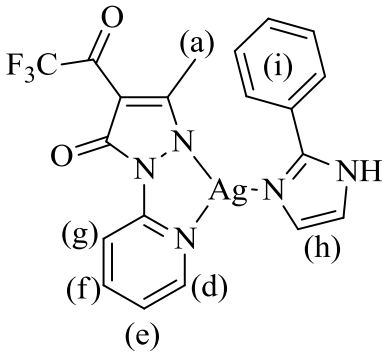

Derivative **5** was obtained similarly to **4**. Yield 85%. It is soluble in methanol and DMSO

Characterization

Molecular weight:	522.23 g mol^{-1}
Molecular formula:	$C_{20}H_{15}AgF_3N_5O_2$

Melting point: 139-142°C

Elemental analysis (%):

Theoretical:	C= 46.06 H= 2.87 N= 13.49
Experimental:	C= 45.04 H= 2.14 N= 12.31

IR (KBr) (ν_{max}/cm^{-1}): 3459m ν, 3060w ν(C arom-H), 1663s ν(C=O), 1592m, 1559m, 1515s, 1434s ν(C=C, C=N, C-N), 1342s, 1302m, 1246s, 953s, 775vs.

^{1}H NMR (DMSO-d6): δ_H 12.99 (1H,s,-NH), 8.67 (1H, d, J(H-H)= 8.46 Hz, H^d), 8.25 (1H, d, J(H-H)= 4.14 Hz, H^g), 7.99 (2H, d, J(H-H)=6.9Hz, H^i, 7.92 (1H, t, J(H-H)= 7.08 Hz, H^f), 7.49-7.41(3H, m, H^i), 7.31 (2H, s, H^h), 7.17 (1H, t, J(H-H) =4.92Hz, H^e), 2.29 (3H, s, H^a) ppm.

TGA-DTA (mg% vs. °C): heating from 30 to 600°C with a speed of 8°C/min; from 100 to 600°C progressive decomposition, with a final black residual of 7% weight.

4.7 Synthesis of Ligands 4,4'-bis(hydroxymethyl)-2,2'-bipyridine, bpy-OH

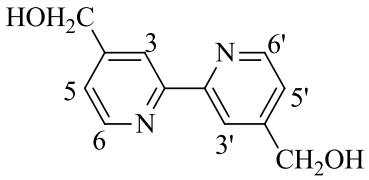

The bpy-OH ligand was prepared in three steps:

Step I: Synthesis of the precursor 4,4'-dicarboxylic-2,2'-bipyridine acid, II

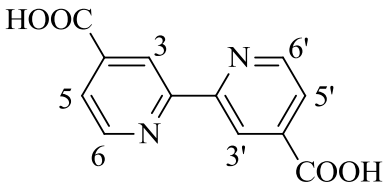

5.0 g (0.026 mmol) of 4,4'-dimethyl-2,2'-bipyridine were dissolved in 175 ml of sulfuric acid. The reaction was carried out under stirring and at a temperature of about 70 °C. To the resulting solution are added 32 g (0.106 mmol) of potassium dichromate, constantly monitoring the temperature so that it does not exceed 80 °C. Once all the added potassium dichromate has gone into solution, the mixture is allowed to cool to room temperature and is then slowly added to a mixture of water and ice of about 500 ml. The precipitate obtained is filtered, washed with distilled water and dried under reduced pressure. The resulting pale yellow solid is then purified by refluxing it in 175 ml of 65% nitric acid, under magnetic stirring. After six hours, the yellowish solution is poured again into a mixture containing water and ice to obtain a precipitate, which has been filtered, washed with water and acetone and dried under reduced pressure. The product **II** was obtained as a white solid with a yield of 92%.

Characterization

Molecular weight: 244.20 g mol^{-1}

Molecular formula: $C_{12}H_8O_4N_2$

Melting point: > 300 ° C

Elementary analysis (%):

	C	H	N
Theoretical:	59.02	3.30	11.47
Experimental:	58.90	3.17	11.38

IR(KBr) (ν_{max}/cm^{-1}): 3113 (OH), 1732 (C=O), 1600-1450 (C-C).

^{1}H-NMR (300 MHz, DMSO-d_6): δ_H, 13.77 (2H, s, OH), 8.91 (2H, d, $H^{5,5'}$), 8.83 (2H, s, $H^{3,3'}$), 7.91 (2H, d, $H^{6,6'}$) ppm.

II step: Synthesis of the precursor, 4,4'-dicarboxylate-diethyl-2,2'-bipyridine ***III***

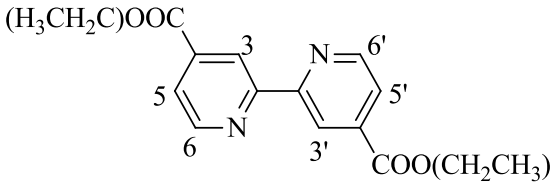

A suspension of the precursor **II** (3.0 g, 12.29 mmol) in 130 ml of ethanol and 7.5 ml of sulfuric acid was kept under magnetic stirring at 80 ° C for 24 h. The solvent is then removed by evaporation under reduced pressure. The obtained residue was extracted from chloroform and a saturated solution of sodium bicarbonate. The organic phase is extracted 4 times, dried with anhydrous sodium sulfate and filtered. After having removed the solvent by evaporation, the residue is recrystallized from chloroform/methanol. Product **III**, a white solid, was obtained with a yield of 91%.

<u>Characterization</u>

Molecular weight: 300.31 g mol^{-1}

Molecular formula: $C_{16}H_{16}O_4N_2$

Melting point: 150°C

Elementary analysis (%):

Theoretical:	C= 63.99	H= 5.37	N= 9.33
Experimental:	C= 63.45	H= 5.11	N= 9.27

IR (KBr) (ν_{max}/cm^{-1}): 2990-2908 (CH), 1726 (C=O), 1595-1450 (C-C).

^{1}H-NMR (300 MHz, $CDCl_3$): δ_H, 8.96 (s, 2H, $H^{6,6'}$), 8.87 (d, 2H, J = 4.89 Hz, $H^{5,5'}$), 7.92 (d, 2H, J = 4.89 Hz, $H^{3,3'}$), 4.46 (q, 4H, -OCH_2CH_3), 1.45 (t, 6H, J = 7.21 Hz,-CH_3) ppm.

III step: synthesis of **Bpy-CH_2OH**

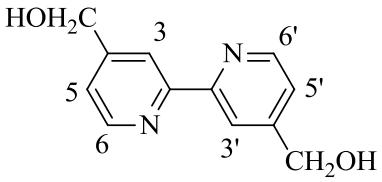

To a solution of the precursor **III** (3.17 g, 10.5 mmol), in 200 ml of ethanol, an excess of boron hydride of sodium (8 g, 221.67 mmol) was added. The white suspension obtained was left to reflux for 3 h. It is then continued with the addition of 320 ml of an aqueous solution saturated with ammonium chloride, maintaining the agitation. The ethanol was removed from the resulting solution at reduced pressure. The residue obtained was then extracted with ethyl acetate. The organic phase is anhydrified with sodium sulfate anhydrous, The solid was recrystallized from ethanol / n-hexane. The ligand **Bpy-CH_2OH** product is a white solid, obtained with a 95% yield.

Characterization

Molecular weight: 216.24 g mol^{-1}

Molecular formula: $C_{12}H_{12}O_2N_2$

Melting point: 181 °C

Elementary analysis (%):

Theoretical:	C= 66.59	H= 5.56	N= 12.95
Experimental:	C= 66.55	H= 5.34	N= 12.70

IR (KBr) (ν_{max}/cm^{-1}): 3369 (OH), 2886-2832 (CH), 1601-1458 (C-C).

^{1}H-NMR (300 MHz, DMSO-d_6 δ_H): δ_H, 8.58(dd, 2H, J_m = 0.74 Hz, J_o = 20.46 Hz ,$H^{5,5'}$), 8.36 (s, 2H, $H^{6,6'}$), 7.35 (dd, 2H, J_m = 0.74 Hz, J_o = 10.27 Hz ,$H^{3,3'}$), 5.53(s, 2H, -OH),4.62 (d, 4H, $J_{(H,H)}$ = 4.4 Hz, -CH_2) ppm.

4.8 Synthesis and characterization of [(Bpy-OH)$_2$Ag][CH$_3$COO], complex 6

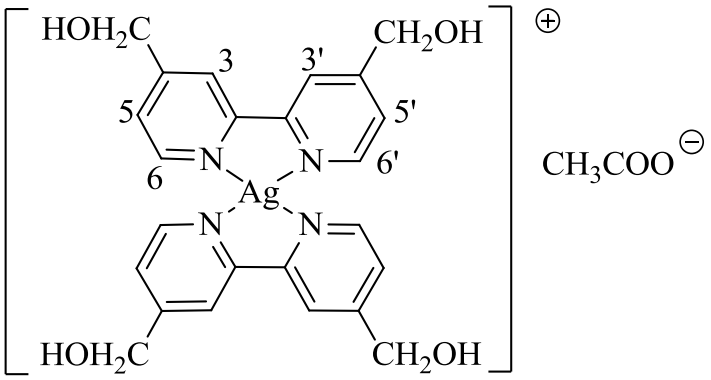

To a solution of 2 eq. of Bpy-OH (100 mg, 0.46 mmol) in EtOH was added 1 eq. of $AgOOCCH_3$ (30 mg, 0.23 mmol). The solution was stirred 4 h under nitrogen in a vessel protected from light. The solution was filtered, washed with EtOH, concentrate under reduced pressure and recrystallized from n-hexane the product is obtained with a 72% yield.

Characterization

Molecular weight:	619.42 g mol^{-1}
Molecular formula:	$C_{26}H_{31}O_7AgN_4$
Melting point:	182°C

Elemental analysis (%):

Theoretical:	C= 50.42 H= 5.04 N= 9.05
Experimental:	C= 50.41 H= 4.77 N= 9.14

IR (KBr) (ν_{max}/cm^{-1}): 3369 (OH), 2920-2818 (C-H), 1602 (C=C), 1560 (n_{asy} C=O), 1407 (n_{sym} C=O).

^{1}H NMR (300MHz, MeOD): δ_H 8.58 (4H, d, J(H-H)= 5.07 Hz, H$^{6,6'}$), 8.39 (4H, s, H$^{3,3'}$), 7.58 (4H, d, J(H-H)= 4.66 Hz, H$^{5,5'}$), 4.91 (8H, s, CH_2), 1.89(3H, s, CH_3).

4.9 Preparation of the EC-*n*x films

4.9.1 Preparation of the EC-0 films

The EC-0 film was prepared through dissolution of EC powder polymer (500 mg) in CH_2Cl_2 (45 mL). The resulting mixture was stirred at room temperature for 6 hours to give a transparent colorless solution. Then 6,5 mL of this solution were poured into a silica glass disk (diameter 9.7 cm). The solvent was evaporated at room temperature for 24 hours and the transparent films obtained were desorbed with 5 mL of distilled water from the glass surface. The obtained films were dried in an oven at 70 °C for 12 hours.

4.9.2 Preparation of EC-($AgNO_3$)a films

The EC-($AgNO_3$)a film was prepared as control film. It is prepared through dissolution of EC powder polymer (500 mg) in CH_2Cl_2 (45 mL). when the mixture as clear the quantity of $AgNO_3$ salt was added to the solution, to getting 40:1 w/w ratio.

The resulting mixture was stirred at room temperature for 6 hours to give a transparent colorless solution. Then 6,5 mL of this solution were poured into a silica glass disk (diameter 9.7 cm). The solvent was evaporated at room temperature for 24 hours and the transparent films obtained were desorbed with 5 mL of distilled water from the glass surface. The obtained films were dried in an oven at 70 °C for 12 hours.

4.9.3 Preparation of the EC-*n*x films in solution

All the EC-n films were prepared according to the procedure below. The polymer EC-nx (500 mg) were dissolved in CH_2Cl_2 (45 mL) and then the quantity of Ag(I) complexes *n* (*n*= 1-6) was added to the solution, to getting the appropriate w/w ratio, as shown in the Table 1. The resulting mixture was stirred at room temperature for 6 hours to give a transparent colorless solution. Then 6,5 mL of this solution were poured into a silica glass disk (diameter 9.7 cm). The solvent was evaporated at room

temperature for 24 hours and the transparent films obtained were desorbed with 5 mL of distilled water from the glass surface. The obtained films were dried in an oven at 70 °C for 12 hours.

Table 1. Specific ratios used for the preparation of the **EC-*n*x** films, expresses in terms of w/w

	x (w/w)	EC (g)	Complex *n* (g)
EC-0	-	0.50	-
EC-*n*a[a)]	1/40	0.50	1.25×10^{-2}
EC-*n*b	1/2000	0.50	2.5×10^{-4}
EC-*n*c	1/5000	0.50	1×10^{-4}

[a)] *n* = **1-6** complexes; x = a-c, weigh ratios n/EC

4.9.4 Preparation of the EC-*n*x film-forming solutions through Liquid Assisted Grinding

The white powder of EC together with Ag(I) complexes **1-2** in the ratio of 40:1 w/w (Table 1) and have been grinded in an agate ball miller for 4 hours in the presence of a small amount, 60 µL, of CH_2Cl_2. The obtained waxy solid has been solubilized with CH_2Cl_2 (45 mL) and the solution was stirred at room temperature for 6 hours. After mixing 6.5 mL of the solution was poured into a silica glass disk (diameter 9.7 cm). The solvent was evaporated at room temperature, transparent films were obtained and desorbed with 5 mL of water from the glass surface.

4.10 Antibacterial activity

The antibacterial activity by contact of all EC-*n*x films was tested in agreement to the ISO standard. [350] EC-*n***x** films were prepared as square with dimensions of 5 x 5 cm and tested, in triplicate, against *Escherichia coli (E. coli)*. Unloaded EC-0 sample

[350] ISO-22196: Plastics –Measurement of Antibacterial Activity on Plastics Surface, **2011**

was used as negative control and EC loaded with $AgNO_3$ was used as positive control. Firstly, bacterial aqueous suspension of E. coli (217 CFU mL^{-1}, 20 mL) was filtered with a nitrocellulose membrane filter under vacuum and placed over a plate containing *Glucoxane Agar*. Petri dish agar was incubated overnight at 35±1 °C for 24 h. After incubation, the dish was evaluated by visual inspection using manual colony counter to count the numbers of bacteria present. The EC-*n*x films were total immersed in 20 mL of this bacterial aqueous suspension in sterile Petri dishes, for 24 h at room temperature. In this way, both faces of EC-*n*x films were in contact with bacterial aqueous suspension. After contact test, every bacterial aqueous suspension was filtered with a nitrocellulose membrane filter and these were placed over a plate containing *Glucoxane Agar* and incubated overnight at 35±1 °C for 24 h. In order to evaluate the antibacterial activity of EC-*n*x films the % of bacteria growth reduction was calculated by counting the number of bacteria survived and comparing this value with the number of colonies of the negative control, EC-0. The percentage of reduction was calculated as follows:

$$\%\ of\ \ reduction = \frac{B - A}{B}$$

where:

B = CFU mL^{-1}average recovered from unloaded EC-0

A = CFU mL^{-1}average recovered from EC-*n*x films.

4.11 Release tests for specific migration of Ag(I)

The migration of Ag(I) ion was tested by using three simulants: distilled water (simulant A), ethanol 10% (v/v) (simulant B) and acetic acid 3% (v/v) (simulant C), under two conditions of simulations, 40 °C for ten days and 70 °C for 2 hours, according to EU Legislation of chemicals from plastic materials.[351]

[351] EU Food Contact Regulations for Plastics (food packaging and food Regulations 1935/2004, 79/112/EEC and 89/109/EEC) and EU Regulation 10/2011 (The Plastics Regulation), which indicates the rules for measuring overall and specific migration. http://ec.europa.eu/food/food/chemicalsafety/foodcontact/index_eu.htm

All the EC-*n*x films have been cut to size in order to have a surface/volume ratio equal to 1. The sample were total immersed in 100 mL of simulant in a beaker, in this way both faces of the sample were contact with simulant. The experiments were made in triplicate test for to evaluate the repeatability of determination. After the migration test time, the samples were removed and the simulants were prepared and acidified with nitric acid (3%) to analyze the Ag(I) released in the simulants by using inductively coupled plasma spectroscopy with mass spectrometry detection (ICP-OES). Calibration curves for investigated of Ag^+ ion were obtained by using aqueous standard solutions of standards appropriately acidified with nitric acid (3%).

CONCLUSIONS

Novel antibacterial Ag(I) containing Ethylcellulose EC-*n*x solid films have been successfully prepared and fully characterized. The novel EC-*n*x films, prepared in different weigh ratios *n*/EC (*n* = complexes **1**-**6** and x = a-c, which correspond to the amounts of complexes) have been obtained following the casting method. Casting solutions have been prepared by mixing the components either in solution or in solid state. The preparation in the solid state has been performed using the principle of Liquid Assisted Grinding (LAG). In both cases, after solvent casting evaporation, transparent films have been obtained. With the purpose of an eco-friendly preparation, 2-methyltetrahydrofuran, a derivative product of biomass, has been chosen as solvent, owe to its "greener" character with respect to dichloromethane primary used in the preparation of EC films. The silver complexes chosen as active additives differ for their nature (neutral *vs*. ionic) and the substituents grafted onto the employed ligands. Neutral acylpyrazolonato Ag(I) complexes containing different substituted imidazoles, are chosen for their known antibacterial action exhibited against numerous bacterial families, while the ionic bis-bypiridine Ag(I) complex was chosen for its interesting liquid crystalline proprieties. Most of the acylpyrazolonato Ag(I) complexes, as well as the precursor ligands, have been synthesized and fully characterized by the Prof. Fabio Marchetti and co-workers from the University of Camerino.

The Ag(I) complexes, designed with different structural characteristics, allow to highlight the formation of different type of interactions with the polymer matrix when the films are formed. Antibacterial activity and silver release have been studied for all the new EC-*n*x prepared films. All the physical-chemical characterizations have been performed on the most concentrated films in Ag(I) complexes, (EC-*n*a, 1:40), allowing the identification of all possible differences of their chemical and physical properties and therefore the nature and the relative effects of the non-covalent interactions between the Ag(I) additives and the polymeric EC matrix.

Efficiencies and performances of all EC-*n*x films were compared with two different controls, first EC-0, pure Ethylcellulose film and second EC-($AgNO_3$)x, films containing silver nitrate in an equal weight/ratio compared to the EC-*n*x prepared films. All controls have been prepared following the identical procedure employed

for the other silver containing films. Several significant differences in both structural and physical-chemical properties within the new films have been observed according to the specific interactions established by the Ag(I) complexes and the polymer matrix.

The presence of the N-H hydrogen bond donor on the imidazole ligands favor the formation of hydrogen bonds with the suitable acceptor groups present on the polymeric EC matrix, both on the surface and in the inner structure, giving rise to different aggregation mode in the formation of the derived films. The neutral acylpyrazolone silver complexes without the N-H group on the imidazole ring are characterized by new local sub-organization of the polymer backbone, with the coexistence of local hexagonal and chiral nematic orders (N* and H), as proved by the PXRD and POM analysis. These complexes are able to reach the inner structure of the EC polymeric matrix, presumably embedding between EC inner chains. Instead, the silver complexes with the N-H group on the imidazole ancillary ligand as well as the ionic complex, are, probably, retained on the matrix surface through the formation of hydrogen bond interactions, leaving, then, the EC film inner structure unmodified. In these cases, the formation of microcrystals of the complex on the surface of the polymeric matrix has been proved by AFM, POM, DSC and PXRD characterizations.

The different type of interactions between the Ag(I) additives and the matrix induces interesting differences in the obtained films in terms of Ag(I) antibacterial activity and eventual Ag(I) ion release. In this work, the attention has been focused on the antimicrobial activity against the model gram-negative bacteria, Escherichia coli, being the most important pathogenic bacteria found in food industry. This property would make these new films potentially used in important applicative fields such as in food packaging and in biomedical devices.

All silver containing films have exhibited antimicrobial activity, independently on the concentration of complex used.

Ag(I) migration from the new EC-*n*x films has been tested by using three food simulants: water (A), ethanol 10% v/v (B) and acetic acid 3% v/v (C). The tests were conducted under two different experimental conditions, 70 °C for 2 h and 40 °C for ten days, according to the EU Legislation on the migration of chemicals from plastic materials. All the films prepared, with the exception of the EC-*n*a films, showed a

release of Ag(I) ions below the limit set by the EU legislation of 0.05 mg Kg^{-1} and for the films with the smallest amount of silver content, the eventual release was below the instrumental limit of quantification (LOQ) of 0.004 mg L^{-1}. This interesting reduced release of Ag^{+} ions occurs in all simulation conditions tested in terms of type of simulant, temperature, and exposure time tested.

Significant differences were observed in the case of the EC-*n*a films, where the behaviour varies according to the simulant used, and for the same simulant, variations are observed with increase of temperature and relative exposure time.

When distilled water is used as simulant, those films in which the silver complexes are embedded between the EC chains displayed the lowest level of release, independently of the temperature;

When acetic acid (3%) is used as simulant, a similar behaviour as in the case of distilled water is observed, but only at low exposure time and at high temperature. Instead, for the 10 days exposure period, for all EC-*n*a films, regardless of the nature of the interactions established between complex and polymer matrix, high release values were observed. Since after the exposure of 10 days, the films have maintained their integrity, this higher release might be correlated to eventual instability of the silver complexes in an acid environment over long periods of time.

Particularly interesting is the release behaviour observed when ethanol is used as simulant. In this case, a new factor must be invoked to understand the obtained results. Indeed, while at low temperature and exposure of 10 days, results are identical to the ones observed for distilled water, instead at high temperature and for an exposure of 2 hours an opposite trend of release has been observed in the series of the EC-*n*a films. Indeed, in these last conditions that films, which leave the EC structure unmodified, are characterised by a lower release of Ag^{+} ions–compared with that films for which the complexes are deeply embedded into the EC matrix. This specific behaviour of release has been correlated, through PXRD studies, to the swelling phenomenon of the EC matrix that occurs when using ethanol as simulant. This swelling in ethanol is due to the high solubility of the EC in this solvent. The films without the polymer structure modifications and characterized by the presence of microcrystals on their surface, hamper the swelling of the polymeric matrix, delaying the release of Ag^{+} ions to the medium. Instead for EC-*n*a films with complexes that formed intimate interactions with the EC matrix, the swelling is

observed allowing an easier diffusion of the Ag^+ ions to the external medium to form intimate interactions with the EC matrix.

The herein presented doctoral research studies demonstrated the possibility of using Silver(I) complexes as suitable candidates for the preparation of ethyl cellulose films with antibacterial activity and low silver release, that could find use in food packaging or biomedical applications. Noteworthy, the present work shows the importance of controlling the establishment of specific interactions between the chemical functionalities of the complexes and the polymer matrix. Intercalation of the complexes within the polymer matrix seems to result in low Ag^+ level of release, but this is true only if the external medium cannot provoke swelling phenomenon to the polymer matrix. In this latter case, indeed, the formation of microcrystals of complexes into the polymer matrix can be a viable strategy to decrease the release of silver ions.

Noteworthy, the results including in these Ph.D studies have been presented at the "XLVII Congresso Nazionale della Divisione di Chimica Inorganica della Società Chimica Italiana" (Bari, September 2019) receiving the committee prize for the best poster of the congress. Furthermore, part of the work carried out herein has been recently object to publication in an international peer-reviewed journal (Preparation and characterization of Ag(I) Ethylcellulose thin films as potential food packaging materials, ChemPlusChem, 2020, DOI: 10.1002/cplu.201900681) and studies of the evaluation of the effectiveness of antimicrobial food packaging for these class of materials carried out by monitoring biomarkers of food dysregulation via SPME GC/MS analysis are currently under progress. Preliminary results of this study have been presented at the international congress E-WISPOC 2020, held in Bressanone, in early 2020.

SUPPORTING AND INFORMATION

Complex 1

Table S 1. Crystal data and structure refinement for Complex **1**.

Identification code	shelx	
Empirical formula	$C_{21}\ H_{0.25}\ Ag_{1.50}\ F_3\ N_{5.50}\ O_{1.50}$	
Formula weight	572.32	
Temperature	298(2) K	
Wavelength	0.71073 Å	
Crystal system	Monoclinic	
Space group	P 21/n	
Unit cell dimensions	a = 7.1520(9) Å	α= 90°.
	b = 8.8634(11) Å	β= 90.472(5)°.
	c = 33.158(4) Å	γ = 90°.
Volume	2101.8(4) $Å^3$	
Z	4	
Density (calculated)	1.809 Mg/m^3	
Absorption coefficient	1.464 mm^{-1}	
F(000)	1097	
Crystal size	? x ? x ? mm^3	
Theta range for data collection	2.379 to 25.812°.	
Index ranges	-8<=h<=8, -10<=k<=10, -40<=l<=40	
Reflections collected	34735	
Independent reflections	3967 [R(int) = 0.0651]	
Completeness to theta = 25.242°	99.9 %	
Refinement method	Full-matrix least-squares on F^2	
Data / restraints / parameters	3967 / 0 / 289	
Goodness-of-fit on F^2	1.122	
Final R indices [I>2sigma(I)]	R1 = 0.1170, wR2 = 0.3139	
R indices (all data)	R1 = 0.1327, wR2 = 0.3224	
Extinction coefficient	n/a	
Largest diff. peak and hole	1.095 and -1.514 e.$Å^{-3}$	

Table S 2. Atomic coordinates (x 10^4) and equivalent isotropic displacement parameters ($Å^2$x 10^3) for Complex **1**. U(eq) is defined as one third of the trace of the orthogonalized U^{ij} tensor.

	x	y	z	U(eq)
Ag	2417(2)	2255(1)	4489(1)	56(1)
F(1)	2846(15)	-565(12)	6533(3)	75(3)
N(1)	2882(16)	1498(12)	5103(3)	43(2)
F(3)	4886(16)	920(14)	6826(3)	89(3)
F(2)	5849(15)	-610(13)	6366(3)	83(3)
N(2)	2799(15)	-39(11)	5193(3)	41(2)
O(2)	4240(20)	2875(14)	6281(4)	83(4)
N(5)	2439(18)	4479(13)	3356(3)	51(3)
N(3)	1772(17)	-431(13)	4546(4)	51(3)
N(4)	1883(19)	3406(14)	3940(4)	57(3)
O(1)	3329(18)	-1629(12)	5736(3)	67(3)
C(3)	3310(20)	-326(16)	5594(5)	51(3)
C(11)	2173(18)	-1045(14)	4887(4)	41(3)
C(2)	3655(19)	1104(15)	5755(4)	45(3)
C(1)	3396(19)	2196(17)	5441(5)	51(3)
C(5)	4110(20)	1540(18)	6152(5)	54(3)
C(16)	4320(20)	4320(20)	2729(5)	62(4)
C(8)	980(20)	-2820(20)	4283(6)	65(4)
C(10)	2030(20)	-2547(15)	4955(5)	56(4)
C(9)	1390(20)	-3451(19)	4652(6)	64(4)
C(15)	3440(30)	5280(20)	3031(5)	69(5)
C(6)	4470(20)	323(18)	6467(5)	55(4)
C(12)	380(20)	3250(20)	3703(6)	74(5)
C(4)	3590(20)	3861(17)	5448(5)	58(4)
C(19)	6020(50)	2500(50)	2130(8)	146(15)
C(21)	3990(30)	4490(30)	2316(6)	87(6)
C(7)	1180(20)	-1314(19)	4239(5)	61(4)
C(14)	3050(20)	4196(19)	3729(4)	59(4)
C(13)	720(30)	3870(30)	3347(6)	87(6)
C(20)	4700(40)	3780(40)	1999(9)	125(10)
C(17)	5590(30)	3180(30)	2811(7)	89(6)
C(18)	6280(40)	2280(30)	2518(10)	124(10)

Table S 3. Bond lengths [Å] and angles [°] for Complex **1**.

Ag-N(4)	2.119(12)
Ag-N(1)	2.166(11)
Ag-N(3)	2.433(12)
F(1)-C(6)	1.422(19)
N(1)-C(1)	1.330(19)
N(1)-N(2)	1.396(15)
F(3)-C(6)	1.336(18)
F(2)-C(6)	1.332(18)
N(2)-C(3)	1.399(18)
N(2)-C(11)	1.421(16)
O(2)-C(5)	1.262(19)
N(5)-C(14)	1.331(18)
N(5)-C(13)	1.35(2)
N(5)-C(15)	1.483(19)
N(3)-C(11)	1.284(18)
N(3)-C(7)	1.35(2)
N(4)-C(14)	1.30(2)
N(4)-C(12)	1.33(2)
O(1)-C(3)	1.248(17)
C(3)-C(2)	1.40(2)
C(11)-C(10)	1.355(19)
C(2)-C(5)	1.40(2)
C(2)-C(1)	1.43(2)
C(1)-C(4)	1.48(2)
C(5)-C(6)	1.52(2)
C(16)-C(17)	1.39(3)
C(16)-C(21)	1.40(2)
C(16)-C(15)	1.46(3)
C(8)-C(7)	1.35(2)
C(8)-C(9)	1.37(2)
C(8)-H(8A)	0.9300
C(10)-C(9)	1.36(2)
C(10)-H(10A)	0.9300
C(9)-H(9A)	0.9300
C(15)-H(15A)	0.9700
C(15)-H(15B)	0.9700

C(12)-C(13)	1.33(3)
C(12)-H(12A)	0.9300
C(4)-H(4A)	0.9600
C(4)-H(4B)	0.9600
C(4)-H(4C)	0.9600
C(19)-C(18)	1.31(4)
C(19)-C(20)	1.54(5)
C(19)-H(19A)	0.9300
C(21)-C(20)	1.33(3)
C(21)-H(21A)	0.9300
C(7)-H(7A)	0.9300
C(14)-H(14A)	0.9300
C(13)-H(13A)	0.9300
C(20)-H(20A)	0.9300
C(17)-C(18)	1.35(3)
C(17)-H(17A)	0.9300
C(18)-H(18A)	0.9300

N(4)-Ag-N(1)	169.0(5)
N(4)-Ag-N(3)	120.3(5)
N(1)-Ag-N(3)	69.6(4)
C(1)-N(1)-N(2)	106.6(11)
C(1)-N(1)-Ag	133.4(9)
N(2)-N(1)-Ag	119.8(8)
N(1)-N(2)-C(3)	111.7(11)
N(1)-N(2)-C(11)	118.2(10)
C(3)-N(2)-C(11)	130.0(11)
C(14)-N(5)-C(13)	103.8(13)
C(14)-N(5)-C(15)	127.4(14)
C(13)-N(5)-C(15)	128.8(14)
C(11)-N(3)-C(7)	119.0(13)
C(11)-N(3)-Ag	116.2(9)
C(7)-N(3)-Ag	124.5(11)
C(14)-N(4)-C(12)	104.8(14)
C(14)-N(4)-Ag	127.7(11)
C(12)-N(4)-Ag	126.6(12)
O(1)-C(3)-C(2)	133.9(15)
O(1)-C(3)-N(2)	122.0(14)

C(2)-C(3)-N(2)	104.0(11)
N(3)-C(11)-C(10)	123.1(13)
N(3)-C(11)-N(2)	115.4(12)
C(10)-C(11)-N(2)	121.4(13)
C(3)-C(2)-C(5)	130.2(13)
C(3)-C(2)-C(1)	108.3(12)
C(5)-C(2)-C(1)	121.4(13)
N(1)-C(1)-C(2)	109.4(13)
N(1)-C(1)-C(4)	120.1(14)
C(2)-C(1)-C(4)	130.6(14)
O(2)-C(5)-C(2)	126.3(15)
O(2)-C(5)-C(6)	114.8(14)
C(2)-C(5)-C(6)	118.9(14)
C(17)-C(16)-C(21)	112.0(19)
C(17)-C(16)-C(15)	125.1(16)
C(21)-C(16)-C(15)	122.9(18)
C(7)-C(8)-C(9)	118.5(16)
C(7)-C(8)-H(8A)	120.8
C(9)-C(8)-H(8A)	120.8
C(11)-C(10)-C(9)	118.8(15)
C(11)-C(10)-H(10A)	120.6
C(9)-C(10)-H(10A)	120.6
C(10)-C(9)-C(8)	119.0(16)
C(10)-C(9)-H(9A)	120.5
C(8)-C(9)-H(9A)	120.5
C(16)-C(15)-N(5)	115.5(14)
C(16)-C(15)-H(15A)	108.4
N(5)-C(15)-H(15A)	108.4
C(16)-C(15)-H(15B)	108.4
N(5)-C(15)-H(15B)	108.4
H(15A)-C(15)-H(15B)	107.5
F(2)-C(6)-F(3)	108.1(12)
F(2)-C(6)-F(1)	107.6(13)
F(3)-C(6)-F(1)	104.9(13)
F(2)-C(6)-C(5)	113.0(13)
F(3)-C(6)-C(5)	111.6(13)
F(1)-C(6)-C(5)	111.3(12)
C(13)-C(12)-N(4)	109.3(16)

C(13)-C(12)-H(12A)	125.3
N(4)-C(12)-H(12A)	125.3
C(1)-C(4)-H(4A)	109.5
C(1)-C(4)-H(4B)	109.5
H(4A)-C(4)-H(4B)	109.5
C(1)-C(4)-H(4C)	109.5
H(4A)-C(4)-H(4C)	109.5
H(4B)-C(4)-H(4C)	109.5
C(18)-C(19)-C(20)	118(3)
C(18)-C(19)-H(19A)	121.1
C(20)-C(19)-H(19A)	121.1
C(20)-C(21)-C(16)	132(3)
C(20)-C(21)-H(21A)	114.2
C(16)-C(21)-H(21A)	114.2
N(3)-C(7)-C(8)	121.6(16)
N(3)-C(7)-H(7A)	119.2
C(8)-C(7)-H(7A)	119.2
N(4)-C(14)-N(5)	113.3(15)
N(4)-C(14)-H(14A)	123.3
N(5)-C(14)-H(14A)	123.3
C(12)-C(13)-N(5)	108.6(15)
C(12)-C(13)-H(13A)	125.7
N(5)-C(13)-H(13A)	125.7
C(21)-C(20)-C(19)	111(3)
C(21)-C(20)-H(20A)	124.3
C(19)-C(20)-H(20A)	124.3
C(18)-C(17)-C(16)	122(2)
C(18)-C(17)-H(17A)	118.9
C(16)-C(17)-H(17A)	118.9
C(19)-C(18)-C(17)	125(3)
C(19)-C(18)-H(18A)	117.7
C(17)-C(18)-H(18A)	117.7

Symmetry transformations used to generate equivalent atoms:

Table S 4. Anisotropic displacement parameters ($Å^2 x\ 10^3$) for Complex **1**. The anisotropic displacement factor exponent takes the form: $-2\pi^2[\ h^2a^{*2}U^{11} + ... + 2\ h\ k\ a^*\ b^*\ U^{12}\ ]$

	U^{11}	U^{22}	U^{33}	U^{23}	U^{13}	U^{12}
Ag	83(1)	41(1)	44(1)	10(1)	1(1)	9(1)
F(1)	94(7)	78(7)	53(5)	15(5)	16(5)	-11(6)
N(1)	51(6)	33(6)	46(6)	1(5)	11(5)	-2(5)
F(3)	91(8)	103(9)	72(7)	11(6)	-29(6)	2(6)
F(2)	76(7)	90(8)	83(7)	6(6)	3(5)	28(6)
N(2)	51(6)	32(5)	39(5)	-2(4)	4(5)	4(5)
O(2)	132(12)	58(7)	59(7)	-4(6)	-12(7)	-7(7)
N(5)	71(8)	47(7)	36(6)	12(5)	6(5)	-8(6)
N(3)	50(7)	40(6)	64(8)	-2(6)	2(6)	1(5)
N(4)	76(9)	46(7)	49(7)	4(6)	-2(6)	-4(6)
O(1)	99(9)	36(5)	66(7)	1(5)	-3(6)	6(5)
C(3)	46(7)	43(8)	64(9)	18(7)	14(6)	15(6)
C(11)	41(7)	37(7)	45(7)	-4(5)	4(5)	-1(5)
C(2)	45(7)	41(7)	49(8)	6(6)	0(6)	-4(6)
C(1)	40(7)	49(8)	63(9)	2(7)	3(6)	9(6)
C(5)	47(8)	56(9)	60(9)	1(7)	6(7)	-3(7)
C(16)	59(9)	75(11)	51(9)	17(8)	1(7)	-4(8)
C(8)	44(8)	75(11)	75(11)	-23(9)	4(7)	2(8)
C(10)	77(10)	27(7)	63(9)	-5(6)	-2(8)	11(6)
C(9)	49(8)	46(8)	95(13)	-12(8)	-5(8)	-5(7)
C(15)	94(13)	60(10)	52(9)	19(8)	3(8)	-11(9)
C(6)	57(9)	53(9)	56(9)	-3(7)	-7(7)	11(7)
C(12)	53(9)	85(13)	85(13)	4(10)	-6(9)	-8(9)
C(4)	52(9)	51(9)	70(10)	-5(7)	-2(7)	5(7)
C(19)	150(30)	210(40)	81(17)	-40(20)	61(17)	-110(30)
C(21)	96(15)	111(17)	55(10)	5(11)	-13(10)	-25(13)
C(7)	55(9)	59(10)	70(10)	3(8)	-5(8)	-5(7)
C(14)	75(10)	62(10)	39(7)	4(7)	-1(7)	-8(8)
C(13)	62(11)	125(18)	73(12)	24(12)	-23(9)	-19(11)
C(20)	120(20)	140(30)	120(20)	-36(19)	-18(18)	-46(19)
C(17)	106(16)	82(14)	80(13)	8(11)	18(12)	16(12)
C(18)	130(20)	110(20)	140(30)	31(18)	49(19)	22(16)

Table S 5. Torsion angles [°] for Complex **1**.

C(1)-N(1)-N(2)-C(3)	-1.5(14)
Ag-N(1)-N(2)-C(3)	174.2(8)
C(1)-N(1)-N(2)-C(11)	176.4(11)
Ag-N(1)-N(2)-C(11)	-7.9(14)
N(1)-N(2)-C(3)-O(1)	179.9(13)
C(11)-N(2)-C(3)-O(1)	2(2)
N(1)-N(2)-C(3)-C(2)	2.1(14)
C(11)-N(2)-C(3)-C(2)	-175.5(12)
C(7)-N(3)-C(11)-C(10)	0(2)
Ag-N(3)-C(11)-C(10)	-174.8(12)
C(7)-N(3)-C(11)-N(2)	179.4(12)
Ag-N(3)-C(11)-N(2)	4.9(15)
N(1)-N(2)-C(11)-N(3)	1.4(17)
C(3)-N(2)-C(11)-N(3)	178.8(13)
N(1)-N(2)-C(11)-C(10)	-179.0(13)
C(3)-N(2)-C(11)-C(10)	-2(2)
O(1)-C(3)-C(2)-C(5)	-2(3)
N(2)-C(3)-C(2)-C(5)	175.6(14)
O(1)-C(3)-C(2)-C(1)	-179.3(16)
N(2)-C(3)-C(2)-C(1)	-1.9(15)
N(2)-N(1)-C(1)-C(2)	0.2(15)
Ag-N(1)-C(1)-C(2)	-174.7(9)
N(2)-N(1)-C(1)-C(4)	-179.1(12)
Ag-N(1)-C(1)-C(4)	6(2)
C(3)-C(2)-C(1)-N(1)	1.1(16)
C(5)-C(2)-C(1)-N(1)	-176.6(13)
C(3)-C(2)-C(1)-C(4)	-179.7(15)
C(5)-C(2)-C(1)-C(4)	3(2)
C(3)-C(2)-C(5)-O(2)	-173.7(16)
C(1)-C(2)-C(5)-O(2)	4(2)
C(3)-C(2)-C(5)-C(6)	6(2)
C(1)-C(2)-C(5)-C(6)	-176.6(13)
N(3)-C(11)-C(10)-C(9)	-2(2)
N(2)-C(11)-C(10)-C(9)	178.7(13)
C(11)-C(10)-C(9)-C(8)	3(2)
C(7)-C(8)-C(9)-C(10)	-2(2)

C(17)-C(16)-C(15)-N(5)	-55(3)
C(21)-C(16)-C(15)-N(5)	126.7(18)
C(14)-N(5)-C(15)-C(16)	100(2)
C(13)-N(5)-C(15)-C(16)	-80(2)
O(2)-C(5)-C(6)-F(2)	-122.4(16)
C(2)-C(5)-C(6)-F(2)	57.8(19)
O(2)-C(5)-C(6)-F(3)	0(2)
C(2)-C(5)-C(6)-F(3)	179.8(13)
O(2)-C(5)-C(6)-F(1)	116.4(16)
C(2)-C(5)-C(6)-F(1)	-63.4(17)
C(14)-N(4)-C(12)-C(13)	4(2)
Ag-N(4)-C(12)-C(13)	-165.5(15)
C(17)-C(16)-C(21)-C(20)	-1(3)
C(15)-C(16)-C(21)-C(20)	177(2)
C(11)-N(3)-C(7)-C(8)	1(2)
Ag-N(3)-C(7)-C(8)	175.2(12)
C(9)-C(8)-C(7)-N(3)	0(2)
C(12)-N(4)-C(14)-N(5)	-4(2)
Ag-N(4)-C(14)-N(5)	165.0(11)
C(13)-N(5)-C(14)-N(4)	3(2)
C(15)-N(5)-C(14)-N(4)	-177.1(15)
N(4)-C(12)-C(13)-N(5)	-2(3)
C(14)-N(5)-C(13)-C(12)	0(2)
C(15)-N(5)-C(13)-C(12)	179.7(17)
C(16)-C(21)-C(20)-C(19)	4(4)
C(18)-C(19)-C(20)-C(21)	-1(4)
C(21)-C(16)-C(17)-C(18)	-5(3)
C(15)-C(16)-C(17)-C(18)	177(2)
C(20)-C(19)-C(18)-C(17)	-5(4)
C(16)-C(17)-C(18)-C(19)	9(4)

Symmetry transformations used to generate equivalent atoms:

Complex 2

Table S 1. Crystal data and structure refinement for Complex **2**.

Identification code	shelx	
Empirical formula	C_{18} H_{19} Ag F_3 N_5 O_2	
Formula weight	502.25	
Temperature	296(2) K	
Wavelength	0.71073 Å	
Crystal system	Triclinic	
Space group	P -1	
Unit cell dimensions	a = 7.7583(10) Å	α= 104.268(6)°.
	b = 11.6991(15) Å	β= 91.117(6)°.
	c = 11.9243(15) Å	γ = 102.264(6)°.
Volume	1022.0(2) $Å^3$	
Z	2	
Density (calculated)	1.632 Mg/m^3	
Absorption coefficient	1.036 mm^{-1}	
F(000)	504	
Crystal size	0.210 x 0.100 x 0.060 mm^3	
Theta range for data collection	1.767 to 26.525°.	
Index ranges	-9<=h<=9, -14<=k<=14, -14<=l<=14	
Reflections collected	44220	
Independent reflections	4204 [R(int) = 0.0405]	
Completeness to theta = 25.242°	100.0 %	
Refinement method	Full-matrix least-squares on F^2	
Data / restraints / parameters	4204 / 0 / 271	
Goodness-of-fit on F^2	1.152	
Final R indices [I>2sigma(I)]	R1 = 0.0362, wR2 = 0.1018	
R indices (all data)	R1 = 0.0608, wR2 = 0.1260	
Extinction coefficient	n/a	
Largest diff. peak and hole	0.571 and -0.644 e.$Å^{-3}$	

Table S 2. Bond lengths [Å] and angles [°] for Complex **2**.

Ag-N(4)	2.125(3)
Ag-N(1)	2.194(3)
Ag-N(3)	2.417(3)
Ag-Ag#1	3.2725(7)
N(1)-C(1)	1.316(4)
N(1)-N(2)	1.407(4)
N(2)-C(11)	1.404(4)
N(2)-C(3)	1.406(4)
N(3)-C(11)	1.332(4)
N(3)-C(7)	1.342(4)
N(4)-C(14)	1.308(6)
N(4)-C(12)	1.385(6)
N(5)-C(14)	1.340(6)
N(5)-C(13)	1.349(7)
N(5)-C(15)	1.461(8)
O(1)-C(3)	1.236(4)
O(2)-C(5)	1.212(5)
F(1)-C(6)	1.331(4)
F(2)-C(6)	1.336(6)
F(3)-C(6)	1.334(6)
C(1)-C(2)	1.418(5)
C(1)-C(4)	1.500(5)
C(2)-C(5)	1.427(5)
C(2)-C(3)	1.440(5)
C(5)-C(6)	1.558(6)
C(7)-C(8)	1.356(6)
C(8)-C(9)	1.376(6)
C(9)-C(10)	1.382(5)
C(10)-C(11)	1.385(5)
C(12)-C(13)	1.325(8)
C(15)-C(16)	1.379(9)
C(16)-C(17)	1.495(9)
C(17)-C(18A)	1.41(5)
C(17)-C(18B)	1.48(4)
N(4)-Ag-N(1)	165.31(12)

N(4)-Ag-N(3)	120.75(12)
N(1)-Ag-N(3)	71.02(10)
N(4)-Ag-Ag#1	109.38(10)
N(1)-Ag-Ag#1	83.63(8)
N(3)-Ag-Ag#1	61.41(7)
C(1)-N(1)-N(2)	106.1(3)
C(1)-N(1)-Ag	134.8(2)
N(2)-N(1)-Ag	117.34(19)
C(11)-N(2)-C(3)	128.6(3)
C(11)-N(2)-N(1)	119.6(3)
C(3)-N(2)-N(1)	111.8(2)
C(11)-N(3)-C(7)	118.2(3)
C(11)-N(3)-Ag	114.4(2)
C(7)-N(3)-Ag	126.9(2)
C(14)-N(4)-C(12)	104.5(4)
C(14)-N(4)-Ag	122.7(3)
C(12)-N(4)-Ag	132.6(3)
C(14)-N(5)-C(13)	106.8(4)
C(14)-N(5)-C(15)	125.3(6)
C(13)-N(5)-C(15)	127.8(5)
N(1)-C(1)-C(2)	111.8(3)
N(1)-C(1)-C(4)	119.4(3)
C(2)-C(1)-C(4)	128.8(3)
C(1)-C(2)-C(5)	123.8(3)
C(1)-C(2)-C(3)	106.8(3)
C(5)-C(2)-C(3)	129.3(3)
O(1)-C(3)-N(2)	123.9(3)
O(1)-C(3)-C(2)	132.7(3)
N(2)-C(3)-C(2)	103.5(3)
O(2)-C(5)-C(2)	125.7(4)
O(2)-C(5)-C(6)	115.7(4)
C(2)-C(5)-C(6)	118.6(3)
F(1)-C(6)-F(3)	107.0(4)
F(1)-C(6)-F(2)	106.7(4)
F(3)-C(6)-F(2)	108.0(4)
F(1)-C(6)-C(5)	110.0(4)
F(3)-C(6)-C(5)	112.7(4)
F(2)-C(6)-C(5)	112.1(4)

N(3)-C(7)-C(8)	123.8(4)
C(7)-C(8)-C(9)	117.4(3)
C(8)-C(9)-C(10)	120.7(4)
C(9)-C(10)-C(11)	117.6(3)
N(3)-C(11)-C(10)	122.3(3)
N(3)-C(11)-N(2)	116.1(3)
C(10)-C(11)-N(2)	121.6(3)
C(13)-C(12)-N(4)	109.7(5)
C(12)-C(13)-N(5)	107.2(4)
N(4)-C(14)-N(5)	111.7(4)
C(16)-C(15)-N(5)	120.1(5)
C(15)-C(16)-C(17)	119.9(6)
C(18A)-C(17)-C(16)	113.1(16)
C(18B)-C(17)-C(16)	126.9(15)

Symmetry transformations used to generate equivalent atoms:

#1 -x+1,-y+1,-z+2

Table S 3. Torsion angles [°] for Complex **2**.

C(1)-N(1)-N(2)-C(11)	-178.4(3)
Ag-N(1)-N(2)-C(11)	-11.3(4)
C(1)-N(1)-N(2)-C(3)	-0.7(4)
Ag-N(1)-N(2)-C(3)	166.5(2)
N(2)-N(1)-C(1)-C(2)	0.5(4)
Ag-N(1)-C(1)-C(2)	-163.3(3)
N(2)-N(1)-C(1)-C(4)	180.0(3)
Ag-N(1)-C(1)-C(4)	16.2(6)
N(1)-C(1)-C(2)-C(5)	176.1(4)
C(4)-C(1)-C(2)-C(5)	-3.4(7)
N(1)-C(1)-C(2)-C(3)	-0.2(4)
C(4)-C(1)-C(2)-C(3)	-179.6(4)
C(11)-N(2)-C(3)-O(1)	-2.2(6)
N(1)-N(2)-C(3)-O(1)	-179.7(3)
C(11)-N(2)-C(3)-C(2)	178.0(3)
N(1)-N(2)-C(3)-C(2)	0.5(4)
C(1)-C(2)-C(3)-O(1)	-180.0(4)
C(5)-C(2)-C(3)-O(1)	4.1(7)
C(1)-C(2)-C(3)-N(2)	-0.2(4)
C(5)-C(2)-C(3)-N(2)	-176.2(4)
C(1)-C(2)-C(5)-O(2)	9.2(7)
C(3)-C(2)-C(5)-O(2)	-175.4(5)
C(1)-C(2)-C(5)-C(6)	-171.3(4)
C(3)-C(2)-C(5)-C(6)	4.1(7)
O(2)-C(5)-C(6)-F(1)	-3.7(6)
C(2)-C(5)-C(6)-F(1)	176.7(4)
O(2)-C(5)-C(6)-F(3)	115.6(5)
C(2)-C(5)-C(6)-F(3)	-64.0(5)
O(2)-C(5)-C(6)-F(2)	-122.3(5)
C(2)-C(5)-C(6)-F(2)	58.1(5)
C(11)-N(3)-C(7)-C(8)	-0.1(6)
Ag-N(3)-C(7)-C(8)	171.2(3)
N(3)-C(7)-C(8)-C(9)	-1.0(6)
C(7)-C(8)-C(9)-C(10)	1.1(7)
C(8)-C(9)-C(10)-C(11)	-0.2(6)
C(7)-N(3)-C(11)-C(10)	1.1(5)

Ag-N(3)-C(11)-C(10)	-171.3(3)
C(7)-N(3)-C(11)-N(2)	-179.4(3)
Ag-N(3)-C(11)-N(2)	8.2(4)
C(9)-C(10)-C(11)-N(3)	-1.0(6)
C(9)-C(10)-C(11)-N(2)	179.5(4)
C(3)-N(2)-C(11)-N(3)	-176.0(3)
N(1)-N(2)-C(11)-N(3)	1.2(4)
C(3)-N(2)-C(11)-C(10)	3.5(5)
N(1)-N(2)-C(11)-C(10)	-179.3(3)
C(14)-N(4)-C(12)-C(13)	-0.6(6)
Ag-N(4)-C(12)-C(13)	-176.1(4)
N(4)-C(12)-C(13)-N(5)	1.5(6)
C(14)-N(5)-C(13)-C(12)	-1.8(6)
C(15)-N(5)-C(13)-C(12)	179.9(6)
C(12)-N(4)-C(14)-N(5)	-0.6(5)
Ag-N(4)-C(14)-N(5)	175.5(3)
C(13)-N(5)-C(14)-N(4)	1.5(6)
C(15)-N(5)-C(14)-N(4)	179.9(5)
C(14)-N(5)-C(15)-C(16)	57.7(11)
C(13)-N(5)-C(15)-C(16)	-124.3(9)
N(5)-C(15)-C(16)-C(17)	179.8(7)
C(15)-C(16)-C(17)-C(18A)	162(2)
C(15)-C(16)-C(17)-C(18B)	-170(2)

Symmetry transformations used to generate equivalent atoms:

#1 -x+1,-y+1,-z+2

Table S 4. Hydrogen bonds for Complex **2** [Å and °].

D-H...A	d(D-H)	d(H...A)	d(D...A)	<(DHA)
C(4)-H(4A)...O(2)	0.96	2.26	2.968(6)	130.2
C(4)-H(4B)...F(1)#2	0.96	3.04	3.640(6)	121.6
C(7)-H(7)...F(2)#3	0.93	3.02	3.712(5)	132.6
C(8)-H(8)...O(2)#4	0.93	2.40	3.298(5)	163.1
C(8)-H(8)...F(1)#4	0.93	2.66	3.358(5)	132.9
C(10)-H(10)...O(1)	0.93	2.23	2.856(4)	124.0
C(13)-H(13)...O(1)#5	0.93	2.50	3.298(5)	143.7
C(13)-H(13)...F(3)#5	0.93	2.89	3.410(7)	116.4
C(14)-H(14)...O(1)#3	0.93	2.67	3.311(6)	126.9
C(14)-H(14)...F(2)#3	0.93	2.96	3.825(6)	155.8
C(15)-H(15B)...N(4)#6	0.97	3.03	3.750(8)	131.8
C(15)-H(15B)...N(5)#6	0.97	3.12	3.746(8)	123.8
C(16)-H(16A)...F(3)#1	0.97	2.75	3.665(8)	157.5
C(16)-H(16B)...F(2)#3	0.97	2.70	3.608(8)	155.3

Symmetry transformations used to generate equivalent atoms:

#1 -x+1,-y+1,-z+2 #2 -x+2,-y+1,-z+1 #3 -x+2,-y+1,-z+2

#4 x,y,z+1 #5 x-1,y-1,z #6 -x+1,-y,-z+2

Table S 5. Specific Ag(I) migration from EC-*n*x square films, expressed in mg L^{-1} release in several simulants by heating at 70 °C for 2 hours. Data represent mean ± standard deviation (SD) of least three independent measurements.

Sample	***Simulant*** [a] ***A***	***Simulant*** ***B***	***Simulant*** ***C***
EC-0	0	0	0
EC-1a	$1.63 \times 10^{-1} \pm 9 \times 10^{-3}$	$3.951 \pm 2.6 \times 10^{-2}$	$4.08 \times 10^{-1} \pm 5.3 \times 10^{-2}$
EC-1b	LOQ[b]	$1.4 \times 10^{-2} \pm 2.2 \times 10^{-3}$	$0.6 \times 10^{-2} \pm 1.8 \times 10^{-2}$
EC-1c	LOQ	$0.75 \times 10^{-2} \pm 1.2 \times 10^{-3}$	$0.3 \times 10^{-1} \pm 1.1 \times 10^{-3}$
EC-2a	$0.24 \pm 3 \times 10^{-3}$	$1.01 \pm 1.9 \times 10^{-2}$	$2.53 \times 10^{-1} \pm 2.4 \times 10^{-3}$
EC-2b	$0.8 \times 10^{-2} \pm 1 \times 10^{-3}$	LOQ	$1.1 \times 10^{-2} \pm 1.3 \times 10^{-3}$
EC-2c	LOQ	LOQ	LOQ
EC-3a	$1.18 \pm 6 \times 10^{-3}$	$1.13 \times 10^{-2} \pm 1.6 \times 10^{-3}$	$2.1 \pm 1.8 \times 10^{-2}$
EC-3b	$0.78 \times 10^{-2} \pm 2 \times 10^{-3}$	LOQ	$5 \times 10^{-3} \pm 1 \times 10^{-3}$
EC-3c	LOQ	LOQ	LOQ
EC-4a	$1.111 \pm 6 \times 10^{-3}$	$3.1 \times 10^{-2} \pm 1 \times 10^{-3}$	$1.611 \pm 3.1 \times 10^{-2}$
EC-4b	LOQ	LOQ	LOQ
EC-4c	LOQ	LOQ	$6 \times 10^{-3} \pm 2 \times 10^{-3}$
EC-5a	$0.87 \pm 4 \times 10^{-3}$	$4.7 \times 10^{-1} \pm 3 \times 10^{-3}$	$1.44 \pm 3 \times 10^{-2}$
EC-5b	$0.6 \times 10^{-2} \pm 2 \times 10^{-3}$	$1.46 \times 10^{-2} \pm 1.3 \times 10^{-3}$	$1.8 \times 10^{-2} \pm 1.6 \times 10^{-3}$
EC-5c	LOQ	LOQ	LOQ
EC-6a	$0.48 \pm 2 \times 10^{-3}$	$1.28 \times 10^{-1} \pm 1.4 \times 10^{-3}$	$3.86 \times 10^{-1} \pm 2.1 \times 10^{-3}$
EC-6b	$0.6 \times 10^{-2} \pm 1 \times 10^{-3}$	$1.1 \times 10^{-2} \pm 2.3 \times 10^{-3}$	$1.9 \times 10^{-2} \pm 1.1 \times 10^{-3}$
EC-6c	LOQ	LOQ	LOQ
EC-($AgNO_3$)a	$3.26 \times 10^{-1} \pm 1.50 \times 10^{-2}$	$2.86 \times 10^{-1} \pm 1.7 \times 10^{-2}$	$2.34 \times 10^{-1} \pm 2.9 \times 10^{-2}$
EC-($AgNO_3$)b	$2 \times 10^{-2} \pm 1 \times 10^{-3}$	LOQ	$4 \times 10^{-3} \pm 1 \times 10^{-3}$
EC-($AgNO_3$)c	$5 \times 10^{-3} \pm 2 \times 10^{-3}$	LOQ	$5.30 \times 10^{-2} \pm 2 \times 10^{-3}$

Table S 6. Specific Ag(I) migration from EC-*n* square films, expressed in mg L^{-1} release in several simulants by heating at 40 °C for 10 days. Data represent mean ± standard deviation (SD) of least three independent measurements.

Sample	***Simulant*** [a] ***A***	***Simulant B***	***Simulant C***
EC-0	0	0	0
EC-1a	$2.13 \times 10^{-1} \pm 7.1 \times 10^{-3}$	$1.37 \times 10^{-2} \pm 1.84 \times 10^{-3}$	$1.791 \pm 2.52 \times 10^{-2}$
EC-1b	LOQ[b]	LOQ	LOQ
EC-1c	LOQ	LOQ	LOQ
EC-2a	$0.52 \pm 5.1 \times 10^{-3}$	$4.8 \times 10^{-2} \pm 3.1 \times 10^{-3}$	$9.98 \times 10^{-1} \pm 3.9 \times 10^{-3}$
EC-2b	$1.1 \times 10^{-2} \pm 1.6 \times 10^{-3}$	$2.8 \times 10^{-2} \pm 1.5 \times 10^{-3}$	$1.7 \times 10^{-2} \pm 1.9 \times 10^{-3}$
EC-2c	LOQ	LOQ	LOQ
EC-3a	$1.1 \pm 2.3 \times 10^{-2}$	$2.0 \pm 3.2 \times 10^{-2}$	$1.64 \pm 7.3 \times 10^{-2}$
EC-3b	$2.21 \times 10^{-2} \pm 2.1 \times 10^{-3}$	$1.0 \times 10^{-2} \pm 1.9 \times 10^{-3}$	$0.45 \times 10^{-1} \pm 1.3 \times 10^{-3}$
EC-3c	LOQ	LOQ	LOQ
EC-4a	$5.36 \times 10^{-1} \pm 3.9 \times 10^{-2}$	$2.112 \pm 2.87 \times 10^{-2}$	$1.651 \pm 2.3 \times 10^{-2}$
EC-4b	LOQ	LOQ	$2.5 \times 10^{-2} \pm 9.1 \times 10^{-3}$
EC-4c	LOQ	LOQ	$4.4 \times 10^{-2} \pm 3.1 \times 10^{-3}$
EC-5a	$0.42 \pm 2 \times 10^{-2}$	$1.12 \pm 3 \times 10^{-2}$	$2.27 \pm 6.4 \times 10^{-2}$
EC-5b	$1.23 \times 10^{-2} \pm 2 \times 10^{-3}$	$1.1 \times 10^{-2} \pm 1.8 \times 10^{-3}$	$2.7 \times 10^{-2} \pm 2.2 \times 10^{-3}$
EC-5c	LOQ	LOQ	LOQ
EC-6a	$1.21 \times 10^{-1} \pm 3 \times 10^{-3}$	$0.12 \pm 4 \times 10^{-2}$	$1.246 \pm 6.4 \times 10^{-2}$
EC-6b	$1.2 \times 10^{-2} \pm 1.1 \times 10^{-3}$	$1.2 \times 10^{-2} \pm 2.3 \times 10^{-3}$	$1.9 \times 10^{-2} \pm 2.2 \times 10^{-3}$
EC-6c	LOQ	LOQ	LOQ
EC-($AgNO_3$)a	$5.26 \times 10^{-1} \pm 2.6 \times 10^{-2}$	$1.4 \times 10^{-2} \pm 1.5 \times 10^{-3}$	$1.08 \times 10^{-1} \pm 1.3 \times 10^{-2}$
EC-($AgNO_3$)b	$1.3 \times 10^{-2} \pm 2 \times 10^{-3}$	LOQ	$2.1 \times 10^{-2} \pm 3 \times 10^{-3}$
EC-($AgNO_3$)c	$1.5 \times 10^{-2} \pm 2 \times 10^{-3}$	LOQ	$2.8 \times 10^{-2} \pm 2 \times 10^{-3}$

List of Publications

Fabio Marchetti*, Riccardo Pettinari, Corrado Di Nicola, Claudio Pettinari, Anup Paul, Alessandra Crispini, Eugenia Giorno, Francesco Lelj, Sonia Stoia, Mario Amati*, **Effects of methyl groups in a pyrimidine-based flexible ligand on the formation of silver(I) coordination networks,** *New Journal of Chemistry,* **2018**, 42, 13998

F. Scarpelli, A. Crispini*, E. Giorno*, F. Marchetti*, R. Pettinari, C. Di Nicola, M. Penelope De Santo, E. Fuoco, R. Berardi, P. Alfano, P. Caputo, D. Policastro, C. Oliviero Rossi and I. Aiello, **Preparation and Characterization of Silver(I) Ethylcellulose Thin Films as Potential Food Packaging Materials**, *ChemPlusChem*, Wiley, **2020,** 85, 426-440

Side projects:

Andrea Bloise*, Claudia Ricchiuti , Eugenia Giorno, Ilaria Fuoco, Patrizia Zumpano, Domenico Miriello, Carmine Apollaro, Alessandra Crispini, Rosanna De Rosa, Rosalda Punturo, **Assessment of Naturally Occurring Asbestos in the Area of Episcopia (Lucania, Southern Italy)**, *Fibers* **2019**, *7*, 5, 45; https://doi.org/10.3390/fib7050045

ACKNOWLEDGEMENTS

I would like to express my gratitude to my supervisors Prof.ssa Alessandra Crispini for guiding me and to Prof.ssa Iolinda Aiello for her continuous human and scientific support..

I would like a special thanks I would like to do to Dott. Riccardo Berardi and Dott. Pasquale Alfano for making me always feels welcome in their company..

I would like to thanks my family for always believed in me and my colleagues for the goods moment spent together..